Fibre reinforced polymer nanocomposites

Proefschrift

Ter verkrijging van de graad van doctor
aan de Technische Universiteit Delft,
op gezag van de Rector Magnificus prof. dr. ir. J.T. Fokkema
voorzitter van het College van Promoties,
in het openbaar te verdedigen op dinsdag 11 oktober 2005 om 10:30 uur
door

Daniël Petrus Nicolaas VLASVELD

scheikundig ingenieur
geboren te Leiderdorp

Dit proefschrift is goedgekeurd door de promotor:
Prof. dr. S.J. Picken

Toegevoegd promotor:
Dr. ir. H.E.N. Bersee

Samenstelling promotiecommissie:

Rector Magnificus, voorzitter
Prof. dr. S.J. Picken, Technische Universiteit Delft, promotor
Dr. ir. H.E.N. Bersee, Technische Universiteit Delft, toegevoegd promotor
Prof. ir. A. Beukers, Technische Universiteit Delft
Prof. dr. ir. A. Posthuma de Boer, Technische Universiteit Delft
Prof. dr. C.E. Koning, Technische Universiteit Eindhoven
Dr. ir. A. Stroeks, DSM Research
Dr. A.D. Gotsis, Technical University of Crete, Greece

The research described in this thesis forms part of the research program of the Dutch Polymer Institute, DPI project 279.

Copyright © 2005: D.P.N. Vlasveld
All rights reserved

No part of the material protected by this copyright notice may be reproduced or utilized in any form or by any means, electronic or mechanical, including photocopying, recording or by any information storage retrieval system, without permission from the author.

ISBN-10: 90-9019883-0
ISBN-13: 978-90-9019883-5

Cover design and photography: Daniël Vlasveld
Photos: Carbon fibres and mica crystals

Printed at Haveka, the Netherlands

Fibre reinforced polymer nanocomposites

Contents Fibre reinforced polymer nanocomposites

Chapter 1 General Introduction 1

1.1 Fibre reinforced polyamide 6 nanocomposite 1
1.2 Reinforcement of thermoplastic polymers 2
1.2.1 Properties of filled polymers 2
1.2.2 Types of reinforcing fillers for polymers 3
1.3 Nanocomposites 5
1.3.1 Nanocomposites compared to traditional filled polymers 6
1.3.2 Layered silicates 8
1.3.3 Layered silicate as reinforcement 10
1.3.4 Properties of layered silicate nanocomposites 12
1.4 Thermoplastic continuous fibre composites 16
1.5 Fibre composites with nanocomposite matrix 21
1.5.1 The concept of a three phase composite 21
1.5.2 Previous research in this field 22
1.6 Outline of the thesis 23
1.7 References 25

Chapter 2 Moisture absorption in PA6 silicate nanocomposites and its influence on the mechanical properties 29

2.1 Introduction 29
2.2 Theory 30
2.2.1 Water diffusion in polymers and nanocomposites 30
2.2.2 Influence of water on mechanical properties 33
2.3 Experimental 33
2.3.1 Materials 33
2.3.2 Preparation 34
2.3.3 Testing 35
2.4 Results and Discussion 36
2.4.1 Moisture absorption 36
2.4.2 Diffusion coefficient 37
2.4.3 Aspect ratios 41
2.4.4 Mechanical properties 42
2.5 Conclusions 45
2.6 References 47

Chapter 3 **Analysis of the modulus of PA6 silicate nanocomposites using moisture controlled variation of the matrix properties** 49

3.1 Introduction 49
3.2 Theory 50
3.2.1 The Halpin-Tsai model 51
3.2.2 Calculation of the matrix modulus using the Halpin-Tsai model 54
3.2.3 Calculation of the effective platelet aspect ratio 56
3.3 Experimental 57
3.3.1 Materials 57
3.3.2 Sample preparation 57
3.3.3 Testing 58
3.4 Results and Discussion 59
3.4.1 Silicate content, matrix crystallinity and T_g 59
3.4.2 Silicate platelet and crystalline orientation 61
3.4.3 Calculation of the modulus of the matrix phase 63
3.4.4 Modulus of the nanocomposites and calculation of the aspect ratios 66
3.5 Conclusions 68
3.6 References 70

Chapter 4 **A comparison of the temperature dependence of the modulus, yield stress and ductility of nanocomposites based on high and low MW PA6 and PA66.** 73

4.1 Introduction 73
4.2 Experimental 76
4.2.1 Material 76
4.2.2 Preparation 77
4.2.3 Testing 78
4.3 Results and Discussion 79
4.3.1 Modulus 79
4.3.2 Yield- or fracture stress 83
4.3.3 Elongation at break 84
4.3.4 Glass transition temperature and crystallinity 86
4.3.5 Brittle to ductile transition temperatures 87
4.4 Conclusions 89
4.5 References 91

Chapter 5 The relation between rheological and mechanical properties in PA 6 nanocomposites and microcomposites 93

5.1 Introduction 93
5.2 Theory 94
5.2.1 Modulus of elasticity 94
5.2.2 Melt rheology 95
5.3 Experimental 99
5.3.1 Materials 99
5.3.2 Specimen preparation 100
5.3.3 Testing 101
5.4 Results and Discussion 102
5.4.1 Dispersion and particle size 102
5.4.2 Dynamic moduli 103
5.4.3 Rheological tests 107
5.4.4 Calculation of the aspect ratios from viscosity data 111
5.4.5 Comparison between the modulus increase and the viscosity increase 113
5.5 Conclusions 115
5.6 References 116

Chapter 6 Creep and physical aging behaviour of PA6 nanocomposites 119

6.1 Introduction 119
6.2 Experimental 121
6.2.1 Materials 121
6.2.2 Sample preparation 122
6.2.3 Testing 123
6.4 Results and Discussion 123
6.5 Conclusions 133
6.6 References 134

Chapter 7 Fibre-matrix adhesion in glass-fibre reinforced PA6 silicate nanocomposites 135

7.1 Introduction 135
7.2 Theory 136
7.2.1 Influence of the matrix shear yield stress 136
7.2.2 Influence of the matrix modulus 137
7.2.3 Influence of the maximum strain of the matrix 139
7.2.4 The influence of the melt flow behaviour 140
7.2.5 Determination of the critical aspect ratio from the test data 140
7.3 Experimental 141
7.3.1 Materials 141
7.3.2 Preparation 142
7.3.3 Testing 143

7.4 Results and Discussion 144
7.4.1 SFFT PA6 and glass fibres with various sizings 145
7.4.2 SFFT glass fibres and dry PA-6 nanocomposites 146
7.4.3 SFFT glass fibres and moisture conditioned PA-6 nanocomposites 147
7.4.4 Matrix properties: tensile modulus, yield stress, yield strain and melt flow behaviour 148
7.4.5 General discussion of the results 151
7.5 Conclusions 153
7.6 References 154

Chapter 8 Continuous fibres reinforced thermoplastic composites with a PA6 nanocomposite matrix 157

8.1 Introduction 157
8.2 Experimental 159
8.2.1 Materials 159
8.2.2 Preparation 160
8.2.3 Testing 162
8.3 Results and Discussion 163
8.3.1 The influence of the temperature on the flexural strength of PA6 glass and carbon fibre composites 163
8.3.2 Nanocomposite matrix materials 165
8.3.3 The flexural strength of fibre composites with a nanocomposite matrix 168
8.4 Conclusions 172
8.5 References 174

Chapter 9 Conclusions 175

9.1 Production processes 175
9.2 Brittleness 176
9.3 Crystallization and orientation of crystals and particles 176
9.4 Water absorption and diffusion 177
9.5 Aspect ratios from the various models 177
9.6 Creep and physical ageing 178
9.7 Melt flow behaviour and fibre impregnation 178
9.8 Adhesion 179
9.9 Combination nanocomposites and continuous fibres 180
9.10 Recommendations 181
9.11 References 183

Summary 185
Samenvatting 189
Dankwoord 193
Curiculum vitae 197
Publications 199

Chapter 1

General Introduction

1.1 Fibre reinforced polyamide 6 nanocomposite

Polymer nanocomposites are a relatively new type of composite material, of which the possibilities are numerous but not yet fully explored.
Thermoplastic continuous fibre reinforced composites are another relatively new development within the field of composites, in which thermoplastic polymers are replacing crosslinked resins as matrix material for continuous fibre reinforced composites.
In this thesis the results are described of the research into the possibilities of a combination of these two new types of composites. This combination consists of a three-phase composite, in which the main reinforcing phase are continuous fibres and the matrix consists of a thermoplastic polymer nanocomposite. To be able to successfully produce this new type of composite and to understand the properties, several aspects of the individual components need to be understood first. For this reason most of the research has been focussed on the nanocomposite matrix material, followed by an investigation of the properties of fibre composites and the three-phase thermoplastic fibre reinforced nanocomposite.
The matrix polymer chosen to investigate this new three-phase composite with is polyamide 6 (PA6), because it is known from previous research that good nanocomposites can be produced with this polymer. Polyamide 6 is an engineering plastic that is positioned between the cheap commodity plastics and the high performance polymers, because it has good mechanical properties while being relatively cheap. The goal of this research is to improve the properties of the matrix material of the fibre composite by reinforcement on the nanometer level and thereby upgrading the properties of this relatively low cost thermoplastic composite.
In this general introduction first the various types of reinforcement used in thermoplastic polymers will be discussed, followed by a more detailed description of nanocomposites and thermoplastic continuous fibre composites. This will be followed by a short overview of the limited amount of research that was done on the

combination of fibre composites and nanocomposites. In the last section an overview will be given of the topics that will be investigated in each chapter of this thesis.

1.2 Reinforcement of thermoplastic polymers

Thermoplastic polymers have been developed and produced since the 1930s and where used since then in ever growing quantities. A large part of the thermoplastic polymers are not used in their pure form, but mixed with some form of rigid filler or reinforcement to modify the mechanical properties. Polymers containing rigid fillers are known as compounds or composites, because they consist of at least two different phases.

1.2.1 Properties of filled polymers

The initial reason for the use of fillers in polymers was to reduce the cost of the compound [1], but fillers also change the mechanical and other properties of the compound. While the price per weight of some fillers might be cheaper than the polymer, per volume the differences are less because of the generally high density of mineral fillers. The addition of fillers to the polymers also adds extra cost in the form of more processing steps, and sometimes addition of extra components such as surface modifiers are necessary. Therefore, the use of fillers is mainly driven by the property enhancements, which can often justify the extra cost [1,2].

Beneficial properties that fillers can give to a compound or composite are mainly:

- Increased modulus.
- Increased useful temperature range due to the higher modulus at high temperatures (increased heat distortion temperature (HDT)).
- Better dimensional stability, because of the reduced shrinkage upon crystallization, and the reduced thermal expansion.
- Reduced flammability.
- Sometimes increased toughness, in certain combinations of filler and polymer.

Fillers in polymers can also have some disadvantages, which should be reduced as much as possible:

- Increased viscosity, which makes processing more difficult.

- Usually reduced toughness, although sometimes an increase is found.
- Often increased surface roughness, transparency is usually lost and the compound can get coloured by the filler.
- Higher density, because most mineral fillers have a higher density than polymers.
- Ageing performance can be negatively affected.

1.2.2 Types of reinforcing fillers for polymers

Many of the rigid fillers used for reinforcing or stiffening of polymers, including the nano-particles described in this thesis, are of inorganic origin. However, also synthetic organic fibres are used as reinforcement. For fillers from natural origin only grinding and filtration is enough to obtain the desired particles, for synthetic fillers many different processes can be involved such as dissolving, melting, precipitation, and (in the case of fibres) spinning, heat treatments, surface treatment and chopping. There are several ways to classify the various types of filler particle, such as based on their origin (natural or synthetic), chemical composition (organic or inorganic), size (micrometers or nanometers) or based on the shape (spherical, platelet or fibre) or aspect ratio. The aspect ratio is the ratio between the longest and the shortest dimension of the particle, and is an important factor for the composite properties.

Low aspect ratio fillers (aspect ratio ≅ 1)

- Ground calcium carbonate is a very cheap filler for thermoplastics, and is used in large quantities, mostly in polyvinylchloride (PVC), polypropylene (PP) and polyamides (PA). Because of the granular structure resulting from the wet or dry grinding process it has a low aspect ratio, resulting in a limited increase in modulus of the filled polymer. Sometimes the particles are coated with fatty acids to improve dispersion [1,2].
- Precipitated calcium carbonate is a semi-synthetic filler obtained from natural calcium carbonate. The precipitation process gives much more freedom for tuning purity, crystal structure, and particle shape and size compared to grinding of natural calcium carbonate. Usually the aspect ratio is quite low, and the main application is in PVC [1,2].
- Clay, when used as a traditional filler in thermoplastics (not exfoliated such as in nanocomposites), is limited mainly to kaolinite. Usually kaolinite is used after a calcination process, which is a heat treatment at temperatures between 500 and

1000 °C that changes the crystal structure of the clay or makes it amorphous. Uncoated it is used in PVC cable insulation and coated with organo-silane it is used in polyamides [1,2].

- Silica can be produced in several synthetic ways, which all result in small, low aspect ratio (usually spherical) particles. Silica is mainly used in rubbers for enhancement of the mechanical properties, and in smaller quantities in thermoplastics [1,2].

Platelet shaped reinforcement (high aspect ratio)

- Talc seems to be a very soft material because it consists of layers that can be very easily cleaved. However, the magnesium-silicate structure within the layers is very strong and stiff. The milling process used for talc results in decreasing the size of the particles but also in delamination into moderately high aspect ratio platelets. The aspect ratio combined with the high modulus in the platelet direction is the reason that talc can give a significant increase in modulus to the compound, combined with a reduction in shrinkage. Talc is mainly used in polypropylene for increasing the modulus and is usually not coated in this application [1,2].
- Mica has a similar very stiff platelet-shaped structure as talc, and therefore it is also used to increase the modulus or reduce the shrinkage of the compound. Mica can be coated with organo-silane to obtain a better adhesion between particle and polymer. The aspect ratio and therefore the efficiency of reinforcement, depends on the milling process and the compounding step [1,2].
- Exfoliated layered silicate can be obtained from certain types of natural clay via a special dispersion process [3,4]. These particles are very thin and can give large increases in modulus due to the high aspect ratio. This type of composite will be discussed in detail in section 1.3.

Short fibre reinforcement (high aspect ratio)

- Glass fibres are used in large amounts in thermoplastics because of the property enhancement they give. Because of the high aspect ratio they can provide a large increase in modulus and strength, without affecting the toughness too much. The source for glass is of mineral origin, but the composition can be changed by mixing different components. Fibres are spun with diameters

between 5 and 20 microns, which are cut in small fragments for extrusion. The extrusion process reduces the fibre length, but if the fibres are carefully processed the aspect ratio can remain higher, improving the effectiveness of the fibre. Glass is always coated, often with organo-silane, to improve the adhesion with the matrix [5]. Glass can also be produced in the form of platelets and spherical beads.

- Carbon fibre has a much higher modulus than glass fibre while having a much lower density. It is therefore an excellent reinforcement for reaching very high modulus without sacrifices in weight, but the higher price somewhat limits the use. Carbon fibres are not of mineral origin but are based on pitch or polymer fibres (PAN), which are carbonised at high temperatures in an inert atmosphere to obtain a strong graphite structure in fibre form [5].
- Aramid fibres are synthetic polymer fibres with a very high modulus, strength and temperature resistance. Used as short fibre reinforcement they combine very high modulus with low weight at a relatively high price [5].

When the function of the filler is taken into account, it becomes clear that there is a difference between particles with low aspect ratios (approximately spherical particles) and particles with high aspect ratios (platelets and fibres). Low aspect ratio fillers are not very effective in increasing the modulus of a compound, so they are often cheap fillers used in large quantities, while large aspect ratio fillers are effective in smaller quantities and can provide large increases in the modulus at higher filler loadings.

1.3 Nanocomposites

The term nanocomposites is in the broadest sense referring to every type of material with fillers in the nanometer size range at least in one dimension. In this thesis only nanocomposites with a polymer matrix will be discussed and investigated. More specifically, these nanocomposites are polymers that are reinforced with highly anisotropic rigid inorganic particles, which have at least one dimension in the nanometer size-range.

The fillers used in polymer nanocomposites are usually inorganic fillers, although carbon nanotubes and carbon black (extensively used in rubbers) are exceptions.

Nanofillers can have different shapes:

- **Spherical** (silica, carbon black),
- **Rod** / **fibre** (synthetic whiskers, carbon nanotubes, boehmite, sepiolite)
- **Sheet** / **platelet** (layered silicates such as montmorillonite and similar synthetic structures such as synthetic mica, fluorohectorite and laponite).

The class of nanocomposites that will be used in this thesis are the exfoliated layered silicate nanocomposites with a thermoplastic polymer matrix.

1.3.1 Nanocomposites compared to traditional filled polymers

The main difference between conventional layered fillers for polymers, such as clay, mica and talc, is the particle size and the aspect ratio of the filler. In the case of conventional layered silicate fillers, the dispersed particles are relatively large aggregates of primary particles (silicate sheets). Although talc and mica can be cleaved into thin particles, there is a limit to this break-up by mechanical methods. The mechanical break-up also limits the aspect ratio of the sheets, since the particles do not only cleave between the layers, but also break up in the long direction.
The primary particles of layered minerals such as talc, mica and many types of clay (including the smectite clays) are crystalline layers of approximately one nanometer thickness. The characteristic property of layered silicate nanocomposites is the fact that these 1 nm thin silicate sheets (the primary particles) are individually dispersed in the polymer matrix [6]. To achieve this fine dispersion, mechanical forces alone are not enough; there should be a thermodynamic driving force as well to separate the layers into the primary silicate sheets [7]. This thermodynamic driving force is introduced by inserting a certain coating of surfactants on each individual layer. These surfactant molecules increase the layer distance, improve the compatibility with the polymer and can give an increase in entropy because they can mix with the polymer [8]. To enable each layer to be coated with the surfactant, the layers should be accessible for the surfactant molecules from the solution, and for this reason the clay layers need to swell of exfoliate in the solvent (usually water). For this reason natural mica and talc cannot be used: the layers in mica have collapsed in a non-swellable state and talc-sheets are not charged, so they do not swell either.
Smectite clay, such as montmorillonite, is negatively charged and swells in water, and can therefore be coated with a cationic surfactant in an aqueous suspension. The surfactant provides a hydrophobic nature to the silicate surface, which causes

the layers to precipitate as organophilic clay, also known as organoclay. The dried organoclay can be used to produce nanocomposites with several different methods, although only a limited number of combinations of surfactant and polymers will result in a good dispersion.

The additional benefits of layered silicate nanocomposites compared to the polymers filled with traditional micrometer-scale particles (besides the general benefits of filled polymers mentioned in section 1.1.1):

- Increased modulus at very low filler concentration: 5 % nanofiller can typically provide the same increase in modulus as 40 % traditional mineral filler (such as talc) or 15 % glass fibres [9].
- Lower density, because the layered silicate filler is used in much smaller quantities.
- Increased barrier properties against gas transport through the nanocomposite. The high aspect ratio of the impermeable silicate layers increase the path length for diffusion of molecules [10-12].
- Reduced rate of moisture uptake in polymers such as polyamides, because of the barrier property [10-12].
- Reduced flammability; the barrier function of the silicate layers reduces the transport of oxygen and waste-gasses and a silicate-platelet char layer forms that blocks the burning polymer from the atmosphere [13-16].
- Better surface and optical properties; due to the small particle size the surface of a nanocomposite is very smooth, and nanocomposites can be transparent because the particle size is below the wavelength of visible light [6].

Layered silicate fillers in polymers do not only have advantages, but some important disadvantages have to be taken into account:

- A reduced toughness for normally tough polymers such as polyamides can occur [17-21]. Compared to traditional filled compounds the loss of ductility might be less important.
- An increased viscosity and often a melt yield stress [22-26].

Although the raw material of the nanofillers might be very cheap, the extensive processing to change natural clay into a polymer-compatible nanofiller can increase the cost of the filler much more than the traditional fillers. However, the reduced quantities of filler can lead to a competitive price of nanocomposites [6].

1.3.2 Layered silicates

Layered silicates are natural or synthetic minerals that consist of very thin crystalline layers. The layers usually consist of a crystalline alumino- or magnesio-silicate, and the total sheet can be charged due to charge deficiencies when metal ions are exchanged for other types [9,27]. Examples of layered silicates are talc, mica and smectite clays such as montmorillonite.

The basic building blocks of layered silicates are the tetrahedral sheet (or silicate sheet) in which silicon is surrounded by 4 oxygen atoms, and the octahedral sheet (or gibbsite sheet) in which a metal such as aluminium or magnesium is surrounded by 8 oxygen atoms.

In 1:1 layered structures a tetrahedral sheet is fused with one octahedral sheet, in which the oxygen atoms are shared, an example is kaolinite.

In 2:1 layered silicates two tetrahedral layers surround one octahedral layer, and the oxygen atoms are shared, an example is montmorillonite.

The basic 2:1 structure with silicon in the tetrahedral sheets and aluminium in the octahedral sheet without any substitution of atoms is known as pyrophyllite ($Al_2Si_4O_{10}(OH)_2$), in which the layers are held together by weak Van der Waals forces. The layers cannot be expanded in water due to the lack of charge, so pyrophyllite has only an external surface area and essentially no cation exchange capacity (CEC).

Talc ($Mg_3Si_4O_{10}(OH)_2$) has the same structure as pyrophyllite, but with magnesium instead of aluminium in the octahedral layer. Talc is also a non-swellable mineral, which is very soft because the layers are very weakly bound together. Because talc has no charged layers, the sheets are only bound by weak Van der Waals forces and is has no CEC.

When a part if the silicon in the tetrahedral sheet is substituted by aluminium, the structure is called mica (muscovite, one form of mica: $(K)Al_2(AlSi_3O_{10})(F,OH)_2$). Due to the substitution of some Si by Al, the mineral has a large amount of excess negative charge, which is balanced by interlayer potassium cations. Because the size of the potassium ions matches with the hexagonal hole created by the Si/Al tetrahedral layer, it is able to fit tightly between the layers. Consequently, the interlayers are collapsed and the 2:1 layers are held tightly together by the electrostatic attraction between the negatively charged tetrahedral layer and the potassium cations. Since the layers have collapsed upon the interlayer potassium

ions, micas are non-swellable in water and have no internal surface area to give them a CEC.

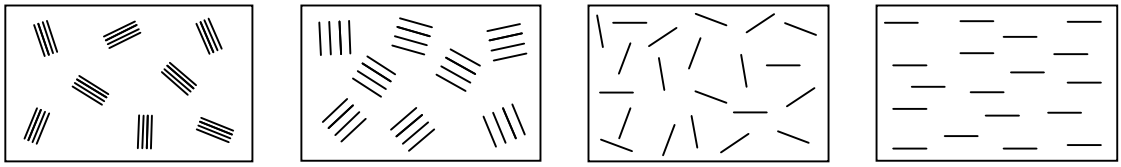
The structure of montmorillonite ($(Na,Ca)_{0.33}(Al, Mg)_2(Si_4O_{10})(OH)_2 - nH_2O$) is derived from the original pyrophyllite structure by partial substitution of the trivalent Al-cation in the octahedral layer by the divalent Mg-cation. Because of the difference in charge between the Al and Mg ions the centre layer of the 2:1 silicate is negatively charged, and the negative charge is balanced by sodium and/or calcium ions between the 2:1 sheets. These ions do not fit in the tetrahedral layer such as in mica and the negative charge is located in the octahedral layer, thus making the attractive forces between the layers weaker. Therefore, the layers are not collapsed upon each other such as in mica. Montmorillonite can absorb water between the charged layers because of this weak binding and the large spacing and it is therefore member of a group of water-expandable clay minerals known as smectites or smectite clays. Because of the water-swellable nature, the surface of montmorillonite is easily accessible for surface ion-exchange reactions and therefore it is the most widely used natural clay in nanocomposites. A characteristic number of these types of clay is the cation exchange capacity (CEC), which is a number for the amount of cations between the surfaces. The CEC of montmorillonite can range from 80 to 120 meq/100g (milli-equivalents per 100 grams).

Synthetic fluorine mica is a water-swellable layered silicate synthesised by heating talc and Na_2SiF_6 for several hours at high temperature [28,29]. If this same reaction is done with K_2SiF_6 instead of Na_2SiF_6, non-swellable fluorine mica is obtained. The structure of synthetic mica is $(Na)Mg_3(Si_4)O_{10}F_2$ or $(Na)Mg_3(AlSi_3)O_{10}F_2$ (with K instead of Na for the non-swellable variety). Since the water-swellable synthetic mica has a charge deficiency and therefore a CEC (70-80 meq/100g), they can be used for ion exchange reactions with organophilic surfactants for use in polymer nanocomposites.

Sepiolite ($Mg_4Si_6O_{15}(OH)_2 - 6H_2O$) has a rod- or fibre-like shape instead of a sheets form. The rods are porous, consisting of narrow but long 2:1 silicate layers joined together at the corners, with open channels in between. These open channels are usually filled with water, but at high temperatures the water can be expelled. Sepiolite has a small CEC, so it can be ion exchanged with a small amount of organic cationic surfactant.

1.3.3 Layered silicate as reinforcement

Montmorillonite is the most used type of layered silicate in polymer nanocomposites because of the swellable layered structure. However, the charged nature of the silicate sheets in the clay makes the silicate sheets incompatible with hydrophobic polymers. Therefore, unmodified montmorillonite will not swell when mixed with a hydrophobic polymer and the sheets will stay together in thick stacks with low aspect ratio, as is schematically shown in figure 1.1 a.



a: Non-exfoliated clay composite

b: Intercalated nanocomposite

c: Exfoliated nanocomposite

d: Aligned exfoliated nanocomposite

Figure 1.1: Different levels of dispersion in layered silicate nanocomposites.

The incompatibility can be reduced by exchanging the sodium and calcium ions between the layers with cationic organic surfactants (see figure 1.2).

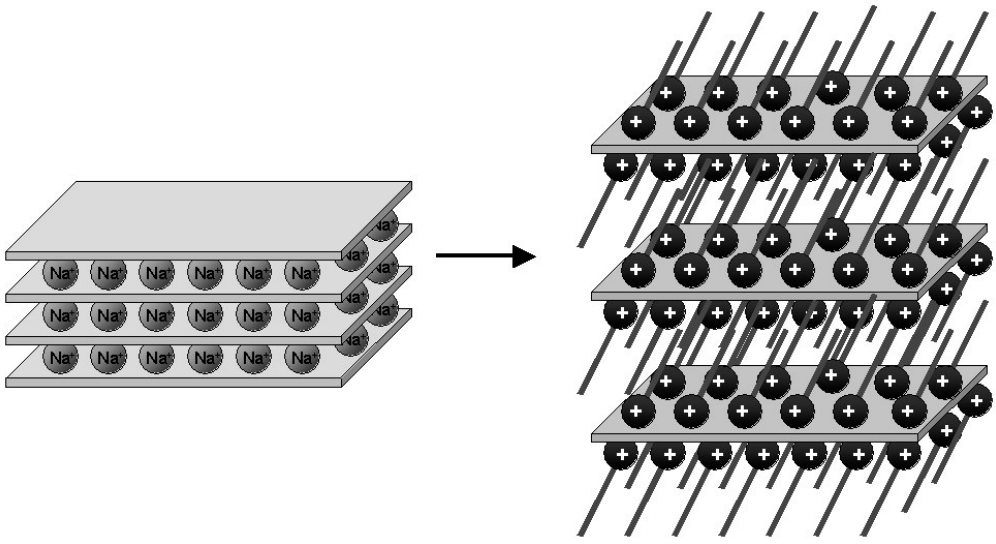


Figure 1.2: Ion exchange with cationic surfactant.

In the swollen or exfoliated state, when all the sheets are individually dispersed in water, the counter ions are accessible and can be exchanged with other cations. Organic surfactant molecules, usually containing a hydrocarbon chain with a length between 10 and 20 carbon atoms, provide a more hydrophobic surface. In addition, due to the larger size compared to the sodium ions the distance between the sheets

increases and therefore the force holding them together decreases. The layered silicate with the organic surfactant between the layers is known as an organoclay or an organically modified layered silicate (figure 1.2). The improved compatibility with the polymer allows polymer molecules to diffuse between the silicate layers and to mix with the surfactant molecules, further increasing the distance between the sheets. This process is known as intercalation. In an intercalated nanocomposite the silicate layers remain at a fixed distance from each other as can be seen in figure 1.1 b. The fixed but increased distance shows up in wide-angle x-ray scattering (WAXS) as a distinct peak, shifted to lower angles compared to the non-intercalated clay.

When the layers completely separate from each other, this is known as the exfoliated state, shown in figure 1.1 c. In the exfoliated state the silicate layers have no fixed distance and therefore the peak corresponding to the layer distance in the WAXS spectrum disappears. The disappearance of the layer distance peak is often used as proof of a well-exfoliated nanocomposite [30].

The complete exfoliation results in special properties for nanocomposites, because the surface in contact with the polymer will be very large (600-800 m^2 per gram of silicate) [11] and the aspect ratio of the primary particles will be very high. The exfoliated particles can be locally ordered at higher particle concentrations in the same way as discotic liquid crystals [31] and the particles can become macroscopically aligned when the polymer in which they are dispersed experiences a flow field [32], leading to oriented structures as shown in figure 1.1 d.

Several methods can be used to produce nanocomposites from layered silicates in polymers [6,30]:

- **In situ polymerization:** Organically modified silicate is swollen in a monomer and the polymerization reaction takes place in the mixture. The growing polymer chains can push the layers apart leading to an exfoliated structure. Instead of a linear polymerization, also in situ crosslinking can be used. In this case, the modified silicate is swollen in one of the reactants, or in the mixture, and the reaction takes place to form a crosslinked network, either rubbery or glassy depending on the glass transition temperature of the network.
- **Melt mixing:** An organoclay is mixed with a thermoplastic polymer in a mixer, usually a co-rotating twin-screw extruder, where high shear forces help the dispersion of the particles in the polymer.
- **Solution mixing:** A polymer is dissolved in a solvent in which the organoclay exfoliates, and after mixing the solvent is evaporated.

The first nanocomposites based on PA6 were made by in-situ polymerization of ε-caprolactam in the presence of swollen organically modified montmorillonite clay. The silicate sheets are forced apart by the polymer chains growing between the layers, forming an exfoliated PA6 nanocomposite [4,33]. Soon after this method based on intercalation by monomers, the direct melt intercalation route for polymer nanocomposites was developed [34]. The melt mixing and exfoliation route has been shown to be just as effective for the production of polyamide nanocomposites as the in-situ polymerization of PA6 [9,18,35]. In the case of melt-intercalation a standard PA6 grade is mixed in a co-rotating twin-screw extruder with organically modified clay.

There are many other systems reported in literature, usually made by melt-blending of a polymer with modified clay or by in-situ polymerization or crosslinking. Some examples of other thermoplastic polymers that have been used as matrix for nanocomposites are: maleic anhydride modified polypropylene (MA-PP) [36], MA-polyethylene [37], polyamide-12 [24,38,39], polyamide 66 [15,40-43], poly (ε-caprolactone) [23,44], poly (vinyl alcohol) [45], polyetherimide [46], styrene-acrylonitrile copolymer (SAN) [47] and polystyrene [48]. Some examples of nanocomposites based on crosslinked elastomers are those based on MA-ethylene-propylene rubber [37], polystyrene-polyisoprene copolymer [49], polyurethane [50,51], elastomeric epoxy [52,53] and poly (dimethylsiloxane) [54]. In addition, an extensive amount of literature has been published about nanocomposites based on crosslinked glassy epoxy resin [55-61].

1.3.4 Properties of layered silicate nanocomposites

Due to the nanometer-scale dimensions and the high aspect ratios of exfoliated silicate layers, nanocomposites show different properties than traditional filled polymers. The high aspect ratio of exfoliated layered silicate fillers results in a more effective modulus increase and the small dimensions of the particles leads to much larger interfacial areas than in traditional microcomposites. The amount of polymer at an interface is much higher: in nanocomposites a significant fraction of the polymer can be considered to be at an interface, in contrast to microcomposites. The larger amount of interfacial polymer can have various effects, such as increased viscosity [23,25], different crystallization behaviour [62,63] and altered polymer dynamics [8,64,65]. The large surface area and large aspect ratio of the silicate layers creates a two-dimensional confined environment for the polymers chains, and on a larger

scale the possibility of local or global ordering of the silicate sheets can create variations in many properties.

Influence of the production method on exfoliation

The modulus of a nanocomposite depends on the aspect ratio of the dispersed particles. The primary silicate sheets are very thin (around 1 nm) and wide, but the aspect ratio of the particles present in the nanocomposite is strongly dependent on the degree of exfoliation, which is influenced by the production method.

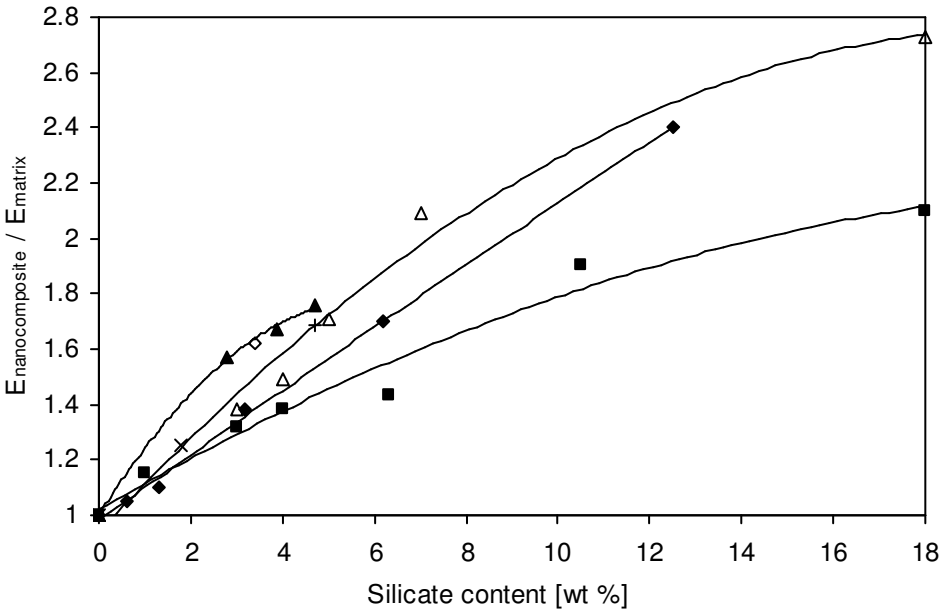


Figure 1.3: Relative modulus for various polyamide-6 nanocomposites
(◆ [35], ◇ [35], ■ [18] , × [66], ▲ [67], + [3])

Several literature data for the tensile moduli of PA6 nanocomposites are collected in figure 1.3, and it can be seen in these results that the increase in modulus is approximately 100% at 10 wt% silicate. Only a small number of results are published about nanocomposites with a silicate content higher than 12 wt% and the results suggest that there is a reduction in modulus-increase above 12 wt%. The results also show that there is no fundamental difference between the modulus increase between the different production methods; for PA6 similar results can be achieved with melt mixing as with in-situ polymerization.

Influence of the organic surfactant on exfoliation

The type of modification used in most organically modified layered silicates is the ion exchange with ammonium-based cationic surfactants. In figure 1.4 the most commonly used types of quaternary ammonium ion surfactants are displayed. The ammonium ions (N^+) can contain one aliphatic chain, as in examples A and C, or two as in example B. The other places can be occupied by methyl groups as shown in 1.4.A or by hydroxyethyl groups as shown in 1.4.C, which results in a more bulky and hydrophilic ammonium group. In many cases the chains consist of (hydrogenated) tallow, which has approximately 65% C-18, 30% C-16 and 5% C-14 [68] or coco oil, which has mainly chain sizes between C 12 and C 16 [69].

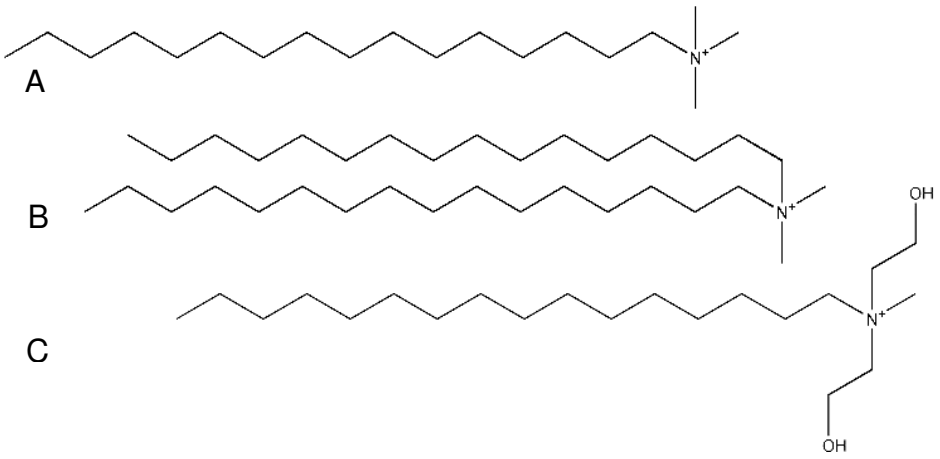


Figure 1.4: Examples of surface modifiers for charged layered silicate nanofillers.

Most organic modifiers used on the layered silicates have one aliphatic chain, and the length of this chain has an influence on the exfoliation and the mechanical properties. The influence of the chain length on the modulus of PP nanocomposites has been investigated [70]. The results showed a dramatic improvement when the chain length reaches 12 C-atoms, with an optimum in the chain length around 16 C-atoms for this system. Identical measurements were done on epoxy nanocomposites [60], which showed that C4 and C6 chains are very ineffective. A big improvement in modulus could be seen in C8 chains, and longer chains showed a small decrease. While the tensile modulus increased a lot with C8 and longer chains, the tensile strength decreased however, which is a trade-off in properties that is often seen in nanocomposites.

A certain minimum chain length is necessary because a longer chain increases the interlayer distance and reduces the bonding strength between the layers, enabling the polymer chain to intercalate [8]. In addition, the longer chains increase the gain in

entropy of mixing when the surfactant chains mix with the polymer, which is the thermodynamic driving force for exfoliation, compensating the loss of conformational freedom of the confined polymer chains [8,71].

Besides the chain length, also the amount of chains (usually one or two), the presence of double bonds in the chains, and the other groups on the ammonium ion are important. The combination of groups determines the amount of hydrophobic or hydrophilic behaviour of the clay and as a result of this the interaction with the polymer. Research on the influence of the chain length on the properties of PA6 nanocomposites has shown that a chain length of approximately C18 is optimal [67]. However, the difference in modulus compared to C12 and C22 surfactant chains is not very high. Therefore, it is clear that the commercially available modified silicates containing chains based on tallow or coco-oil are in the optimal range. Several papers have been published on the influence of the other surfactant architecture parameters, besides in the chain length, on the exfoliation behaviour and the mechanical properties of PA6. The results show without exception that surfactants with one long alkyl chain on the ammonium group lead to better exfoliation and a higher modulus than surfactants with two chains or zero chains [17,21,67]. The chains based on natural products such as tallow can be used in the natural, partially unsaturated state or can be hydrolysed to decrease the amount of double bonds, but it has been shown that hydrolysation has a slight disadvantage for the exfoliation properties in melt-compounded nanocomposites [67]. Replacing two of the three methyl groups on a quaternary ammonium surfactant by more hydrophilic hydroxyl-ethyl groups has also a negative effect on the modulus, as well as surfactant over-saturation of the silicate (addition of more surfactant than the CEC allows to bind) [67]. No significant difference on the exfoliation and mechanical properties has been found between quaternary ammonium ions and tertiary ammonium ions (where one methyl group is replaced by hydrogen) in surfactants with one long chain. It is important to realize when comparing the influence of the surfactant architecture, that the factors that improve the amount of exfoliation and increase the modulus, usually decrease the maximum elongation; usually a trade-off between modulus and elongation was observed [67].

Thermal stability of the surfactant groups can be influenced by the amount of chains and the other side groups on the ammonium ion: surfactants with more than one long chain and with hydroxyl-ethyl groups instead of methyl groups are less stable at higher temperatures than surfactants with one chain [72,73].

Edge modification

While the surface area of the smectite type of layered silicate is negatively charged and can therefore be covered with cationic surfactants, the edges of the plates usually have a different charge. The edges are charged because of the presence of broken bonds at the crystal edges. The surface properties depend greatly on the exposed atoms that may act as electron donors or acceptors. In acid solutions the net charge of the broken-bond surface is positive and the positive charge increases with decreasing pH. In this process protons occupy positions near oxygen atoms. In alkaline solution the net charge of the broken-bond surface is negative. The negative charge is increasing with increasing pH. In the latter case hydroxyl groups occupy positions near protons or metallic cations. Because of the relatively small edge area, a small amount of anions can modify the edges of the clay platelets [74]. This small amount of surface modification at the edges leaves most of the surface area uncovered and can therefore not provide the same thermodynamic driving force for exfoliation as the surface modification can. However, it can help in preventing edge-to-face interactions in solution or in the melt, and it could influence the rheological behaviour this way.

1.4 Thermoplastic continuous fibre composites

The type of thermoplastic fibre composites described in this section is fundamentally different from the short fibre reinforced polymers, which are described in section 1.1. Continuous fibre composites have fibres that run through the entire sample or object, and the orientation of the fibres is not random. The fibre orientation is usually either unidirectional or in the form of 0°/90° woven fibre fabric, but it can be optimized for the best properties in the desired directions. The volume fraction of fibres is usually maximised to achieve the ultimate composite properties, and can be up to 70 volume% in unidirectional composites or 50 volume% in woven fibre composites. This type of thermoplastic fibre composite should therefore be seen as the thermoplastic replacement for crosslinked epoxy or polyester based composites, which are often used in aerospace applications, boats, high performance cars, sport equipment and other applications where high strength combined with low weight are important. Because of the continuous fibre architecture, traditional thermoplastic processing techniques such as extrusion and injection moulding are impossible, and

new forming techniques derived from thermoset composite or sheet-metal forming have been developed [75,76].

Thermoplastic matrix polymers can have several important advantages over thermoset resins for fibre composites in mechanical properties, production methods, and environmental and economical issues. During the past two decades the development of these thermoplastic composites was driven by different factors: the development was initially focussed on the potential advances in mechanical properties, followed by a focus on the advantages found in the new production methods.

The driving force for the first thermoplastic composites around 1980 was the improvement of properties that where difficult to achieve with thermoset resins and epoxy in particular, such as better toughness and impact resistance [75]. By variation of the composition of the epoxy system many properties can be changed, but usually an improvement of one (for example toughness) results in a decrease of another (such as modulus). For this reason, carbon fibre composites with a poly-ether-ether-ketone matrix (PEEK) were developed [76]. PEEK is a semi-crystalline polymer that combines very good toughness, high temperature resistance and high solvent resistance. PEEK is by far the most studied thermoplastic polymer for high performance composites and is mainly used in military aircraft structures. However, the use of this composite is limited because of the high price of the polymer and very high processing temperatures (~ 400 °C). For this reason many composites based on other polymers in combination with several types of fibres (mainly glass and carbon fibres) have been developed, resulting in composite materials that are cheaper and easier to process. With the development of these new thermoplastic composites also other properties besides mechanical properties received more attention: especially the processing possibilities. These new materials could lead to rapid production processes and in this way continuous fibre composites could be used in markets where thermoset composites would be too expensive in production.

Some important differences between thermoset and thermoplastic matrices can be found in:

- **Polymer structure**

Thermoset resins are usually build up from 2 components, reacting together to form an amorphous crosslinked network which is rigid (glassy) at temperatures below the glass transition temperature (T_g), and rubbery above the T_g.

Thermoplastic polymers have usually high molecular weight linear polymer chains, which are not chemically linked to each other as in thermosets. Depending on the flexibility of the chain, the side-groups and the stereo-regularity of the polymer can form an amorphous or semi-crystalline structure. Amorphous polymers below T_g derive their properties from the entanglements formed by the long chains. These entanglements act as temporary crosslinks, giving strength to the matrix. Semi-crystalline polymers have besides amorphous regions also crystalline regions containing densely packed chains, which increase the modulus even above T_g of the amorphous regions.

- **Solvent/moisture resistance**

Thermoset polymers such as epoxy-resins are usually very resistant to solvents, because of the densely crosslinked network. For thermoplastics there is an inherent difference between semi-crystalline and amorphous polymers. Semi-crystalline polymers are more resistant to solvents because the densely packed crystalline areas generally have good solvent resistance and form a barrier shielding the amorphous areas. Amorphous thermoplastics can suffer from swelling or brittleness induced by contact with organic fluids (solvent-crazing), although the sensitivity is highly dependent on the chain architecture.

- **Mechanical properties**

The temperature dependence of the modulus of thermosets and amorphous thermoplastics is similar: the modulus remains more or less at the same level up to the glass transition temperature (T_g), and drops a few decades to a rubber-level (several MPa) above T_g. The difference above T_g is more pronounced, because crosslinked polymers above T_g behave as crosslinked rubbers, while amorphous thermoplastics can flow relatively easily above the T_g. Semi-crystalline thermoplastics have a different behaviour: the modulus drops a bit at T_g, but stays at a useful level (GPa-level instead of MPa-level) due to the crystals up to the melting point of the crystalline regions. The amount of modulus reduction above T_g is dependent on the ratio of amorphous and crystalline regions.

The toughness of thermoset polymers below T_g is not very high because the polymer cannot flow due to the crosslinks. This limits the possibilities for deformation and therefore the energy-dissipating capabilities, which usually leads to relatively brittle fracture behaviour with low maximum strains. Thermoplastic polymers can have some more possibilities for deformation, because chains can slide over each other and crystal structures can deform. There is however a big difference between

different polymers: toughness depends on many parameters such as the exact chain structure, chain length, entanglement density, crystal structure, strain rate and temperature. Creep can be more pronounced in thermoplastic polymers because they lack the dense network of chemical crosslinks that thermoset resins have.

- **Adhesion**

The adhesion between thermoplastic polymers and fibres can be different then with thermoset resins, and often different fibre coatings are necessary to provide good adhesion. Thermoset resins usually give excellent adhesion because the reactive groups on the polymer can chemically bind with the fibre sizing, whereas thermoplastic polymers have usually less reactive sites.

- **Viscosity**

Thermoplastic polymers have a much higher viscosity than the precursor resins for thermoset polymers, because the polymer has already been completely formed into a high molecular weight linear chain. While thermoset resin provide excellent wet-out of the fibres, this process is much more difficult in the case of thermoplastic polymers. Several solutions to solve the viscosity problem are the use of low molecular weight precursors, solvents, high temperatures and pressures, and the reduction of the flow distance for the polymer.

- **Processing properties**

There are big differences in processing possibilities between thermosets and thermoplastic polymers and both have their advantages and disadvantages.
The advantages in the processing of thermoplastic polymers compared to thermosets are mainly associated with the fact that thermosets should still undergo a crosslinking reaction to obtain a polymer structure.

Problems with crosslinking reactions in thermosets are:

1. It takes a lot of time to obtain a good curing reaction, and elevated temperatures are often necessary during the long curing process.
2. The shelf life of the resin components is limited, and when the two components are mixed very limited. Pre-impregnated composites (pre-pregs) need refrigeration to slow down the curing reactions.
3. The chemicals involved in the reactions are usually harmful for the environment and the people working with them, and when not using closed mould techniques

such as vacuum-assisted resin infusion (VARI) and resin transfer moulding (RTM) harmful emissions of volatile compounds occur.

Thermoplastic polymers as matrix material for fibre composites can improve these issues, because:

1. Fast processing of products is possible because a pre-fabricated sheet of composite material can be used and the heating, shaping, and cooling steps can be done very fast. The polymer impregnation of the fibres to produce the pre-fabricated composite sheets can be done in a previous step, and this step is also fast, because this also only requires melting, fibre impregnation, and cooling.
   These two steps of impregnation of the fibres and shaping of the product can be easily separated in time and place, which is more difficult for thermoset composites.
2. The shelf life of thermoplastic polymers is almost unlimited, and the same applies to the pre-impregnated composite sheets.
3. Emissions of volatile and toxic substances are eliminated, because the polymerization process is already complete and therefore no volatile compounds are involved in the processing. However, this is not the case if it is necessary to dissolve the polymer before impregnation, although even then only the impregnation step has solvents involved, the shaping step of the composite part is also emission-free.

The main disadvantage of thermoplastic polymers with respect to the processing properties is the much higher viscosity. This makes impregnation of the fibre bundles more difficult, and it makes typical thermoset processes such as VARI and RTM of complex shapes with high fibre fractions impossible. Therefore, for thermoplastic polymers new ways of processing had to be developed, both for the fibre-impregnation step and for the shaping of the products. These new ways of processing also have their benefits, because the fibre impregnation step and the product-formation step can easily be separated. This makes the use of pre-impregnated sheets as half product very easy, and the shaping step into products very fast and therefore potentially cheaper for larger volumes. In the fibre impregnation step the flow-distance for the polymer melt is usually reduced as much as possible by bringing the polymer and fibres very close together before or during melting. This close contact can be achieved by stacking alternating layers of fibres and polymer film, by impregnation of the fibres with a powdered polymer or by co-mingling of polymer fibres with reinforcing fibres. The fibre impregnation can be done under pressure in a press or (for unidirectional composites) in a pultrusion machine.

1.5 Fibre composites with nanocomposite matrix

1.5.1 The concept of a three phase composite

The length scales of microcomposites, such as glass and carbon fibre composites, and nanocomposites are so different that the two can be combined. On the scale of the fibres the nanofiller particles are still very small; for example, the thickness of an exfoliated silicate sheet is 10000 times smaller that the diameter of an average glass fibre. In figure 1.5 a schematic drawing shows how this concept would look. The fibres are long, continuous fibres and the particles fit between them without reducing the fibre volume fraction. In this three phase composite it is not the goal to replace any of the fibres with nanofillers, the goal is still to use a high volume fraction of fibres as the main reinforcement.

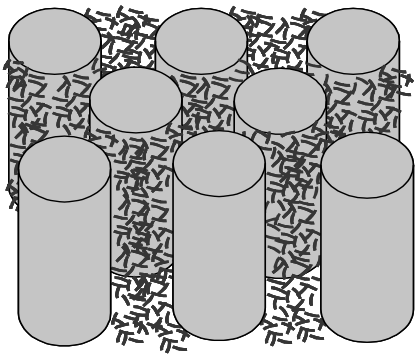


Figure 1.5: Nano-particle reinforcement of the matrix in a fibre composite

The nanoparticles that are present in the matrix polymer are only intended to improve the matrix-dominated properties of the fibre composite. The modulus and the tensile strength of the fibre composite is mainly determined by the fibres, and therefore the increased modulus of the matrix is not expected to provide any significant increase in the modulus of the entire fibre-composite.

The most important improvement that the nanocomposite matrix could provide is an increase in the compressive and flexural strength of the fibre composite. The compressive strength, and therefore also the flexural strength of a continuous fibre composite, depends on the modulus of the matrix [77-85]. Because the modulus of the composite matrix increases with the addition of nanofillers, the compressive and flexural strength of the composite are expected to increase in such a three-phase composite.

1.5.2 Previous research in this field

It appears that not much research has been done on the combination of fibres and nano-fillers in polymers, in view of the limited amount of literature published on this subject. Four different systems were found in the literature, of which three contain continuous fibres in combination with a nanocomposite matrix.
Of the four different systems that have been described, one was made with PA6 nanocomposites in combination with short glass- and carbon fibres [9,86], two with continuous carbon fibre reinforced epoxy in which the epoxy was filled with montmorillonite [87,88] or silicon-carbide whiskers [89] and one with continuous carbon fibre reinforced polyimide nanocomposite [90].

PA6 / montmorillonite nanocomposite with short glass fibres

When a combination of discontinuous fibres and exfoliated layered silicate is used, they both have a similar effect on the modulus. Short fibres (shorter than 1 mm), "long" fibres (LFT) (length of several mm) and exfoliated layered silicates all increase the modulus of the composite. Layered silicate in typical concentrations of 5 wt% can replace almost 40 wt% of low aspect ratio mineral filler or 15 wt% short glass fibres [9]. In a combination of short fibres and layered silicate 4 wt% layered silicate can add approximately 2 GPa to short glass fibre reinforced composites, both in wet and dry conditions, independent of the fibre content [9]. The layered silicate can therefore reduce the amount of glass fibres, or replace larger amounts of low aspect ratio mineral fillers, reducing the density of the compound. However, the increased impact strength that short fibres can give to PA6 composites is reduced by the use of a nanocomposite matrix [9].

Epoxy resin / silicon-carbide whiskers nanocomposite with carbon fibres

The use of silicon-carbide (SiC) whiskers was intended to improve the matrix-dominated properties of high performance continuous fibre composites [89]. The modulus increase of the epoxy resin was approximately 20 % with addition of 10 volume % SiC whiskers in the dry state, and 50% in hot/wet conditions. When 15 volume% SiC was added an increase in fracture energy of the epoxy matrix was found, and the transverse strength of the unidirectional composite increased. However, the three-phase composite showed a slightly reduced compressive strength and a strongly reduced tensile strength compared to the control composite without SiC particles. This unexpected behaviour was caused by the fact that the

carbon fibres were damaged in the resin impregnation process by the very hard and sharp SiC particles, which could be seen in SEM pictures [89].

Epoxy resin / montmorillonte nanocomposite with carbon fibres

In the articles about carbon fibre / epoxy composites with montmorillonite filled matrix [87,88] several natural montmorillonite clays with different surfactants were used, mixed with and without the help of a solvent. The resulting nanocomposite matrices showed slightly increased storage moduli in the glassy state up to 20%, but the fracture toughness and the failure strain were somewhat reduced. The impregnation of the carbon fibre bundles with the nanocomposite resins was more difficult than with the unfilled epoxy resin, because of the much higher viscosity. No improvement in flexural strength of the fibre composites was found with nanofillers [88].

Polyimide nanocomposite with carbon fibres

Research at NASA on nanocomposites for fibre composites was based on the resin PMR-15, which is a highly crosslinked high-temperature resistant thermosetting polyimide [90]. The addition of exfoliated layered silicate reduced oxidation during ageing at high temperatures and reduced matrix cracking. The nanocomposite matrix was reported to increase the flexural strength, flexural modulus and interlaminar shear strength by up to 30 %.

1.6 Outline of the thesis

In this thesis several aspects of nanocomposites, thermoplastic fibre composites and a combination of these two types of composite will be discussed.

In chapter 2 the influence of the type and concentration of layered silicate and the moisture content on the modulus, the strength and the maximum elongation of PA6 nanocomposites is measured and discussed. In addition, the speed of moisture uptake for various concentrations of silicate is measured and the diffusion coefficient is calculated. From the ratio of diffusion coefficients an estimate for the aspect ratio of the particles is calculated. The aspect ratio of the exfoliated particles is a very important factor that determines the moisture transport rate (chapter 2), the elastic modulus (chapter 3) and the melt rheology of the nanocomposites (chapter 5).

In chapter 3 the modulus of nanocomposites with different concentrations of layered silicate at three different moisture levels is used to calculate the aspect ratio of the particles with a mechanical composite model (Halpin-Tsai [91,92]). To be able to

make the correct calculations, the crystallinities of the various nanocomposites are measured, as well as the orientation of the silicate platelets and the crystals in the injection moulded samples. With the crystallinity and the measured influence of the moisture level the matrix modulus for each nanocomposite is calculated, which is used to calculate the aspect ratio of the reinforcing particles.

In chapter 4 the modulus, strength and elongation of various concentrations of layered silicate in PA6 is measured at different temperatures. Both a low and a high molecular weight PA6 matrix material are used to investigate the influence of the MW on the mechanical properties. Besides nanocomposites based on organically modified layered silicate, also one concentration in both PA6 matrices is made with the same silicate without the organic surfactant. A new extrusion process is used to improve the exfoliation with this unmodified silicate and the effect on the mechanical properties is measured. In addition, a PA66 matrix polymer is used to investigate the properties of nanocomposites based on this polymer, and all these melt-mixed nanocomposites are compared with commercial nanocomposites produced by in-situ polymerization. Brittle to ductile transition temperatures were determined and compared between the various types of nanocomposite.

In chapter 5 the influence of various silicate concentrations in PA6 on the viscosity and the modulus is measured. A comparison is made between nanocomposites based on organically modified silicate and un-modified silicate with respect to these properties. In addition, the viscosity and modulus is measured for a range of particle shapes and sizes, both in the nanometer and the micrometer range. The goal of this chapter is to understand which particle size, shape, concentration and modification can provide the best compromise of high modulus without influencing the melt behaviour too much.

In chapter 6 the creep and physical ageing behaviour of PA6 nanocomposites is investigated. Nanocomposites with different concentrations of organically modified silicate are compared with a commercial nanocomposite and one based on unmodified silicate.

In chapter 7 the adhesion between various nanocomposites and glass fibres is measured using a single fibre fragmentation test. The influence of the fibre type, the silicate content, the silicate modification and the moisture level in the matrix is measured.

In chapter 8 the influence of the silicate level, the silicate modification, the moisture level and the temperature on the flexural strength of continuous fibre composites is measured. The composites are based on glass and carbon fibres and have matrices of unfilled PA6 and PA6 nanocomposites.

In chapter 9 the main conclusions from this research are summarised and an outlook is given regarding possible future research on this subject.

1.7 References

1. Rothon R. Particulate-filled polymer composites: Longman; 1995.
2. Rothon RN. Mineral Fillers in Thermoplastics: Filler Manufacture and Characterisation. Advances in Polymer Science 1999;139:67-104.
3. Kojima Y, Usuki A, Kawasumi M, Okada A, Fukushima Y, Kurauchi T, Kamigaito O. Mechanical-Properties of Nylon 6-Clay Hybrid. Journal of Materials Research 1993;8(5):1185-1189.
4. Usuki A, Kojima Y, Kawasumi M, Okada A, Fukushima Y, Kurauchi T, Kamigaito O. Synthesis of Nylon 6-Clay Hybrid. Journal of Materials Research 1993;8(5):1179-1184.
5. Hull D, Clyne TW. An Introduction to Composite Materials. Cambridge; 1996.
6. Giannelis EP. Polymer layered silicate nanocomposites. Advanced Materials 1996;8(1):29.
7. Manias E, Chen H, Krishnamoorti R, Genzer J, Kramer EJ, Giannelis EP. Intercalation kinetics of long polymers in 2 nm confinements. Macromolecules 2000;33(21):7955-7966.
8. Giannelis EP, Krishnamoorti R, Manias E. Polymer-silicate nanocomposites: Model systems for confined polymers and polymer brushes. Advances in Polymer Science 1999;138:107-147.
9. Akkapeddi MK. Glass fiber reinforced polyamide-6 nanocomposites. Polymer Composites 2000;21(4):576-585.
10. Kojima Y, Usuki A, Kawasumi M, Okada A, Kurauchi T, Kamigaito O. Sorption of Water in Nylon-6 Clay Hybrid. Journal of Applied Polymer Science 1993;49(7):1259-1264.
11. LeBaron PC, Wang Z, Pinnavaia TJ. Polymer-layered silicate nanocomposites: an overview. Applied Clay Science 1999;15(1-2):11-29.
12. Murase S, Inoue A, Miyashita Y, Kimura N, Nishio Y. Structural characteristics and moisture sorption behavior of nylon-6/clay hybrid films. Journal of Polymer Science Part B-Polymer Physics 2002;40(6):479-487.
13. Kashiwagi T, Harris RH, Zhang X, Briber RM, Cipriano BH, Raghavan SR, Awad WH, Shields JR. Flame retardant mechanism of polyamide 6-clay nanocomposites. Polymer 2004;45(3):881-891.
14. Morgan AB, Gilman JW, Nyden M, Jackson CL. New approaches to the development of fire-safe materials. Gaithersburg, MD: NIST, National Institute of Standards and Technology; 2000. Report nr NISTIR 6465.
15. Qin HL, Su QS, Zhang SM, Zhao B, Yang MS. Thermal stability and flammability of polyamide 66/montmorillonite nanocomposltes. Polymer 2003;44(24):7533-7538.
16. Flammability of polymer-clay nanocompositesMorgan AB, Gilman JW, Kashiwagi T, Jackson CL. Flammability of polymer-clay nanocomposites. NIST, National Institute of Standards and Technology; 2000.
17. Dennis HR, Hunter DL, Chang D, Kim S, White JL, Cho JW, Paul DR. Effect of melt processing conditions on the extent of exfoliation in organoclay-based nanocomposites. Polymer 2001;42(23):9513-9522.
18. Liu L, Qi Z, Zhu X. Studies on Nylon 6/Clay Nanocomposites by Melt-intercalation Process. Journal of Applied Polymer Science 1999;71:1133-1138.
19. Usuki A, Koiwai A, Kojima Y, Kawasumi M, Okada A, Kurauchi T, Kamigaito O. Interaction of Nylon-6 Clay Surface and Mechanical-Properties of Nylon-6 Clay Hybrid. Journal of Applied Polymer Science 1995;55(1):119-123.
20. Fornes TD, Yoon PJ, Keskkula H, Paul DR. Nylon 6 nanocomposites: the effect of matrix molecular weight. Polymer 2001;42(25):9929-9940.

21. Fornes TD, Hunter D, Paul DR. Nylon-6 Nanocomposites from Alkylammonium-Modified Clay: The Role of Alkyl Tails on Exfoliation. Macromolecules 2003.
22. Lim YT, Park OO. Rheological evidence for the microstructure of intercalated polymer/layered silicate nanocomposites. Macromolecular Rapid Communications 2000;21(5):231-235.
23. Krishnamoorti R, Giannelis EP. Rheology of end-tethered polymer layered silicate nanocomposites. Macromolecules 1997;30(14):4097-4102.
24. Hoffmann B, Kressler J, Stoppelmann G, Friedrich C, Kim GM. Rheology of nanocomposites based on layered silicates and polyamide-12. Colloid and Polymer Science 2000;278(7):629-636.
25. Krishnamoorti R, Yurekli K. Rheology of polymer layered silicate nanocomposites. Current Opinion in Colloid & Interface Science 2001;6(5-6):464-470.
26. Solomon MJ. Rheology of Polypropylene/Clay Hybrid Materials. Macromolecules 2001;34:1864-1872.
27. Brindley GW, Brown G. Crystal Structures of Clay Minerals and their X-ray Indentication: Mineralogical Society; 1980.
28. Breu J, Seidl W, Stoll AJ, Lange KG, Probst TU. Charge homogeneity in synthetic fluorohectorite. Chemistry of Materials 2001;13(11):4213-4220.
29. Tateyama H, Tsunematu K, Noma H, Adachi Y, Takeuchi H, Kohyama N. Formation of expandable mica from talc using the intercalation procedure. Journal of the American Ceramic Society 1996;79(12):3321-3324.
30. Pinnavaia T, Beall G. Polymer-Clay Nanocomposites: John Wiley & Sons Ltd; 2001.
31. Balazs AC, Singh C, Zhulina E, Lyatskaya Y. Modeling the phase behavior of polymer/clay nanocomposites. Accounts of Chemical Research 1999;32(8):651-657.
32. Krishnamoorti R, Ren JX, Silva AS. Shear response of layered silicate nanocomposites. Journal of Chemical Physics 2001;114(11):4968-4973.
33. Usuki A, Kawasumi M, Kojima Y, Okada A, Kurauchi T, Kamigaito O. Swelling Behavior of Montmorillonite Cation Exchanged for Omega-Amino Acids by Epsilon-Caprolactam. Journal of Materials Research 1993;8(5):1174-1178.
34. Vaia RA, Ishii H, Giannelis EP. Synthesis and Properties of 2-Dimensional Nanostructures by Direct Intercalation of Polymer Melts in Layered Silicates. Chemistry of Materials 1993;5(12):1694-1696.
35. Cho JW, Paul DR. Nylon 6 nanocomposites by melt compounding. Polymer 2001;42(3):1083-1094.
36. Hasegawa N, Okamoto H, Kato M, Usuki A. Preparation and mechanical properties of polypropylene-clay hybrids based on modified polypropylene and organophilic clay. Journal of Applied Polymer Science 2000;78(11):1918-1922.
37. Hasegawa N, Okamoto H, Kawasumi M, Kato M, Tsukigase A, Usuki A. Polyolefin-clay hybrids based on modified polyolefins and organophilic clay. Macromolecular Materials and Engineering 2000;280(7-8):76-79.
38. Kim GM, Lee DH, Hoffmann B, Kressler J, Stoppelmann G. Influence of nanofillers on the deformation process in layered silicate/polyamide-12 nanocomposites. Polymer 2001;42(3):1095-1100.
39. Reichert P, Kressler J, Thomann R, Mulhaupt R, Stoppelmann G. Nanocomposites based on a synthetic layer silicate and polyamide-12. Acta Polymerica 1998;49(2-3):116-123.
40. Nair SV, Goettler LA, Lysek BA. Toughness of nanoscale and multiscale polyamide-6,6 composites. Polymer Engineering and Science 2002;42(9):1872-1882.
41. Liu XH, Wu QJ. Polyamide 66/clay nanocomposites via melt intercalation. Macromolecular Materials and Engineering 2002;287(3):180-186.
42. Liu XH, Wu QJ, Berglund LA. Polymorphism in polyamide 66/clay nanocomposites. Polymer 2002;43(18):4967-4972.
43. Lu YL, Zhang GB, Feng M, Zhang Y, Yang MS, Shen DY. Hydrogen bonding in polyamide 66/clay nanocomposite. Journal of Polymer Science Part B-Polymer Physics 2003;41(19):2313-2321.
44. Kubies D, Pantoustier N, Dubois P, Rulmont A, Jerome R. Controlled ring-opening polymerization of epsilon-caprolactone in the presence of layered silicates and formation of nanocomposites. Macromolecules 2002;35(9):3318-3320.
45. Strawhecker KE, Manias E. Structure and properties of poly(vinyl alcohol)/Na+ montmorillonite nanocomposites. Chemistry of Materials 2000;12(10):2943-2949.

46. Huang JC, Zhu ZK, Yin J, Qian XF, Sun YY. Poly(etherimide)/montmorillonite nanocomposites prepared by melt intercalation: morphology, solvent resistance properties and thermal properties. Polymer 2001;42(3):873-877.
47. Kim SW, Jo WH, Lee MS, Ko MB, Jho JY. Preparation of clay-dispersed poly(styrene-co-acrylonitrile) nanocomposites using poly(epsilon-caprolactone) as a compatibilizer. Polymer 2001;42(24):9837-9842.
48. Hasegawa N, Okamoto H, Kawasumi M, Usuki A. Preparation and mechanical properties of polystyrene-clay hybrids. Journal of Applied Polymer Science 1999;74(14):3359-3364.
49. Ren JX, Silva AS, Krishnamoorti R. Linear viscoelasticity of disordered polystyrene-polyisoprene block copolymer based layered-silicate nanocomposites. Macromolecules 2000;33(10):3739-3746.
50. Wang Z, Pinnavaia TJ. Nanolayer reinforcement of elastomeric polyurethane. Chemistry of Materials 1998;10(12):3769-+.
51. Chang JH, An YU. Nanocomposites of polyurethane with various organoclays: Thermomechanical properties, morphology, and gas permeability. Journal of Polymer Science Part B-Polymer Physics 2002;40(7):670-677.
52. Wang Z, Pinnavaia TJ. Hybrid organic-inorganic nanocomposites: Exfoliation of magadiite nanolayers in an elastomeric epoxy polymer. Chemistry of Materials 1998;10(7):1820-1826.
53. Wang Z, Lan T, Pinnavaia TJ. Hybrid organic-inorganic nanocomposites formed from an epoxy polymer and a layered silicic acid (magadiite). Chemistry of Materials 1996;8(9):2200-&.
54. Shia D, Hui CY, Burnside SD, Giannelis EP. An interface model for the prediction of Young's modulus of layered silicate-elastomer nanocomposites. Polymer Composites 1998;19(5):608-617.
55. Kornmann X, Lindberg H, Berglund LA. Synthesis of epoxy-clay nanocomposites: influence of the nature of the clay on structure. Polymer 2001;42(4):1303-1310.
56. Lan T, Pinnavaia TJ. Clay-Reinforced Epoxy Nanocomposites. Chemistry of Materials 1994;6(12):2216-2219.
57. Lan T, Kaviratna PD, Pinnavaia TJ. Mechanism of Clay Tactoid Exfoliation in Epoxy-Clay Nanocomposites. Chemistry of Materials 1995;7(11):2144-2150.
58. Chin IJ, Thurn-Albrecht T, Kim HC, Russell TP, Wang J. On exfoliation of montmorillonite in epoxy. Polymer 2001;42(13):5947-5952.
59. Jiankun L, Yucai K, Zongneng Q, Xiao-su Y. Study on Intercalation and Exfoliation Behavior of Organoclays in Epoxy Resin. Journal of Polymer Science Part B-Polymer Physics 2001;39:115-120.
60. Zilg C, Thomann R, Finter J, Mulhaupt R. The influence of silicate modification and compatibilizers on mechanical properties and morphology of anhydride-cured epoxy nanocomposites. Macromolecular Materials and Engineering 2000;280(7-8):41-46.
61. Lee A, Lichtenhan JD. Thermal and viscoelastic property of epoxy-clay and hybrid inorganic-organic epoxy nanocomposites. Journal of Applied Polymer Science 1999;73(10):1993-2001.
62. Fornes TD, Paul DR. Crystallization behavior of nylon 6 nanocomposites. Polymer 2003;44(14):3945-3961.
63. Devaux E, Bourbigot S, El Achari A. Crystallization behavior of PA-6 clay nanocomposite hybrid. Journal of Applied Polymer Science 2002;86(10):2416-2423.
64. Anastasiadis SH. Local dynamics in nanocomposites. Journal De Physique Iv 2000;10(P7):255-258.
65. Anastasiadis SH, Karatasos K, Vlachos G, Manias E, Giannelis EP. Nanoscopic-confinement effects on local dynamics. Physical Review Letters 2000;84(5):915-918.
66. Hasegawa N, Okamoto H, Kato M, Usuki A, Sato N. Nylon 6/Na–montmorillonite nanocomposites prepared by compounding Nylon 6 with Na–montmorillonite slurry. Polymer 2003;44(10):2933-2937.
67. Fornes TD, Yoon PJ, Hunter DL, Keskkula H, Paul DR. Effect of organoclay structure on nylon 6 nanocomposite morphology and properties. Polymer 2002;43(22):5915-5933.
68. Southern Clay Products website

69. Xie W, Gao ZM, Liu KL, Pan WP, Vaia R, Hunter D, Singh A. Thermal characterization of organically modified montmorillonite. Thermochimica Acta 2001;367:339-350.
70. Reichert P, Nitz H, Klinke S, Brandsch R, Thomann R, Mulhaupt R. Poly(propylene)/organoclay nanocomposite formation: Influence of compatibilizer functionality and organoclay modification. Macromolecular Materials and Engineering 2000;275(2):8-17.
71. Vaia RA, Giannelis EP. Polymer melt intercalation in organically-modified layered silicates: Model predictions and experiment. Macromolecules 1997;30(25):8000-8009.
72. Vanderhart DL, Asano A, Gilman JW. Solid-state NMR investigation of paramagnetic nylon-6 clay nanocomposites. 2. Measurement of clay dispersion, crystal stratification, and stability of organic modifiers. Chemistry of Materials 2001;13(10):3796-3809.
73. Fornes TD, Yoon PJ, Paul DR. Polymer matrix degradation and color formation in melt processed nylon 6/clay nanocomposites. Polymer 2003;44(24):7545-7556.
74. Güven N. Rheological aspects of aqueous smectite suspensions. In: Güven N, Pollastro RM, editors. Clay–water interface and its implications: CMS Workshop Lectures; 1992.
75. Carlsson LA. Thermoplastic composite materials. Amsterdam: Elsevier; 1991.
76. Cogswell FN. Thermoplastic aromatic polymer composites. Oxford: Butterworth-Heinemann; 1992. 277 p.
77. Bazhenov SL, Kuperman AM, Zelenskii ES, Berlin AA. Compression failure of unidirectional glass-fiber-reinforced plastics. Composites Science and Technology 1992;45:201-208.
78. Lo KH, Chim SM. Compressive strength of Unidirectional Composites. Journal of Reinforced Plastics and Composites 1992;11:838-896.
79. Rosen B. Mechanics of composite strengthening. Fiber Composite Materials: ASM; 1965. p 37-75.
80. Chen F, Bazhenov S, Hiltner A, Baer E. Flexural Failure Mechanisms in Unidirectional Glass-Fiber- Reinforced Thermoplastics. Composites 1994;25(1):11-20.
81. Budiansky B, Fleck NA. Compressive Failure of Fiber Composites. Journal of the Mechanics and Physics of Solids 1993;41(1):183-211.
82. Fleck NA, Zhao LG. Microbuckle tunnelling in fibre composites. Journal of the Mechanics and Physics of Solids 2000;48(9):1865-1891.
83. Marissen R, Brouwer HR. The significance of fibre microbuckling for the flexural strength of a composite. Composites Science and Technology 1999;59(3):327-330.
84. Naik NK, Kumar RS. Compressive strength of unidirectional composites: evaluation and comparison of prediction models. Composite Structures 1999;46(3):299-308.
85. Hahn HT, Williams JG. Compression Failure Mechanisms in Unidirectional Composites. In: Whitney JM, editor; 1986. American Society for Testing and Materials. p 115-139.
86. Wu SH, Wang FY, Ma CCM, Chang WC, Kuo CT, Kuan HC, Chen WJ. Mechanical, thermal and morphological properties of glass fiber and carbon fiber reinforced polyamide-6 and polyamide-6/clay nanocomposites. Materials Letters 2001;49(6):327-333.
87. Chen CG, Curliss D. Resin matrix composites: Organoclay-aerospace epoxy nanocomposites, Part II. Sampe Journal 2001;37(5):11-18.
88. Rice BP, Chen CG, Cloos L, Curliss D. Carbon fiber composites: Organoclay-aerospace epoxy nanocomposites, Part I. Sampe Journal 2001;37(5):7-9.
89. Garcia R, Evans RE, Palmer RJ. Structural Property Improvements Through Hybridized Composites. In: Johnston NJ. Toughened Composites. Volume ASTM STP 937. Philadelphia: American Society for Testing and Materials; 1987. p 397-412.
90. Campbell S, Scheiman D, Faile M, Papadopoulos D. PMR-15/ layered silicate nanocomposites for improved thermal stability and mechanical properties. 2002.
91. Halpin JC, Kardos JL. Halpin-Tsai Equations - Review. Polymer Engineering and Science 1976;16(5):344-352.
92. Halpin JC. Stiffness and Expansion Estimates for Oriented Short Fiber Composites. Journal of Composite Materials 1969;3:732-734.

Chapter 2

Moisture absorption in PA6 silicate nanocomposites and its influence on the mechanical properties

2.1 Introduction

One property common to all polyamides is that they absorb water from the environment, both from the air and from liquid water. The equilibrium moisture content of PA6 at 23 °C in a 50% relative humidity environment is around 2.5 wt% and at 100 % relative humidity as high as 9 wt% [1]. Absorbed water in polyamide has a large influence on many properties: decrease of T_g, modulus and yield stress, while both elongation at break and toughness increase [1]. PA6 is often filled with mineral fillers or short fibres such as glass, carbon or aramid fibres to increase the modulus. With the addition of rigid fillers the decrease of the modulus under the influence of water can be compensated. The addition of this type of fillers can be very effective when the polymer is used as an engineering plastic in injection-moulded products. Filler levels up to 60 volume percent are possible, leading to very stiff materials. However, for fibre and film applications these types of fillers are not very useful, because the relatively large size of the filler particles has a negative influence on the toughness, transparency and surface appearance. In addition, high contents of traditional mineral and glass fillers lead to a large increase in the density of the compound. Layered silicate nanocomposites provide several advantages compared to traditional filled compounds, such as lower amounts of fillers and, therefore, lower density, increased barrier properties, improved transparency and better surface appearance.

Nanocomposites consisting of exfoliated silicate layers in PA6 can be produced by in-situ polymerization, in which organically modified silicate layers were swollen by the monomer for PA6 (ε-caprolactam) and exfoliated during polymerization [2-4], or by dispersion in the melt by high shear mixing in a twin-screw extruder [5-8].

Because of the large aspect ratio and surface area of the exfoliated silicate layers they act as efficient barriers against transport through the material [9]. The transport speed of gasses and vapours through the polymer is reduced because the impenetrable silicate layers cause an increase in the path length for molecules

diffusing through the polymer [10,11]. The reduced transport rate reduces the rate of moisture uptake in PA6. Because absorption of water reduces the glass transition temperature and the modulus of PA6, the addition of nanoparticles to reduce the negative effects of water uptake is very useful. The nanoparticles influence the properties of moisture-conditioned nanocomposites in two ways: they reduce the water uptake speed due to the barrier properties, and they increase the modulus of the plasticized nanocomposite.

Despite the importance of the influence of moisture in practical applications, only a few papers containing data for mechanical properties of moisture-conditioned nanocomposites have been published [7,11-14]. However, for a complete understanding of PA6 nanocomposites it is important to understand both how the moisture absorption takes places and how this influences the mechanical properties. In this chapter the influence of different types and amounts of layered silicate and the relative humidity on the diffusion coefficient and the maximum amount of absorbed moisture is described. In addition, the influence of different amounts of moisture on the mechanical properties is measured and discussed. From the ratio of diffusion coefficients in the matrix and the nanocomposites the aspect ratio of the particles is calculated. The aspect ratio of the exfoliated particles is a very important factor that influences the moisture transport rate, the elastic modulus of the nanocomposite (chapter 3) and the viscosity (chapter 5).

2.2 Theory

2.2.1 Water diffusion in polymers and nanocomposites

The moisture absorption speed in polymers and nanocomposites can be quantified by determining the diffusion coefficient. Fick's second law of diffusion (equation 2.1) describes the accumulation of water in a sample as a function of time with a diffusion coefficient D [15].

$$\frac{\partial c}{\partial t} = \frac{\partial}{\partial x}\left(D\frac{\partial c}{\partial x} \right) \qquad 2.1$$

In the initial stage of the absorption, up to approximately $\frac{M_t}{M_\infty} \cong 0.5$, the increase in mass shows a linear relationship with the square root of time [15]. M_t is the mass increase of the sample at time t, and M_∞ the final mass increase of the sample at

saturation. In this initial absorption phase, the diffusion profiles on the different sides of the sample do not overlap and develop independently. Therefore, as long as the diffusion profiles do not overlap, the mass flux of moisture, j, and its time dependence through the sample surface is the same everywhere and is equal to the flux of a semi infinite geometry:

$$j = \Delta c\sqrt{D/\pi t} \qquad 2.2$$

Here Δc is the difference in mass density of the initial (free of moisture) and the final (saturated) stage. To get the change in sample mass per unit time one has to integrate the flux over the surface of the sample. If the diffusion profiles, which arise by penetration of moisture from the different sides of the sample, do not overlap, the flux through the sample surface is the same everywhere. As stated previously, significant overlap does not occur up to $\frac{M_t}{M_\infty} \cong 0.5$ [15]. Up to that point, the time derivative of the sample mass is given simply by the flux times the total surface area, A_{tot}. The value of the flux is then given by that of a semi-infinite geometry in equation 2.2. By integration of the flux times the area one finds for the mass increase:

$$\frac{M_t}{M_\infty} \cong \frac{2A_{tot}}{V}\sqrt{\frac{Dt}{\pi}} \qquad 2.3$$

A_{tot} is the total area of the sample and V the total volume. In equation 2.3 the fact has been used that the final mass of the sample is given by $M_\infty = \Delta c \cdot V$. Equation 2.3 can be used to calculate the diffusion coefficient of a polymer or nanocomposite by plotting (M_t / M_∞) versus $\sqrt{t}$. Then by using equation 2.3 the diffusion coefficient can be determined from the slope. Since we analyze dogbone samples and not films we use the generalized equation for the mass increase where the total area and volume of the sample are significant parameters. The region of validity where the mass increase scales with the square root of time now is slightly less than that of a slab geometry. This analysis is restricted to the data points that follow the square root law to determine the diffusion coefficient. The speed of water absorption in PA6 nanocomposites is reduced compared to the unfilled polymer because of the impermeable silicate layers in the polymer. These layers increase the path-length for diffusion through the polymer [16]. This increased path length predicts the better barrier properties of nanocomposites very well [17]. Contrary to what is sometimes

suggested [13], the amount of water that can be absorbed by PA6 nanocomposites is not reduced; only the rate of absorption is reduced due to the lower diffusion coefficient [11]. In PA6 the water is absorbed in the amorphous phase, because the crystalline part is inaccessible for water [1]. The amorphous fraction is not much different in nanocomposites [10,18] and therefore the amount of absorbed water can reach approximately the same level as in unfilled polyamide, if sufficient time is available. However, data obtained according to (for example) the ISO-62 or ASTM D570-98 standards can give the impression that nanocomposites absorb less moisture. These standards describe procedures in which the moisture absorption is performed in a fixed time, with a maximum of 24 hours, which is clearly not adequate to compare nanocomposites and unfilled polymers. Due to the lower transport rate nanocomposites do not reach the equilibrium moisture content within the fixed time (depending on the sample thickness and conditioning temperature), which was probably the reason for the low moisture absorption reported in several articles [13,14]. Only repeated measurement of the weight increase during moisture absorption until no more increase is observed can ensure that the equilibrium moisture content has been reached.

The diffusion coefficients D can be used to compare the diffusion speed in the unfilled polymer and nanocomposite and to estimate how much time total moisture saturation of a sample takes, depending on the dimensions. In addition, it is possible to calculate the aspect ratio of the silicate sheets in the nanocomposites from the ratio of diffusion coefficients of the nanocomposite and the matrix. Nielsen [16] has derived a simple theory, which relates the diffusion coefficient to the increased path that molecules have to travel when diffusing around impenetrable platelets. Many simplifications have been made in this theory, which reduce the accuracy of the results. An important difference between Nielsen's model and real nanocomposites is the fact that Nielsen's theory is a 2 dimensional theory in which the third dimension of the plates is considered infinitely long. In addition, it assumes perfectly overlapping ribbons, while real particles are randomly oriented, at least in the long dimensions of the platelets. Therefore, this theory underestimates the real diffusion coefficient. Van Es [17] has derived a more accurate equation for diffusion in nanocomposites filled with aligned platelets, which is based on a combination of models by Brydges *et al.* [19] and Hatta *et al*. [20] (equation 2.4).

$$\left(\frac{D_{\text{matrix polymer}}}{D_{\text{nanocomposite}}}\right) = \left(\varphi_{filler}\beta + 1 - \varphi_{filler}\right) \cdot \left(\varphi_{filler}\beta \cdot \gamma(1-\gamma) + 1\right) \qquad 2.4$$

$$\beta = \frac{8}{5\pi} \cdot \frac{w}{t} \qquad \frac{w}{t} = \text{With / Thickness = aspect ratio platelets}$$

γ = Overlap factor: γ = 0.5 for perfect overlap of the platelets, 0 for no overlap and 0.25 for platelets that are randomly oriented in 2 dimensions.

Equation 2.4 is valid for diffusion with a wide variety of particle concentrations, and the validity was confirmed by comparison with three-dimensional finite element modelling. This equation is based on diffusion through a material around impenetrable platelets that are all aligned parallel to each other. This is a reasonable assumption in injection-moulded samples [21-23], especially on the outside of the sample where the first diffusion is measured. However, within the plane of the platelets there is no specific ordering, so the random placement of the sheets leads to an overlap factor γ of 0.25 in this model.

2.2.2 Influence of water on mechanical properties

Absorbed moisture decreases T_g in PA6 and other polyamides [1] because the water molecules interfere with the hydrogen bonds between the polymer chains and this increases the chain mobility. The reduced T_g in the presence of water results in a strong reduction of the amorphous modulus in the temperature range around T_g, which leads to a decrease of the modulus of the semi-crystalline polymer. Because of the reduction of the matrix modulus, also polyamide nanocomposites suffer from a modulus reduction after moisture conditioning. In addition, the increased mobility reduces the yield stress and increases the ductility and elongation at break.

2.3 Experimental

2.3.1 Materials

Polyamide 6, low molecular weight (LMW PA6):

- Akulon® K122D, injection-moulding grade PA6 from DSM, the Netherlands.
  M_n = 16000, M_w = 32000 g/mol, T_m = 220 °C
  (Similar in properties to K222D and K123 used in other chapters.)

Organically modified layered silicate

Three organically modified platelet-shaped silicates were used, the first two based on purified natural montmorillonite clay, and the third on a synthetic layered silicate:

Cloisite® 30 B from Southern Clay Products, USA. (Montmorillonite)

Surfactant: methyl bis-2-hydroxyethyl tallow quaternary ammonium (32 wt%)

- Nanomer® I 30 TC from Nanocor, USA. (Montmorillonite)
  Surfactant: tri-methyl tallow quaternary ammonium (33 wt%)
- Somasif® MAE from Unicoop, Japan. (Synthetic Mica®)
  Surfactant: di-methyl di-tallow quaternary ammonium (40 wt%)

The manufacturers have added organic surfactants on the silicate platelets to enhance the exfoliation, because the surfactants increase the layer distance and improve the interaction with the polymer. The amount of organic surfactant was determined with thermo-gravimetric analysis (TGA) in a Perkin Elmer TGA-7 Thermal Gravimetric Analyzer at 800°C for 1 hour in air.

2.3.2 Preparation

Extrusion

The nanocomposites were prepared by mixing organically modified silicate nanofillers in PA6 in a Werner and Pfleiderer ZDS-K28 co-rotating twin-screw extruder. The modified silicate powder was mixed with the PA6 granules and fed into the extruder at a constant rate via a Plasticolor 2500 feeding unit. The extruder was operated at a screw speed of 200 RPM and a feeding rate of approximately 3 kg per hour, which resulted in an average residence time of 3 minutes in the extruder.

Temperature in the feeding zone was 150°C, all the other zones where heated to 230°C. Cooling was applied to keep the temperature constant, because the high shear in the melt can produce too much heat. First a master batch was made with a silicate content of approximately 10 wt% (based on the inorganic content of the silicate), and the other concentrations were made by mixing this master batch with unfilled K122D in a second extrusion step.

Injection moulding

Dumbbell shaped samples according to ISO 527 standards were injection moulded on an Arburg Allrounder 221-55-250 injection-moulding machine. The feeding zone was heated to 150 °C, the melting and mixing zones were heated to 240 °C and the

nozzle was kept at 260 °C. The mould was heated to a temperature of 90 °C to reduce the cooling speed and ensure a more homogeneous crystallization.

Determination of silicate content

Thermogravimetric analysis (TGA) measurements were used to determine the exact silicate content in the tested samples after processing. A Perkin Elmer TGA-7 Thermal Gravimetric Analyser was used to determine the weight fraction of silicate by heating a sample in air at 800 °C for 1 hour.

2.3.3 Testing

Mechanical properties

The samples were tested on a Zwick 1445 tensile tester with a 10 kN force cell. For the modulus measurement Zwick clip-on extensometers were used. The test speed was 5 mm per minute and the temperature was 23 °C.

Moisture absorption

Dry as moulded samples were dried in a vacuum oven at 80 °C for at least 48 hours before testing.

The moisture conditioning was performed at 70°C to increase the speed of moisture transport. Samples containing 3% water were prepared by conditioning in a Heraeus climate chamber at 70 °C and 65% relative humidity and samples containing 6% water were prepared by conditioning at 70 °C and 92% relative humidity. The sample weight was measured after drying and conditioning on a Mettler AE-240 to calculate the moisture level. The moisture content was calculated based on the amount of matrix material (PA6 and surfactant), so the weight of the silicate phase was not included.

Several samples were stored without further treatment for 270 days in a room with an average temperature of 20 °C and an average relative humidity of 50 %, which resulted in a variable moisture content depending on the silicate content. The diffusion coefficients were determined from rectangular samples of 27 X 20 X 4 mm, cut from the wide part of the ISO 527 test bars.

2.4 Results and Discussion

Nanocomposites with a range of concentrations of layered silicate filler as shown in table 2.1 are used. The silicate content shown in table 2.1 are the quantities determined with TGA measurements.

Silicate type	Silicate content [wt %]				
Cloisite® 30B	2.6	4.7	6.8	8.3	10.6
Nanomer® I30TC	2.5	4.4	6.6	8.3	10.2
Somasif® MAE	2.5	3.6	5.6	7.1	9.1

Table 2.1: Silicate content in the nanocomposites determined by TGA.

2.4.1 Moisture absorption

The maximum moisture content absorbed by the PA6 samples was determined at 70 °C as a function of the relative humidity between 55 and 100 % (figure 2.1). Two different moisture levels, 3 and 6 wt%, were chosen to measure the mechanical properties, which corresponds to moisture conditioning levels of 65 % and 92 % RH at 70 °C.

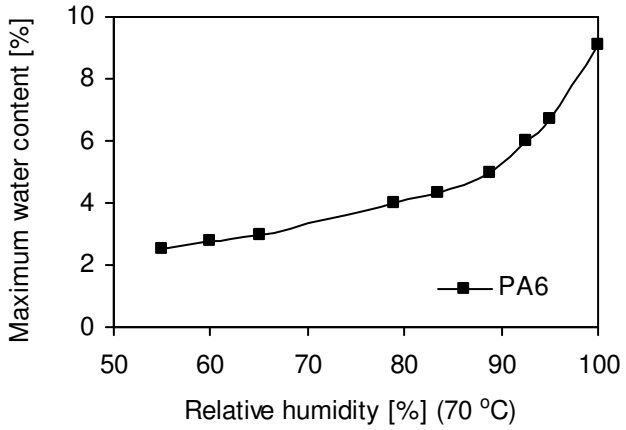


Figure 2.1: Maximum water content in PA6 as a function of the relative humidity at 70 °C.

Water is only absorbed by the amorphous part of PA6 [1]. However, in nanocomposites containing organically modified layered silicate, the surfactant on the platelets can be considered as another amorphous fraction of the material, which can be mixed with the polymer. Therefore, the question arises if the moisture is absorbed by the PA6 phase only, or also by the surfactant. In figure 2.2A the moisture content in the different concentrations of Cloisite® 30 B nanocomposites

after conditioning at 92% RH is shown, calculated with respect to the amorphous PA6 phase and with respect to the total amorphous matrix (amorphous PA6 and surfactant). The volume fractions of amorphous PA6, crystalline PA6, silicate and surfactant used in the calculation (calculated from TGA and DSC data) are shown in figure 2.2B. Keeping in mind that the water concentration of approximately 9.5 wt% in the amorphous phase equals approximately 6 wt% water in the total matrix phase, figure 2.2A shows that nanocomposites can indeed absorb approximately the same equilibrium amount of moisture (in the matrix) as the unfilled polymer and that it is likely that the water is distributed in the entire amorphous matrix (PA6 and surfactant). If the water would only be in the amorphous PA6 phase, an increase in silicate content would imply an increase in the moisture content, which is unlikely.

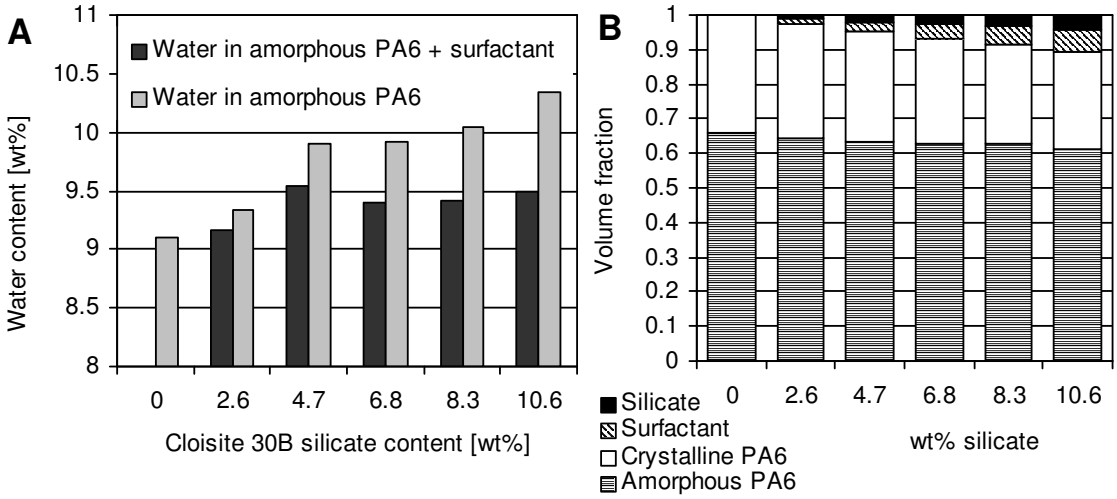


Figure 2.2: **A**: Moisture content in the amorphous phase after 70 °C / 92% RH conditioning, calculated with and without the surfactant phase.
B: Composition Cloisite® 30B nanocomposites.

2.4.2 Diffusion coefficient

The increase in water content of the nanocomposites and unfilled PA6 was measured at 70 °C, both at 65% and 92% RH. An example is shown in figure 2.3 for Cloisite® 30B nanocomposites at 65% RH, where the absorption results are shown as (M_t / M_∞) versus $\sqrt{t}$. The initially straight line levels off above (M_t / M_∞) > 50%.
The speed of moisture absorption is reduced with increasing amounts of exfoliated silicate, due to the barrier properties. Equation 2.3 is used to calculate the diffusion coefficient form the slope in the initial part of the curve, which equals $\left(\frac{A_{total}}{2V}\times\frac{4}{\sqrt{\pi}}\right)\bullet\sqrt{D}$. The constant $\frac{A_{total}}{2V}\times\frac{4}{\sqrt{\pi}}$ is equal to 771 for the samples used for

the moisture absorption experiments. From the slopes of the linear fit at low moisture content the diffusion coefficients are calculated for all nanocomposites at 65 % RH and 92 % RH.

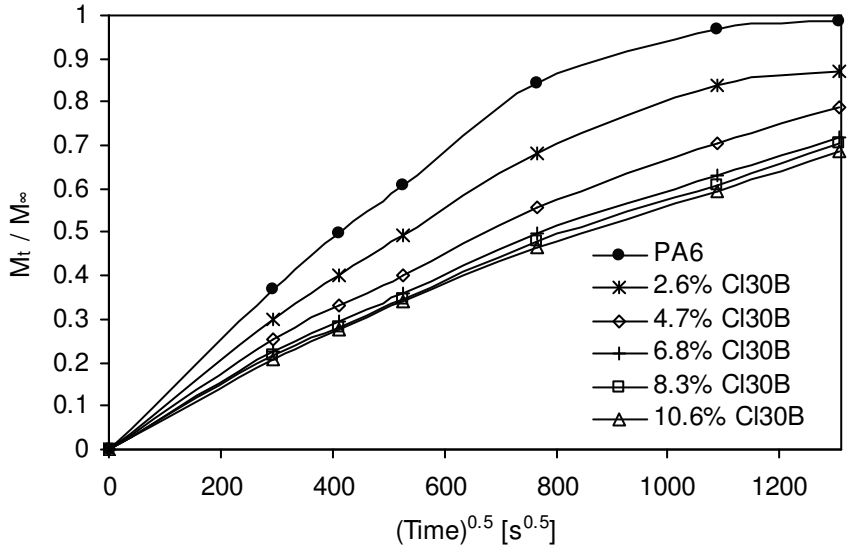


Figure 2.3: Water absorption Cloisite® 30B nanocomposites at 70 °C / 65% RH.

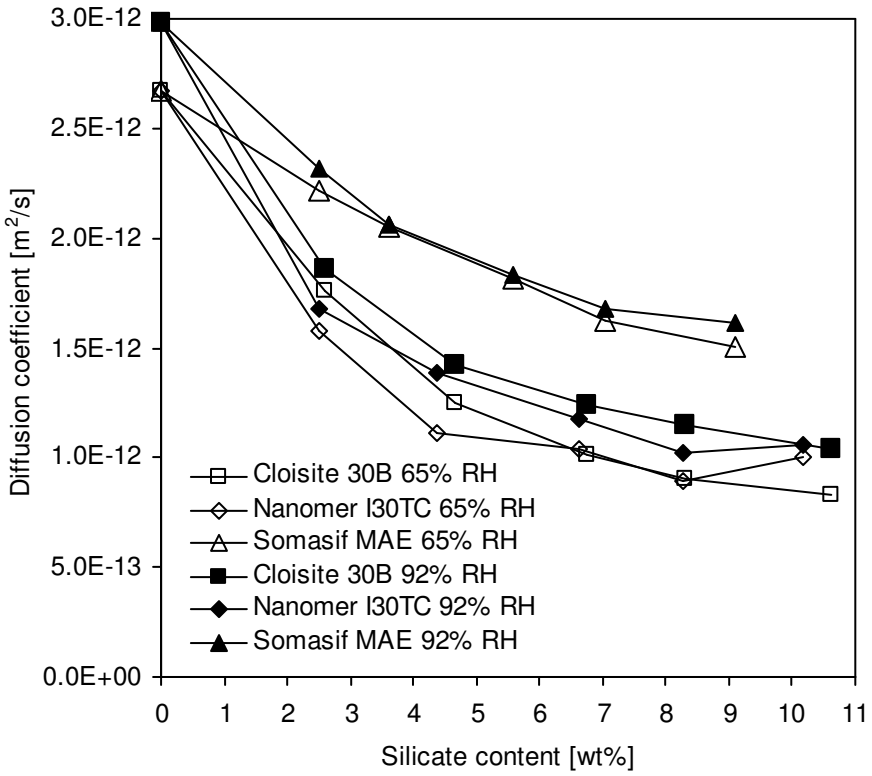


Figure 2.4: Diffusion coefficients nanocomposites.

In figure 2.4 the diffusion coefficients are plotted versus the silicate content. The Cloisite® 30B and Nanomer® I30TC nanocomposites show a similar strong decrease

of the diffusion coefficient with increasing silicate content, while the Somasif® MAE nanocomposites show a smaller decrease. This is probably the result of reduced exfoliation and consequently smaller aspect ratios of the particles in the MAE nanocomposites (see figure 2.7). The diffusion coefficients at the highest silicate content are almost three times smaller than that of the unfilled PA6, which means that the nanocomposites will take approximately three times longer to reach saturation. The results also show that the diffusion coefficient depends on the moisture content during conditioning. A higher relative humidity leads to a higher moisture content in the sample, and this leads to a higher diffusion coefficient. This concentration dependence is a known phenomenon in polyamides [1,24,25], which is caused by the swelling of the amorphous phase with the absorbed water. The effect is not very strong in these samples, probably because the absorption temperature (70°C) is above T_g of the material. In this case the absorption of water has less effect on the chain mobility, because the amorphous phase is already mobile without the addition of water. The influence of the temperature on the diffusion coefficient is much stronger than the influence of the moisture content. It has been shown that diffusion coefficient for water in PA6 has an exponential temperature dependence, with an activation energy E_s = 0.49 eV [24]:

$$D=D_0\exp\left(-\frac{E_s}{kT}\right) \qquad 2.5$$

D_0 depends on variables such as the crystallinity. Equation 2.5 is used to calculate the temperature dependence of D (figure 2.5), using the value we found at 70 °C and high RH ($D = 3.0\cdot10^{-12}$ m^2/s).

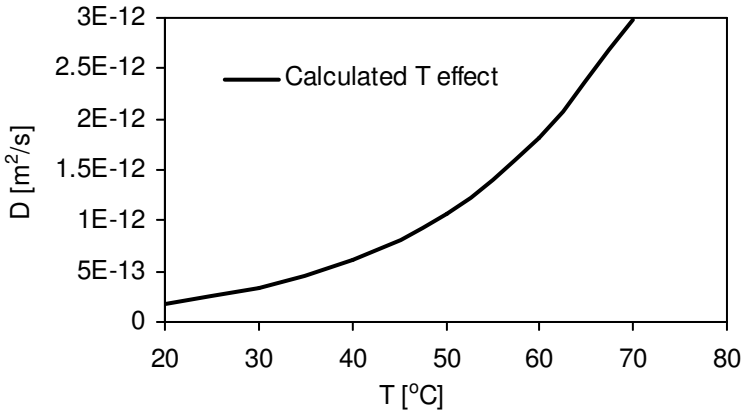


Figure 2.5: Calculated effect of the temperature on the diffusion coefficient in PA6 (eq. 2.5).

The diffusion coefficient is approximately 17 times smaller at 20 °C compared to 70 °C and the moisture saturation will take approximately 17 times longer at room temperature. Therefore, in normal atmospheric conditions (20 °C / 50% RH) it will take a very long time to reach the equilibrium moisture concentration in the 4 mm thick samples. The unfilled PA6 samples reached total saturation at 70 °C in 3 weeks, so a rough estimation shows that it takes one year for total saturation at room temperature. Therefore, it is clear that absorption at elevated temperature is necessary to reach the desired moisture content within a reasonable time, especially in nanocomposites where the diffusion coefficient is up to 3 times smaller then in unfilled PA6. This is illustrated by the moisture content of several samples that have been stored in a room with average conditions of 20 °C and 50% RH for 270 days.

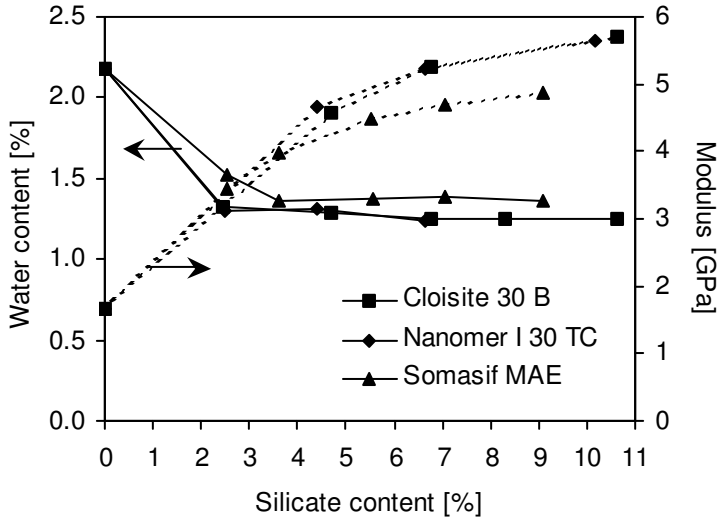


Figure 2.6: Moisture content (solid lines) and modulus (dotted lines) after 270 days conditioning at approximately 20 °C and 50 % RH.

This resulted in moisture contents as shown in figure 2.6, (the concentrations are not the equilibrium moisture content; it is just one moment in a continuing process to reach equilibrium). It can be seen that even the unfilled PA6 did not reach the equilibrium moisture content (ca. 2.5%) and the nanocomposites only reached half of this value in the available time. The strongest influence on the time required for total moisture saturation is the thickness of the samples, because Fick's second law results in a quadratic influence of the thickness on the time. When designing products with polyamide and its nanocomposites it is important to realize that the properties of the materials will continuously change in search of equilibrium over long time periods, up to several years.

These results make very clear that time-limited moisture-conditioning standards such as ISO-62 and ASTM D570-98 are not appropriate for measuring moisture absorption or mechanical properties on nanocomposites. This type of methods might give the impression that nanocomposites absorb less water, while the presented results show that only the speed of water absorption is different.

2.4.3 Aspect ratios

The aspect ratios of the platelets (figure 2.7) are calculated from the diffusion coefficients for the matrix and the nanocomposites, using equation 2.4.

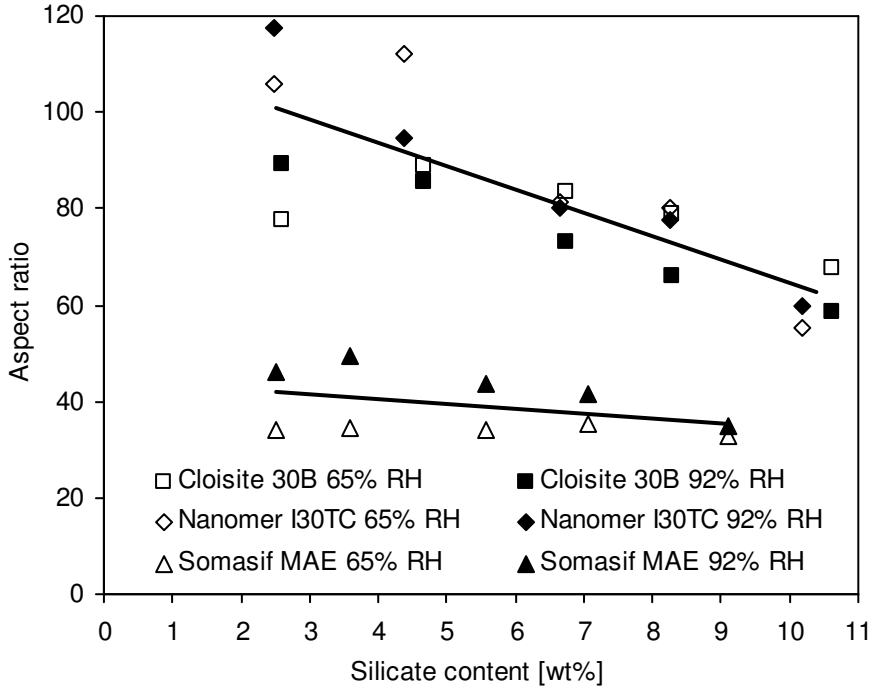


Figure 2.7: Aspect ratios calculated from diffusion coefficients.

In figure 2.7 two lines are drawn as a best fit through the average aspect ratios of Somasif® MAE, and through the combined results of Cloisite® 30B and Nanomer® I30TC. The calculated aspect ratios suggest that Somasif® MAE particles have a lower average aspect ratio than the other two (~ ½), which can be caused by a reduced degree of exfoliation in the MAE nanocomposites. Visual indications for the imperfect exfoliation were seen in the melt: the MAE nanocomposite showed a much lower melt viscosity and an opaque instead of a transparent melt. The fact that Somasif® MAE has two aliphatic chains on each quaternary ammonium group in instead of one for the Cloisite® 30B and Nanomer® I30TC samples, is probably the cause of the reduced exfoliation. The double amount of chains leaves less space for

interactions of polymer chains with the silicate surface and provides a more hydrophobic surface than surfactants with a single chain. In general, relatively hydrophilic modified layered silicates have a better interaction with the hydrophilic PA6 chains [26].

Another general trend that can be seen in figure 2.7 is the decrease of the calculated aspect ratios with increasing silicate content. This could be caused by reduced exfoliation and can be an explanation for the observation that the effectiveness of reinforcement in nanocomposites is often reduced at high silicate content [7,17,27] (see also chapter 3).

2.4.4 Mechanical properties

Modulus

The tensile moduli of the nanocomposites at various moisture contents are shown in figure 2.8.

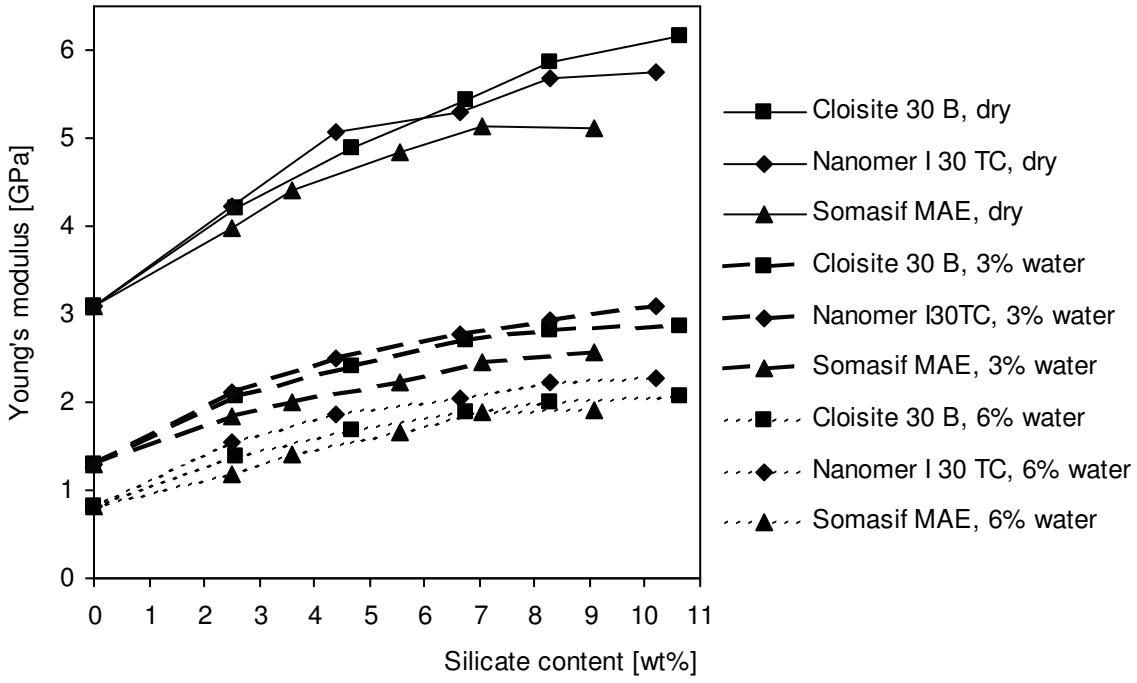


Figure 2.8: Young's modulus versus silicate content for various moisture contents.

It is found that the two different montmorillonite-based fillers (Cloisite® 30B and Nanomer® I30TC) give more or less equal moduli, while Somasif® MAE synthetic mica gives a slightly lower modulus. This is in agreement with the results for the diffusion coefficients and aspect ratios, and is probably the result of imperfect exfoliation of the MAE nanoparticles. When the samples are moisture conditioned,

the modulus of PA6 and the nanocomposites is significantly reduced. The reduction of the modulus in the presence of water is common to all polyamides to a certain degree, and it is caused by the plasticizing action of water molecules in polyamides [28]. All polyamides form hydrogen bonds between the amide groups, and water can bind in between these hydrogen-bonding groups [1]. This increases the mobility of the polymer chains due to weaker interactions, causing a reduction of the glass transition temperature. PA6 has a glass transition temperature around 60 °C in dry conditions, but in moisture conditioned samples this can decrease to room temperature and below [1]. The associated drop of the modulus around T_g can be seen in figure 2.9.

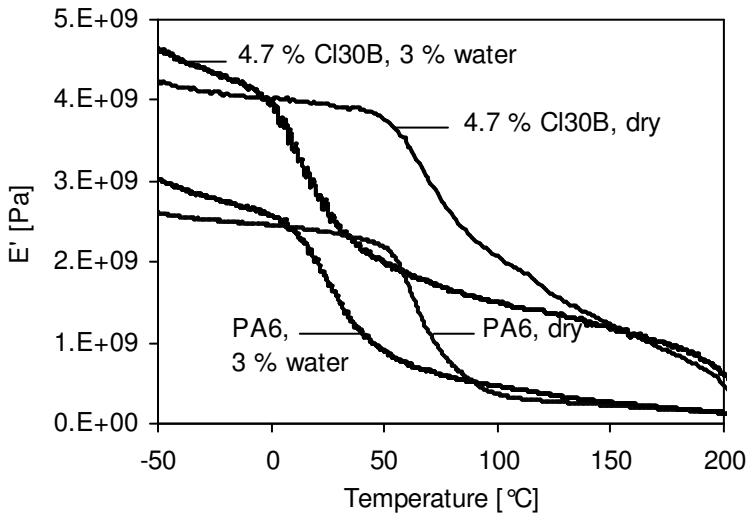


Figure 2.9: Storage modulus from DMA for dry and moisture conditioned PA6 and 4.7 wt% Cloisite 30B nanocomposite.

The presence of the silicate filler does not change T_g and the amount of T_g reduction due to moisture conditioning is similar for nanocomposites and unfilled PA6 (figure 2.9). Both samples show that the reduction of the modulus at room temperature is due to the reduction of T_g. Far above T_g the modulus is not affected much and far below T_g the modulus shows a slight increase, which has been reported before [1]. The importance of the modulus enhancement for the temperature range at which PA6 nanocomposites will often be used can be seen in figure 2.9. If for a certain application a modulus value of for example at least 1 GPa is necessary, figure 2.9 shows that nanocomposites can provide a very large increase in the temperature range at which a material can be applied, up to 100 °C higher. This is closely related to the observed increase in the heat distortion temperature (HDT). The behaviour of T_g in PA6 explains the amount of modulus reduction found for various moisture

contents as shown in figure 2.8. The modulus reduction upon addition of the first 3 % water has a larger influence on the modulus than the addition of large amounts of water, because the addition of the first 3 % water causes the T_g to decrease to around the testing temperature.

The reduced water absorption speed, combined with the influence of moisture on the T_g and modulus has important implications for the use of PA6 nanocomposites. This is illustrated by the moduli of samples that have been exposed for 270 days to standard atmospheric conditions (ca. 20 °C - 50 % RH), shown in figure 2.6. The modulus of the nanocomposites is hardly reduced after this long time, unlike the unfilled PA6. However, with the diffusion coefficients of the nanocomposites (figure 2.4) and the influence of temperature (figure 2.5) it can be estimated that it will take a few years to reach moisture saturation, and thus the modulus of the nanocomposites will eventually drop.

Yield and fracture behaviour

In figure 2.10 the yield or fracture stress of all the samples is shown. The solid points show yield stresses (the maximum in the stress-strain curve), the open points show the brittle fracture stress if the yield point was reached.

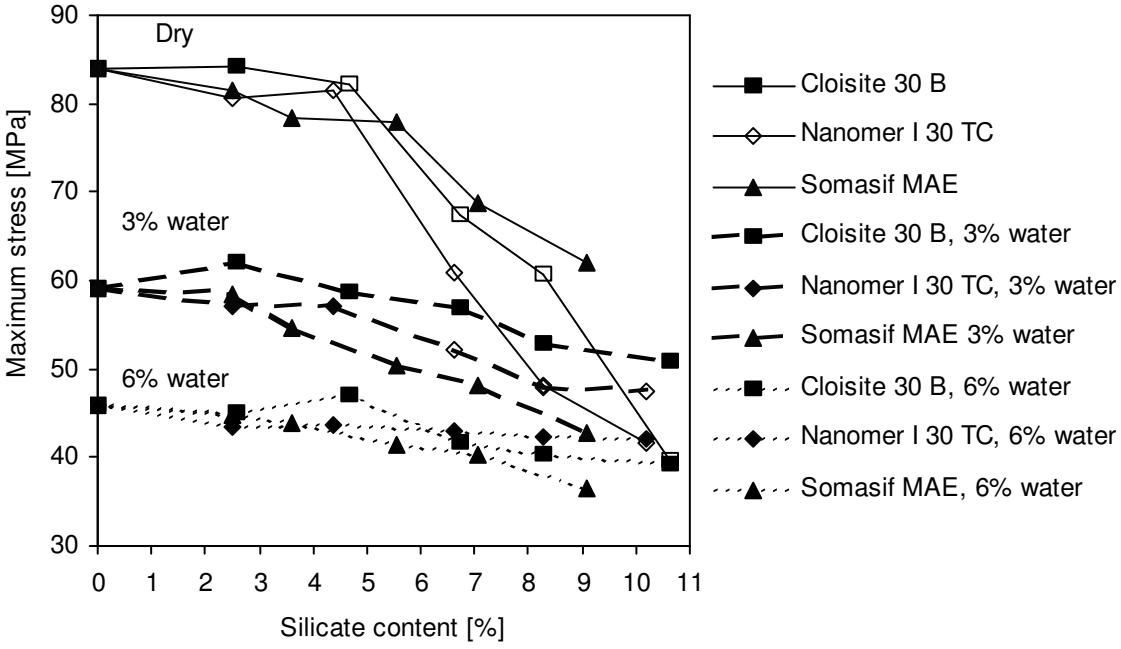


Figure 2.10: Maximum stress versus silicate concentration for various moisture contents. Closed symbols represent the yield stress, open symbols the brittle fracture stress when the yield point was not reached.

In general, increasing the silicate content causes more brittle fracture behaviour, while increasing the moisture content causes a reduction of the yield stress and more ductile fracture behaviour. The ductile behaviour of wet samples could have been expected because this lowers the T_g, which increases the chain mobility of the amorphous phase. There seems to be a trade-off between modulus and ductility; the samples with the highest modulus show the most brittle fracture behaviour. The nanocomposites based on Nanomer® I30TC are most brittle; they are all brittle in the dry state and the samples with 3% water are brittle above 4.4% silicate. The less perfectly exfoliated Somasif® MAE nanocomposites show ductile fracture behaviour up to 9% silicate, even in the dry state. This ductile yield behaviour is accompanied by a reduction of the yield stress with increasing silicate content. A decrease in yield stress can be an indication of a weak adhesion between the particles and the matrix polymer. Rigid particles with a weak interaction with the polymer can de-bond from the matrix at a stress below the yield point. This results in small voids in the polymer and this can reduce the yield stress and increase the ductility, in the same way as cavitated rubber particles in impact modified blends [29-31]. The de-bonding mechanism seems to play a role in the Somasif® MAE nanocomposites, illustrated by the stress whitening that was visible just before the yield stress was reached. Well-bonded particles do not de-bond from the matrix at stress levels below the yield stress and are, therefore, not capable of decreasing the yield stress of the samples. The less exfoliated particles like Somasif® MAE in PA6 give a smaller increase in modulus, but they do not cause brittle fracture behaviour, which can be an important advantage. However, the nanocomposite samples that were kept for 270 days at atmospheric conditions were all brittle (results not shown), including the MAE nanocomposites, despite the absorption of a small amount of water. This change in ductility could be a result of the physical aging of the polymer during this period. The increase in the density of the amorphous phase due to molecular re-arrangements associated with physical aging [28,32], can cause a reduction of the ductility. This can counteract the increased mobility and ductility caused by the absorption of water.

2.5 Conclusions

The nanocomposites absorb water at a slower rate than the unfilled PA6 samples, as expected. However, when given sufficient time the nanocomposites are capable of absorbing similar quantities of water in the matrix phase as the unfilled polymer. The diffusion coefficients of the nanocomposites are reduced to approximately 1/3 of the

original value at the highest silicate loading. The conditioning temperature has a much stronger influence on the time needed to reach saturation. Therefore, increased temperature conditioning is necessary with samples of several mm thick; in moderate conditions (20 °C - 50% RH) the samples absorb moisture so slowly that it takes very long times, up to several years for nanocomposites, to reach complete saturation. Constant monitoring of the weight-increase should be used to determine if the equilibrium has been reached. The moisture absorption results show that time-limited moisture absorption standards like ISO-62 and ASTM D570-98 are not suitable to compare unfilled polymers with nanocomposites, because they would give a wrong impression of the moisture absorption capabilities

The modulus of the nanocomposites increases continuously with increasing silicate content, at around 10 wt% the moduli of the Cloisite® and Nanomer® nanocomposites are twice that of the unfilled resin. At higher silicate content the modulus increase levels off, while the Somasif® MAE nanocomposites have a lower modulus at all concentrations, probably due to reduced exfoliation.

The modulus of moisture-conditioned nanocomposites shows a reduction just like the unfilled polymer. At around 6% silicate the modulus of the moisture conditioned nanocomposite is equal to the modulus of the dry unfilled polymer (at room temperature). This way one of the main drawbacks of polyamides, the large decrease of the modulus in wet conditions, can be compensated by the addition of a small quantity of exfoliated silicate.

The fracture behaviour of the nanocomposites is influenced by the type and concentration of filler, the moisture content and the aging time. In general the addition of silicate filler reduces the ductility, in the dried samples only the Somasif® MAE samples and the lowest concentration of Cloisite® 30B were ductile. Nanomer® I30TC gave the most brittle samples; even at a moisture content of 3% they were all brittle while all the other samples were completely ductile at that water content. At a moisture level of 6% all samples were ductile. The fact that the Somasif® MAE nanocomposites tested after conditioning for 270 days at atmospheric conditions were brittle while the fresh dry samples were ductile shows that physical aging also has an influence on ductility. The physical aging properties of nanocomposites are investigated further in chapter 6.

From the ratio of the matrix and composite diffusion coefficients the average aspect ratio can be estimated. The aspect ratios from the diffusion coefficients are around 100 in the low concentration and decrease somewhat at higher filler levels to around 70. The MAE nanocomposites show lower aspect ratios, which can be explained by the reduced interaction with the polymer.

Remarkably, the aspect ratios as calculated from diffusion data shows a good agreement with aspect ratios calculated from mechanical properties using the Halpin-Tsai composite model and from melt rheology measurements (see chapter 3 and 5) [33,34]. The combined results of moisture diffusion in PA6 nanocomposites and the influence of moisture on the mechanical properties as presented in this chapter, indicate that parts with a thickness of several mm will be subject to large changes in (mechanical) properties over long time periods. Polyamide parts and especially nanocomposites will be in a non-equilibrium state during moisture absorption, leading to constantly changing mechanical properties for periods up to several years. The modulus will eventually drop after enough moisture is absorbed to lower T_g below the use temperature, and the fracture behaviour will probably become more ductile at that point. It has to be realized that besides the moisture absorption, also physical aging plays an important role in the development of the properties of PA 6 nanocomposites over long time scales. However, the reduced moisture transport rate of nanocomposites means that the properties will be less sensitive to short term fluctuations in environmental conditions than unfilled polyamide. Pre-conditioning at elevated temperatures can speed up the moisture absorption process and lead to more stable and predictable properties.

2.6 References

1. Kohan MI. Nylon Plastics Handbook: Carl Hanser Verlag; 1995.
2. Kojima Y, Usuki A, Kawasumi M, Okada A, Fukushima Y, Kurauchi T, Kamigaito O. J. Mater. Res. 1993;8(5):1185-1189.
3. Usuki A, Kawasumi M, Kojima Y, Okada A, Kurauchi T, Kamigaito O. J. Mater. Res. 1993;8(5):1174-1178.
4. Usuki A, Kojima Y, Kawasumi M, Okada A, Fukushima Y, Kurauchi T, Kamigaito O. J. Mater. Res. 1993;8(5):1179-1184.
5. Vaia RA, Giannelis EP. Macromolecules 1997;30(25):8000-8009.
6. Kawasumi M, Hasegawa N, Kato M, Usuki A, Okada A. Macromolecules 1997;30(20):6333-6338.
7. Akkapeddi MK. Glass fiber reinforced polyamide-6 nanocomposites. Polym. Compos. 2000;21(4):576-585.
8. Cho JW, Paul DR. Polymer 2001;42(3):1083-1094.
9. Giannelis EP. Adv. Mater. 1996;8(1):29.
10. Es MAv, Xiqiao F, Turnhout Jv, Giessen Evd. In: Al-Malaika Sea, editor. Specialty Polymer Additives: Blackwell Science; 2001, Chapter 21.
11. Kojima Y, Usuki A, Kawasumi M, Okada A, Kurauchi T, Kamigaito O. J. Appl. Polym. Sci. 1993;49(7):1259-1264.
12. Murase S, Inoue A, Miyashita Y, Kimura N, Nishio Y. J. Polym. Sci. Pt. B-Polym. Phys. 2002;40(6):479-487.
13. Liu XH, Wu QJ. Macromol. Mater. Eng. 2002;287(3):180-186.
14. Wang H, Zeng CC, Elkovitch M, Lee LJ, Koelling KW. Polymer Engineering and Science 2001;41(11):2036-2046.
15. Crank J. The Mathematics of Diffusion. Oxford: Oxford University Press; 1975.

16. Nielsen LE. Journal of Macromolecular Science, Part A 1967;5(1):929-942.
17. Es MAv. Polymer clay nanocomposites. The importance of particle dimensions. Delft: Delft University of Technology; 2001.
18. Lincoln DM, Vaia RA, Wang ZG, Hsiao BS, Krishnamoorti R. Polymer 2001;42(25):9975-9985.
19. Brydges WT, Gulati ST, Baum G. J. Mater. Sci. 1975;10(12):2044-2049.
20. Hatta H, Taya M, Kulacki FA, Harder JF. Journal of Composite Materials 1992;26(5):612-625.
21. Kojima Y, Usuki A, Kawasumi M, Okada A, Kurauchi T, Kamigaito O, Kaji K. J. Polym. Sci. Pt. B-Polym. Phys. 1995;33(7):1039-1045.
22. Varlot K, Reynaud E, Kloppfer MH, Vigier G, Varlet J. J. Polym. Sci. Pt. B-Polym. Phys. 2001;39(12):1360-1370.
23. Fornes TD, Paul DR. Polymer 2003;44(17):4993-5013.
24. Hanspach J, Pinno F. Acta Polym. 1992;43(4):210-213.
25. Lim LT, Britt IJ, Tung MA. J. Appl. Polym. Sci. 1999;71(2):197-206.
26. Fornes TD, Hunter D, Paul DR. Macromolecules 2003.
27. Liu L, Qi Z, Zhu X. J. Appl. Polym. Sci. 1999;71:1133-1138.
28. Struik LCE. Polymer 1987;28(9):1521-1533.
29. Zuiderduin WCJ, Westzaan C, Huetink J, Gaymans RJ. Polymer 2003;44(1):261-275.
30. Wilbrink MWL, Argon AS, Cohen RE, Weinberg M. Polymer 2001;42(26):10155-10180.
31. Zuiderduin WCJ, Vlasveld DPN, Huetink J, Gaymans RJ. Polymer 2004;45(11):3765-3779.
32. Spinu I, McKenna GB. Polymer Engineering and Science 1994;34(24):1808-1814.
33. Vlasveld DPN, Groenewold J, Bersee HEN, Mendes E, Picken SJ. Polymer 2005;46:6102-6113.
34. Vlasveld DPN, Jong Md, Bersee HEN, Gotsis AD, Picken SJ. Polymer 2005;46: In Press.

The results described in this chapter have been published as:

D.P.N. Vlasveld, J. Groenewold, H.E.N. Bersee, S.J. Picken,

Moisture absorption in polyamide-6 silicate nanocomposites and its influence on the mechanical properties. Polymer 2005, (Revised version under review).

Chapter 3

Analysis of the modulus of PA6 silicate nanocomposites using moisture controlled variation of the matrix properties

3.1 Introduction

The most obvious enhancement in mechanical properties that layered silicates can provide is a relatively large increase in modulus at very low filler concentrations. The modulus increase is mainly in the long directions of the particles because of the high aspect ratio of the layered silicate particles. Compared to short fibre reinforcement the particle shape in layered silicate nanocomposites is more effective, because they can reinforce in two dimensions instead of one [1,2]. The high modulus and anisotropy of the particles also reduces thermal expansion and shrinkage upon crystallization in the long direction of the platelets [3], although due to the anisotropy the expansion is larger in the thickness direction of the platelets [4,5].

Despite all the research on nanocomposites, there is still discussion about the reason of the large modulus increase by using such small amounts of filler. The nature of the mechanism is a subject of debate were various contrasting ideas seem to exist:

- The increased modulus could be contributed to the reduced mobility of a constrained polymer phase close to the silicate layers. The large surface area of the exfoliated platelets is considered to be responsible for this constrained polymer phase with a higher modulus [6-8].
- The strong ionic bond between the polymer and the silicate platelets is sometimes assumed to be the main reason for the increased modulus [9].
- The reinforcement mechanism in nanocomposites could be similar to traditional composites. In that case the modulus of the composite is dependent on the modulus of the matrix, the modulus of the filler and the shape and orientation of the filler particles. According to this view traditional composite theories can explain most of the properties of nanocomposites without assuming a change in the polymer properties [1,2].

In the first two theories the high modulus of the silicate particles is considered to be of minor importance, or even completely ignored. As has been shown by Van Es et al. and Fornes et al. [1,2] the presence of very stiff, high aspect ratio particles is

expected to give a large increase in modulus and should not be ignored, as is sometimes done [6]. It is unlikely that the type of bond is very important for the modulus, because the bonding strength is not important for the modulus, although it is important for the strength of the composite. It has been reported that it is possible to make nanocomposites with layered silicates without any surfactant, which can give similar moduli [10], despite the lack of modification on the silicate filler (see also chapter 4 and 5). By analysing the modulus of PA6 nanocomposites with different moisture content and describing this with a mechanical model the nature of the modulus enhancement of nanocomposites can become clearer.

In this chapter results from chapter 2, the influence of the silicate content and moisture content on the modulus of PA6 nanocomposites, are used to test the validity of the Halpin-Tsai composite theory for nanocomposites. The experimental results are used to estimate the average platelet aspect ratio using the Halpin-Tsai composite model. The results of the model can show if nanocomposites behave like conventional composites or that the modulus of the matrix is changed by the presence of the nanoparticles, as is often suggested [6-9]. Composite models such as the series model, parallel model and Halpin-Tsai model assume that the matrix phase and the reinforcing phase do not change the properties of the other phase, so it is interesting to see to which extend this traditional composite model can predict the properties of nanocomposites. By changing the moisture content the modulus of the matrix can be varied over a wide range while the composition and morphology of the nanocomposites remains constant. The influence of the silicate on the crystallinity is measured with DSC and the orientation of the reinforcing platelets and the PA6 crystals is measured with WAXS. These parameters are used in the Halpin-Tsai model to estimate the matrix modulus in the nanocomposites and the effective aspect ratio of the silicate platelets. The calculated effective aspect ratios of the nanoparticles in nanocomposites with a wide variety of matrix moduli are compared to determine if the mechanism of modulus enhancement in layered silicate nanocomposites is similar to that of conventional (micro)composites.

3.2 Theory

The modulus of PA6 is strongly influenced by moisture absorption. Therefore, different moisture levels can be used to change the modulus of the matrix material without changing the microstructure of the nanocomposite.

The amount of water that can be absorbed by PA6 nanocomposites is not reduced compared to unfilled PA6, however, the rate of absorption is reduced due to the lower diffusion coefficient [11,12]. The water is absorbed in the amorphous part of PA6 [13], so in the model it is assumed that the absorbed water does not influence the mechanical properties of the crystalline phase. However, the amorphous phase shows a dramatic change in modulus because the absorbed moisture causes a decrease of the glass transition temperature to below room temperature. The matrix moduli are measured on the conditioned unfilled polymer, and they are subsequently compensated for the differences in crystallinity and the presence of surfactant with the Halpin-Tsai model. The aspect ratio of the reinforcing particles in each nanocomposite is calculated using the Halpin-Tsai model with the measured modulus of the nanocomposites and the different matrix moduli for the three different moisture contents as input.

3.2.1 The Halpin-Tsai model

The semi-empirical Halpin-Tsai model [14,15] is used, because it is a relatively simple but accurate model that takes into account the shape and the aspect ratio of the reinforcing particles. Polydispersity of the reinforcing particles in such a semi-empirical model will lead to an average particle size as a result. The Halpin-Tsai model was originally developed to describe the properties of semi-crystalline polymers [5,14], which are in essence also nanocomposites, and can also be used for composites reinforced with fibre and platelet shaped particles. Van Es [1,5,14] has derived a set of shape factors for platelet-reinforced composites by comparing results from the Halpin-Tsai equations to results from more fundamental approaches i.e. the Eshelby theory, the Mori-Tanaka theory and 3D finite element modelling [5,14]. Equation 3.1 shows the traditional form [14] of the Halpin-Tsai equations:

$$\frac{E_c}{E_m} = \frac{1+\varsigma\eta\varphi_f}{1-\eta\varphi_f} \quad \text{in which} \quad \eta = \frac{\left(\frac{E_f}{E_m}-1\right)}{\left(\frac{E_f}{E_m}+\varsigma\right)} \qquad 3.1$$

E_c = Composite Young's modulus.

E_f = Filler modulus, E_m = Matrix modulus.

ς = Shape factor, depending on the geometry, orientation and aspect ratio of the particles.

φ_f = Volume fraction filler

The shape factors for the tensile moduli of platelet reinforced composites are [1]:

E_{11} or E_{22} $\quad \zeta = 2/3 \cdot (L/D)$ (in the radial direction of the platelets)

E_{33} $\quad \zeta = 2$ (perpendicular to the platelets)

(L/D) = aspect ratio (= width of platelet / thickness of platelet)

When equation 3.1 is rewritten in one equation as is shown in equation 3.2, the nature of the Halpin-Tsai model becomes clearer.

$$E_c = E_m \frac{E_f(1+\zeta\varphi_f) + E_m(\zeta - \zeta\varphi_f)}{E_f(1-\varphi_f) + E_m(\zeta+\varphi_f)} \qquad \text{(Halpin-Tsai)} \qquad 3.2$$

When the aspect ratios are much smaller then the ratio of filler and matrix modulus ($\zeta << E_f/E_m$) the Halpin-Tsai model gives results close to a series model:

$$E_c \approx \frac{E_m E_f}{E_f(1-\varphi_f) + E_m(\varphi_f)} = \left(\frac{1-\varphi_f}{E_m} + \frac{\varphi_f}{E_f} \right)^{-1} \qquad \text{(Series model)} \qquad 3.3$$

When the aspect ratios are much larger then the ratio of filler and matrix modulus ($\zeta >> E_f/E_m$) the Halpin-Tsai model gives results close to a parallel model:

$$E_c \approx E_m \frac{E_f \zeta \varphi_f + E_m \zeta (1-\varphi_f)}{E_m \zeta} = E_f \varphi_f + E_m (1-\varphi_f) \qquad \text{(Parallel model)} \qquad 3.4$$

For nanocomposites the series model underestimates the modulus, because the volume fraction of filler is very low, resulting in domination of the first term in equation 3.3 and thus in values close to the matrix modulus. However, the parallel model overestimates the composite modulus at low matrix moduli, since it assumes a continuous reinforcing phase. The Halpin-Tsai model (equation 3.2) leads to results that are in between these two extremes when the aspect ratio is of the same order of magnitude as the ratio of moduli ($\zeta \approx E_f/E_m$). The aspect ratio of the particles has a strong influence on the results and, therefore, determines how close the results are to either the series or parallel model.

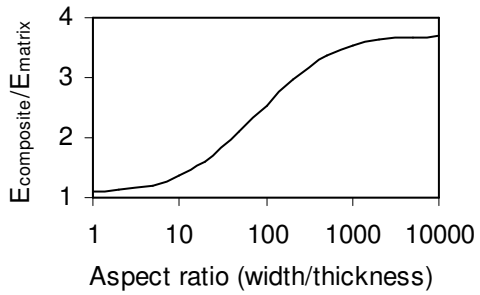


Figure 3.1: Relative modulus as a function of the aspect ratio.
(5 vol%, E_m=3.1GPa, E_f=172 GPa)

The calculated effect of the aspect ratio on the relative modulus ($E_{composite}$ / E_{matrix}) in the Halpin-Tsai model for a platelet filled composite (E_{matrix} = 3.1 GPa, E_{filler} = 172 GPa, φ_f = 0.05) is shown in figure 3.1, which shows that the particles are hardly effective below L/D = 10, and only when L/D is above 1000 the maximum effect is reached. This means that for typical platelet sizes in nanocomposites, the influence of the aspect ratio and, therefore, also of the exfoliation, on the modulus is very important. Platelet aspect ratios for layered silicate nanocomposites are around 100-200. Consequently, when exfoliation is not optimal the resulting reduction in aspect ratio has a large effect on the modulus. The Halpin-Tsai model can, besides calculation of the composite modulus, also be used to calculate the aspect ratio of the reinforcing particles when the modulus of the composite, matrix and filler are known. The Halpin-Tsai model can only give an effective aspect ratio, because the particles can have different shapes, sizes and thicknesses. The effective aspect ratio represents the best fit with the measured moduli and can be considered a useful parameter to compare different nanocomposite compositions, as well as providing a reasonable estimate of the average aspect ratio.

In this chapter the Halpin-Tsai model for a platelet reinforced composite is used twice:

1. To calculate the modulus of the matrix, based on the crystallinity and the amount of surfactant (section 3.2).
2. To calculate the effective aspect ratio of the reinforcing particles in the nanocomposite (section 3.3).

In the second model the results of the first model, i.e. the matrix moduli for each composition and moisture content, are used as input.

3.2.2 Calculation of the matrix modulus using the Halpin-Tsai model

As mentioned before, the Halpin-Tsai model for nanocomposites assumes that the filler does not influence the properties of the matrix. However, the addition of the layered silicate filler can influence the modulus of the matrix because of its influence on the crystallinity and the presence of the surfactant.

- Surfactant: By adding the modified layered silicate also approximately half of its weight in anionic surfactant is added. The volume fraction is even larger than the weight fraction due to the lower density of the surfactant, and, therefore, the surfactant fraction should not be neglected.
- Crystallinity: It is known that the addition of layered silicates can influence the crystallinity. The crystallinity has a strong influence on the modulus of the matrix, especially above T_g, where the modulus mainly depends on the crystalline phase.

These two factors are accounted for by using a different matrix modulus for each silicate concentration in the Halpin-Tsai model to calculate the aspect ratios in the nanocomposites. The matrix moduli are calculated with the Halpin-Tsai equations because the semi-crystalline polymer can be considered to be a composite with an amorphous polymer matrix reinforced with crystalline polymer platelets (lamellae).
Although a nanocomposite based on a semi-crystalline polymer is a very complex system containing many different phases that can influence each other, we have assumed a simplified composition to be able to estimate the properties with a relatively simple composite model. The four phases of the simplified composition that is assumed in this model is shown in figure 3.2.

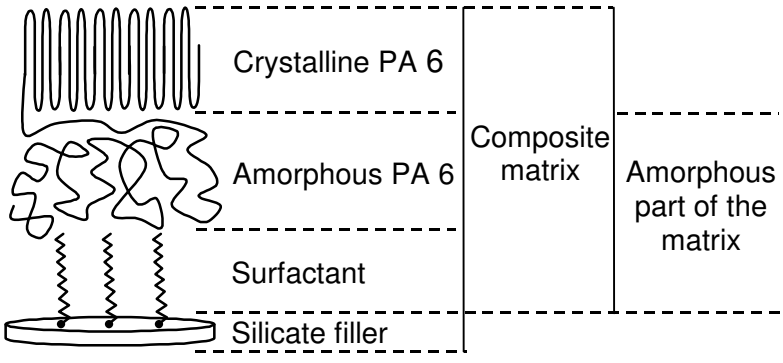


Figure 3.2: Simplified composition of the nanocomposite for the Halpin-Tsai model.

It consists of a crystalline PA6 phase, an amorphous PA6 phase, a surfactant phase and an inorganic silicate phase. The nanocomposite matrix consists of the crystalline PA6 phase, the amorphous PA6 phase and the surfactant phase. The modulus of the

nanocomposite matrix is calculated with the Halpin-Tsai model that considers an amorphous matrix reinforced with crystalline platelets. The amorphous part of the matrix consists of amorphous PA6 and surfactant, and it is assumed in this model that the surfactant has no stiffness ($E_{surfactant}=0$). Therefore, the modulus of the amorphous matrix is calculated with equation 3.5:

$$E_{amorphous\ matrix} = E_{amorphous\ PA6} * (1-\varphi_{surfactant}) \qquad 3.5$$

($\varphi_{surfactant}$ = volume fraction surfactant in amorphous matrix)

The result is that the modulus of the amorphous phase in the model is slightly reduced when the modified silicate is added. The input for the Halpin-Tsai model to calculate the matrix modulus is the amorphous PA6 modulus, the modulus of the crystalline phase, the volume fraction of the crystalline phase, and the aspect ratio of the crystalline lamellae:

- **Modulus of amorphous PA6**

The value used for the modulus of dry amorphous PA6 at room temperature is 2.2 GPa, which is calculated from literature results for moduli at different amounts of crystallinity [16]. For moisture-conditioned samples with 3 and 6% water the value for the amorphous modulus is calculated with the Halpin-Tsai model from the measured sample modulus and the calculated crystalline modulus.

- **Crystalline volume fraction**

The heat required for melting in the tested samples was measured with DSC and with the use of the mass fractions of silicate and surfactant and the heat of crystallization of the crystals ($\Delta H_{alpha\ crystal}$ = 243 J/g, $\Delta H_{gamma\ crystal}$ = 213 J/g [1]) the crystalline volume fraction of the matrix has been calculated.

- **Aspect ratio of the crystalline lamellae**

For the aspect ratio of the crystalline lamellae a constant value of 1000 is chosen in the model. Consequently, at these high values the modulus is almost independent on the exact aspect ratio, which was shown in figure 3.2. It is believed such a high aspect ratio is a reasonable assumption because the lamellae are very thin, around 5 nm [13], but relatively wide (several μm). It will be explained in the discussion why the exact value is not important in these calculations.

- **Modulus crystalline phase**

The crystalline phase can consist of several different crystalline structures, such as the α and γ crystal structures. In this composite model it is assumed that the modulus of all crystal structures is identical. In the model the modulus in the long direction of

the crystalline platelet is used, which is perpendicular to the chain axis. In the literature not much data is available for this direction of the crystal, and the values that have been reported are rather diverse [17]. However, it is possible to calculate the effective crystalline modulus with the Halpin-Tsai model by using the measured modulus of the dry polyamide 6 samples and the amorphous modulus. The calculated value for the crystalline modulus is used for all other samples to calculate how the matrix modulus changes with the crystallinity.
The result of this approach is a different matrix modulus for each nanocomposite sample, which depends on the crystallinity, the amount of surfactant and the moisture content.

3.2.3 Calculation of the effective platelet aspect ratio

The calculated matrix moduli for each sample can be used in the Halpin-Tsai model to calculate the effective aspect ratio of the silicate particles in the samples. Besides the matrix modulus, the input for this model is the modulus of each nanocomposite sample as measured on the injection moulded samples, the volume fraction silicate platelets as calculated from TGA measurements and the silicate modulus. The degree of alignment of the platelets is investigated using WAXS. In this model the modulus of the silicate platelets is assumed to be 172 GPa, equal to the modulus of a perfect mica crystal [18], which is comparable in structure to the layered silicates in the nanocomposite samples. The volume fractions are calculated from the mass fractions by using the following densities: ρ surfactant = 0.93 g/cm^3 [19], ρ amorphous PA6 = 1.08 g/cm^3, ρ α-crystalline PA6 = 1.24 g/cm^3, ρ γ-crystalline PA6 = 1.18 g/cm^3 [13,20], ρ silicate = 2.8 g/cm^3 (equal to the density of mica [21]).
The modelled aspect ratios for each silicate concentration and moisture content are plotted versus silicate content to see if they show the same trend for each matrix modulus. If the aspect ratios are independent of the matrix modulus, this provides support to the idea that the modulus increase in nanocomposites is based on the same mechanism as valid for traditional composites.
Many simplifications in the composition for the model have been made and of several parameters the exact values are uncertain or subject of debate. However, small variations in the assumed values do not have a significant influence on the results and do not change the overall conclusions.

3.3 Experimental

3.3.1 Materials

Polyamide 6, low molecular weight (LMW PA6)

- Akulon® K122D, injection-moulding grade PA6 from DSM, the Netherlands.
  M_n = 16000, M_w = 32000 g/mol, T_m = 220 °C
  (Similar in properties to K222D and K123 used in other chapters.)

Organically modified layered silicate

- Cloisite® 30B from Southern Clay Products (USA), was used as nanoparticles. The manufacturer has added an organic surfactant (methyl bis-2-hydroxyethyl tallow quaternary ammonium) on the silicate platelets to enhance the exfoliation by improving the interaction with the polymer. The amount of organic surfactant, approximately 32 wt%, is determined using thermo-gravimetric analysis (TGA).

Five different concentrations of Cloisite® 30B in PA6 were used; all concentrations were conditioned to reach three different moisture levels.

3.3.2 Sample preparation

Extrusion

The nanocomposites were prepared by mixing Cloisite® 30B in PA6 in a Werner and Pfleiderer ZDS-K28 co-rotating twin-screw extruder. The modified layered silicate powder was mixed with the polymer granules and fed into the extruder at a constant rate via a Plasticolor 2500 feeding unit. The extruder was operated at a screw speed of 200 RPM and a feeding rate of approximately 3 kg per hour, which resulted in an average residence time of 3 minutes in the extruder.

Temperature in the feeding zone was 150 °C, all the other zones were heated to 230 °C. Cooling was applied to keep the temperature constant since the high shear forces in the melt can produce too much heat. First a 10.6 wt% (based on the inorganic content of the filler) master batch was made. Other concentrations were made by diluting the master batch with unfilled K122D in a second extrusion step.

Injection moulding

Dumbbell shaped samples according to the ISO 527 standard were injection moulded on an Arburg Allrounder 221-55-250 injection-moulding machine. The feeding zone was heated to 150 °C, the melting and mixing zones were heated to

240 °C and the nozzle was kept at 260 °C. The mould was heated to a temperature of 90 °C to reduce the cooling speed and ensure a more homogeneous crystallization.

Moisture conditioning

Dry as moulded samples were dried in a vacuum oven at 80 °C for at least 48 hours before testing. The moisture conditioning was performed at 70 °C to increase the speed of moisture transport, which is necessary because of the barrier properties of nanocomposites. The sample weight was measured after drying and conditioning on a Mettler AE-240 to calculate the moisture level. The moisture content was calculated based on the amount of polyamide 6, so the silicate and surfactant weight were not included.

Samples with 3% water in the PA6 phase were prepared by conditioning in a Heraeus climate chamber at 70 °C and 65% relative humidity and samples with 6% water in the PA6 phase were prepared by conditioning at 70 °C and 92% relative humidity.

3.3.3 Testing

Measurement of silicate content

Thermogravimetric analysis (TGA) measurements were done to determine the exact silicate content in the tested samples after processing. A Perkin Elmer TGA-7 Thermal Gravimetric Analyzer was used to determine the weight fraction of silicate by heating a sample in air at 800 °C for 1 hour.

Measurement of the crystallinity

The level of crystallinity of the samples and the ratio of the two crystal phases, α and γ, was determined with Differential Scanning Calorimetry on a Perkin-Elmer DSC-7. DSC samples of approximately 5 mg were cut from the centre of the tensile test bar. The DSC measurements were performed at a heating rate of 10 °C per minute between 25 °C and 270 °C. The crystallinity was calculated using a heat of fusion of 213 J/g for the gamma crystals, and 243 J/g for the alpha crystals [5].

Measurement of the glass transition temperature

The glass transition temperatures (T_g) of the samples were determined with Dynamic Mechanical analysis. Samples of 0.5 mm thin were cut from the injection moulded

test bars and tested in three point bending in a Perkin-Elmer DMA 7e at a temperature range from –130 °C to 210 °C. The temperature at the highest point of the largest peak in the loss modulus spectrum was used to represent the T_g. The tests were done for unfilled PA6 and 6.7% silicate filled samples at moisture contents of 0, 3 and 6 wt% water in the PA6 phase.

Measurement of the average crystal and silicate platelet orientation

Wide angle X-ray scattering (WAXS) has been performed on a Bruker D8 Discover diffractometer with a 2D (1024x1024) detector using a 10cm sample to detector distance and incident Cu radiation of 1.54Å. An incident beam cross-section of 0.5 mm was used. A 0.5 mm thin cross section was cut through the thickness and the width of the moulded sample tensile test bar and x-ray measurements were taken at different positions starting from the edge and each next measurement 0.5 mm further inside the moulded sample.

Measurement of the modulus

The samples were tested on a Zwick 1445 tensile tester with a 10 kN force cell. For the modulus measurement Zwick clip-on extensometers were used. The test speed was 5 mm per minute and the temperature was 23 °C.

3.4 Results and Discussion

3.4.1 Silicate content, matrix crystallinity and T_g

The silicate levels as measured with TGA and the results are shown in the first row in table 3.1. These values were used to calculate the silicate volume fraction, which is shown in the second row of table 3.1.

Properties nanocomposites	PA6	2.6 %	4.7 %	6.8 %	8.3 %	10.6 %
wt % silicate (TGA)	0	2.6	4.7	6.8	8.3	10.6
vol% silicate	0	1.1	1.9	2.8	3.5	4.5
Fraction α crystals (vs α+γ crystals)	0.9	0.5	0.25	0.2	0.15	0.15
wt% crystalline PA6 in PA6	36.3	36.5	36.0	35.0	33.8	33.2
vol% surfactant in matrix	0	1.5	2.8	4.1	5.1	6.7
vol% crystalline PA6 in matrix	33.4	33.4	32.8	31.4	30.1	29.1

Table 3.1: Results TGA and DSC with calculated volume fractions.

The melting curves of the first heating sequence in the DSC measurements are shown in figure 3.3 (curves are shifted up for clarity).

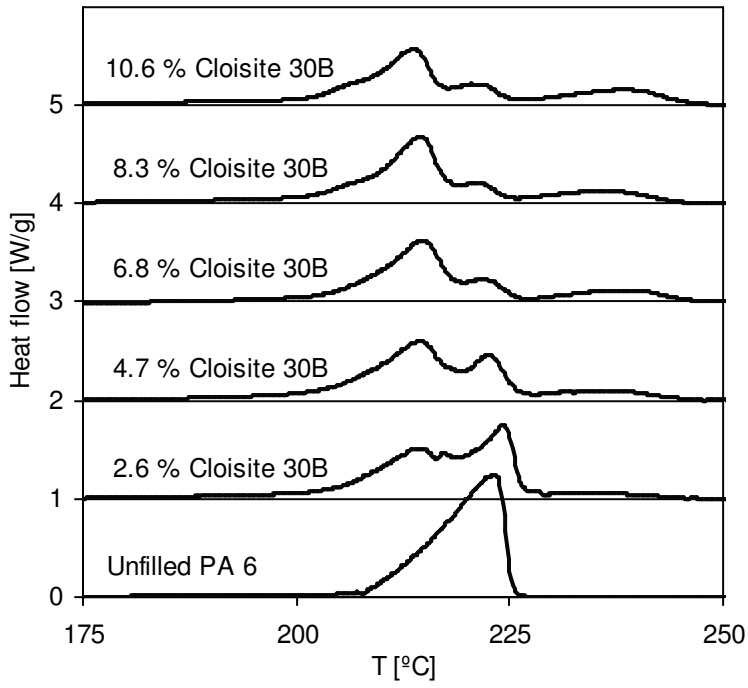


Figure 3.3: DSC melting curves first heating (curves are shifted up for clarity).

The peak surface for the γ crystal phase around 213 °C increases while the peak surface for the α crystal phase around 220 °C decreases upon addition of silicate. In addition a new peak around 240 °C appears, which is also associated with the γ crystal phase, as was shown by IR results [5]. The higher melting point could be the result of a higher lamellar thickness or of a stabilization of the crystals due to interactions with the silicate. The ratio of α to γ phase is estimated based on the relative peak areas in the DSC curves (fourth row in table 3.1). The exact value of the ratio does not influence the results much because the heat of melting is very similar. The results for the heat of melting in combination with the α to γ crystal ratio are used to calculate the percentage crystallinity in the samples. The crystallinity (wt%) based on the total PA6 content is shown in the third row of table 3.1. In the last two rows of table 3.1 the volume fractions of surfactant and crystalline PA6 are shown with respect to the total matrix of the nanocomposite, so this includes the PA6 and surfactant, but not the silicate filler. It can be seen that the volume fraction of crystalline matrix decreases slightly with increasing silicate content, while the surfactant fraction increases. Both changes probably lead to a reduction in matrix modulus at increasing filler levels, because the amorphous modulus is lower than the

crystalline modulus and the surfactant does not add stiffness to the polymer. These results are used in the Halpin-Tsai model for the calculation of the matrix modulus.
The glass transition temperatures determined from the loss peak of the DMA measurements are 65 °C for the dry PA6, 25 °C for the PA6 with 3 wt% water and 0 °C for the PA6 with 6% water. The T_g's were similar in unfilled PA6 and nanocomposites for similar water content.

3.4.2 Silicate platelet and crystalline orientation

Two typical 2D WAXS scattering spectra are displayed in figure 3.4. The intensity rings at high scattering angles relate to the crystalline PA6 phases.

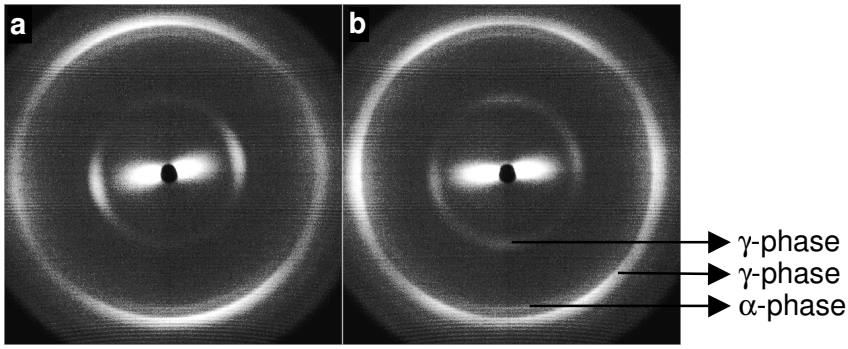


Figure 3.4: WAXS spectrum 4.7% Cloisite® 30B nanocomposite.
a) 1 mm from the edge, b) 0.5 mm from the edge

The brightest high angle ring is associated with the γ-phase and the fainter ring inside is associated with the α-phase, the ring at intermediate angles is also associated with the γ-phase [13]. It can be seen from figure 3.4 that for a given spatial position inside the moulded bar, partial orientation of crystallites is observed. Such partial crystal orientation is strongly coupled to the observed oriented central scattering pattern present at smaller angles. This central scattering is the high angle limit of the form factor of the silicate platelets that are oriented with the flow direction. Although there is partial coupling between the orientation of platelets and the crystallites, the full dependence of crystal orientation inside the macroscopic sample seems a complex issue. This can be seen from the comparison of figures 3.4a and for 3.4b taken at two neighbouring positions inside the sample: in figure 3.4a the crystallite scattering seems to fully align with the platelets (central scattering) while in figure 3.4b, it seems that a biaxial orientation is present. Also, as it can be seen from the same figures, the α and γ phases seem to orient differently along the sample. Furthermore, the

average crystal orientation along the macroscopic sample may be evaluated by considering data grouped along the 2θ direction for different positions within the sample as displayed in figure 3.5.

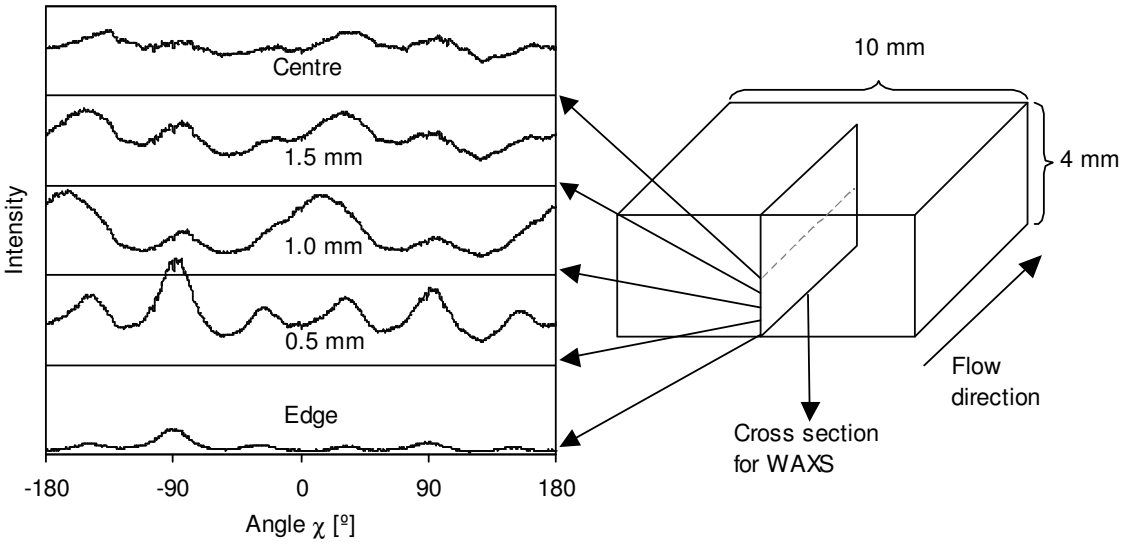


Figure 3.5: WAXS peaks for the γ-crystalline phase (peak around 21°) at various depths within the injection moulded sample (4.7 wt% Cloisite® 30B). Curves are shifted up for clarity; the horizontal line below each curve is the baseline. On the right the orientation of the cross section within the injection moulded test bar is shown. It is also shown at which points the measurements were done.

It can be seen from data on the γ phase that even from this phase, which is strongly induced by the silicate surface, crystal orientation at different positions along the sample seem to be uncorrelated. It is therefore reasonable to assume an average random orientation of crystallites along the macroscopic sample.

The absence of an inter-particle maximum in the scattering spectra indicates a very high degree of exfoliation. Consequently, the quantification of a degree of alignment by considering a silicate peak is impossible using WAXS. One way to relatively estimate the variation of the degree of orientation of the platelets along the sample is to consider integrating the data associated with the shoulder of the central scattering around the beam stop along the 2θ direction. It was decided to arbitrarily integrate data in 2θ between 1.1° (next to the beam stop) and 7.9°. The resulting intensity as a function of the azimuthal angle χ is displayed in figure 3.6. In order to estimate the orientation, the "shoulder width" at half of the peak height was then calculated for each position along the sample and the values are displayed in figure 3.6. They vary between 10 and 19°, suggesting a very high degree of orientation along the sample.

Performing the same set of measurements on the perpendicular cross section of the moulded bar we were able to construct a map of the platelets alignment through the entire cross-section of the injection moulded sample and subsequently calculate an average orientation. The average "shoulder width" at this local length scales is 13.7° and $\langle\cos^2(\delta\chi)\rangle = 0.94$. This value is close to 1, which is an indication of a very good alignment of the platelets in injection moulded samples, and it confirms the results of several authors [2,22,23]. The real orientation is probably even higher, as it would require deconvolution of the scattering signal with the x-ray line width. In any case, it seems to be a reasonable assumption that there is a very high degree of platelets orientation in the mechanical modelling below. Any misalignment that might affect the calculated effective aspect ratio has the same influence on all moisture concentrations, and will not influence the conclusions.

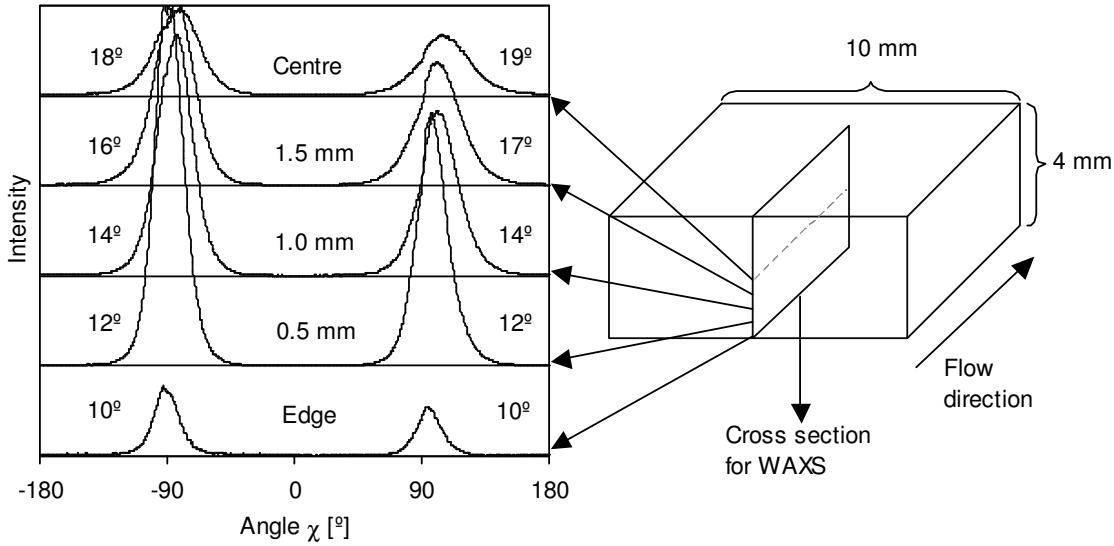


Figure 3.6: WAXS results for the shoulder of the central scattering around the beam stop, which is used to estimate the orientation of the layered silicate at various depths. (4.7 wt% Cloisite® 30B). Curves are shifted up for clarity; the horizontal line below each curve is the baseline. The angles next to the peaks are the width at half the height. On the right the orientation of the cross section within the injection moulded test bar is shown. It is also shown at which points the measurements were done.

3.4.3 Calculation of the modulus of the matrix phase

The moduli of the amorphous part of the matrix (consisting of amorphous PA6 and surfactant), which are used in the calculation of the nanocomposite matrix modulus, are shown in the fourth row in table 3.2.

Properties matrix (PA6 + surfactant)	**Pure PA6**	**2.6 %**	**4.7 %**	**6.8 %**	**8.3 %**	**10.6 %**
wt % silicate (TGA)	0	2.6	4.7	6.8	8.3	10.6
vol % surfactant in matrix	0	1.52	2.79	4.11	5.12	6.71
Volume fraction surfactant in the amorphous matrix	0	0.022	0.042	0.060	0.073	0.093
$E_{\text{amorphous matrix}}$, dry [GPa]	2.20	2.15	2.11	2.07	2.04	2.00
$E_{\text{amorphous matrix}}$, 3% water [GPa]	0.31	0.30	0.30	0.29	0.29	0.28
$E_{\text{amorphous matrix}}$, 6% water [GPa]	0.038	0.037	0.037	0.036	0.036	0.035

Matrix moduli (calculated)	**Pure PA6**	**2.6 %**	**4.7 %**	**6.8 %**	**8.3 %**	**10.6 %**
E_{matrix}, dry [GPa]	3.10	3.06	3.01	2.94	2.87	2.81
E_{matrix}, 3% water [GPa]	1.29	1.28	1.25	1.20	1.15	1.09
E_{matrix}, 6% water [GPa]	0.82	0.82	0.80	0.76	0.72	0.67

Table 3.2: Results matrix modulus calculation with the Halpin-Tsai model

The modulus of dry PA6 is 3.10 GPa (measurement) and the amorphous modulus of dry PA6 is assumed to be 2.2 GPa (calculated from measurements [16]). With the Halpin-Tsai model a crystalline modulus of 5.25 GPa is calculated based on the crystalline volume fraction as shown in table 3.2. This value for the crystalline modulus is similar to literature data, calculated from PA6 fibres [24]. It is assumed in the model that the α and γ crystals have equal moduli, which is believed to be a reasonable assumption because the hydrogen bond density is very similar. The value of 5.25 GPa for the crystalline phase is assumed to be independent of moisture conditioning and is used in all further calculations.

The Halpin-Tsai model is also used to estimate the amorphous modulus in moisture conditioned samples. The measured values for moisture conditioned PA6 are 1.29 GPa for 3% water and 0.82 GPa for 6% water, and with the value of 5.25 GPa for the crystalline modulus this leads to the amorphous moduli shown in table 3.2. For a moisture level of 3% the calculated amorphous modulus is 0.31 GPa and for a moisture level of 6% it is 0.038 GPa; this large drop in amorphous modulus is expected because at 3 % water the amorphous part of the PA6 has crossed T_g, reaching the rubber plateau. In the fourth row the results for the dry amorphous modulus at the various filler levels are shown, in the fifth and sixth row the results for the moisture-conditioned amorphous moduli are shown. The decrease in the amorphous modulus with increasing silicate content is caused by the increasing amount of surfactant.

In the next step for each silicate concentration and moisture content a value for the nanocomposite matrix modulus was calculated using the Halpin-Tsai equation. The

values for the modulus (5.25 GPa) and the aspect ratio (L/D=1000) of the crystalline lamellae are chosen to be constant. For each sample the specific crystalline volume fraction (table 3.1) and the amorphous matrix modulus (table 3.2) were used.

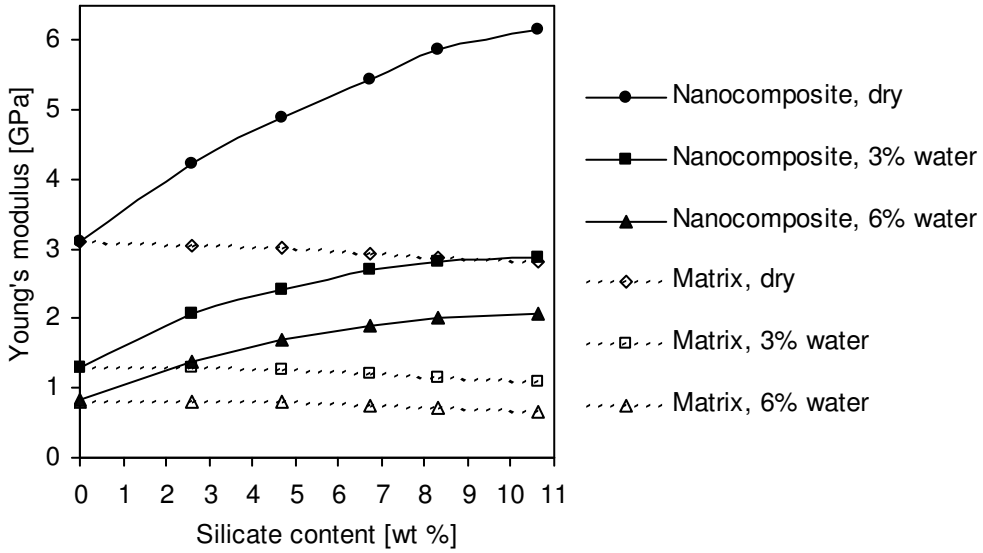


Figure 3.7: Influence of silicate and moisture content on the Young's modulus

The resulting nanocomposite matrix modulus for each sample is shown in the last three rows of table 3.2 and in figure 3.7. The results of the calculated matrix moduli are independent on the average orientation or on the aspect ratio of the crystalline plates that is assumed. This is because the modulus of the moisture-conditioned amorphous phase is basically a fit-parameter to describe the measured modulus of the moisture-conditioned unfilled PA6 samples. Therefore, if the aspect ratio would be assumed to be smaller, the estimated modulus of the moisture conditioned amorphous matrix would be higher, and vice versa. The same applies for the orientation; if the platelets would not be considered completely random but partially aligned, the model would result in a lower amorphous matrix modulus. The calculated dependence of the matrix modulus on the silicate content is independent on the crystalline aspect ratio or orientation (within reasonable limits). It is important to realize that the Halpin-Tsai model that is used to calculate the matrix modulus is not intended to provide an accurate prediction of the aspect ratio of the crystalline lamellae or the moduli of the different phases. It is only used to calculate the influence of the modified silicate particles on the matrix modulus by introducing the effect of the surface modification and the small change in crystallinity.

3.4.4 Modulus of the nanocomposites and calculation of the aspect ratios

Modulus

The measured results for the tensile modulus of the nanocomposite samples at various moisture contents and silicate concentrations are shown in figure 3.7, along with the calculated matrix moduli that are used in the model. A reduction of the modulus is clear for both the unfilled polymer (at 0% silicate) and the nanocomposites when water is absorbed during conditioning.

Nanocomposite moduli	**Pure PA6**	**2.6 %**	**4.7 %**	**6.8 %**	**8.3 %**	**10.6 %**
Dry [GPa]	3.10	4.21	4.88	5.44	5.86	6.21
3% water [GPa]	1.29	2.07	2.41	2.70	2.81	2.86
6% water [GPa]	0.82	1.39	1.69	1.90	2.01	2.07

Effective aspect ratios	**2.6 %**	**4.7 %**	**6.8 %**	**8.3 %**	**10.6 %**
Dry	152	114	95	89	70
3% water	155	110	94	82	64
6% water	145	117	102	94	75

Table 3.3: Nanocomposite moduli and calculated aspect ratios from Halpin-Tsai model

The previously calculated matrix moduli (see table 3.2) were used in the Halpin-Tsai model to calculate the effective aspect ratios. These calculated aspect ratios are shown in the last three rows in table 3.3 and in figure 3.8.

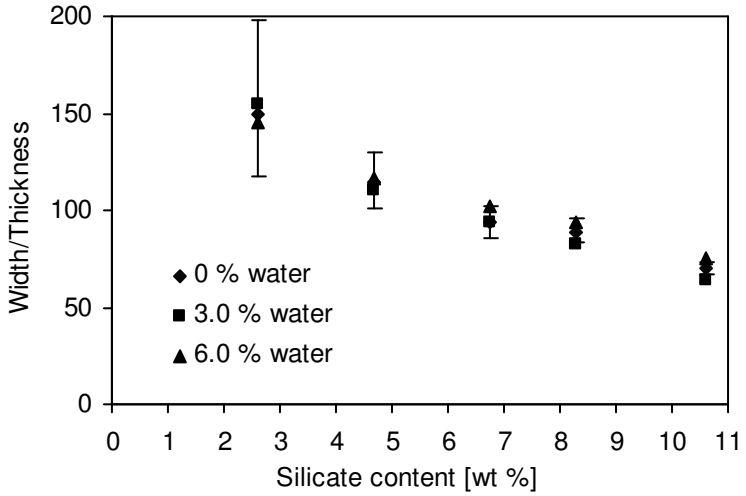


Figure 3.8: Calculated aspect ratios versus silicate content

The calculated effective aspect ratios are based on particles aligned with their long dimensions along the test axis, which is a reasonable assumption as was shown in section 3.4.2. It can be seen in figure 3.8 that the effective aspect ratio decreases with increasing silicate content, which can be explained by a less effective exfoliation at higher silicate loadings. The reduced exfoliation at higher silicate content has been shown previously by several authors [5,25,26]. It is also in agreement with calculations based on diffusion data (chapter 2) and melt-viscosity data (chapter 5).

The most important result from these aspect ratio calculations is the fact that the data for three different moisture contents overlap in figure 3.8. This shows that the modulus of a nanocomposite can be explained by the combination of a very stiff filler particle with a high aspect ratio and the normal matrix modulus, which in this case is varied by changing the moisture content. Apparently, the Halpin-Tsai composite theory can be used to describe the modulus of nanocomposites for a wide variety of matrix moduli, both below and above T_g of the matrix polymer, with the same aspect ratio for all matrix moduli. The fact that the modulus of nanocomposites can be explained by the Halpin-Tsai theory, independent of the modulus of the matrix, proves that the reinforcing mechanism in nanocomposites is similar to traditional composites. No additional stiffening of the matrix due to confinement of the polymer has to be assumed to explain the high modulus of nanocomposites.

To show the influence of errors in the modulus measurements, error bars are displayed for the dry series in figure 3.8 (for clarity the other series do not show the error bars). The error bars correspond to a constant error of $\pm$ 0.1 GPa in the modulus measurement. It can be seen that at low silicate concentrations a small error in the modulus measurement has large effects on the calculated aspect ratio; however, for higher concentrations the error is much smaller and the calculated aspect ratios are more reliable. It is clear that based on these calculations it has to be concluded that the effective reinforcing effect of the particles seems to decrease with increasing silicate loading. The effective aspect ratios from the model are realistic values: the aspect ratios are between 70 and 150, which is in the range of what can be observed in the TEM image shown in figure 3.9. With increasing concentration the exfoliation becomes less perfect, resulting in an effective aspect ratio that is half of the highest value. This means that when perfect exfoliation is assumed in the low concentrations, an average stack size of 2 platelets is present in the highest concentrations.

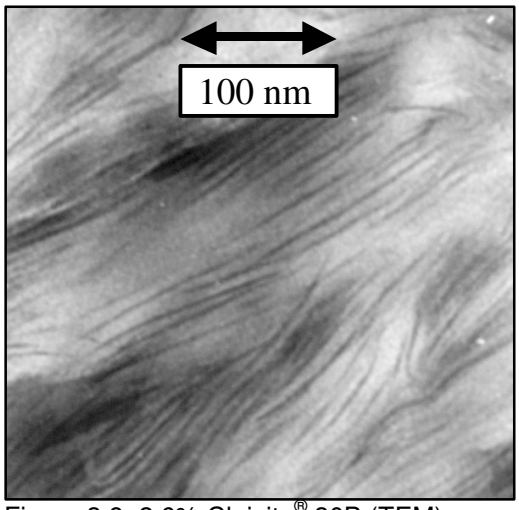


Figure 3.9: 2.6% Cloisite® 30B (TEM)

As a final point of discussion it is emphasized that the Halpin-Tsai model is a semi-empirical model. The aspect ratio's reported here are, therefore, effective values, incorporating effects of distribution, polydispersity and shape variability. It appears from this study that the Halpin-Tsai model is sufficiently accurate to describe the reinforcing power of nano-platelets in a single parameter, the effective aspect ratio. Note that the effective aspect ratio is more than a fitting parameter, since the nanocomposite modulus at all the different moisture levels can be explained by the same effective aspect ratio (for each silicate content).

3.5 Conclusions

Because the modulus of the PA6 matrix can be adjusted by varying the amount of absorbed water, the nanocomposite series used in this study is very useful to investigate if the nanocomposite modulus can be described with a conventional composite theory such as the Halpin-Tsai theory.

The layered silicate used in this study induces a different crystalline phase in the polymer, and causes a small reduction of the crystallinity. WAXS measurements on the injection-moulded samples have shown that the PA6 crystals show a certain degree of alignment at the local level. However, when all different areas and both crystal phases are considered, the average alignment in the entire sample seems to be almost isotropic. Therefore, the Halpin-Tsai model with shape factors for platelet-shaped reinforcement and random alignment is used to estimate the modulus of the matrix in the nanocomposites as a function of crystallinity and surfactant content. The

calculations show that with increasing silicate content the matrix modulus decreases slightly compared to the reference polymer, due to the reduced crystallinity and the dilution of the matrix by the surfactant.

The WAXS measurements through the cross section revealed that the silicate layers are very well aligned in the flow direction in most of the sample volume. The calculated matrix modulus and the measured nanocomposite modulus for each sample is used in the Halpin-Tsai model for aligned platelets to calculate the effective aspect ratio of the silicate platelets for each concentration and moisture content. If the nanocomposite modulus is governed by the same mechanism as traditional composites, the effective aspect ratios that are calculated with the model should not depend on the matrix modulus. This is indeed found to be the case; all nanocomposites with different moisture content can be described with one aspect ratio for each silicate concentration. With increasing silicate concentration the calculated effective aspect ratio decreases, probably because of a reduced exfoliation of the silicate filler at higher loading. The effective aspect ratios derived from the model show a good similarity with the aspect ratios as they are observed in transmission electron microscopy, and the reduction of the effective aspect ratio can be explained by the appearance of small stacks of on average two platelets at the highest concentration. Therefore, it can be concluded that the high aspect ratio and high modulus of the platelets are the main reason for the strong increase of the modulus at a much lower filler content compared to micro-composites. The present results show that with the same microstructure (i.e. equal aspect ratio particles) the model is able to predict the measured modulus without requiring any major change of the matrix properties. The small change in modulus due to the different crystallinity and the addition of surfactant molecules was taken into account. In addition, a reduced mobility of the polymer phase would be unlikely to have much effect at temperatures below T_g, since the amorphous phase is rigid at those temperatures, but would have a larger influence above T_g. The Halpin-Tsai composite theory can be used to describe the modulus of nanocomposites both below and above T_g of the matrix polymer using the same aspect ratios. The results described here for different matrix moduli support the theories of Van Es and Fornes [1,2]. The shape and modulus of the reinforcing particles is sufficient to account for the observed moduli, without a special influence of their exceptionally small size or surface area, and without significantly influencing the modulus of the matrix. Changes on the molecular level due to the presence of the silicate layers apparently only have a small influence on the modulus. The reduced efficiency of reinforcement of the silicate sheets at increasing filler levels can be partially explained by the reduction of the matrix

modulus due to the presence of surfactant and reduced crystallinity, and partially by the occurrence of small stacks of platelets.

3.6 References

1. Es MAv, Xiqiao F, Turnhout Jv, Giessen Evd. Comparing Polymer-Clay Nanocomposites with Conventional Composites using Composite Modeling. In: Al-Malaika Sea, editor. Specialty Polymer Additives: Blackwell Science; 2001.
2. Fornes TD, Paul DR. Modeling properties of nylon 6/clay nanocomposites using composite theories. Polymer 2003;44(17):4993-5013.
3. Yoon PJ, Fornes TD, Paul DR. Thermal expansion behavior of nylon 6 nanocomposites. Polymer 2002;43(25):6727-6741.
4. Okada A, Usuki A. The chemistry of polymer-clay hybrids. Materials Science & Engineering C 1995;3(2):109-115.
5. Es MAv. Polymer clay nanocomposites. The importance of particle dimensions. Delft: Delft University of Technology; 2001.
6. Shelley JS, Mather PT, DeVries KL. Reinforcement and environmental degradation of nylon-6/clay nanocomposites. Polymer 2001;42(13):5849-5858.
7. Kojima Y, Usuki A, Kawasumi M, Okada A, Fukushima Y, Kurauchi T, Kamigaito O. Mechanical-Properties of Nylon 6-Clay Hybrid. Journal of Materials Research 1993;8(5):1185-1189.
8. Giannelis EP. Polymer layered silicate nanocomposites. Advanced Materials 1996;8(1):29.
9. Usuki A, Koiwai A, Kojima Y, Kawasumi M, Okada A, Kurauchi T, Kamigaito O. Interaction of Nylon-6 Clay Surface and Mechanical-Properties of Nylon-6 Clay Hybrid. Journal of Applied Polymer Science 1995;55(1):119-123.
10. Hasegawa N, Okamoto H, Kato M, Usuki A, Sato N. Nylon 6/Na–montmorillonite nanocomposites prepared by compounding Nylon 6 with Na–montmorillonite slurry. Polymer 2003;44(10):2933-2937.
11. Vlasveld DPN, Bersee HEN, Picken SJ. Moisture Absorption in Polyamide-6 Silicate Nanocomposites and its Influence on Mechanical Properties. Polymer (Revised version under review) 2005.
12. Kojima Y, Usuki A, Kawasumi M, Okada A, Kurauchi T, Kamigaito O. Sorption of Water in Nylon-6 Clay Hybrid. Journal of Applied Polymer Science 1993;49(7):1259-1264.
13. Kohan MI. Nylon Plastics Handbook: Carl Hanser Verlag; 1995.
14. Halpin JC, Kardos JL. Halpin-Tsai Equations - Review. Polymer Engineering and Science 1976;16(5):344-352.
15. Halpin JC. Stiffness and Expansion Estimates for Oriented Short Fiber Composites. Journal of Composite Materials 1969;3:732-.
16. Bureau MN, Denault J, Cole KC, Enright GD. The role of crystallinity and reinforcement in the mechanical behavior of polyamide-6/clay nanocomposites. Polymer Engineering and Science 2002;42(9):1897-1906.
17. Hsia KJ, Xin YB, Lin L. Numerical-Simulation of Semicrystalline Nylon-6 - Elastic-Constants of Crystalline and Amorphous Parts. Journal of Materials Science 1994;29(6):1601-1611.
18. Shell HR, Ivey KH. Fluorine Micas: Bureau of Mines, US Department of the Interior; 1969.
19. Akzo Nobel Surface Chemistry website. 2004.
20. Fornes TD, Paul DR. Crystallization behavior of nylon 6 nanocomposites. Polymer 2003;44(14):3945-3961.
21. Rothon R. Particulate-filled polymer composites: Longman; 1995.
22. Kojima Y, Usuki A, Kawasumi M, Okada A, Kurauchi T, Kamigaito O, Kaji K. Novel Preferred Orientation in Injection-Molded Nylon 6-Clay Hybrid. Journal of Polymer Science Part B-Polymer Physics 1995;33(7):1039-1045.

23. Varlot K, Reynaud E, Kloppfer MH, Vigier G, Varlet J. Clay-reinforced polyamide: Preferential orientation of the montmorillonite sheets and the polyamide crystalline lamellae. Journal of Polymer Science Part B-Polymer Physics 2001;39(12):1360-1370.
24. Murthy NS, Grubb DT. Deformation of lamellar structures: Simultaneous small- and wide-angle X-ray scattering studies of polyamide-6. Journal of Polymer Science Part B-Polymer Physics 2002;40(8):691-705.
25. Liu L, Qi Z, Zhu X. Studies on Nylon 6/Clay Nanocomposites by Melt-intercalation Process. Journal of Applied Polymer Science 1999;71:1133-1138.
26. Akkapeddi MK. Glass fiber reinforced polyamide-6 nanocomposites. Polymer Composites 2000;21(4):576-585.

The results described in this chapter have been published as:

D.P.N. Vlasveld, J. Groenewold, H.E.N. Bersee, E. Mendes, S.J. Picken, Analysis of the modulus of polyamide-6 silicate nanocomposites using moisture controlled variation of the matrix properties. Polymer 2005 (46) 6102-6113.

Chapter 4

A comparison of the temperature dependence of the modulus, yield stress and ductility of nanocomposites based on high and low MW PA6 and PA66.

4.1 Introduction

Nanocomposites based on a PA6 matrix containing exfoliated layered silicate particles have been produced by in-situ polymerization of ε-caprolactam [1-3] and by high shear mixing in the melt in an extrusion process [4-9]. In both processes an organic modification on the silicate layers is necessary to achieve good exfoliation. An alternative type of process has recently been reported, in which unmodified layered silicate has been used to reach an adequate level of exfoliation in PA6 [10,11]. In this process water is used to swell the silicate layers and make the inter-gallery accessible for the polymer and thereby improve exfoliation. The possibility to use unmodified silicate is interesting because of the potential reduction of the raw materials cost, the increased thermal stability due to the absence of the thermally unstable surfactants and the lower viscosity of this type of nanocomposite due to the reduced degree of exfoliation [12] (see also chapter 5).
The interaction between the polymer chain and the silicate for the three types of PA6 nanocomposite are schematically shown in figure 4.1.

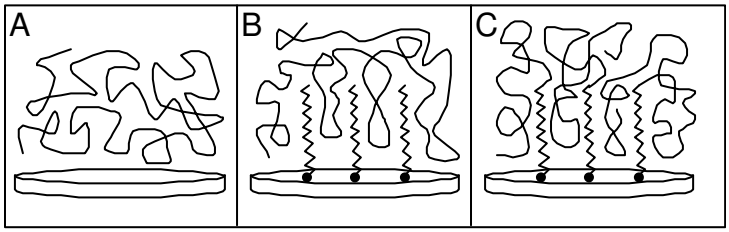


Figure 4.1: Schematic representation of the three types of nanocomposite used:

A Non-modified silicate with polymer,

B Modified silicate mixed with polymer (melt-mixed),

C Modified silicate connected with polymer (in-situ polymerization)

Figure 4.1A shows the non-modified silicate nanocomposite, figure 4.1B shows the melt-exfoliated modified silicate nanocomposite in which the surfactant chains are mixed with the polymer, and figure 4.1C shows the in-situ polymerised nanocomposite in which the polymer has reacted with the surfactant resulting in ionic bonds with the silicate particles. In this chapter these three types will be investigated and compared.

In extrusion processes the degree of exfoliation does not only depend on favourable thermodynamic interactions between the polymer chains and the surfactant, but also on the amount of shear that can be transmitted to the particles [13]. Therefore intermeshing twin screw extruders are capable of producing a better exfoliation than single screw extruders, and high shear screw designs provide better results than low shear screws [8]. Apart from the type of mixer, also the type of matrix material plays a role in the amount of stress that can be transferred to the platelets. It has been shown that a higher molecular weight of the polymer can result in an improved exfoliation, and therefore higher moduli [14], although the effects on the modulus are not that large. The yield stress of PA6 nanocomposites usually increases upon addition of layered silicate, but at higher silicate content samples often become brittle, resulting in a lower strength at high silicate content [7,15]. The more brittle fracture behaviour of PA6 nanocomposites is evident from the large reduction in elongation at break shown in chapter 2 and reported by several authors [7,8,14,16-18]. It has been shown that the elongation at break in nanocomposites depends on the molecular weight of the matrix polymer; a higher MW leads to much higher elongations [14]. It is often reported that impact strength is not much affected by the addition of layered silicate fillers, but the values reported are usually of brittle fractures in all cases, including the unfilled reference polymer [7,19]. In the case of brittle fractures not much influence of the filler can be measured, only at elevated temperatures the PA6 matrix polymer becomes ductile in notched impact tests [6] and can be compared with the nanocomposites. Increasing the test temperatures will eventually lead to ductile fracture behaviour, as was shown for both in-situ polymerized and melt processed nanocomposites [6,19,20]. It has been shown that in nanocomposites the temperature at which the samples becomes ductile (T_{bd}) increases more or less linearly with increasing silicate content [6].

The fracture behaviour of polymers depends on many molecular factors such as the chain architecture, the molecular weight and the intermolecular order of the polymer (such as crystallinity), and in addition on test conditions such as test speed, temperature and sample size [21,22]. In composites also stress concentrations, the size and orientation of the particles and the interfacial adhesion play a role. In

general the transition from brittle to ductile fracture behaviour is explained by the existence of two different failure mechanisms, one leading to brittle failure and one leading to ductile shear yielding. In this scheme, known as the Ludwig-Davidenkov-Orowan hypothesis [23], the failure mechanism that requires the lowest stress under certain conditions is the one determining the failure mechanism: when the yield stress is lower than the brittle failure stress ductile failure occurs, when the brittle stress is lower brittle failure occurs. Because the brittle failure mechanism is less temperature dependent than the yield stress, which decreases strongly with increasing temperature, a temperature exists above which the failure behaviour becomes ductile. This transition temperature is known as the brittle to ductile transition temperature (T_{bd}). The brittle fracture stress is increased by increasing the molecular weight of the polymer, both for amorphous and for semi-crystalline polymers, which causes a reduction of T_{bd}. The underlying mechanism for this is that higher MW chains can form more intermolecular connections such as entanglements in amorphous polymers and tie-chains in semi-crystalline polymers. These connections between the chains form a network with improved load carrying capabilities, which increases the ductility. The effect of MW is especially strong at MW below 20000, such as is the case in PA6, at very high MW (>100000) the effects are less pronounced [21]. Increasing crystallinity increases the modulus and the yield stress, decreases the ductility and increases T_{bd} [23]. For polyamide 66 it has been shown that reduction of the size of the spherulites increases the modulus and yield stress, while reducing the elongation at break [24]. In (nano)composites the reinforcing particles can influence the fracture behaviour by additional factors such as the introduction of stress concentrations, other deformation mechanisms and by influencing the intermolecular structure.

In the last years several authors have reported the successful production of polyamide 66 (PA66) nanocomposites [25-29] with a similar extrusion process as used for PA6 nanocomposites. One important issue with respect to the production of PA66 nanocomposites is the thermal stability of the surfactant molecules. It is known that the most commonly used quaternary ammonium surfactants are not very stable at temperatures above 200 °C [30]. It has been shown that the combination of high processing temperatures in combination with high shear stresses causes even more degradation than at high temperatures without shear. For short processing times the degradation is not much of a problem in the case of PA6 (processed at 230-240 °C), but at the temperatures required for PA66 melt processing (minimum 270 °C) the problem is more serious. It has been reported that PA66 nanocomposites cannot be

made via the same process and with the same modified silicates [29], while other authors have shown that it is possible, with reasonably good results [25].

In this chapter the mechanical properties of various types of polyamide nanocomposite are described. Various concentrations of organically modified silicate in two different MW PA6 matrix materials are compared. In addition, nanocomposites with several silicate concentrations in PA66 have been prepared, using the same modified silicate. The two different MW PA6 matrix materials are also used to make a nanocomposite with the same silicate without surfactant, to compare the influence of the surfactant on exfoliation and mechanical properties. All these nanocomposites have been tested over a temperature range varying from 20 °C to 120 °C, to compare the modulus, yield stress and fracture behaviour. From this data brittle to ductile transitions are determined and the influence of the matrix polymer and the type of modification becomes clearer.

4.2 Experimental

4.2.1 Material

Polyamide 6, low molecular weight (LMW PA6)

- Akulon® K222D, injection-moulding grade PA6 from DSM, the Netherlands.
  M_n = 16000, M_w = 32000 g/mol, T_m = 220 °C
  (Similar in properties to K122D and K123D used in other chapters.)

Polyamide 6, high molecular weight (HMW PA6)

- Akulon® K136, film / extrusion grade PA6 from DSM, the Netherlands.
  M_n = 35600, M_w = 71000 g/mol, T_m = 220 °C

Polyamide 66, low molecular weight (PA66)

- Akulon® S223D, injection-moulding grade PA66 from DSM, the Netherlands.
  M_n = 16000, M_w = 32000 g/mol, T_m = 260 °C

Commercial polyamide 6 nanocomposites

Two commercial PA6 nanocomposites are used (MW unknown):

- From Ube, Japan, containing 2.5% silicate.
- Unitika M1030D, from Unitika, Japan, containing 4.6% silicate.

These nanocomposites are made by in-situ hydrolytic polymerization of ε-caprolactam in the presence of swollen organically modified silicates. The organic

surfactant is the initiator for polymerization, so the polymer chains are bound to the surfactant via covalent bonds. Because the surfactants have an ionic bond with the silicate layers, the polymer is ionically bound to the silicate layers, unlike in the melt-processed nanocomposites.

Organically modified layered silicate

- Somasif® MEE (Synthetic Mica®) from Unicoop, Japan.
  This is synthetic fluorine mica, covered with a methyl bis-2-hydroxyethyl coco quaternary ammonium surfactant (28.5 wt%).

The manufacturer has added the organic surfactant on the silicate platelets, and the amount of organic surfactant was determined with thermo-gravimetric analysis (TGA) in a Perkin Elmer TGA-7 Thermal Gravimetric Analyzer at 800 °C for 1 hour in air.

Unmodified layered silicate

- Somasif® ME-100 (Synthetic Mica®) from Co-op Chemicals, Japan.
  This is water-swellable synthetic fluorine mica, which does not contain any organic surfactant. The inorganic part is identical to Somasif® MEE.

4.2.2 Preparation

Extrusion

The nanocomposites with Somasif® MEE were prepared by mixing in PA6 and PA66 in a Werner and Pfleiderer ZDS-K28 co-rotating twin-screw extruder. The screw layout was designed to produce high shear stresses, achieved by incorporating several kneading blocks followed by small backflow elements. The modified layered silicate powder was mixed with the polymer granules and fed into the extruder at a constant rate via a Plasticolor 2500 feeding unit. The extruder was operated at a screw speed of 200 RPM and a feeding rate of approximately 3 kg per hour.

The temperature in the feeding zone was 150 °C, for PA6 all the other zones where heated to 230 °C and for PA66 all the other zones where heated to 270 °C. Cooling was applied to keep the temperature constant since the high shear forces in the melt can produce too much heat.

First a master batch with a high concentration (11.9 wt% for PA6, 10.3 wt% for PA66, based on the inorganic content of the filler) was made. Other concentrations were made by diluting the master batch with unfilled polymer in a second extrusion step.

The nanocomposites with Somasif® ME-100 were made by feeding a mixture of cryogenically milled PA6 and ME-100 powder in a Werner and Pfleiderer ZSK 30/44 D co-rotating twin-screw extruder. To enhance the exfoliation of the water-swellable ME-100 silicate, water was injected into the extruder at a rate of 25 ml/min, and removed by venting at the end of the extruder. The extruder was operated at a temperature of 240 °C at a rotation speed of 200 rpm and a feeding rate of approximately 10 kg/h.

Injection moulding

Dumbbell shaped samples according to ISO 527 standards were injection moulded on an Arburg Allrounder 221-55-250 injection-moulding machine. For PA6 the feeding zone was heated to 150 °C, the melting and mixing zones heated to 240 °C and the nozzle was heated to 270 °C. For PA66 the melting and mixing zones were heated to 275 °C and the nozzle was heated to 290 °C.

4.2.3 Testing

Determination of silicate content

Thermo-gravimetric analysis (TGA) measurements were done to determine the exact silicate content in the tested samples after processing. A Perkin Elmer TGA-7 Thermal Gravimetric Analyzer was used to determine the weight fraction of silicate by heating a sample in air at 800 °C for 1 hour. The silicate levels mentioned are the weight percentages of the inorganic part of the filler as measured with TGA, the weight of the surfactant is not included in this value. The resulting ash had a black colour, which is caused by graphite layers that get formed between well-exfoliated silicate layers. These graphite layers are single layers [31], and therefore they cause only a negligible error in the calculated silicate content.

Conditioning

All samples have been tested dry; the injection-moulded samples were dried further in a vacuum oven at 80 °C for at least 48 hours before testing.

Measurement of the crystallinity

The level of crystallinity of the samples and the ratio of the two crystal phases, α and γ, was determined with Differential Scanning Calorimetry on a Perkin-Elmer DSC-7. DSC samples of approximately 5 mg were cut from the centre of the tensile test bar.

The DSC measurements were performed at a heating rate of 10 °C per minute between 25 °C and 270 °C. The crystallinity was calculated using a heat of fusion of 213 J/g for the gamma crystals, and 243 J/g for the alpha crystals [9,32].

Measurement of the glass transition temperature

The glass transition temperatures (T_g) of the samples were determined with Dynamic Mechanical analysis. Samples of 0.2 mm thick were pressed at 240 °C and tested in tension in a Perkin-Elmer DMA 7e at a temperature range from –100 °C to 200 °C. The temperature at the maximum of the loss modulus is used to represent T_g.

Mechanical properties

The samples were tested on a Zwick 1445 tensile tester with a 10 kN force cell, equipped with a climate chamber. For the modulus measurement Zwick clip-on extensometers were used. The test speed was 5 mm per minute and the temperature in the climate chamber was varied between 20 °C and 120 °C. For each temperature and composition five samples were tested to determine the average values.

4.3 Results and Discussion

4.3.1 Modulus

The modulus of the nanocomposites is plotted versus temperature in figure 4.2; figure 4.2A shows the results for low MW PA6, 4.2B for high MW PA6, 4.2C for PA66 and 4.2D for two commercial PA6 nanocomposites. The modulus increases with increasing silicate content and decreases with increasing temperature, as expected. The largest drop in modulus can be seen between 40 °C and 80 °C, which is the temperature range at which T_g is crossed. This causes a strong modulus decrease of the amorphous part of the polymer, but it is clear that the nanoparticles are also very effective for increasing the modulus above T_g. The three different matrix polymers have slightly different moduli and therefore the moduli of the nanocomposites have been divided by the matrix modulus to compare the efficiency of reinforcement between the various nanocomposites. This way the relative modulus ($E_{nanocomposite}$ / E_{matrix}) is calculated, and the values for 23 °C are shown in figure 4.3 as a function of silicate content. Figure 4.3 shows that the modulus increase for the high MW nanocomposites is comparable to the increase for low MW nanocomposites,

although previously a higher modulus for higher MW matrix polymers due to higher shear forces during extrusion has been reported [14]. Probably the exfoliation in the low MW nanocomposites was already very efficient due to the high shear screw design in the extruder; therefore the extra shear due to the higher MW does not improve the exfoliation much. However, the high melt viscosity of the high MW nanocomposites apparently induced some additional degradation due to extra heat created in the extrusion process, which resulted in a stronger discoloration in the high MW nanocomposites.

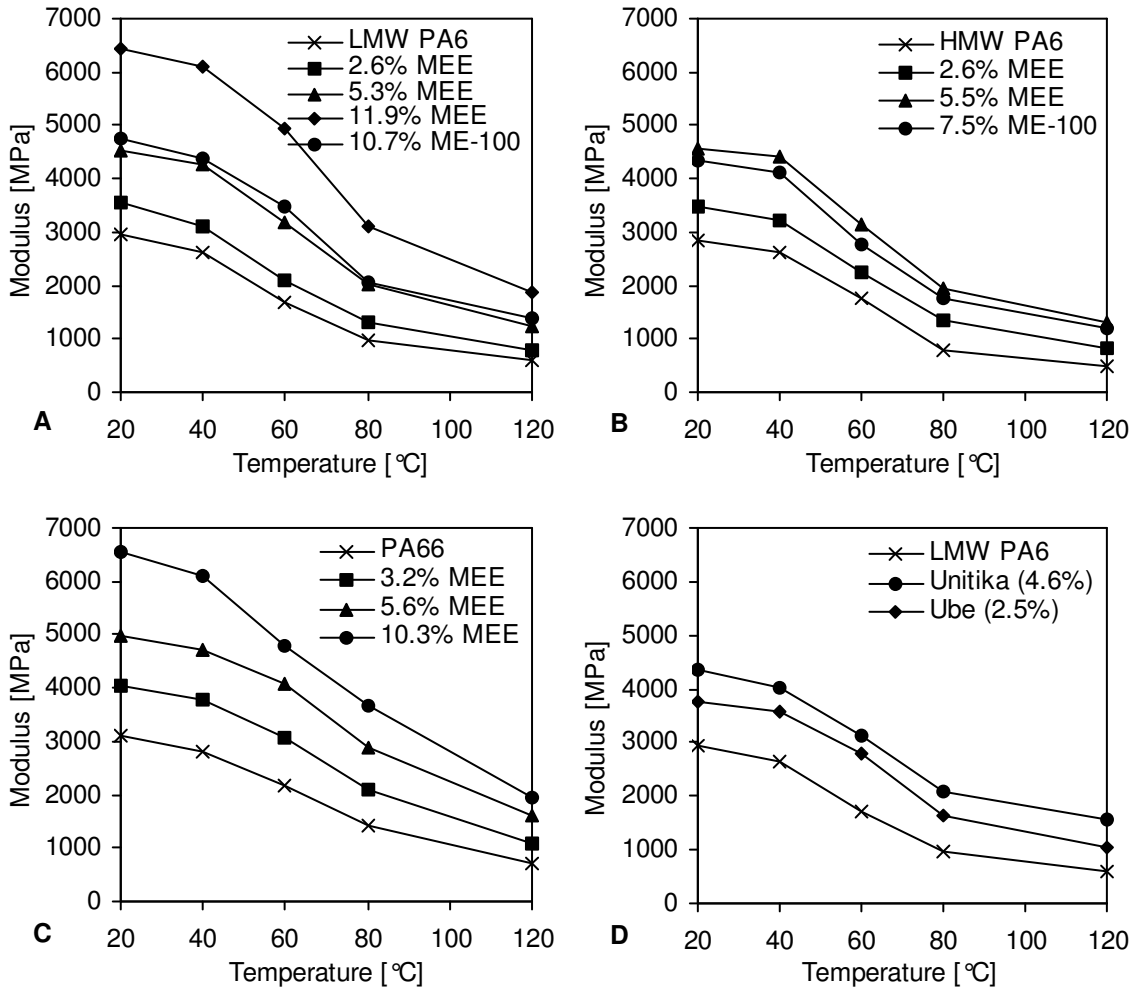


Figure 4.2: Young's modulus as a function of temperature,

A) Low MW PA6 nanocomposites, B) High MW PA6 nanocomposites,

C) Low MW PA66 nanocomposites, D) Commercial nanocomposites

If the moduli of the PA66 nanocomposites in figure 4.2C are compared with the nanocomposites based on the low MW PA6 in figure 4.2A (both have comparable MW), it is clear that the PA66 nanocomposites have a slightly higher modulus at all concentrations. The unfilled PA66 has a higher modulus than PA6, and from figure

4.3 it becomes clear that the increase in modulus with increasing silicate content is equal to the increase in PA6. The increase in modulus is higher than reported before for PA66 [25,28], while no difference in compatibilizer or mixing procedure compared to PA6 nanocomposites was necessary. Apparently, despite the higher processing temperatures the degradation of the surfactant was not so severe that the degree of exfoliation was reduced. It has been shown previously that increasing the extrusion temperature for PA6 nanocomposites from 240 °C to 280 °C does not have any significant influence on the mechanical properties [6]. In addition, no more discoloration was seen in these PA66 samples than in the low MW PA6 nanocomposites. These results for PA66 show that this type of organically modified silicate and the same extrusion process can be used just as effectively in nanocomposites based on PA66 as for those based on PA6, contrary to previous observations [29,33].

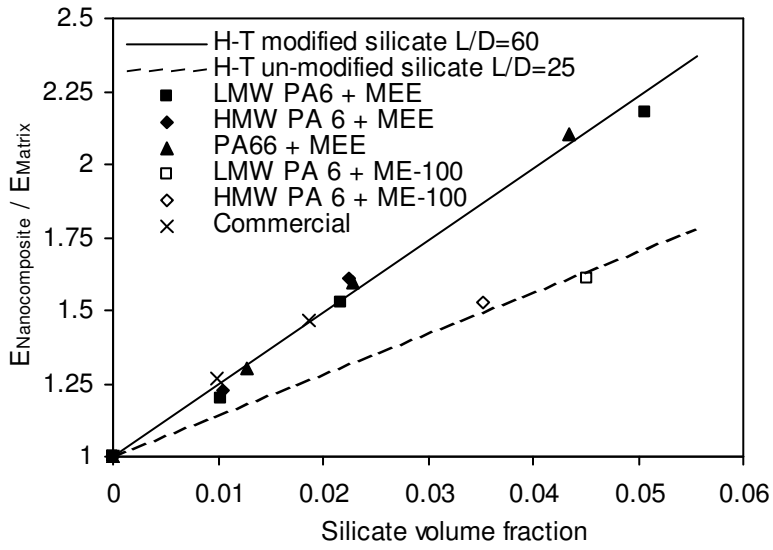


Figure 4.3: Relative modulus as a function of silicate content (20 °C).

The moduli of commercially available in-situ polymerized nanocomposites, shown in figure 4.2D, are comparable with the moduli of the melt-exfoliated nanocomposites with equivalent silicate content. Figure 4.3 shows that the relative modulus increase of all melt exfoliated nanocomposites with organically modified nanoparticles, whether they are based on low MW PA6, high MW PA6 or PA66, is equal to the modulus increase obtained in the commercially produced in-situ polymerized nanocomposites. The increase in modulus in all these materials is approximately 10% per wt% silicate, which is in line with previous results [6].

However, the nanocomposites containing unmodified silicate particles (ME-100) are exceptions to this rule. The 10.7% ME-100 in low MW PA6 has a modulus that is similar to the modulus of 5.3% MEE nanocomposite. The fact that nanocomposites based on unmodified silicate need a higher filler content to reach a similar modulus than with organically modified silicate, can be explained by a reduced degree of exfoliation. This can be the result of a reduced thermodynamic driving force for exfoliation due to the absence of the surfactant. On the other hand, the fact that the 10.7% ME-100 nanocomposite has a modulus comparable with a nanocomposite with 5.3% well exfoliated modified particles (MEE), shows that the exfoliation process with water works rather well. In figure 4.3 it can also be seen that the modulus increase with unmodified silicate is at a lower level compared to the increase with modified silicates, the slope is approximately half, i.e. about 5% modulus increase per wt% silicate. In a comparable process to exfoliate unmodified silicate with the help of water in an extrusion process, a modulus increase equal to that of organically modified silicate was reported [11], although the reported value was at a much lower silicate content of 1.6 wt% and it is, therefore, difficult to compare with these results at 10 wt% silicate. The superior modulus increase at low silicate content reported previously [11] could be a result of the longer time available to the silicate to swell in water when clay slurry is used, compared to the process used here, in which the silicate only comes into contact with water in the extruder.

Using the Halpin Tsai composite model [34,35], the effective aspect ratio (L/D) of the platelets can be estimated [32]. In figure 4.3 two lines are added which are calculated with the Halpin Tsai model, showing a best fit through the collective data of the modified silicate series and the unmodified series. The modulus increase depends on the aspect ratio of the reinforcing particles, and therefore on the degree of exfoliation. The fit for the modified silicate corresponds to an effective aspect ratio of 60, while the fit for unmodified silicate corresponds to an effective aspect ratio of 25. This means that the average stack size of the silicate layers is approximately 2.4 times larger for the unmodified silicate nanocomposites. The reduced exfoliation is in line with expectation due to the lower compatibility between the unmodified nanoparticles and the matrix polymer. These aspect ratios are in line with those calculated in chapter 2, 3 and 5 for higher silicate concentrations, but lower than those calculated for low concentrations. As mentioned in chapter 3, the errors in the calculation of the aspect ratio are much larger at low silicate concentrations. However, taking this into account, the results seem to suggest a somewhat worse exfoliation of the Somasif MEE nanofiller in the lower concentrations compared to the Nanomer I30TC and

Cloisite 30B used in chapter 2 and 3 and the Somasif MEE nanocomposites used in chapter 5.

4.3.2 Yield- or fracture stress

The yield stress of the nanocomposites has been determined, but some nanocomposite samples broke in a brittle way before reaching the yield point. In that case the fracture stress was determined. Figure 4.4A shows the yield- or fracture stress for low MW PA6, 4.4B for high MW PA6, 4.4C for PA66 and 4.4D for commercial nanocomposites. When the yield stress was not reached, the maximum stress shown in figure 4.4 is the brittle fracture stress.

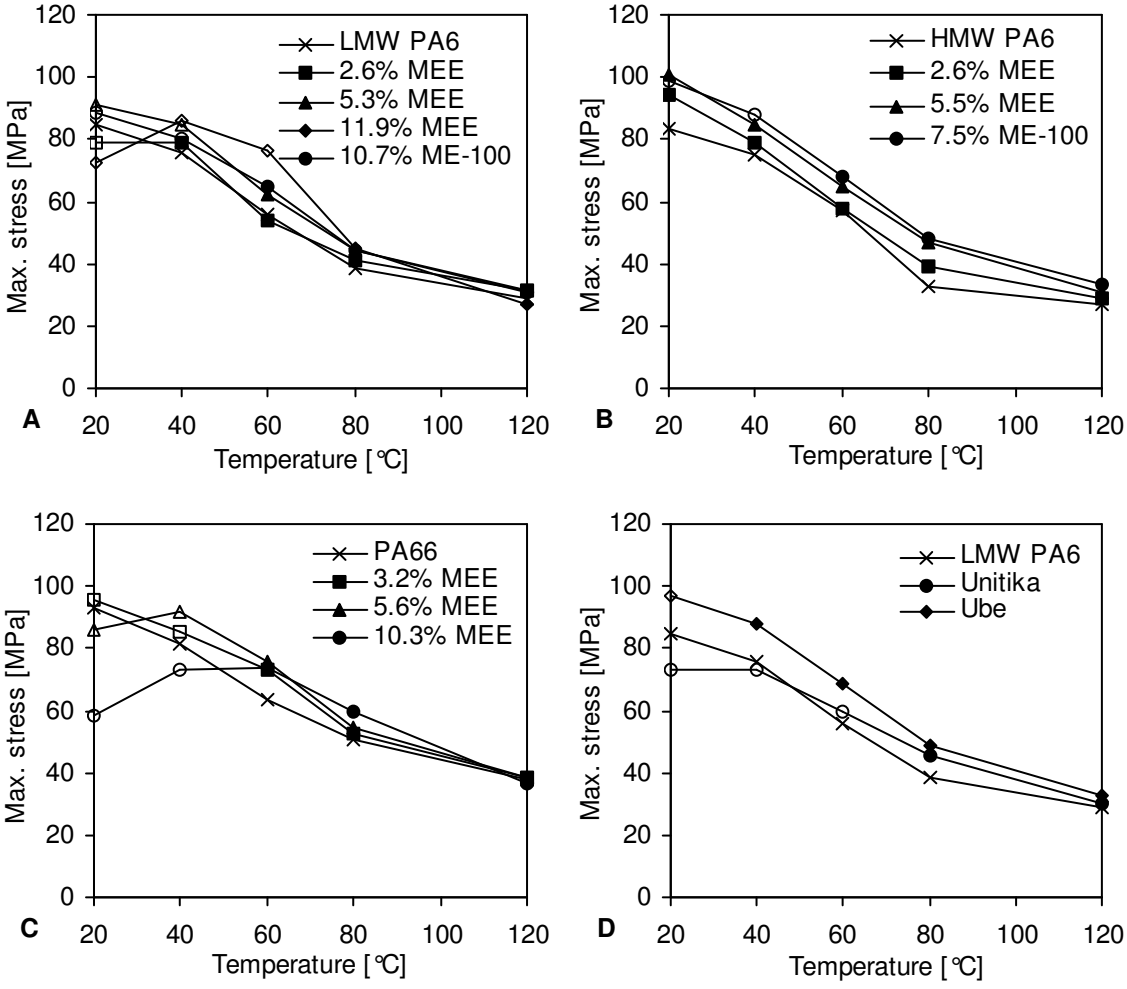


Figure 4.4: Maximum stress as a function of temperature,

A) Low MW PA6 nanocomposites, B) High MW PA6 nanocomposites,

C) Low MW PA66 nanocomposites, D) Commercial nanocomposites

Open symbols: brittle failure stress, solid symbols: yield stress

The maximum stresses when samples fractured in a brittle manner are indicated by open symbols and yield stresses are shown by solid symbols. All unfilled polyamide samples, low and high MW PA6 and PA66, are ductile and show yielding and neck formation. However, the nanocomposites based on low MW PA6 and PA66 are brittle at room temperature, even at the lowest silicate concentrations. With increasing temperature ductile yield behaviour is reached, and for higher silicate concentrations the temperature has to be raised further to reach ductile behaviour. The use of unmodified silicate (ME-100) results in a yield stress, yield/fracture behaviour and modulus, which is similar to nanocomposites containing approximately half the amount of modified silicate (MEE). The use of higher MW PA6 for the melt processing has a very positive effect on the fracture behaviour, while it does not have much effect on the modulus as was shown in figure 4.3. Nanocomposites based on high MW PA6 are ductile at all temperatures, even at room temperature. However, concentrations above 5.5% silicate were not investigated because of the extremely high melt viscosity at higher loadings. The nanocomposite based on ME-100 was not ductile at room temperature, but only at 60 °C, which is higher than expected based on the results for low MW PA6. A reason for this more brittle behaviour could be a decrease in MW due to the extrusion process in the presence of water. Evidence for the reduction of MW can also be found in the viscosity data in chapter 5. The PA66 nanocomposites showed a similar trend as the low MW PA6 nanocomposites, the yield point was not reached at room temperature, but at elevated temperatures the samples became ductile. In the high MW PA6 series and at higher temperatures for the other matrix polymers the influence of the silicate content on the yield stress can be seen clearly. The nanocomposites show an increase in yield stress, approximately 10 % at 2.6% silicate and 20% at 5.5% silicate, which is a much smaller increase than the increase in modulus.

4.3.3 Elongation at break

The elongation at break of the nanocomposites is shown in figure 4.5: 4.5A shows the elongation for low MW PA6, 4.5B for high MW PA6, 4.5C for PA66 and 4.5D for commercial nanocomposites. The displacement of the clamps that could be reached in the tests was limited by the size of the climate chamber. Therefore, in the case of fully ductile samples, the tests were stopped at 50% strain, which in that case is shown in figure 4.5 as the maximum strain. The samples would probably reach a much higher strain than 50% if not limited by the test equipment. In each graph in figure 4.5 a line is drawn at 7.5 % strain, which is approximately the borderline

between brittle and ductile behaviour. Samples that break below this value are brittle, samples that break around this value are breaking just at or around the yield point, and samples that break at much higher values show yielding and neck formation.

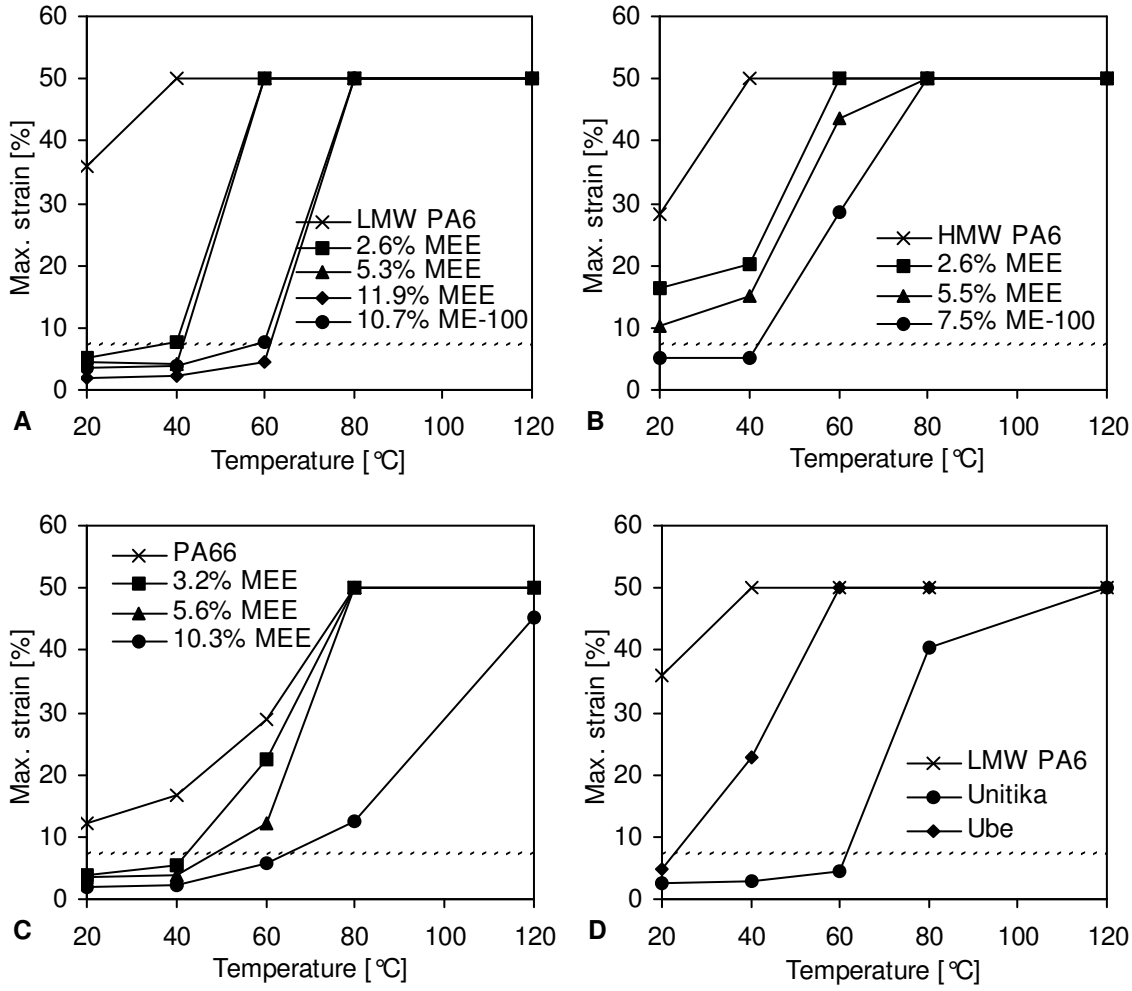


Figure 4.5: Maximum strain as a function of temperature (tests were stopped at 50% strain),
A) Low MW PA6 nanocomposites, B) High MW PA6 nanocomposites,
C) Low MW PA66 nanocomposites, D) Commercial nanocomposites

It can be seen in figure 4.5 that all unfilled samples are ductile, although the PA66 samples show a much smaller elongation; at room temperature PA66 samples break just after reaching the yield point, before a neck could be formed. The nanocomposites show a sharp transition from a low elongation at break to a high elongation, which is known as the brittle to ductile transition. When the brittle to ductile transition has been passed, all samples, including the nanocomposites with the highest silicate concentrations, can form a neck that can propagate trough the entire sample to reach high elongations. The two commercially available nanocomposites (figure 4.5D) show the same transition behaviour, although the

nanocomposite with the highest silicate concentration (Unitika) is brittle up to quite high temperatures; only at 80 °C and above it shows neck-formation and high elongations.

4.3.4 Glass transition temperature and crystallinity

The dynamic loss modulus was measured for the low MW PA6 MEE nanocomposites to see if the silicate layers influence the glass transition temperature. In figure 4.6 the loss modulus curves are shown, and from the position of the peak maximum it is clear that T_g is not significantly changed by the presence of the silicate layers. However, the loss peaks show a broadening with increasing silicate content at temperatures above T_g. This may indicate that a part of the polymer has a higher T_g due to interactions with the silicate sheet.

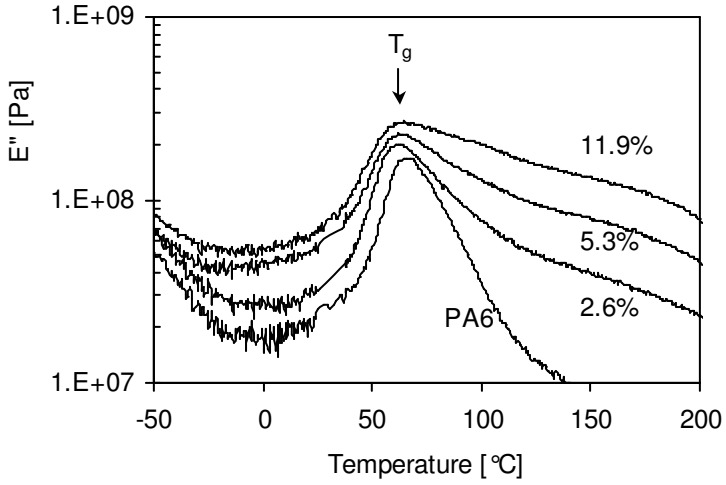


Figure 4.6: Loss modulus as function of T for low MW PA6 / MEE nanocomposite

In figure 4.7 the crystallinity of the PA6 matrix in the nanocomposites is plotted as a function of the silicate content. It is clear that the crystallinity is hardly changed by the addition of the silicate in these samples. Therefore, it can be concluded that the mechanical properties of the nanocomposites are not significantly affected by differences in crystallinity. In chapter 3 the influence of the silicate content on the crystallinity was investigated in more detail for Cloisite 30B nanocomposites, in which a small decrease above 5 wt% could be seen (see table 3.1). In the samples in chapter 3 the crystallinity of the unfilled PA6 and the lower silicate concentrations was slightly higher than can be seen in figure 4.7. This can be caused by the fact that the samples described in chapter 2 and 3 were injection moulded in a heated mould.

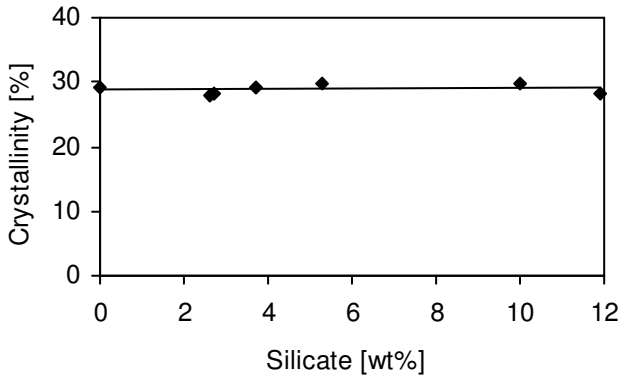


Figure 4.7: Crystallinity as a function of silicate content for low MW PA6 nanocomposites containing MEE and ME-100 silicate.

4.3.5 Brittle to ductile transition temperatures

The low MW nanocomposite PA6 and PA66 samples for each silicate content show a transition from brittle to ductile fracture behaviour upon increasing temperature as is clear from figure 4.5. The high MW samples are ductile at all test temperatures, so for this series no transition was determined. Figure 4.8 shows the temperatures at which the transition from brittle to ductile fracture behaviour takes place (the brittle to ductile transition temprature, or T_{bd}), as a function of silicate content. The T_{bd} for PA66 nanocomposites is approximately 10 °C higher than T_{bd} of PA6, and both series show approximately the same increase of the T_{bd} with increasing silicate content. The T_{bd} increases roughly with 3 °C with a 1 wt% increase of the silicate content, which confirms the trend that was found for melt compounded PA6 nanocomposites in Izod impact tests [6].

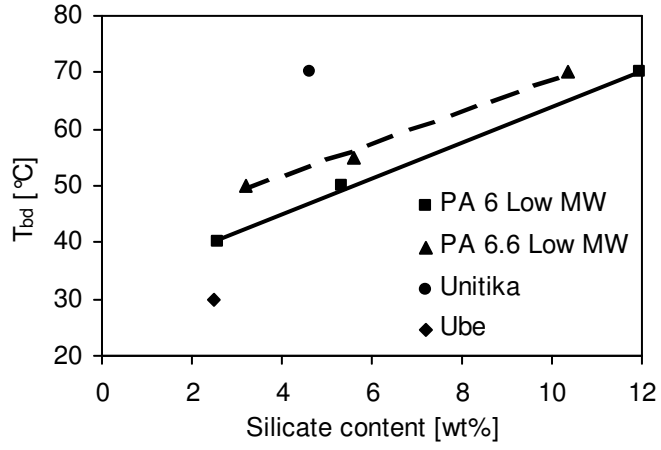


Figure 4.8: Brittle to ductile transition temperature (T_{bd}) in the tensile tests as a function of silicate content, for commercial and low MW PA6 nanocomposites.

The commercial nanocomposites show a somewhat unexpected behaviour: the nanocomposite with the highest silicate content (Unitika) has an unusually high T_{bd} for the amount of silicate it contains, while the nanocomposite with the lowest amount of silicate (Ube) has a lower T_{bd} than the melt processed low MW samples. Because the commercial nanocomposites are from different manufacturers, the MW and the silicate particle size might vary. Therefore, it is difficult to determine the reason for the differences in fracture behaviour between the two commercial nanocomposites.

At first sight it seems interesting that the brittle to ductile transition occurs around the glass transition temperature of the matrix polymer, which is around 55 °C for PA6 and around 60 °C for PA66. However, the change in fracture behaviour around the T_{bd} cannot be simply attributed to the extra mobility associated with the glass transition phenomenon. Evidence for this can be found in the fact the nanocomposite with 11.9% silicate in low MW PA6 is still completely brittle above T_g of PA6, while nanocomposites based on high MW PA6 are already ductile at room temperature up to 5.5% silicate. However, the loss moduli curves in figure 4.6 suggest that, although the main T_g peak is not changed in nanocomposites, a part of the polymer might have a higher T_g due to the interaction with the particle.

The MW of the matrix polymer is very important for the yield or fracture behaviour, as is clear from the differences in maximum elongation in figure 4.5A and 4.5A. It was shown previously that a higher MW of the matrix polymer increases the elongation at break and the results in this chapter confirm this [14].

Fracture behaviour is dependent on many sample and test parameters, and it is therefore difficult to determine the exact reason why the fracture behaviour of nanocomposites differs from unfilled polymers on the basis of these results. However, a few possible causes for the decreased ductility and increased T_{bd} in nanocomposites can be suggested:

- As has been shown in section 4.3.2 (figure 4.4), the yield stress increases with the addition of silicate and decreases with increasing temperature. This means that higher temperatures are necessary to reduce the yield stress of a nanocomposite sample below the brittle failure stress, which can explain the higher T_{bd} in line with the Ludwig-Davidenkov-Orowan hypothesis [23].
- In general higher MW increases the ductility, and from these results it is clear that this is valid for nanocomposite too. A reduction of the MW causes a large reduction in ductility, and it has been reported that exfoliated silicate catalyses the reduction of the MW in extrusion processes [36]. Therefore, a reduction in MW caused by the silicate layers during processing could have an effect on

the ductility and T_{bd}. However, viscosity measurements do not indicate a significant decrease of MW due to the extrusion with silicate, but the different extrusion process used for ME-100 nanocomposites does lower the MW (see chapter 5).

- A strong interaction of the polar PA6 chains with the charged silicate layers can exist; therefore the silicate layers could be considered crosslinking points where many polymer chains are connected. These physical crosslinks could significantly reduce the flow possibilities of the polymer in the nanocomposites.
- The loss modulus peak from the dynamic mechanical measurements, see figure 4.6, shows a broadening at higher silicate content. This could indicate that a fraction of the polymer chains only becomes mobile at temperatures above the bulk T_g, which could reduce the deformation possibilities.
- The large amount of impenetrable silicate layers in the material could reduce the amount of tie-chains between crystalline areas, which reduces the possibilities for stress transfer through the sample and leads to more brittle fracture behaviour. In addition, the silicate sheets could reduce the spherulite size, which has been shown to lead to a reduction in elongation at break in PA66 [24].

4.4 Conclusions

Nanocomposites with different concentrations of organically modified silicate based on two different molecular weight grades of PA6 were prepared by mixing in the melt in a twin-screw extruder. The high MW nanocomposites could not be successfully prepared at concentrations above 5.5 wt% because of the extremely high melt viscosity at the processing temperature. With the same process and the same organically modified silicate a series of nanocomposites based on PA66 was successfully prepared; the only necessary difference was the higher processing temperature. In addition, nanocomposites were prepared from unmodified silicate with a water-assisted extrusion process, both with high and low MW PA6. The samples were tested at temperatures ranging from 20 to 120 °C. The modulus increase is in all nanocomposites with organically modified nanocomposites similar: at room temperature an increase of the modulus of approximately 3% for each 1 wt% of silicate is found. This is equal to the increase in modulus achieved in commercially

available nanocomposites (based on an in situ polymerization process leading to nearly perfect exfoliation) and to previously reported results [6].

It is a remarkable result that the PA66 nanocomposites produced in this way have an identical (relative) modulus increase as PA6 nanocomposites, because results reported so far have shown a much lower increase [25,29] or even required a different organic modification [29,33]. The unmodified silicate nanocomposites show a smaller increase of the modulus, approximately equal to nanocomposites containing half the amount of modified silicate.

The yield stress increases also with the addition of layered silicate, but to a smaller extent than the modulus. Low MW PA6 and PA66 nanocomposites show very brittle fracture behaviour at room temperature, while high MW PA6 nanocomposites are ductile. Commercial nanocomposites are brittle too, so the ionic bond between the polymer and the silicate in these in-situ polymerized nanocomposites does not seem to influence the ductility. With increasing temperature all the nanocomposites become ductile at a certain temperature. The temperature at which this transition occurs defines the T_{bd}, which increases with increasing silicate content by approximately 10 °C per 5 wt% silicate, both for low MW PA6 and PA66.

The improved fracture behaviour of high MW nanocomposites seems to be an interesting property, but the downside is a big reduction in processability due to the very high viscosity caused by the high polymer viscosity in combination with the large surface area and aspect ratio of the exfoliated silicate platelets. The use of unmodified silicate can be interesting due to the lower price of the reinforcing material, but the reinforcing effect is not as effective as the modified silicate.

In all tested properties the melt-mixed nanocomposites are approximately equal to in-situ polymerised nanocomposites.

The results in this chapter show that PA66 nanocomposites can be processed in the same way as PA6 nanocomposites; the high processing temperatures do not seem to be a problem for the modified silicate. The higher melting point could be an advantage in some cases, and the modulus has been shown to be even higher that that of PA6 based nanocomposites due to the slightly higher matrix modulus. The reduction of the modulus at temperatures above T_g is almost equal to that in PA6 nanocomposites, because T_g of PA66 is not much higher and the ductility is slightly lower than that of PA6 nanocomposites. For the molecular weight of the matrix polymer a compromise has to be made between processability and mechanical properties, as is the case for unfilled polymers. More about the compromise between processability and mechanical properties will be discussed in chapter 5.

4.5 References

1. Kojima Y, Usuki A, Kawasumi M, Okada A, Fukushima Y, Kurauchi T, Kamigaito O. Mechanical-Properties of Nylon 6-Clay Hybrid. J. Mater. Res. 1993;8(5):1185-1189.
2. Usuki A, Kojima Y, Kawasumi M, Okada A, Fukushima Y, Kurauchi T, Kamigaito O. Synthesis of Nylon 6-Clay Hybrid. J. Mater. Res. 1993;8(5):1179-1184.
3. Usuki A, Kawasumi M, Kojima Y, Okada A, Kurauchi T, Kamigaito O. Swelling Behavior of Montmorillonite Cation Exchanged for Omega-Amino Acids by Epsilon-Caprolactam. J. Mater. Res. 1993;8(5):1174-1178.
4. Maxfield M, Cristiani BR, Sastri VR; Polymer nanocomposites comprising a polymer and an exfoliated particulate material derivatized with organo silanes, organo titanates, and organo zirconates dispersed therein and process of preparing same. USA patent 5,514,734. 1996.
5. Akkapeddi MK. Glass fiber reinforced polyamide-6 nanocomposites. Polym. Compos. 2000;21(4):576-585.
6. Cho JW, Paul DR. Nylon 6 nanocomposites by melt compounding. Polymer 2001;42(3):1083-1094.
7. Liu L, Qi Z, Zhu X. Studies on Nylon 6/Clay Nanocomposites by Melt-intercalation Process. J. Appl. Polym. Sci. 1999;71:1133-1138.
8. Dennis HR, Hunter DL, Chang D, Kim S, White JL, Cho JW, Paul DR. Effect of melt processing conditions on the extent of exfoliation in organoclay-based nanocomposites. Polymer 2001;42(23):9513-9522.
9. Es MAv. Polymer clay nanocomposites. The importance of particle dimensions. Delft: Delft University of Technology; 2001.
10. Korbee R; Process for the preparation of polyamide nanocomposite composition. NL patent WO 99/29767 DSM. 1999.
11. Hasegawa N, Okamoto H, Kato M, Usuki A, Sato N. Nylon 6/Na–montmorillonite nanocomposites prepared by compounding Nylon 6 with Na–montmorillonite slurry. Polymer 2003;44(10):2933-2937.
12. Vlasveld DPN, Parlevliet PP, Bersee HEN, Picken SJ. Fibre–matrix adhesion in glass-fibre reinforced polyamide-6 silicate nanocomposites. Composites Part A: Applied Science and Manufacturing 2005;36(1):1-11.
13. Fornes TD, Yoon PJ, Hunter DL, Keskkula H, Paul DR. Effect of organoclay structure on nylon 6 nanocomposite morphology and properties. Polymer 2002;43(22):5915-5933.
14. Fornes TD, Yoon PJ, Keskkula H, Paul DR. Nylon 6 nanocomposites: the effect of matrix molecular weight. Polymer 2001;42(25):9929-9940.
15. Gloaguen JM, Lefebvre JM. Plastic deformation behaviour of thermoplastic/clay nanocomposites. Polymer 2001;42(13):5841-5847.
16. Usuki A, Koiwai A, Kojima Y, Kawasumi M, Okada A, Kurauchi T, Kamigaito O. Interaction of Nylon-6 Clay Surface and Mechanical-Properties of Nylon-6 Clay Hybrid. J. Appl. Polym. Sci. 1995;55(1):119-123.
17. Fornes TD, Hunter D, Paul DR. Nylon-6 Nanocomposites from Alkylammonium-Modified Clay: The Role of Alkyl Tails on Exfoliation. Macromolecules 2003.
18. Fornes TD, Hunter DL, Paul DR. Nylon-6 nanocomposites from alkylammonium-modified clay: The role of alkyl tails on exfoliation. Macromolecules 2004;37(5):1793-1798.
19. Okada A, Usuki A. The chemistry of polymer-clay hybrids. Materials Science & Engineering C 1995;3(2):109-115.
20. Mallick PK, Zhou YX. Yield and fatigue behavior of polypropylene and polyamide-6 nanocomposites. J. Mater. Sci. 2003;38(15):3183-3190.
21. Ezrin M. Plastics failure guide: Hanser Gardner Publications; 1996.
22. Bicerano J, Seitx JT. Molecular origins of toughness in polymers. In: Arends CB, editor. Polymer toughening. New York: Marcel Dekker Inc.; 1996.
23. Ward IM, Hadley DW. An Introducion to the Mechanical Properties of Solid Polymers: Wiley; 1997.
24. Kohan MI. Nylon Plastics Handbook: Carl Hanser Verlag; 1995.

25. Nair SV, Goettler LA, Lysek BA. Toughness of nanoscale and multiscale polyamide-6,6 composites. Polymer Engineering and Science 2002;42(9):1872-1882.
26. Qin HL, Su QS, Zhang SM, Zhao B, Yang MS. Thermal stability and flammability of polyamide 66/montmorillonite nanocomposltes. Polymer 2003;44(24):7533-7538.
27. Lu YL, Zhang GB, Feng M, Zhang Y, Yang MS, Shen DY. Hydrogen bonding in polyamide 66/clay nanocomposite. J. Polym. Sci. Pt. B-Polym. Phys. 2003;41(19):2313-2321.
28. Liu XH, Wu QJ, Berglund LA. Polymorphism in polyamide 66/clay nanocomposites. Polymer 2002;43(18):4967-4972.
29. Liu XH, Wu QJ. Polyamide 66/clay nanocomposites via melt intercalation. Macromol. Mater. Eng. 2002;287(3):180-186.
30. Xie W, Gao ZM, Pan WP, Hunter D, Singh A, Vaia R. Thermal degradation chemistry of alkyl quaternary ammonium montmorillonite. Chem. Mat. 2001;13(9):2979-2990.
31. Fischer HR. Personal communication. 2004.
32. Es MAv, Xiqiao F, Turnhout Jv, Giessen Evd. Comparing Polymer-Clay Nanocomposites with Conventional Composites using Composite Modeling. In: Al-Malaika Sea, editor. Specialty Polymer Additives: Blackwell Science; 2001.
33. Gonzalez I, Eguiazabal JI, Nazabal J. Exfoliated PA6,6 nanocomposites by modification with PA6. Polymer 2005;In press.
34. Halpin JC. Stiffness and Expansion Estimates for Oriented Short Fiber Composites. Journal of Composite Materials 1969;3:732-734.
35. Halpin JC, Kardos JL. Halpin-Tsai Equations - Review. Polymer Engineering and Science 1976;16(5):344-352.
36. Davis RD, Gilman JW, VanderHart DL. Processing degradation of polyamide 6/montmorillonite clay nanocomposites and clay organic modifier. Polym. Degrad. Stabil. 2003;79(1):111-121.

The results described in this chapter have been published as:

D.P.N. Vlasveld, S. G. Vaidya, H.E.N. Bersee, S.J. Picken.

A comparison of the temperature dependence of the modulus, yield stress and ductility of nanocomposites based on high and low MW PA6 and PA66.

Polymer, 2005, Volume 46, Issue 10, Pages 3452-3461

Chapter 5

The relation between rheological and mechanical properties in PA 6 nanocomposites and microcomposites

5.1 Introduction

Particle reinforced polymer composites have been used for decades to increase the modulus and strength of polymers and to reduce thermal expansion. The more recently developed polymer nanocomposites based on exfoliated layered silicates [1-3] show besides improved mechanical properties also good barrier properties and reduced flammability. Compared to composites containing larger dispersed particles (microcomposites), nanocomposites have the advantage of achieving the optimal properties at relatively low filler content due to the large aspect ratio and high modulus of the particles. However, the advantages in mechanical properties of nanocomposites, such as the higher modulus and yield stress, are usually accompanied by a stronger increase in melt viscosity and a change in rheological behaviour compared to microcomposites. The higher melt viscosity is a disadvantage for processing techniques such as extrusion and injection moulding, although it can be beneficial for film extrusion.

In this chapter both the main advantage of the use of nanocomposites, i.e. the increased modulus, and their main disadvantage for processing, i.e. the increased viscosity, are investigated. Both are influenced by the same factors, such as particle shape and concentration. Therefore, some relations between the modulus, the viscosity and the particle shape and concentration are discussed in section 5.2. With an improved understanding of these factors, the optimum morphology can be chosen that leads to the best compromise in properties. Nanocomposites and microcomposites with different amounts and types of fillers have been prepared, and their rheological and mechanical properties are compared. The aspect ratios of the particles were calculated from the storage modulus at room temperature using the Halpin-Tsai composite model, and from the complex viscosity in the melt using viscosity models proposed by Simha, Kuhn and Utracki.

5.2 Theory

5.2.1 Modulus of elasticity

The modulus of a layered silicate nanocomposite is dependent on the modulus and the volume fractions of the components and on the degree of exfoliation of the silicate particles. Improved exfoliation increases the amount of particles and their aspect ratio. The importance of the aspect ratio was already known for fibre composites, in which longer fibres also lead to better properties. This is even more important for nanocomposites because the volume fractions are relatively low. Many composite models take the aspect ratio into account [4]. One such model is the Halpin-Tsai model, which has been described in chapter 3. This model is shown here again in equation 5.1, now with the shape factors for both platelet and fibre reinforcement:

$$\frac{E_c}{E_m} = \frac{1+\varsigma\eta\varphi_f}{1-\eta\varphi_f} \qquad \text{in which} \qquad \eta = \frac{\frac{E_f}{E_m}-1}{\frac{E_f}{E_m}+\varsigma} \qquad 5.1$$

E_c = Composite Young's modulus.

E_f = Filler modulus, E_m = Matrix modulus.

ς = Shape factor, depending on geometry, aspect ratio and orientation.

φ_f = Filler volume fraction

The shape factors for the tensile moduli of platelet reinforced composites are [4]:

ς = ⅔ (a/b) (in the radial direction of the platelets, E_{11} or E_{22})

ς = 2 (perpendicular to the platelets, E_{33})

(a = longest dimension, b = shortest dimension)

The shape factors for the tensile moduli of fibre reinforced composites are [4]:

E_{11} or E_{22}	$\varsigma = 2$	(perpendicular to the fibre direction)
E_{33}	$\varsigma = 2$ (a/b)	(in the fibre direction)

When the modulus of the composite, matrix and filler are known, the Halpin-Tsai model can also be used to back-calculate the aspect ratio of the reinforcing particles. This will be an *effective* aspect ratio, because the particles can have different shapes, sizes and thicknesses. The effective aspect ratio is a reasonable estimate of the average aspect ratio (also calculated from modulus and diffusion data in chapters

2 and 3) and provides a useful parameter to compare different nanocomposite compositions. The Halpin-Tsai equations predict that platelet-shaped particles are hardly effective at very low aspect ratios (< 10). Fibres do not need to have such a high aspect ratio as platelets to increase the modulus of the composite significantly. The maximum stiffening effect is reached at aspect ratios above approximately 1000 for platelets and 100 for fibres [5].

5.2.2 Melt rheology

In this section first the relations that are used to calculate the viscosity from the dynamic measurements will be shown. This will be followed by several equations that relate the viscosity of filled systems with the particle shape and concentration, which will be used to estimate the average particle aspect ratio.

By increasing the filler content the viscosity increases considerably in both exfoliated and intercalated nanocomposites, especially at low shear rates or low frequencies [6-10]. Unfilled polymers have usually a constant viscosity over a large frequency range with shear thinning behaviour at higher frequencies or shear rates. Nanocomposites with filler loading above a few percent show shear thinning over the entire range of frequencies [7]. The unlimited increase of the viscosity when the shear rate approaches zero is caused by the presence of a network structure in the melt that leads to a yield stress. This can be caused by the dispersed particles, which can touch or connect to each other to form a continuous structure. The formation of a network does not require a physical connection between the particles; it is sufficient that the particles feel each other's presence and are able to transfer stresses [7]. The probability that particles form a network depends on the interactions between the particles, on the shape (aspect ratio) and on the inter-particle distance. A reduction of the distance between the particles or increased aspect ratio at constant volume fraction increases the probability that the particles connect. Due to their large aspect ratio, the space the exfoliated silicate layers need to rotate freely in the melt is much larger than the volume they occupy. Therefore, the percolation threshold of exfoliated layered silicates is very low [7].

Flow of polymers in shear experiments

The complex shear modulus G^* is defined in oscillatory shear as:

$$\tau(t) = G^*(\omega)\,\gamma_0\,e^{i\omega t} \qquad 5.2$$

($\tau(t)$ = shear stress, γ_0= shear strain magnitude)

For a viscoelastic material subjected to an oscillatory strain, the oscillatory stress response will be out of phase by an angle δ. For a perfectly elastic system δ=0, whereas for a perfectly viscous liquid, the stress is out of phase by δ=90°. For viscoelastic systems the phase angle shift is between these limiting cases.
The flow behaviour of fluids can be described by the viscosity, η.
In the presence of a yield stress, τ_{yield}, the viscosity is defined as:

$$\tau = \tau_{yield} + \eta\dot{\gamma} \qquad \Rightarrow \qquad \eta = \frac{\tau - \tau_{yield}}{\dot{\gamma}} \quad \text{(Bingham model)} \qquad 5.3$$

$\dot{\gamma}$ = shear rate [s^{-1}].

The apparent yield stress (τ_{yield}) of the network can be estimated by extrapolating the stress versus $\dot{\gamma}$ curve to zero shear rate (or frequency in dynamic measurements).
A complex viscosity can be determined from dynamic melt flow measurements:

$$\eta^* = G^* / \omega \qquad \text{(complex viscosity)} \qquad 5.4$$

A yield stress in the melt means that flow cannot occur below a stress threshold. However, this stress is part of the measured response in the dynamic measurements and leads to an apparent increase of the measured viscosity. A corrected viscosity can be calculated by subtraction of the yield stress from the measured stress:

$$G^* = (\eta^* \cdot \omega) + \frac{\tau_{yield}}{\gamma_0} \qquad \Rightarrow \qquad \eta^*_{corrected} = \frac{G^* - \frac{\tau_{yield}}{\gamma_0}}{\omega} \qquad 5.5$$

Viscosity of filled fluids

For filled systems several relations are defined between the viscosity of the unfilled fluid and the filled fluid. The relative, reduced and intrinsic viscosities are defined as:

$$\eta_{relative} = \frac{\eta}{\eta_0} \qquad \text{relative viscosity} \qquad 5.6$$

$$\eta_{reduced} = \frac{\eta - \eta_0}{\eta_0 \cdot \varphi} \qquad \text{reduced viscosity} \qquad 5.7$$

$$[\eta] = \lim_{\varphi \to 0} \frac{\eta - \eta_0}{\eta_0 \cdot \varphi}$$ intrinsic viscosity 5.8

η = viscosity of the mixture/composite [N.s/m^2]

η_0 = viscosity of the liquid [N.s/m^2]

φ = volume fraction of particles

(Because in equation 5.7 and 5.8 the (dimensionless) volume fraction is used instead of the concentration, the reduced and intrinsic viscosities are also dimensionless.)

Relations between viscosity and particle shape in filled systems

The rheology of suspensions of rigid spheres can be described by Einstein's viscosity equation (eq. 5.9). This linear equation can be used for non-settling and non-interacting spherical particles in a Newtonian liquid at low volume fractions ($\varphi_{spheres}$):

$$\eta = \eta_0 \cdot (1 + 2.5 \cdot \varphi_{spheres}) \quad \rightarrow \quad [\eta] \cong \eta_{reduced} = 2.5 \qquad 5.9$$

(At low filler fractions $\eta_{reduced}$ approximates [η].)

Although polymer nanocomposites do not meet all these requirements, the filler concentrations are low and at low shear rates the melt of the polymer matrix behaves as a Newtonian fluid. Therefore, Einstein's viscosity equation (eq. 5.9) is a good basis to use with some adaptations to account for different particle shapes. The modified Einstein-type equations described hereafter can be used to describe the viscosity of nanocomposite melts. Inversely, effective aspect ratios can be estimated from melt flow measurements using these viscosity models, in a similar way as can be done using the modulus and the Halpin-Tsai equations.

Simha [11] has derived equations for small non-spherical particles, where Brownian motion has to be taken into account. The particle shape is incorporated in a factor v, which replaces the value of 2.5 in equation 5.9. For prolate ellipsoids (~fibre shape) and oblate ellipsoids (~disk shape) different equations are derived. For these low filler concentrations a linear model is assumed, in which $v \cong [\eta]$.

$$\eta = \eta_0 \cdot (1 + v \cdot \varphi_{ellipsoids}) \quad \rightarrow \quad [\eta] \cong \eta_{reduced} = v \qquad 5.10$$

$$[\eta] = \frac{\frac{16}{15}\left(\frac{a}{b}\right)}{\tan^{-1}\left(\frac{a}{b}\right)}$$ (oblate ellipsoids ≅ disks)

$$[\eta] = \left(\frac{\left(\frac{a}{b}\right)^2}{15\left(\ln 2\left(\frac{a}{b}\right)\right)} - \frac{3}{2} \right) + \left(\frac{\left(\frac{a}{b}\right)^2}{5\left(\ln 2\left(\frac{a}{b}\right)\right)} - \frac{1}{2} \right) + \frac{14}{15}$$ (prolate ellipsoids ≅ fibres)

(a = long radius in the ellipsoid, b = short radius)

$[\eta] = 2.5$ (spheres (Einstein, eq. 5.9))

The equation for [η] for prolate ellipsoids (fibres) can be approximated by a quadratic function. For aspect ratios from 10 to 70 the best fit is:

$$[\eta] = 0.049\left(\frac{a}{b}\right)^2 + 1.12\left(\frac{a}{b}\right) - 3.74 \qquad 5.11$$

The equation for $[\eta]$ for oblate ellipsoids (platelets) can be approximated by a linear function for all aspect ratios:

$$[\eta] = 0.679\left(\frac{a}{b}\right) + 0.454 \qquad 5.12$$

Another linear equation that describes the viscosity of fluids filled with disk-shaped particles has been proposed by Luciani *et al.* [12]. They have studied dilute suspensions of mica flakes with various aspect ratios, and used a model proposed earlier by Kuhn [13] to describe the effect of the aspect ratio on the intrinsic viscosity of platelet filled composites. The authors simplified the model for high aspect ratios, and showed a very good fit with experimental measurements [12]:

$$[\eta] = \left(\frac{4}{9}\right) + \frac{4}{3\pi}\left(\frac{a}{b}\right) \qquad \text{Valid for: } 12 < \left(\frac{a}{b}\right) < 150 \qquad 5.13$$

The main difference between the results of Simha's and Kuhn's equations is the strength of the influence of the aspect ratio. This can be seen when equations 5.12 and 13 are compared: the factor in front of the aspect ratio is smaller in equation 5.13 than in equation 5.12 (0.42 vs 0.68). This is probably a result of the fact that the latter model (Kuhn) does not include the effect of Brownian motion.

Without Brownian motion, the particles can align and the viscosity increase is less strong. Therefore, Kuhn's theory is more suitable for composites with relatively large particles, in which Brownian motion can be neglected.
A different form of a relation between the intrinsic viscosity and the particle aspect ratio of disk-shaped particles has been derived by Utracki [14]:

$$[\eta] = 2.5 + 0.025\left(1 + \left(\frac{a}{b}\right)^{1.47}\right) \qquad 5.14$$

Equation 5.14 [14] is an exception from the linear dependence for platelets (Simha and Kuhn), as it assumes power law behaviour.

5.3 Experimental

5.3.1 Materials

Polyamide 6, low molecular weight (LMW PA6):

- Akulon® K123, injection-moulding grade PA6 from DSM, the Netherlands.
  M_n = 16000, M_w = 32000 g/mol, T_m = 220 °C.
  (K123 does not contain a nucleating agent, besides that it is similar in properties to K122D and K222D used in other chapters.)

Nanofillers

To investigate the effect of the amount of filler and the degree of exfoliation in the nanocomposites two platelet-shaped silicates are used, both based on synthetic fluoro-mica:

- Somasif® MEE from Unicoop, Japan: synthetic mica modified with coco bis(2-hydroxyethyl) methyl ammonium surfactant (28.5 wt%).
- Somasif® ME-100 from Unicoop, Japan: unmodified water-swellable synthetic mica.

To examine the influence of the shape of the particles, the nanometer-thin platelet shaped fillers were compared to spherical and fibre-shaped fillers in the same size range:

- Snowtex® (Nissan Chemical Industries): Spherical silica nanoparticles in aqueous dispersion containing 20 wt% particles with sizes between 20 and 50 nm.

- Sivomatic A sepiolite: Fibre-shaped nanoparticles. After dispersion in the polymer the particles have a length of a few hundred nm and a diameter of 10-30 nm. Sepiolite is a naturally occurring silicate mineral with a hollow channel structure, usually containing water (figure 5.1). The tubes consist of silicate layers with a similar structure as in montmorillonite or mica [15] and are connected to each other at the corners.

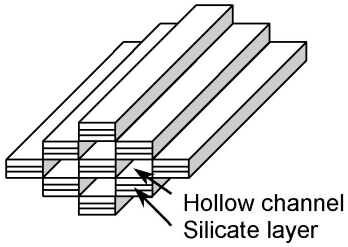


Figure 5.1: Schematic structure of sepiolite.

Microfillers

To study the influence of the size of the particles, the nanoparticles were compared with µm-sized glass particles of approximately the same aspect ratio.

- Sovitex Micropearls (50 20 215) spherical glass beads (average diameter 30 µm).
- Glass fibres (OCF CS 173X-10C) with an initial length of 4 mm and a diameter of 10 µm. After extrusion the length was reduced.
- Glass flakes (GF-300) with an initial diameter range of 50 to 1800 µm and a thickness around 2.5 µm. After extrusion the diameter was also reduced.

The silicate platelets have a modulus of 172 GPa [16]; the modulus of glass is 76 GPa [17]. The density of the silicate platelets is 2.8 g/cm^3 [18], and of glass it is 2.54 g/cm^3 [17]. The modulus and density of sepiolite are estimated form its structure. Since approximately 50 vol% consists of the mica structure, the modulus of sepiolite is estimated to be half that of mica or montmorillonite: 86 GPa. The voids between the tubes (50 volume %) can be filled with water, and the density of non-dried sepiolite is estimated similarly to be 1.9 g/cm^3.

5.3.2 Specimen preparation

Extrusion

Mixtures of cryogenically milled polyamide-6 and filler powder were fed to a Werner & Pfleiderer ZSK 30/44 D co-rotating twin-screw extruder. The extruder was operated at 240 °C, 200 rpm, with an output rate of 10 kg/h.

To enhance the exfoliation of unmodified nano-fillers, water was injected in the extruder at 25 ml/min for the unmodified sepiolite and ME-100 [19]. The same water-assisted extrusion procedure was used for the glass microcomposites and the unfilled matrix to compare the viscosities of the resulting composites. The dispersed silica particles (Snowtex) were injected into the extruder using a suspension in water. In this case the extruder output rate was 4 kg/h. In all these cases the water was removed using a vent at the end of the extruder. The MEE nanocomposites and the unfilled PA6 reference material were extruded without injection of water.

Samples

The samples for dynamic mechanical analysis (DMA) were 2.6 mm wide and 20 mm long. They were cut from 0.2 mm thin films, made by compression moulding of the extrudate in a Fontijne laboratory press at 240 °C. The samples were cooled in the press at an initial cooling rate of approximately 40 °C/min.

The samples for the rheological measurements were 2 mm thick and were also made by compression moulding. Al samples where dried before testing at 80 °C in vacuum for at least 2 days.

5.3.3 Testing

Thermo-gravimetric Analysis (TGA)

A Perkin Elmer TGA 7 thermo-gravimetric analyzer was used for the determination of the amount of surfactant on the MEE organo-silicate and the silicate content in the composites. The samples where heated in air to 800 °C for 30 minutes.

Optical and Transmission Electron Microscopy

A Nikon Eclipse E600 Polarization optical microscope was used to determine the particle size of the glass fillers. Transmission electron microscopy (TEM) was used to check the size and dispersion of the particles in the nanocomposites. Samples for TEM-analysis were prepared from extruded pellets. Films with a thickness of 70 nm were cut with a diamond knife parallel to the extrusion direction at –100 °C and observed with a Philips CM 200 TEM at an acceleration voltage of 120 kV.

Dynamic Mechanical Analysis (DMA)

The storage modulus in the solid state was determined with DMA using a Rheometrics Solids Analyser II at a frequency of 1 Hz (ASTM D5026). The

temperature range was -130 °C to 200 °C, the heating rate was 5 °C/min and the length between the clamps was approximately 11 mm. The thickness of the samples was measured with an accuracy of 1 µm using a Heidenhahn MT30B thickness meter.

Rheological measurements

Dynamic rheological measurements in the melt were performed at 250 °C using a RMS 605 Rheometrics Mechanical Spectrometer. The rheological properties of the PA6 and the nanocomposites were measured in oscillatory shear mode using 50 mm diameter parallel plates at a gap of 1.8 mm. The dynamic moduli, G' and G", were recorded as functions of angular frequency (ω) in the range from 0.1 to 100 rad/s at a strain magnitude of 1%. PA6 can polymerize further in the melt in dry conditions [20]. All results shown are from measurements after 10 minutes conditioning in the melt and are corrected for the polymerization taking place during the measurements.

5.4 Results and Discussion

5.4.1 Dispersion and particle size

Optical microscopy showed that the glass fibres have an average length of approximately 200 µm after extrusion, which corresponds to aspect ratios around 20. The glass platelets have a diameter of approximately 100 µm and aspect ratios around 40 (thickness 2.5 µm).

Figure 5.2 shows TEM images of PA6 nanocomposites with 5 wt% nanoparticles.

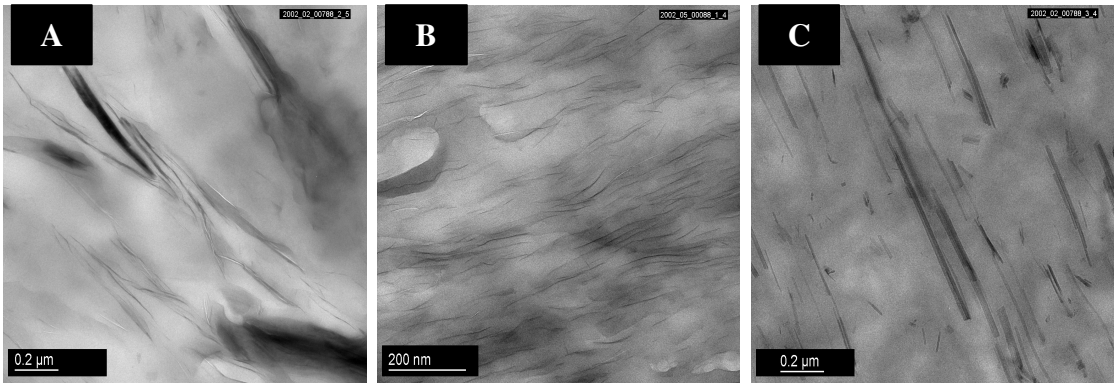


Figure 5.2: TEM-images of PA6 nanocomposite with 5 wt% nanoparticles:
A: Unmodified silicate (ME-100), B: Modified silicate (MEE), C: Sepiolite

ME-100 is not modified and it is not expected to exfoliate as well as silicates with an appropriate organic modification. Agglomerates varying from several to dozens of platelets are, indeed, present. For the MEE nanocomposites a much better dispersion is observed, with the majority of particles being single platelets or very small stacks. The thickness of the silicate platelets is approximate 1 nm, and the observed aspect ratio in the MEE nanocomposites is approximately 200, or less when stacks of several platelets are present. The average aspect ratio of the ME-100 nanocomposites is smaller than that of the MEE nanocomposites due to the presence of thicker stacks of platelets. The fibre shaped sepiolite shows a distribution of lengths and thicknesses of the rods with an average length of 200 nm, thickness of 10 nm, and aspect ratio around 20.

5.4.2 Dynamic moduli

The storage moduli of all tested micro- and nanocomposites are displayed in figures 5.3 - 5.6 as a function of temperature.

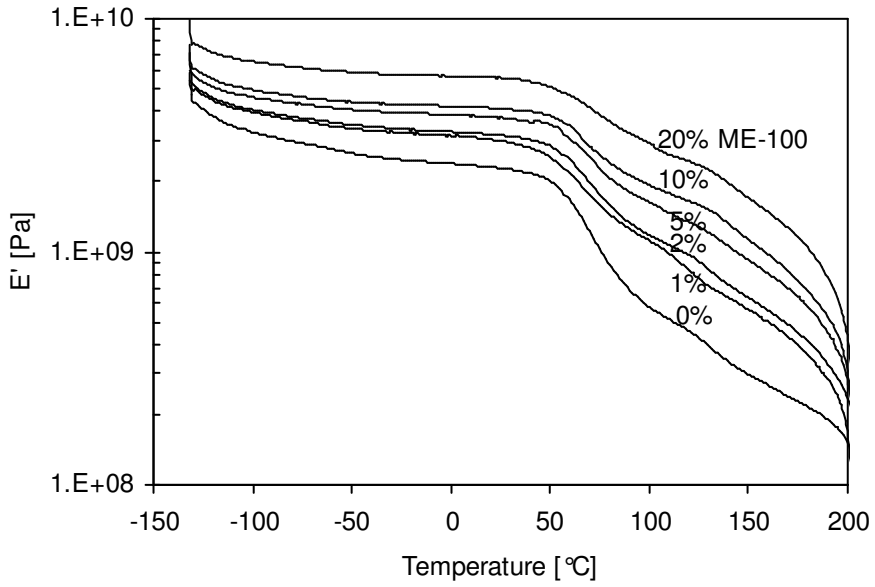


Figure 5.3: The storage modulus of ME-100 nanocomposites at different volume fractions as a function of the temperature.

Figure 5.3 shows the storage modulus for composites with 0-20 wt% of unmodified nanoplatelets (ME-100). Figure 5.4 shows the same for the organically modified nanoplatelets (MEE). Higher silicate concentrations lead to a higher modulus over the entire temperature range. Note that the bulk T_g does not change with the addition of layered silicate in these nanocomposites. The moduli of the nanocomposites with

the modified MEE particles are higher than of those with the unmodified ME-100 particles, because the surface modification improves the exfoliation, leading to more individual particles with higher aspect ratios.

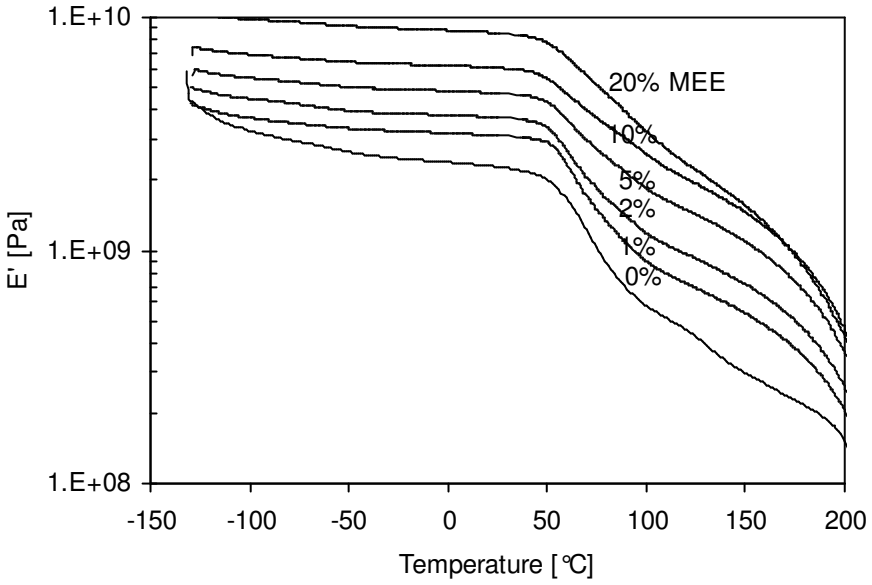


Figure 5.4: The storage modulus of MEE nanocomposites at different volume fractions as a function of the temperature.

Figure 5.5 compares the moduli for various shapes of nanoparticles at 5 wt% loading.

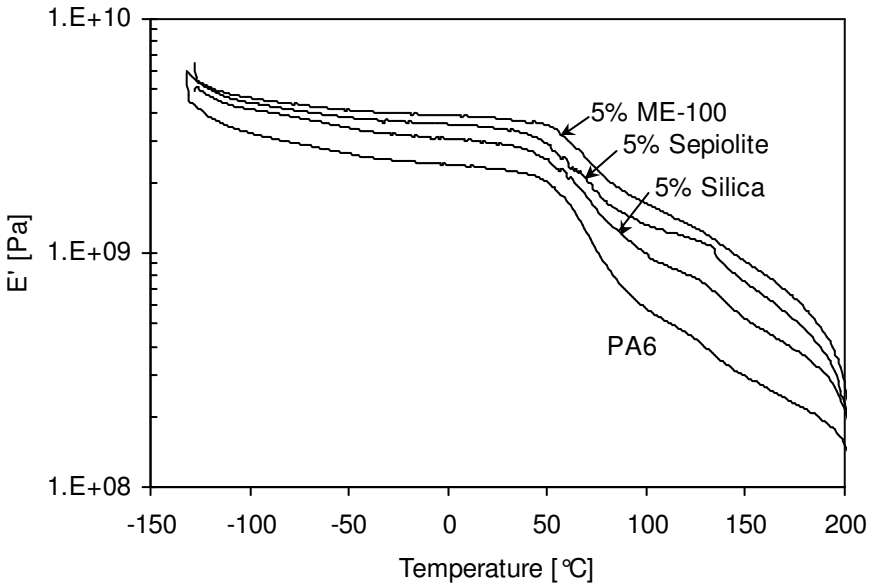


Figure 5.5: The influence of the particle shape on the storage modulus of the nanocomposites. Silica: spherical, sepiolite: fibre, ME-100: platelet.

The spherical particles (silica) result in the smallest modulus enhancement. The platelet (ME-100) is the most effective shape because it reinforces in two directions, while the fibres (sepiolite) just in one. Figure 5.6 shows the effect of the particle shape of the micro-composites. Comparing the modulus values in figure 5.5 with those in figure 5.6, it can be seen that the microparticles are less effective than the nanoparticles. Below T_g there is no significant difference in the modulus between the various shapes, probably because of the relatively low filler content for glass composites. However, above T_g the higher aspect ratio particles are more effective than the glass beads.

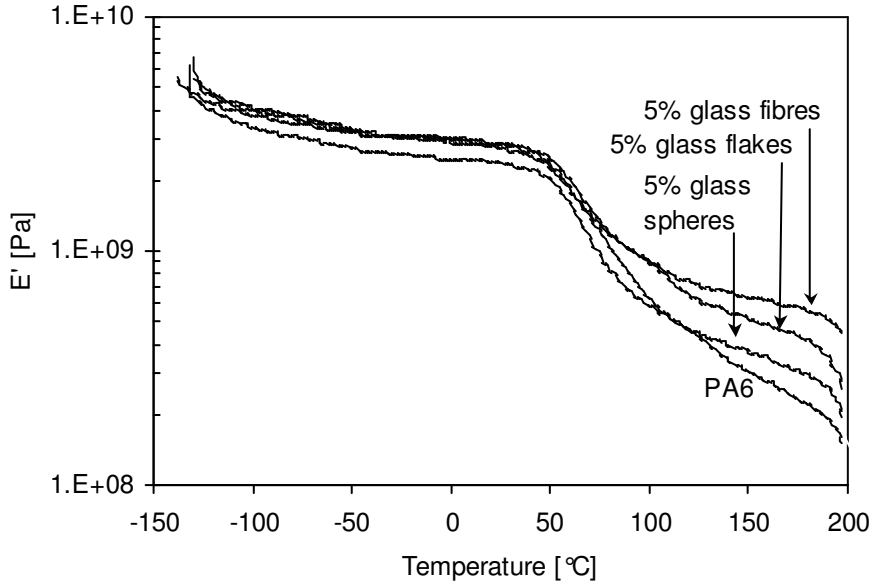


Figure 5.6: The influence of the particle shape on the storage modulus of the microcomposites.

As already mentioned, the Halpin-Tsai model (eq. 5.1) can be used to estimate the effective aspect ratio from composite moduli. There may be a small enhancement of the matrix (PA6) modulus in the nanocomposites, because the particles could induce a slightly higher crystallinity in the matrix (K123 does not contain a nucleating agent). This difference can affect the estimation of the aspect ratio. To compensate for the nucleating effect, the matrix modulus used in the Halpin-Tsai model was estimated by applying the model to the 5% silica nanocomposite, of which the aspect ratio is known (= 1). The matrix modulus from this silica nanocomposite was used in the models of all other nanocomposites. For the MEE nanocomposites an additional correction was used to correct for the relatively large volume fraction of surfactant. It

was assumed that the surfactant does not add stiffness to the matrix and the matrix modulus of the MEE nanocomposites can be calculated from:

$$E_{matrix\ MEE} = (1 - \varphi_{surfactant}) \cdot E_{matrix\ nanocomposites} \quad 5.15$$

Another parameter in the composite model is the particle orientation. Because the flow during pressing of the specimen causes alignment of the particles, the platelets are assumed to be aligned in the plane of the film, while the fibres are assumed to be randomly oriented in the two major dimensions of the film. The calculated composite modulus is then [5]:

$$E_{plate\ composite} = E_{aligned\ plates} \quad 5.16$$

$$E_{fibre\ composite} = 0.375 \cdot E_{aligned\ fibres} + 0.625 \cdot E_{perpendicular} \quad 5.17$$

wt%	Filler type	(a/b) Halpin-Tsai [21]	τ_{yield} [Pa]	(a/b) Simha oblate [11] [1]	(a/b) Kuhn [13] [1,2]	(a/b) Utracki [14] [1,3]	(a/b) Simha prolate [11] [1]
1%	MEE	(61)*	0	173	277	311	
2%	MEE	170	0.5				
5%	MEE	111	1.5				
10%	MEE	77	9.4				
20%	MEE	54	99				
1%	ME-100	31	0	37	59	104	
2%	ME-100	28	0.2				
5%	ME-100	31	0.3				
10%	ME-100	17	0.2				
20%	ME-100	16	0.4				
5%	Glass flake	12	0	21	34	68	
5%	Glass fibre	20	0				12
5%	Sepiolite	20	4				20

Table 5.1: Apparent yield stress (τ_{yield}) and aspect ratios (a/b) calculated from the modulus (Halpin-Tsai) and the viscosity.

* Large error due to low filler content, see text.

[1] Only data at lowest filler content, because it is derived from [η].

[2] Based on linear fit (equation 5.13) by Luciani [12].

[3] Based on power law dependence (Utracki, equation 5.14).

Despite the uncertainty in many factors such as the matrix and filler modulus, filler orientation, polydispersity and density, the effective aspect ratios could be calculated

using the Halpin-Tsai composite theory and compared with calculations from rheological measurements and microscopy observations. These aspect ratios from the Halpin-Tsai theory are shown in table 5.1, in the third column. The results at very low silicate content (e.g. at 1 % MEE) are very sensitive to the value of the modulus and are, therefore, not reliable. The margin of error decreases for higher filler content. The general trend from the modulus data is a decreasing aspect ratio at increasing silicate content, similar to the trend observed in chapter 2 and 3.

5.4.3 Rheological tests

Determination of the yield stress

The complex modulus of unfilled polymers and composites without a yield stress converges to zero at zero shear frequency. However, nanocomposites with high silicate content can form a structure in the melt, which leads to a yield stress. This effect is present in the MEE nanocomposites, as can be seen in figure 5.7.

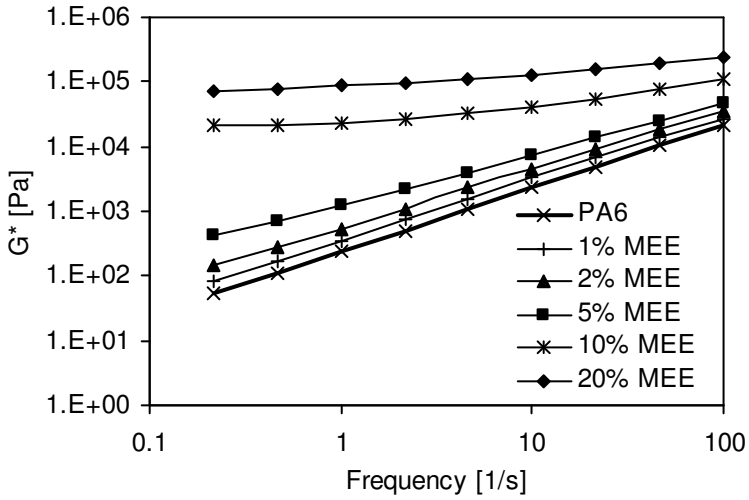


Figure 5.7: Complex modulus MEE nanocomposites.

While for unfilled PA6 and low MEE volume fractions the plot in figure 5.7 shows a straight line converging to zero for $\omega \rightarrow 0$, the modulus for higher concentrations levels off to a finite value. An apparent yield stress can be determined from this value, and is shown in table 5.1 and figure 5.8.

A corrected viscosity, $\eta_{corrected}$, can then be calculated by subtraction of this apparent yield stress from the measured stress, using equation 5.5. The unfilled matrix and the microcomposites have zero yield stress. The nanocomposites containing unmodified particles have very low yield stresses, even up to 20 wt% filler. The MEE

nanocomposites show a steep increase in the yield stress above 5 wt%. At 20 % MEE silicate, τ_{yield} is more than 3 decades higher than at 20 wt% ME-100. A high yield stress can be a disadvantage for applications were flow occurs at low speed, such as in the impregnation of (macro-) fibre composites [22] (chapter 7 and 8).

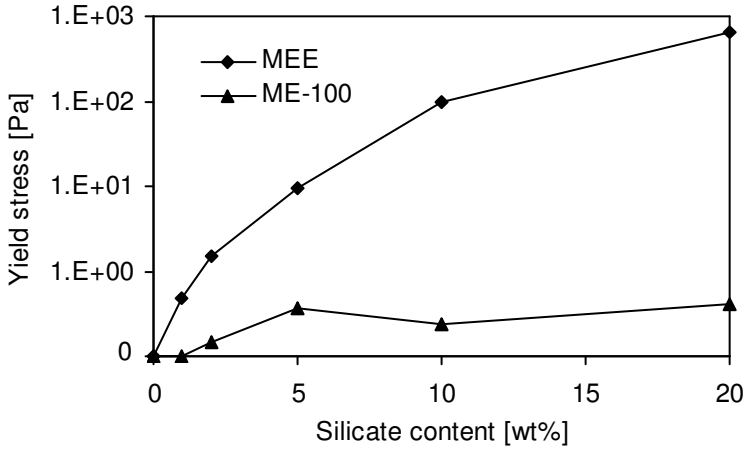


Figure 5.8: The apparent melt yield stress of the MEE and ME-100 nanocomposites.

The influence of size and shape on the viscosity

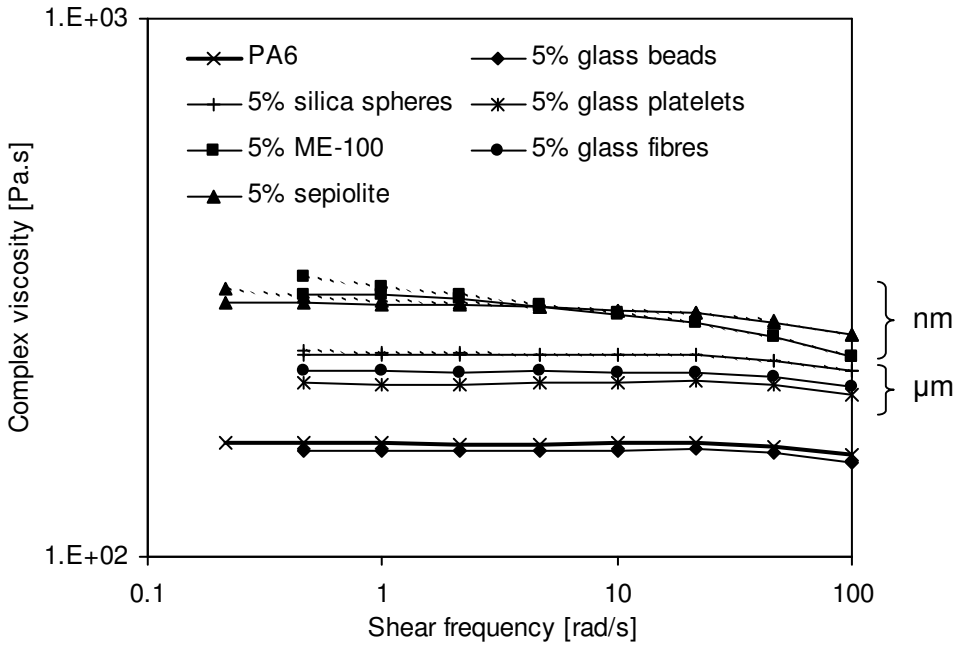


Figure 5.9: Complex viscosity of 5 wt% glass microcomposites and silica(te) nanocomposites at 250 °C. Dotted lines indicate as-measured viscosities (corrected for polymerization during measurement). Solid lines indicate viscosities corrected for the yield stress.

To investigate the influence of the size and shape of the particles on the viscosity, μm-sized glass spheres, fibres and platelets with comparable aspect ratios were compared with the nm-sized unmodified particles. All data were compensated for a small viscosity increase due to some polymerization during the measurement. Figure 5.9 shows the complex viscosity of 5 wt% composites at 250 °C. Subtraction of the apparent yield stress from the raw data results in Newtonian behaviour over a large range of frequencies. The slightly lower viscosity with glass spheres is probably just inaccuracy of the measurement. Two trends regarding the influence of the shape and the size of the particles can easily be seen in figure 5.9. The first trend is that the fibres result in the largest increase in viscosity, closely followed by the platelets (for both μm and nm sized particles). All models described in section 5.2.2 predict this effect of the aspect ratio correctly. Increasing the aspect ratio of the particles can be seen as increasing their *effective* volume fraction, because high aspect ratio particles need more space to rotate and move around. The second trend is that the viscosity of the nano-composites is higher than the viscosity of the equivalent micro-composites. This is probably caused by the surface area of the nanoparticles, which is much larger than that of the microparticles. This could slow down the movement of the polymer chains in the melt.

The influence of the volume fraction

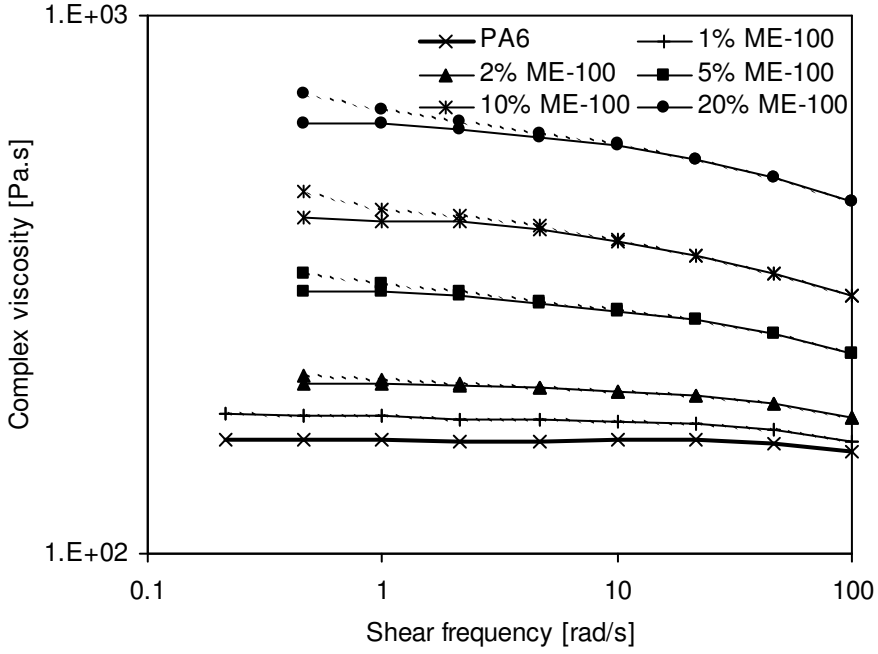


Figure 5.10: Complex viscosity of PA6 ME-100 nanocomposites at 250 °C.
Dotted lines indicate as-measured viscosities (corrected for polymerization during measurement). Solid lines indicate viscosities corrected for the yield stress.

Figure 5.10 shows the complex viscosity obtained from oscillatory shear measurements of ME-100 nanocomposites. The corrected viscosities show a Newtonian plateau at low frequencies and increase linearly as a function of filler content between 0 and 20 wt% ME-100.
Figure 5.11 shows the same for MEE nanocomposites.

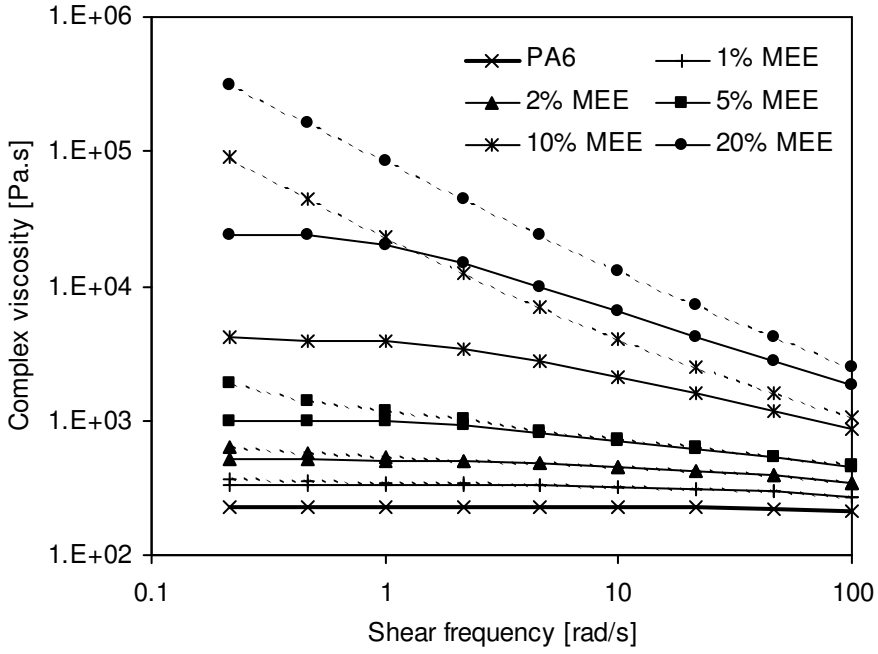


Figure 5.11: Complex viscosity of PA6 MEE nanocomposites at 250 °C.
Dotted lines indicate as-measured viscosities (corrected for polymerization during measurement). Solid lines indicate viscosities corrected for the yield stress.

The viscosity of MEE nanocomposites increases much faster with increasing silicate content compared to the ME-100 nanocomposites, with a strong acceleration above 5%. With increasing volume fraction the platelets or aggregates are more hindered in their rotation and movement, leading to a structure that can cause pseudo-solid behaviour. The high apparent yield stress at these higher concentrations (figure 5.8) is an indication of such a strong structure in the melt. When forced to flow, the nanocomposites are strongly shear thinning, because of the breaking up of the structure. After correction for the apparent yield stress, the viscosity shows a zero shear Newtonian plateau. This viscosity plateau will be used for the calculation of the aspect ratios of the particles.

5.4.4 Calculation of the aspect ratios from viscosity data.

The aspect ratios of the particles are estimated from the complex viscosity data in the melt and compared with those calculated from the storage modulus in the solid state and those estimated from optical microscopy or TEM. The aspect ratios (a/b) are calculated from the complex viscosities after they are corrected for the effect of the yield stress (Newtonian plateau). The intrinsic viscosity is used for these calculations as a common basis for the comparison of composites with several filler types and volume fractions. For the ME-100 and MEE nanocomposites many concentrations have been tested and the intrinsic viscosity can be estimated from the intercept of the plot of $\eta_{reduced}$ versus filler content at zero concentration (figure 5.12).

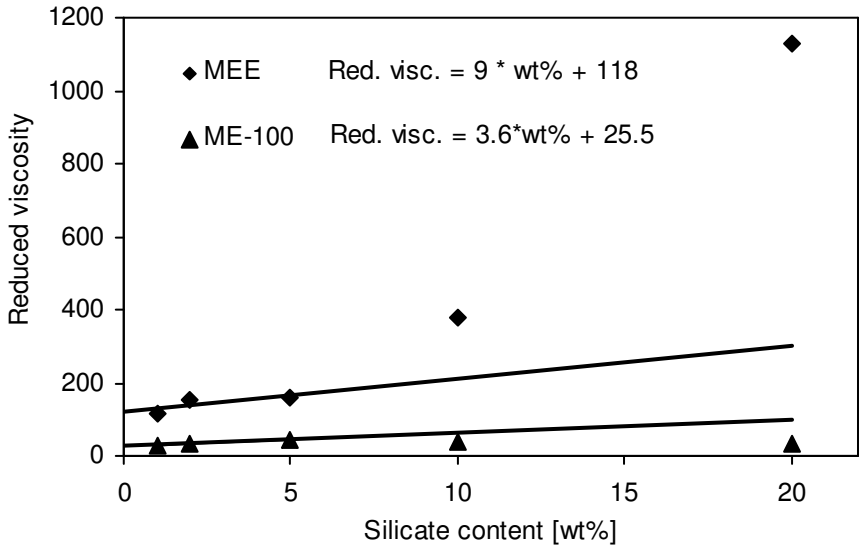


Figure 5.12: Reduced viscosity MEE and ME-100 nanocomposites.

A linear fit through the concentrations up to 5 wt% is used for this. The intrinsic viscosity is 25.5 for the ME-100 nanocomposites and 118 for the MEE nanocomposites (the latter is close to the value for in-situ polymerized nanocomposites (105.5) found by Utracki [14]). A reasonable estimate of the intrinsic viscosity for the other composites is obtained from the reduced viscosity at 5 wt%, as is suggested by figure 5.12: up to 5 wt% the reduced viscosity does not depend strongly on the filler content. Figure 5.13 shows the dependence of the intrinsic viscosity on the platelet aspect ratio described by the theory of Simha (eq. 5.12), Luciani/Kuhn (eq. 5.13) and Utracki (eq. 5.14). The two horizontal lines at 118 and 25.5 indicate the values of the intrinsic viscosity of the MEE and ME-100 nanocomposites. The intersections of these lines with the three theoretical curves determine the aspect ratios of the particles. These are shown in table 5.1 together

with the values estimated from the reduced viscosities for the other composites. The viscosity model by Simha for oblate ellipsoids (platelets) predicts values of the particle aspect ratios close to the values predicted by the Halpin Tsai composite theory for both MEE and ME-100 nanocomposites.

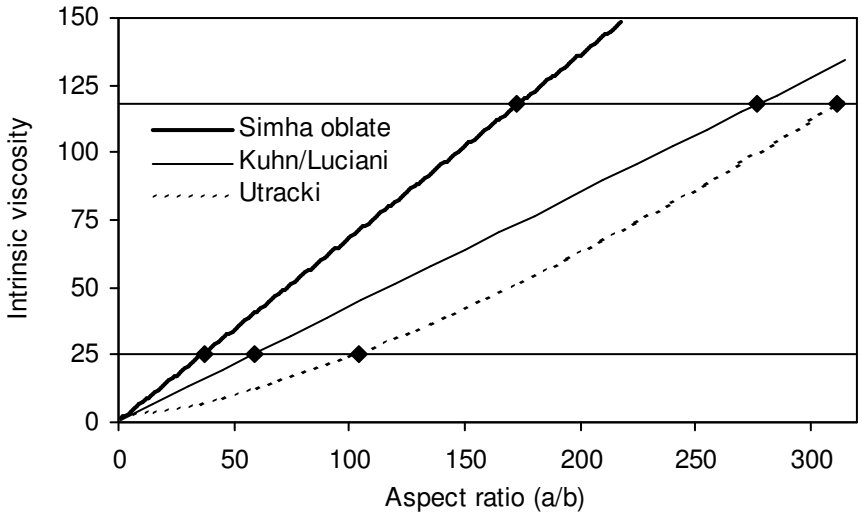


Figure 5.13: Aspect ratio versus intrinsic viscosity for platelet composites.

Although it is impossible to obtain accurate average particle sizes from TEM, figure 5.2 suggests that the Simha model predicts reasonable aspect ratios for these nanoparticles. The viscosity theory of Kuhn/Luciani [12,13] is more suitable for relatively large particles, where Brownian motion can be ignored, and could overestimate the aspect ratio for nanoparticles. It has been shown that this theory correlates very well with experimental results from micro-scale mica composites [12]. This theory indeed seems to overestimate the aspect ratio for nanoparticles, as well as the theory of Utracki. The increase in modulus is very small for the glass filled composites, and, therefore, the error in the Halpin-Tsai results is larger in this case than for the nanocomposites. This can explain the differences between the aspect ratios calculated from the modulus and the viscosity.

The Simha viscosity model for prolate ellipsoids (equation 5.10 and 5.11) yields an aspect ratio for sepiolite close to the one of the Halpin-Tsai model and the TEM results (figure 5.2C). For the (micro) glass fibres the calculated aspect ratio is too low. Therefore, it appears again that the Simha equation (for fibres) applies better for nanocomposites than for micro-composites, just as for the platelets.

5.4.5 Comparison between the modulus increase and the viscosity increase

A comparison between the modulus increase and the viscosity increase should now be made to find the particles that provide the best compromise for specific applications, such as fibre composite matrix. The modulus increase (enhancement of the mechanical properties) can be compared with the viscosity increase (worsening of the processing properties) by plotting the relative modulus ($E_{composite}/E_{matrix}$) at room temperature versus the relative viscosity in the melt. This is shown in figure 5.14 at two shear frequencies: at 0.46 rad/s (figure 5.14A) and at 100 rad/s (figure 5.14B).

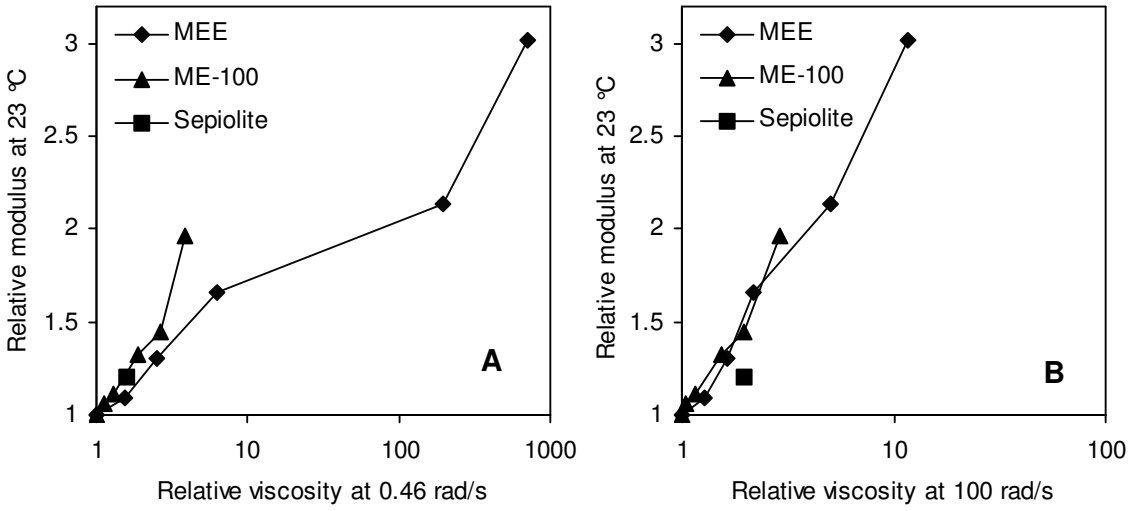


Figure 5.14: Relative modulus compared with relative viscosity (uncorrected for yield stress): **A** 0.46 rad/s, **B** 100 rad/s

All relative viscosities are based on the complex viscosities calculated without subtraction of the yield stress, because this is more representative for the forces in the processing equipment. From figure 5.14A it can be seen that for low shear rate processes, such as fibre impregnation and wetting, nanocomposites based on unmodified silicate have the advantage of a lower viscosity compared to those based on modified silicate for equivalent modulus enhancement, especially at loadings above 5%. The advantage becomes even clearer when also the yield stress is considered (figure 5.8). However, when processes with high shear rates (figure 5.14B) are applied, such as injection moulding, both types of nanocomposite show a similar increase in viscosity. At high shear rates the penalty in the viscosity for better exfoliation is reduced, probably because the platelets become aligned. The fibre shaped sepiolite nanofiller causes a larger increase of the viscosity than the platelet filler at a similar modulus increase at high shear rates. This is supported by the

theories, which predict a quadratic dependence of the viscosity on the aspect ratio for fibres influenced by Brownian motion, and a linear dependence for platelets. The solid-state modulus predicted by the Halpin-Tsai model shows a linear dependence for all shapes.

A remark on the effect of the particle size on the viscosity is due here. When nanofillers are used, there is a much larger area available for interactions between the surface of the particles and the matrix melt. This effect is stronger when the particles are modified to improve the exfoliation, such as in the MEE nanocomposites. Therefore, the simple Einstein-type viscosity models are not expected to hold well in this case. It can be expected that interactions will add a contribution to the friction between particles and matrix and, thus, increase the viscosity. For not too concentrated suspensions this contribution can be expected to be proportional to the existing interfacial surface. For the same volume fraction of particles, φ, the interfacial surface depends on the size of the particles. For example, in a composite with fibres of length b and diameter a, the specific interfacial surface is approximately:

$$S_{spec} \approx n\pi ba \quad \text{with} \quad \varphi = n\pi \frac{b^2}{4} a \quad \rightarrow \quad S_{spec} \approx \frac{\varphi}{b} \qquad 5.18$$

where n is the number of particles per volume. This proportionality is valid for any particle shape, where b is a characteristic size. A better form for the Einstein equation that includes interactions, then, could be:

$$\frac{\eta}{\eta_0} = 1 + \left(k_E + \frac{k_{int}}{b} \right) \varphi \qquad 5.19$$

The factor k_{int} in equation 5.19 gives the degree of interaction between the matrix and the particles, while k_E is the factor 2.5 in Einstein's equation or ν in the theory of Simha. Equation 5.19 describes the fact that the viscosity of filled fluids is not only shape-dependent but also size-dependent. In order to use this equation one needs information on the value of k_{int}, but this is beyond the scope of this thesis. This additional term becomes important when the characteristic size b is small and it can explain some of the differences in the viscosity between the nanocomposites and the microcomposites in figure 5.9.

5.5 Conclusions

Nanocomposites show higher moduli in the solid state at low filler content than glass micro-composites. This higher modulus is accompanied by a stronger increase in melt viscosity. The particle shape and aspect ratio have a strong influence on both the modulus in the solid state and the melt viscosity. The modulus increase is higher for platelets than for fibres for the same volume fraction, because the platelets reinforce in two directions instead of one. The viscosity increases less for platelets than for fibres. This is accounted for by theories, which predict a linear dependence on the aspect ratio for platelets and a quadratic one for fibres. The nanocomposites produced with unmodified nano-platelets have a lower modulus and a lower viscosity than those based on organically modified platelets. The data and models based on the room temperature modulus or on the melt viscosity give an average aspect ratio for the unmodified silicate of approximately ¼ of the modified silicate. This is due to the larger amount of multi-platelet stacks in the unmodified silicate nanocomposite, which were also observed in TEM. In modified silicate nanocomposites the melt yield stress increases rapidly above 5 wt% silicate, suggesting a strong structure of interacting particles. The unmodified particles do not lead to a large yield stress, even up to 20 wt% filler.

The Simha theory for oblate and prolate spheroids predicts aspect ratios from melt viscosity data that are close to the results from the Halpin-Tsai model for nanocomposites. For the glass microcomposites the theory of Kuhn [13], which does not include the effect of Brownian motion, is more accurate, although the modulus increase in the glass microcomposites was too small for an accurate calculation of the aspect ratios.

When the advantages in mechanical properties (high modulus) are compared with the disadvantage of the increased viscosity and yield stress in the melt, it is clear that the choice for the best filler type depends on the type of process that is used to process the nanocomposite. For low shear rate processes, such as fibre impregnation and wetting, nanocomposites based on unmodified silicate have the advantage of a lower viscosity and a much lower yield stress (or no yield stress at all at low filler content) compared to those based on modified silicate for the same modulus enhancement. However, for high shear rate processes, such as injection moulding, both types of nanocomposite show a similar increase in viscosity, probably because the platelets can align in fast flow fields. In this case the modulus advantage

of the modified platelets is the determining criterion. For film blowing or extrusion this high viscosity can be an advantage, similar to high MW polymers.

One factor that viscosity theories based on Einstein's equation do not take into account is the effect of the size of the particles. The viscosity of nanoparticles filled fluids can be shape and size dependent. This is caused by the interaction of the polymer with the large surface area of the filler. A factor containing the degree of interaction divided by the specific filler size could be incorporated in Einstein's equation to describe the effect of surface interactions.

5.6 References

1. Kojima Y, Usuki A, Kawasumi M, Okada A, Fukushima Y, Kurauchi T, Kamigaito O. Mechanical-Properties of Nylon 6-Clay Hybrid. Journal of Materials Research 1993;8(5):1185-1189.
2. Usuki A, Kawasumi M, Kojima Y, Okada A, Kurauchi T, Kamigaito O. Swelling Behavior of Montmorillonite Cation Exchanged for Omega-Amino Acids by Epsilon-Caprolactam. Journal of Materials Research 1993;8(5):1174-1178.
3. Usuki A, Kojima Y, Kawasumi M, Okada A, Fukushima Y, Kurauchi T, Kamigaito O. Synthesis of Nylon 6-Clay Hybrid. Journal of Materials Research 1993;8(5):1179-1184.
4. Es MAv, Xiqiao F, Turnhout Jv, Giessen Evd. Comparing Polymer-Clay Nanocomposites with Conventional Composites using Composite Modeling. In: Al-Malaika Sea, editor. Specialty Polymer Additives: Blackwell Science; 2001.
5. Es MAv. Polymer clay nanocomposites. The importance of particle dimensions. Delft: Delft University of Technology; 2001.
6. Hoffmann B, Kressler J, Stoppelmann G, Friedrich C, Kim GM. Rheology of nanocomposites based on layered silicates and polyamide-12. Colloid and Polymer Science 2000;278(7):629-636.
7. Krishnamoorti R, Yurekli K. Rheology of polymer layered silicate nanocomposites. Current Opinion in Colloid & Interface Science 2001;6(5-6):464-470.
8. Krishnamoorti R, Giannelis EP. Rheology of end-tethered polymer layered silicate nanocomposites. Macromolecules 1997;30(14):4097-4102.
9. Giannelis EP, Krishnamoorti R, Manias E. Polymer-silicate nanocomposites: Model systems for confined polymers and polymer brushes. Advances in Polymer Science 1999;138:107-147.
10. Solomon MJ. Rheology of Polypropylene/Clay Hybrid Materials. Macromolecules 2001;34:1864-1872.
11. Simha R. The influence of Brownian movement on the viscosity of solutions. Journal of Physical Chemistry 1940;44:25–34.
12. Luciani A, Leterrier Y, Manson JAE. Rheological behaviour of dilute suspensions of platelet particles. Rheologica Acta 1999;38(5):437-442.
13. Kuhn W, Kuhn H. Die Abhangigkeit Der Viskositat Vom Stromungsgefalle Bei Hochverdunnten Suspensionen Und Losungen. Helvetica Chimica Acta 1945;28(1):97-127.
14. Utracki LA, Lyngaae-Jorgensen J. Dynamic melt flow of nanocomposites based on poly-epsilon- caprolactam. Rheologica Acta 2002;41(5):394-407.
15. Ruiz-Hitzky E. Molecular access to intracrystalline tunnels of sepiolite. Journal of Materials Chemistry 2001;11(1):86-91.
16. Shell HR, Ivey KH. Fluorine Micas: Bureau of Mines, US Department of the Interior; 1969.
17. Hull D, Clyne TW. An Introduction to Composite Materials. Cambridge; 1996.

18. Rothon R. Particulate-filled polymer composites: Longman; 1995.
19. Korbee R; Process for the preparation of polyamide nanocomposite composition. NL patent WO 99/29767 DSM. 1999.
20. Kohan MI. Nylon Plastics Handbook: Carl Hanser Verlag; 1995.
21. Halpin JC, Kardos JL. Halpin-Tsai Equations - Review. Polymer Engineering and Science 1976;16(5):344-352.
22. Vlasveld DPN, Parlevliet PP, Bersee HEN, Picken SJ. Fibre–matrix adhesion in glass-fibre reinforced polyamide-6 silicate nanocomposites. Composites Part A: Applied Science and Manufacturing 2005;36(1):1-11.

The results described in this chapter have been published as:

D.P.N. Vlasveld, M. de Jong, H.E.N. Bersee, A.D. Gotsis, S.J. Picken.

The relation between rheological and mechanical properties in PA 6 nanocomposites and microcomposites. Polymer 2005, In Press

Chapter 6

Creep and physical aging behaviour of PA6 nanocomposites

6.1 Introduction

Creep is the time dependent deformation of materials subjected to a continuous stress. This deformation can be both elastic and plastic, and therefore it can be non-recoverable when the load is removed. Creep can lead to unacceptable deformation and eventually even to structural failure and is, therefore, a very important property for engineering plastics and composites. The creep response is quantified by the creep compliance, which is the strain divided by the applied stress.

In polymers, the deformation process under load is strongly dependent on the mobility of the chains. The chain mobility is not only temperature dependent, but also time dependent. The time dependent change of the properties in amorphous polymers below T_g is known as physical aging [1]. The physical aging process is driven by the difference between the actual volume and the thermodynamic equilibrium volume of an amorphous polymer when it is quenched from a temperature above T_g to below T_g. Upon fast cooling below T_g the polymer cannot shrink fast enough to keep the equilibrium volume due to the low chain mobility. Therefore, during extended aging periods the polymer slowly evolves towards this equilibrium situation. The physical aging process results in property changes such as an increase in density, modulus and yield stress, and a reduction in ductility, ultimate elongation and creep rate.

In semi-crystalline polymers the physical aging behaviour of the amorphous phase is more complex. It has been shown that physical ageing also occurs well above T_g of the amorphous phase in semi-crystalline polymers [1-9]. An explanation for this extended temperature range at which ageing occurs was proposed by Struik [1,4-6], and involves a range of different amorphous phases. In general, the model assumes that amorphous polymer close to a crystalline region or filler particle has a reduced mobility and therefore a higher T_g. Further from the rigid phase, the T_g decreases towards the bulk T_g. This results in the broadening of the loss modulus peak compared to purely amorphous polymers as is seen in dynamic mechanical

measurements. In the simplified Struik-model two different T_g's are assumed instead of a continuous range: one for the bulk amorphous material and one for the material with a reduced mobility. The aging behaviour below the lowest (bulk) T_g (region 1) is similar to the behaviour in amorphous polymers. Struik [1] has shown that at low deformations (in the linear visco-elastic regime) and below T_g the creep curves for different ageing times can be superimposed on one reference ageing time by shifts along the time axis (see figures 6.1-6.7). A commonly used method to describe the aging behaviour is to plot the shift factor a_{te} versus the aging time t_e on a double logarithmic plot and determine the slope. The slope μ (equation 6.1) in the plot of log (a_{te}) versus log (t_e) is known as the shift rate [1].

$$\mu = \frac{d\log(a_{te})}{d\log(t_e)} \qquad 6.1$$

Measurement of the creep rate at different ageing times can be performed on the same sample if the stress is small enough to prevent permanent deformation. The testing time should be less than 10% of the ageing time to minimise the effect of ageing during the measurement.

PA6 nanocomposites containing exfoliated layered silicate particles have been developed to improve the mechanical properties, and to reduce the flammability and moisture permeability. Due to the large aspect ratio and the high modulus of the particles the optimal properties are reached at lower filler content than with the use of traditional mineral or fibre fillers. Because of the increased modulus of nanocomposites it can be expected that the creep is also reduced. However, hardly any data have been published so far for nanocomposites on this important subject. The physical aging behaviour also remains to be investigated for nanocomposites. It is interesting to see if the reduced ductility and elongation at break of nanocomposites could have a connection with a modified physical aging. Extensive research has been done previously on the physical ageing of unfilled polyamides, for example on PA6 [1] and PA66 [3]. The results revealed a complex behaviour dependent on ageing temperature and applied stress. Annealing temperatures of 150-160 °C were used for the thermal rejuvenation of the PA6 and PA66 samples before quenching to the ageing temperature, and for the applied stress usually less than 25% of the yield stress was used. For (dry) PA6 the double logarithmic shift rate μ at room temperature was found to be around 0.75.

Measurement of the creep is a very practical method to study the physical aging phenomenon, and in creep studies the influence of physical aging needs to be

considered for a correct interpretation of the data. Therefore, the phenomena of creep and physical aging in PA6 nanocomposites are investigated together in this chapter. PA6 reference materials (low and high molecular weight) are compared with melt-exfoliated nanocomposites with a range of silicate concentrations. In addition, a commercially available in-situ polymerized nanocomposite and a nanocomposite containing unmodified (water-swellable) silicate have been investigated. Samples annealed far above T_g (160 °C) were quenched to room temperature and tested after various ageing times. Some tests were done at 80°C and on moisture conditioned samples to investigate the influence of increased polymer mobility on the creep behaviour.

6.2 Experimental

6.2.1 Materials

Polyamide 6, low molecular weight (LMW PA6)

- Akulon® K222D, injection-moulding grade PA6 from DSM, the Netherlands.
  $M_n \approx 16000$, $M_w \approx 32000$ g/mol, $T_m \approx 220$ °C
  (Similar in properties to K122D and K123 used in other chapters.)

Polyamide 6, high molecular weight (HMW PA6)

- Akulon® K136, film / extrusion grade PA6 from DSM, the Netherlands.
  $M_n \approx 35600$, $M_w \approx 71000$ g/mol, $T_m \approx 220$ °C

Commercially available PA6 nanocomposite

- Unitika M1030D, from Unitika, Japan, containing 4.6% silicate.

This nanocomposite is produced by in-situ hydrolytic polymerization of ε-caprolactam in the presence of swollen organically modified silicates. The organic surfactant is the initiator for polymerization, so the polymer chains are bound to the surfactant via covalent bonds. The surfactants have an ionic bond with the silicate layers and in this way the polymer is ionically bound to the silicate layers, unlike melt-processed nanocomposites, which rely on H-bonding and dipolar interactions.

Organically modified layered silicate

- Somasif® MEE (Synthetic Mica®) from Unicoop, Japan.

This is synthetic fluorine mica, covered with a methyl bis-2-hydroxyethyl coco quaternary ammonium surfactant (28.5 wt%, determined with a Perkin Elmer TGA-7 Thermal Gravimetric Analyzer at 800 °C for 1 hour in air).

Unmodified layered silicate

- Somasif® ME-100 (Synthetic Mica®) from Unicoop, Japan.
  This is water-swellable synthetic fluorine mica, which does not contain any organic surfactant; it is the inorganic basis of Somasif® MEE.

6.2.2 Sample preparation

Extrusion

The nanocomposites with Somasif® MEE were prepared by mixing the layered silicate with PA6 (K222D) in a Werner and Pfleiderer ZDS-K28 co-rotating twin-screw extruder. The extruder was operated at a screw speed of 200 RPM and a feeding rate of approximately 3 kg per hour. The temperature in the feeding zone was 150 °C, all the other zones where heated to 230 °C. Cooling was applied to keep the temperature constant, since the high shear forces in the melt can produce too much heat. First a master batch with 11 wt% (based on the inorganic content of the filler) was made and the lower concentrations were made by diluting the master batch with PA6 in a second extrusion step.

The nanocomposites with Somasif® ME-100 were made by feeding a mixture of cryogenically milled PA6 (K222D) and ME-100 powder in a Werner and Pfleiderer ZSK 30/44 D co-rotating twin-screw extruder. To enhance the exfoliation of the water-swellable ME-100 silicate, water was injected into the extruder at a rate of 25 ml/min, and removed by venting at the end of the extruder. The extruder was operated at a temperature of 240 °C at a rotation speed of 200 rpm and a feeding rate of approximately 10 kg/h.

Injection moulding

Dumbbell shaped samples according to the ISO 527 standard were injection moulded on an Arburg Allrounder 221-55-250 injection-moulding machine. The feeding zone was heated to 150 °C, the melting and mixing zones heated to 240 °C and the nozzle was kept at 260 °C.

Annealing

Dry as moulded samples were annealed in a vacuum oven at 160 °C for 15 hours before quenching to the aging temperature. Subsequently the samples were taken from the vacuum oven and immediately stored in a desiccator containing a $CaCl_2$ drying agent, in an air-conditioned room at 23 °C.

6.2.3 Testing

Silicate content

Thermogravimetric analysis (TGA) measurements were done to determine the exact silicate content in the tested samples after processing. A Perkin Elmer TGA-7 Thermal Gravimetric Analyzer was used to determine the weight fraction of silicate by heating a sample in air at 800 °C for 1 hour.

Creep

The samples were tested on a Zwick 1445 tensile tester with a 10 kN force cell. The test machine was equipped with a force feedback loop to be able to test at a constant stress. A constant stress of 16 MPa was used in all ageing experiments, which is approximately 1/5 of the yield stress. This stress was reached and stabilized within 15 seconds after the start of the loading. The loading period was never longer than 10% of the previous ageing time, to reduce the influence of ageing during the test. The temperature of the test equipment and the samples during the ageing and creep tests was maintained at 23 °C ± 0.5 °C by air-conditioning of the room containing the samples and test equipment. The samples were tested inside a climate chamber on the tensile tester, which was flushed with dried air to prevent moisture uptake during the creep tests. After each creep test the samples were stored again in the desiccator to prevent moisture absorption during ageing.

6.4 Results and Discussion

In figures 6.1-6.7 the results are displayed for all the creep tests on the various materials at different ageing times. The creep compliance (strain/stress) in GPa^{-1} is shown on the vertical axis on a linear scale and the time is shown on a logarithmic scale. For clarity the curves that are shown are obtained from a polynomial fit through

the original data, which removes fluctuations due to small inaccuracies in the measurement.

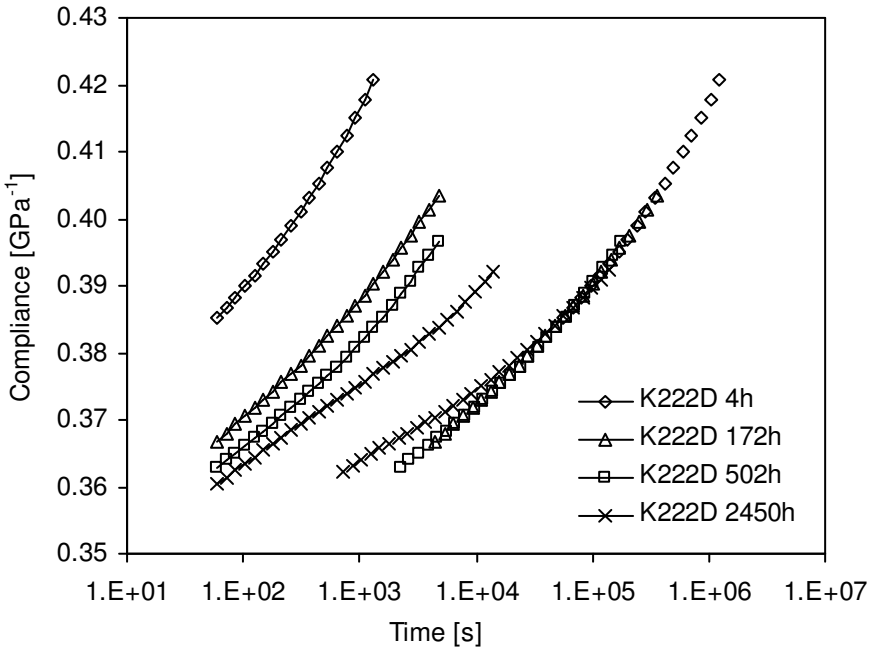


Figure 6.1: Creep compliance for low MW PA6 (K222D) as a function of ageing time. The overlapped curves on the right are the curves shifted over the time axis onto one master curve.

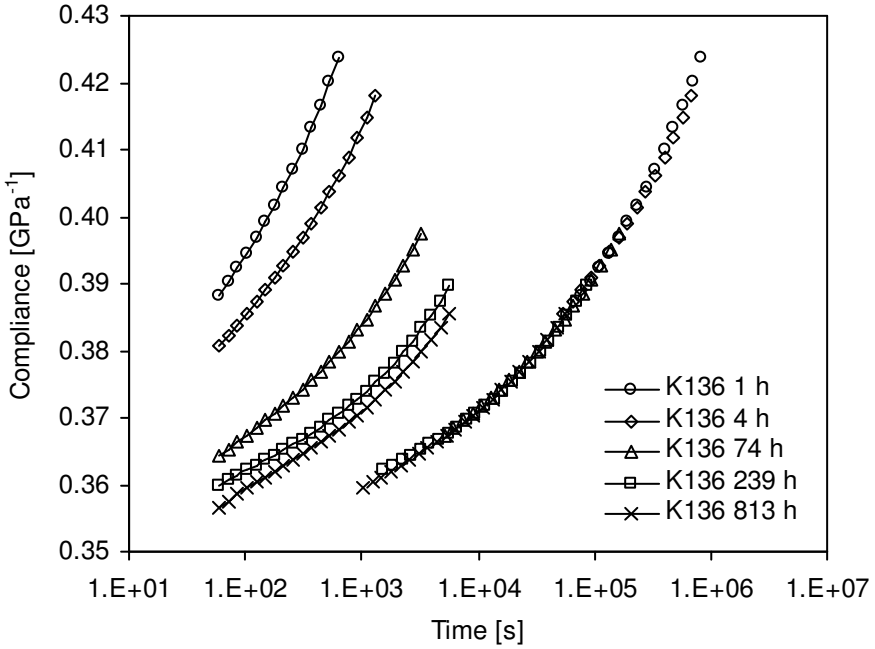


Figure 6.2: Creep compliance for high MW PA6 (K136) as a function of ageing time. The overlapped curves on the right are the curves shifted over the time axis onto one master curve.

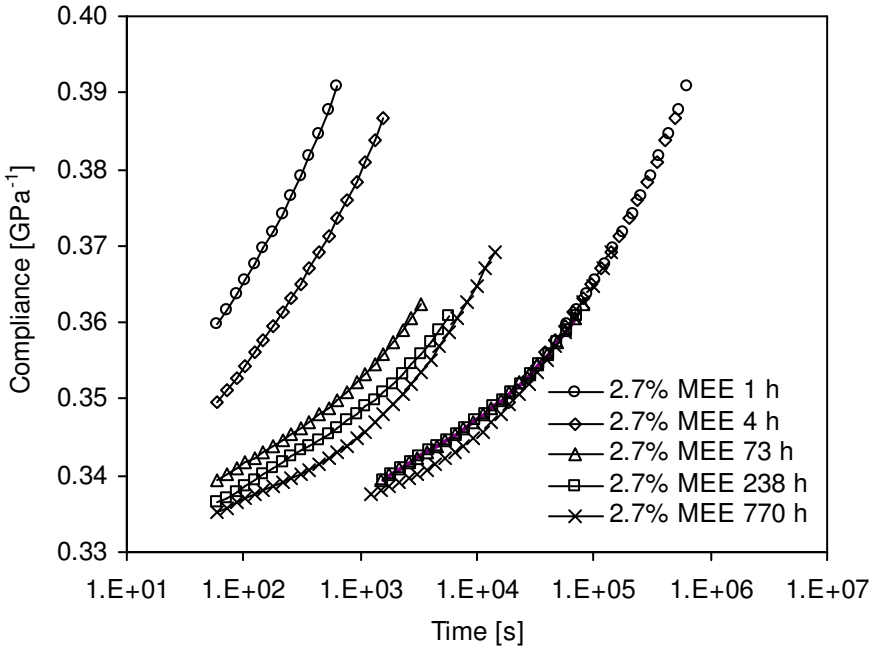


Figure 6.3: Creep compliance for 2.7% MEE nanocomposite as a function of ageing time. The overlapped curves on the right are the curves shifted over the time axis onto one master curve.

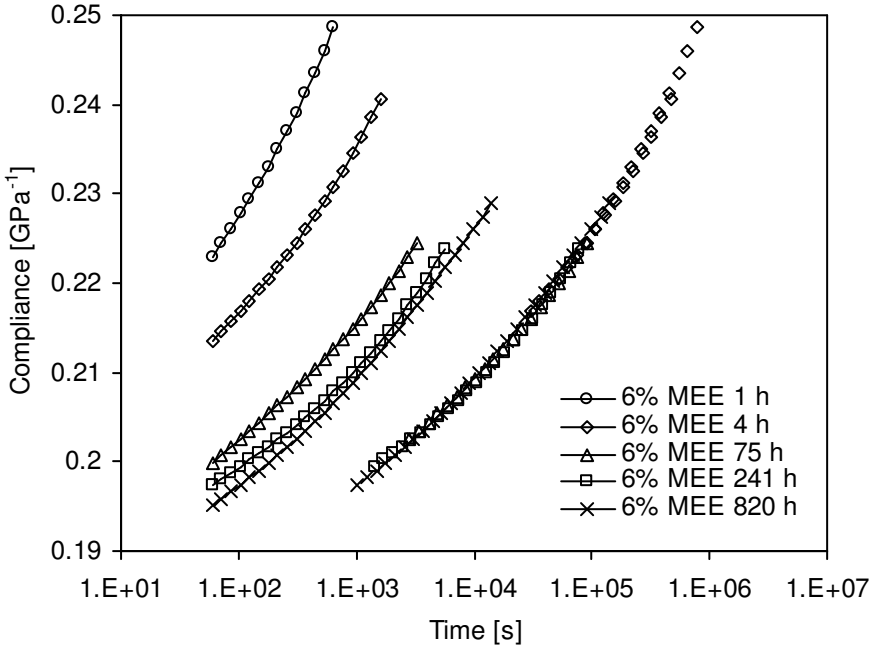


Figure 6.4: Creep compliance for 6% MEE nanocomposite as a function of ageing time. The overlapped curves on the right are the curves shifted over the time axis onto one master curve.

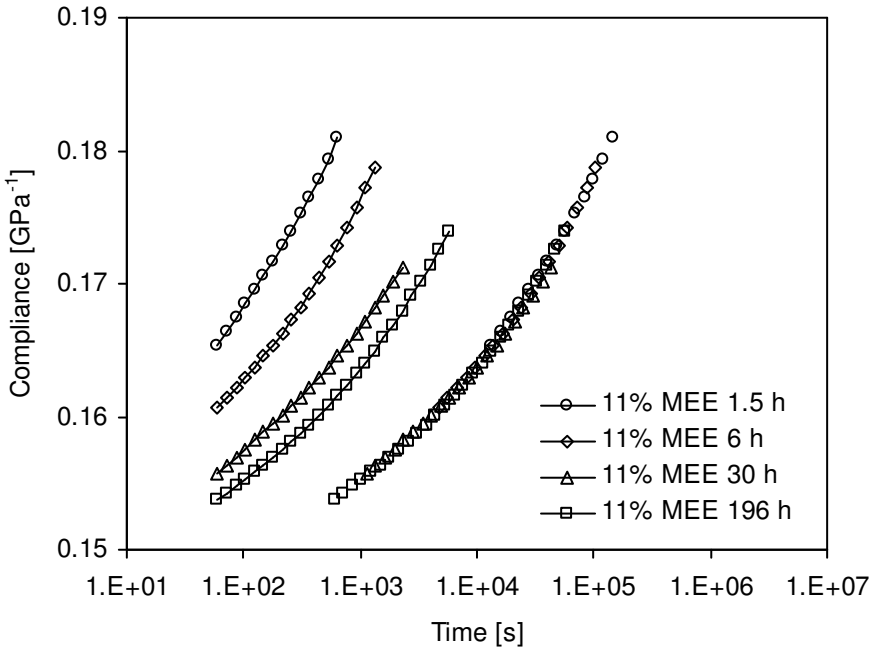


Figure 6.5: Creep compliance for 11% MEE nanocomposite as a function of ageing time. The overlapped curves on the right are the curves shifted over the time axis onto one master curve.

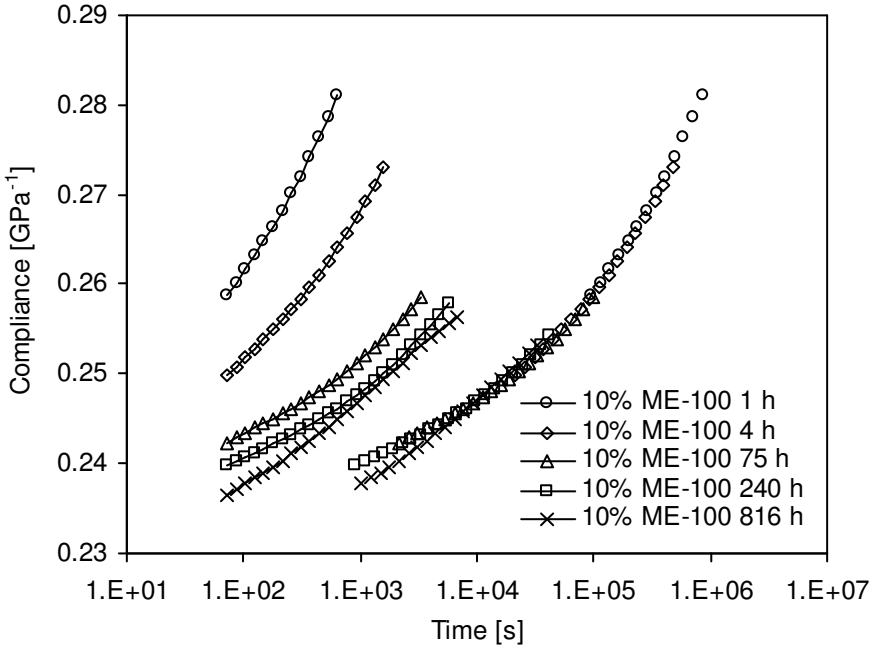


Figure 6.6: Creep compliance for 10% ME-100 (unmodified silicate) nanocomposite as a function of ageing time. The overlapped curves on the right are the curves shifted over the time axis onto one master curve.

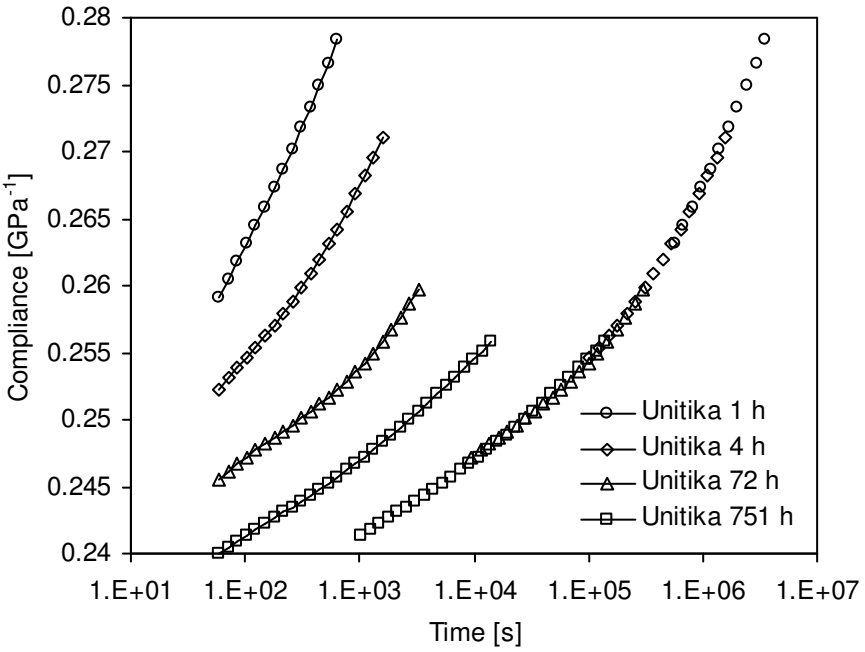


Figure 6.7: Creep compliance for a commercial PA6 nanocomposite (Unitika M1030D) as a function of ageing time. The overlapped curves on the right are the curves shifted over the time axis onto one master curve.

The Kohlrausch-Williams-Watts (KWW) equation, which can describe the ageing behaviour of amorphous polymers [1,3], could not describe every creep curve in these materials accurately enough and, therefore, a polynomial fit of the form $y=a+b\ln t+c\ln^2 t+d\ln^3 t+e\ln^4 t$ (y=compliance, t=time) was used instead. Although the constants in this equation have no physical meaning, the equations can describe all creep curves very accurately and it can be used to determine the slope of the curves. All measurements are performed at 23 °C in a dry environment, well below the T_g of PA6.

In each of the figures 6.1-6.7 the creep curves for different ageing times can be superimposed on one reference ageing time by shifts along the time axis. The master curve was shifted by one decade from the longest ageing time for clarity. In all figures it can be seen that at the highest ageing time (770 h or higher, or approximately one month) the curves have a slightly different shape and that the superposition cannot be done very accurately.

In figures 6.1 and 6.2 the results for two types of unfilled PA6 can be seen. There is virtually no difference in the level of the creep compliance between the two different molecular weights. It shows that below T_g the molecular weight has little influence on the creep behaviour, because only local motion of the chain segments is involved in

the glassy state. Therefore, the creep results will not be influenced by possible differences in MW that might occur due to the processing of the nanocomposites.
In figures 6.3-6.5 the creep results are shown for organically modified nanocomposites containing 2.7, 6 and 11 wt% silicate respectively, figure 6.6 shows the results for a nanocomposite based on unmodified layered silicate and figure 6.7 for a commercial nanocomposite. The shape of the curves in the nanocomposite is very similar to those of the unfilled polymer, but the values of the creep compliance are much lower.

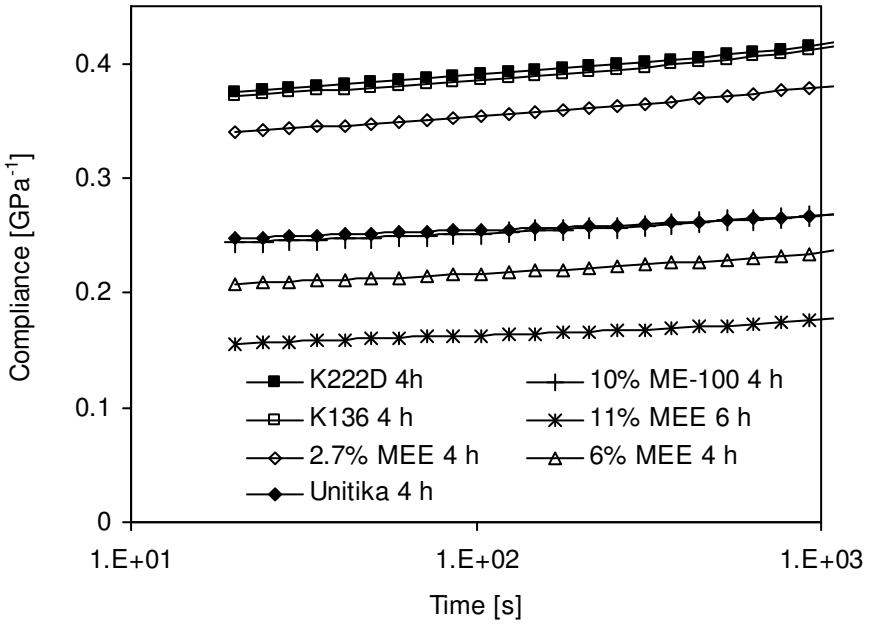


Figure 6.8: Creep compliance after 4 hours ageing for all materials.

In figure 6.8 the creep curves for the different materials after 4 h ageing time (6 h for 11% MEE) are collected, which clearly shows that nanocomposites containing more silicate have a lower creep compliance. A lower initial creep compliance can be expected, because the modulus increases with increasing silicate content (figure 6.9). The modulus at the time that the stress of 16 MPa was first reached (after 20 s) shows an increase as a function of ageing time, see figure 6.9. The increase is approximately linear when plotted versus the logarithm of time. To see if the creep rate is also reduced, besides the initial level of strain due to the higher modulus, the slope of the creep curves is calculated. To eliminate the effect of the differences in the initial compliance due to the differences in modulus, the compliance is normalized by dividing the compliance at time t by the initial compliance at time t_0 (t_0 = 20s, when the maximum stress is first reached) (equation 6.2).

$$J_t / J_0 = \text{normalized compliance} \qquad 6.2$$

The slope of the normalized compliance (SNC), shown in equation 6.3, is plotted in figure 6.10 for all materials after a 4 h ageing time (11% MEE after 6 h).

$$\frac{d\,(J_t/J_0)}{d\,t} = \text{slope of the normalized compliance (SNC)} \qquad 6.3$$

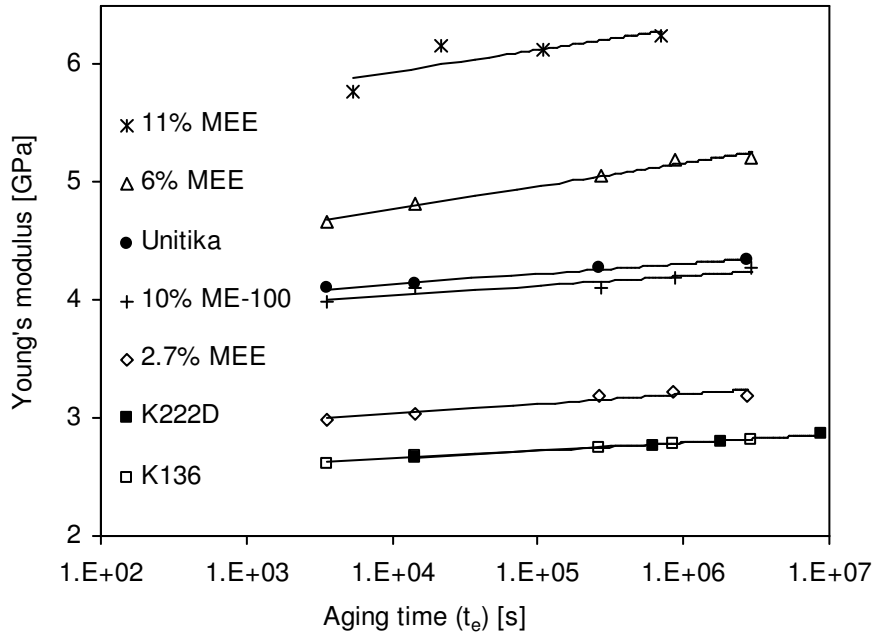


Figure 6.9: Young's modulus as a function of various ageing time, calculated from the initial strain after 20 s, when the maximum stress of 16 MPa was just reached.

The slopes of the normalized compliance (SNC) do not show a large difference between the nanocomposites and the unfilled PA6 (figure 6.10). The in-situ polymerized nanocomposite (Unitika) seems to have a slightly lower SNC. This could indicate a slightly faster physical ageing in this type of nanocomposite.

The logarithm of the shift factors a_{te} are plotted versus the logarithm of the aging time t_e on a double logarithmic plot in figure 6.11. The slope of the curves in figure 6.11 determines the shift rate μ, as was shown in equation 6.1. The slopes are not changed much by the addition of layered silicate nanoparticles. The last points in the curves for the MEE nanocomposites, belonging to ageing times above one month, seem to deviate from the increase in a straight line. This could be a result of the equilibrium situation being approached, as was observed in glassy epoxy networks 5-

10 °C below T_g [10]. However, because of the larger distance from T_g it is more likely that it is related to the change in curve shape observed at the longest ageing times, which makes time-ageing time superposition difficult (see figures 6.1-6.7). If the last point clearly deviates it is not used in the determination of the shift rate.

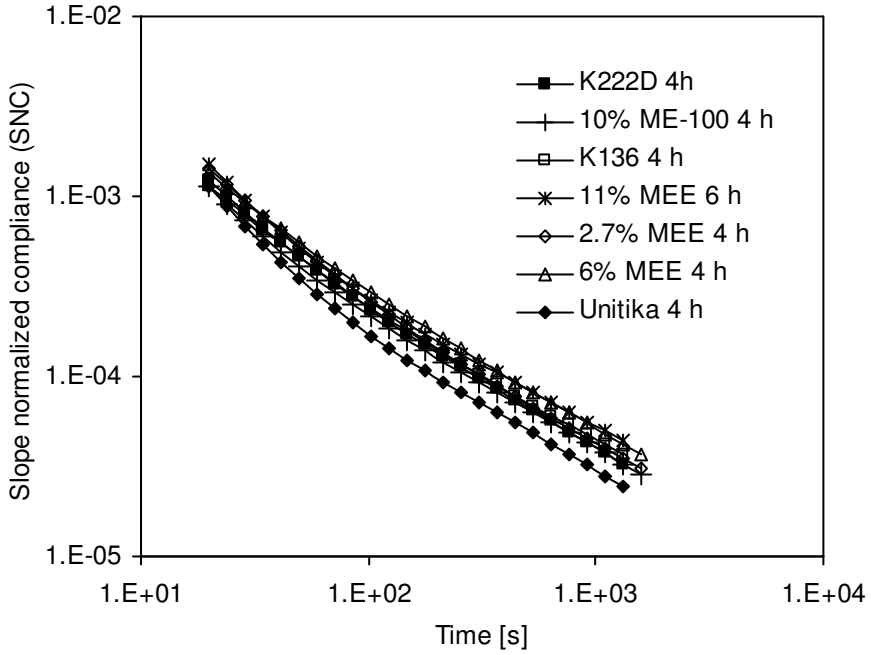


Figure 6.10: Slope of the normalized creep compliance curves after 4 hours of ageing time (6 h for 11% MEE). Equation 6.3 is used for the calculations.

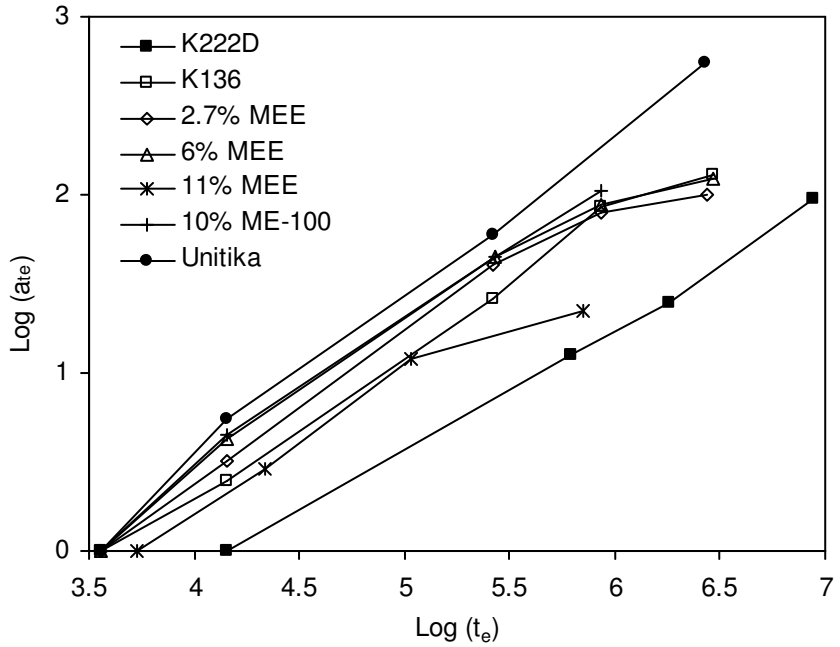


Figure 6.11: Double logarithmic plot of the shift factor a_{te} versus the ageing time t_e. The slope of the curves is the logarithmic shift rate μ (see table 6.1).

Material	Shift rate μ
K222D	0.70
K136	0.76
2.7% MEE	0.82
6% MEE	0.82
11% MEE	0.83
10% ME-100	0.84
Unitika M1030D	0.93

Table 6.1: Double logarithmic shift rate

The shift rates (slopes) for all materials (table 6.1) show a somewhat higher shift rate for the nanocomposites. The effect is not very large, and a difference between the two types of unfilled PA6 can be seen as well. The difference between the two unfilled PA6 samples is probably an indication of the margin of error, because both types of PA6 seem to show the same behaviour in creep compliance (figure 6.1 and 6.2) and modulus (figure 6.9). The values between 0.70 and 0.76 for unfilled PA6 are in the same range as measured by Struik for PA6 at room temperature [1]. The Unitika nanocomposite has a higher shift rate than the other nanocomposites and unfilled PA6 samples, which may indicate a faster physical ageing. Faster physical ageing can also explain the lower SNC of this nanocomposite as can be seen in figure 6.10.

One important property to take into account when using polyamides is the fact that they absorb moisture from the air, which has a strong influence on the mechanical properties. PA6 absorbs around 2.5 % water in a 50 % RH environment, which leads to a lowering of T_g of approximately 30 °C [11]. It is particularly interesting to investigate which effect the use of nanofillers has on the creep and physical ageing properties of PA6 nanocomposites in moisture conditioned samples and at elevated temperatures (above T_g). Around T_g the modulus of PA6 shows a steep decrease, and therefore a strong increase in the creep compliance is expected. It has been shown that the addition of layered silicate nanofillers to PA6 has no significant effect on T_g or on the ultimate moisture absorption capabilities of the polymer [12]. Some results on the creep behaviour of moisture conditioned nanocomposites and nanocomposites tested at temperatures above T_g (published previously [13]), are shown in figure 6.12.

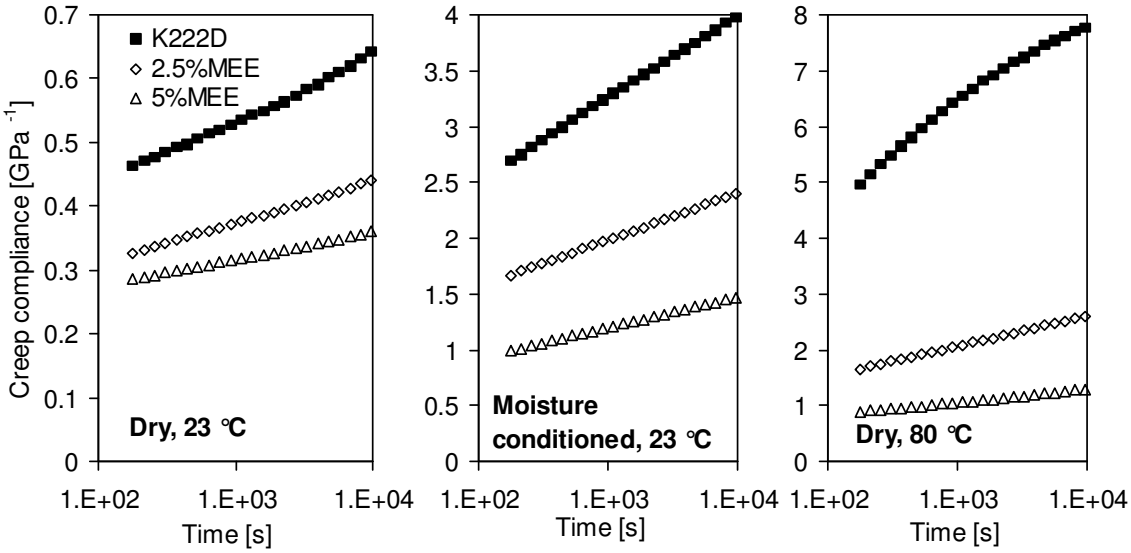


Figure 6.12: Effect of absorbed moisture and temperatures above T_g on the creep behaviour of PA6 and PA6 nanocomposites.

The compliance values in figure 6.12 for dry samples at 23 °C differ slightly from the values in figures 6.1-6.7, because the applied stress was higher and the ageing was performed for several weeks at 80 °C. The stress in the creep tests in figure 6.12 was approximately 2/3 of the yield stress under the tested conditions, and the decrease of the yield stress with increasing temperature and moisture content was taken into account. It can be seen that under these conditions the creep compliance of PA6 is approximately six times higher in moisture-conditioned samples (2.5% water) and twelve times higher in dry samples at 80 °C. However, the addition of nanofillers is very effective in reducing the creep compliance under these conditions, even much more effective than in the dry samples at room temperature. For example, while the addition of 5% MEE nanoparticles results in a reduction of the creep compliance of around 43 % in dry samples at 23 °C, in moisture-conditioned samples this is around 63 % and in the samples tested at 80 °C it is 83 %. The exact physical ageing and creep behaviour of PA6 nanocomposites in moisture conditioned samples and at elevated temperatures should be the subject of further research, but these results clearly show the large benefits of PA6 nanocomposites compared to unfilled PA6 under these conditions.

6.5 Conclusions

The creep compliance is reduced by addition of layered silicate to PA6, as is clear from figure 6.8. The reduction is closely related to the increased modulus of the nanocomposites, which increases with increased ageing time (figure 6.9). The slope of the creep curves decreases strongly (on a linear time scale), which is also evident from the slopes of the normalized creep curves in figure 6.10.

The physical ageing process is not changed much by the addition of the layered silicate, as can be seen from the shape of the creep curves and the shift rate. The shape of the curves is similar in unfilled PA6 and PA6 nanocomposites and the curves for different ageing times can be overlapped onto one master curve by shifts on the time axis, just as in unfilled polymers below T_g. The shift rate is in the same range, although it seems to be slightly higher for nanocomposites (table 6.1), indicating a slightly faster ageing rate in nanocomposites. In addition, the SNC (figure 6.10) shows little influence of the addition of the nanoparticles.

The creep curves for ageing times longer than one month show a change in shape, and are therefore difficult to overlap on the master curve. It is not clear what the reason is for this change in the shape of the creep curves at very long ageing times.

The creep measurements on PA6 nanocomposites conditioned with an equilibrium amount of moisture and tested at elevated temperatures have shown that the effect of nanofillers is much stronger under these conditions. It has been shown that creep compliances above T_g can be reduced by more than 80% by filling PA6 with 5% of exfoliated silicate. Increasing the temperature from 23 °C to 80 °C (crossing T_g) only leads to a three times increase of the creep compliance in the 5% silicate nanocomposite, while this is twelve times for unfilled PA6. These results are very important for applications where PA6 is used as load bearing engineering plastic, because with absorption of moisture T_g can decrease below the use temperature and this strongly increases the creep compliance. Further research on the physical ageing behaviour of moisture conditioned nanocomposites and nanocomposites at temperatures above T_g is needed to understand the complete time- and temperature-dependent deformation behaviour. However, it has been clearly shown that the use of nanocomposites instead of unfilled PA6 can have major advantages for the time dependent deformation behaviour.

6.6 References

1. Struik LCE. The Mechanical and Physical Aging of Semicrystalline Polymers .1. Polymer 1987;28(9):1521-1533.
2. El Shafee E. Effect of aging on the mechanical properties of cold- crystallized poly(trimethylene terephthalate). Polymer 2003;44(13):3727-3732.
3. Spinu I, McKenna GB. Physical Aging of Nylon-66. Polymer Engineering and Science 1994;34(24):1808-1814.
4. Struik LCE. Mechanical-Behavior and Physical Aging of Semi-Crystalline Polymers .4. Polymer 1989;30(5):815-830.
5. Struik LCE. Mechanical-Behavior and Physical Aging of Semi-Crystalline Polymers .3. Prediction of Long-Term Creep from Short-Time Tests. Polymer 1989;30(5):799-814.
6. Struik LCE. The Mechanical-Behavior and Physical Aging of Semicrystalline Polymers .2. Polymer 1987;28(9):1534-1542.
7. Krishnaswamy RK, Geibel JF, Lewis BJ. Influence of semicrystalline morphology on the physical aging characteristics of poly(phenylene sulfide). Macromolecules 2003;36(8):2907-2914.
8. Beckmann J, McKenna GB, Landes BG, Bank DH, Bubeck RA. Physical aging kinetics of syndiotactic polystyrene as determined from creep behavior. Polymer Engineering and Science 1997;37(9):1459-1468.
9. Spinu I, McKenna GB. Physical aging of thin films of nylon and PET. Journal of Plastic Film & Sheeting 1997;13(4):311-326.
10. Lee A, McKenna GB. Effect of Crosslink Density on Physical Aging of Epoxy Networks. Polymer 1988;29(10):1812-1817.
11. Kohan MI. Nylon Plastics Handbook: Carl Hanser Verlag; 1995.
12. Vlasveld DPN, Groenewold J, Bersee HEN, Picken SJ. Moisture Absorption in Polyamide-6 Silicate Nanocomposites and its Influence on Mechanical Properties. Polymer 2005 (Revised version under review).
13. Vlasveld DPN, Bersee HEN, Picken SJ. Nanocomposite matrices for continuous fiber reinforced thermoplastic composites. Conference proceeding SAMPE Europe 2004, Drechsler K, editor; 2004; Paris.

The results described in this chapter have been published as:

D.P.N. Vlasveld, H.E.N. Bersee, S.J. Picken,

Creep and physical aging behaviour of PA6 nanocomposites.

Polymer 2005 (under review).

Chapter 7

Fibre-matrix adhesion in glass-fibre reinforced PA6 silicate nanocomposites

7.1 Introduction

The higher modulus of nanocomposites compared to unfilled PA6 could improve the matrix dominated properties of continuous fibre composites, such as the compressive and flexural strength [1], provided that the interfacial bonding of the fibres with the nanocomposite matrix is not negatively influenced by the addition of the fillers. The effect of the addition of nanofillers to a polymer on the adhesion of the matrix to the fibres is not yet known. Therefore, in this chapter the adhesion of various PA6 nanocomposite matrix materials with glass fibres is investigated.

Many different testing methods for the fibre-matrix adhesion are available. The single fibre fragmentation test (SFFT) [2] has been chosen because it is relatively easy to perform with thermoplastic matrix materials. The SFFT has been used extensively to evaluate the fibre-matrix adhesion and interfacial shear strength by using an analysis based on the Kelly-Tyson theory [3]. A test specimen contains a single fibre embedded in a polymer matrix and a tensile load is applied on the single fibre composite in the axial direction. Once the specimen begins to stretch, the load is transferred from the matrix to the fibre through the interfacial shear stress and the stress in the fibre builds up until it breaks into fragments. The fibre fragmentation process continues until the load transferred through the interface can no longer provide enough stress in the fibre to reach the fibre failure stress. At the moment that the fragments are so small that none of the fragments can be broken further by stress transfer through the interface, a state of total fragmentation is reached, also known as fragmentation saturation. The analysis of the test results is often based on the constant shear model developed by Kelly and Tyson [3], which can be used to estimate the shear strength τ which acts on the interface between the fibre and the matrix. However, Tripathi and Jones [4] have listed several limitations of the Kelly-Tyson constant shear model, and concluded that the calculation of τ from SFFT data

with the constant shear model does not give very accurate results. Therefore, the interfacial shear stress will not be calculated, but the critical aspect ratio will be used as a relative measure to compare the adhesion of a glass fibre with different matrix materials. Single fibre fragmentation tests are performed with E-glass fibres in a PA6 based matrix, both with and without nanofillers. The interfacial bonding of fibres from different manufacturers with PA6 are investigated, and the best fibre type was selected to investigate the influence of the addition of silicate nanofillers and moisture conditioning. Three different concentrations of organically modified silicate and one concentration of non-modified silicate were used in the matrix material. The Young's modulus, the yield stress, the yield strain and the melt flow behaviour of the different matrix materials were measured to see if a relation can be found with the results from the single fibre fragmentation tests.

7.2 Theory

7.2.1 Influence of the matrix shear yield stress

Following the theory of Kelly and Tyson, if a constant interfacial shear stress τ loads every point of a non-failing fibre fragment (with a diameter D and length L), then the maximum tensile stress σ_{max} at the centre of the fibre fragment is given by equation 7.1 [3]:

$$\sigma_{max} = \frac{2\tau L}{D} \qquad 7.1$$

When the maximum stress in the fibre fragment σ_{max} is higher than the failure stress of that fibre fragment, it will fail. With decreasing length of the fibre fragments a length will be obtained at which the shear stress that can be transmitted through the interface is not high enough to reach the fibre failure stress (σ^*_{fibre}), so in this case $\sigma_{max} < \sigma^*_{fibre}$. A critical length L_c exists at which $\sigma_{max} = \sigma^*_{fibre}$ and this defines the critical aspect ratio L_c/D [3] as is shown in equation 7.2:

$$\frac{L_c}{D} = \frac{\sigma^*_{fibre}}{2\tau} \qquad 7.2$$

This critical length is the minimum fibre fragment length that can be fractured by means of stress transfer via the fibre-matrix interface. Below L_c the fibre will be pulled out of the matrix before fibre failure. The fibre pullout can be the result of two different failure mechanisms: failure of the interfacial bond between the matrix and the fibre, and matrix shear yield failure. In the Kelly-Tyson model the matrix is assumed to be elastic up to the yield point, and perfectly plastic above it. If the interfacial bonding strength is higher than the matrix shear yield strength, then matrix failure occurs by local shear yielding of this perfectly plastic matrix around the fibre. On the other hand, when the interfacial bonding strength is lower than the matrix strength, the interface will de-bond after which only frictional forces act on the fibre. Comparing experimental critical fibre fragment aspect ratios with the aspect ratios that would be predicted by the theory of Kelly and Tyson for matrix shear yield failure can show which failure mechanism is occurring in the experiments.

This analysis based on the theory of Kelly and Tyson only allows calculation of the influence of the matrix yield stress on the failure mechanism, while moisture conditioning and addition of silicate nanofillers changes both the elastic behaviour (modulus) and the yield behaviour (yield stress and yield strain) of the matrix and all these factors can influence the results of the SFFT.

7.2.2 Influence of the matrix modulus

Several authors have investigated the influence of the modulus of the matrix and fibres on the stress transfer from the matrix to the fibres, both theoretically and experimentally. The shear-lag theory of Cox [5] describes how a discontinuous fibre in a cylindrical matrix is loaded though shear at the interface when the composite experiences a certain strain. The stress transfer from matrix to fibre depends on the diameter of the fibre, the diameter of the cylindrical matrix around the fibre, the Poisson ratio of the matrix and the moduli of both matrix and fibre. An important result of the shear lag analysis of Cox is that a constant maximum axial fibre stress is reached in the middle of the fibre at a certain distance from the fibre ends, while the maximum interfacial shear stress is reached at the fibre ends and decays to zero in the middle. At both ends of the fibre a certain length is required for reaching the maximum fibre stress. This theory therefore also defines a critical fibre length, which is twice the length from one fibre end to the centre necessary to reach the maximum fibre stress. If a fibre is below this critical length, the fibre cannot be loaded up to the maximum stress and is therefore less efficient in reinforcing the composite and cannot be broken through shear transfer at the interface. When the yield stress is

assumed to be constant, the critical fibre length L_c based on the shear lag theory can be related to the fibre and matrix properties by equation 7.3, as was derived by Galiotis et al. [6] and Asloun et al. [7].

$$L_c = D\left[\frac{(1+\nu_m)(E_f - E_m)\ln(2R/D)}{E_m}\right]^{\frac{1}{2}} \qquad 7.3$$

D = fibre diameter, R = radius of the cylindrical matrix around the fibre, E_f = fibre tensile modulus, E_m = matrix tensile modulus, ν_m = matrix Poisson ratio.

In a single fibre composite the length for R is usually considered to be half the composite thickness, as an approximation. For fibre composites the modulus of the fibres is usually much higher than the modulus of the matrix, and therefore when $E_f >> E_m$ equation 7.3 can be rewritten in the form of 7.4 to describe the critical aspect ratio L_c/D:

$$\frac{L_c}{D} = \left[(1+\nu_m)\ln\frac{2R}{D}\right]^{\frac{1}{2}}\left(\frac{E_f}{E_m}\right)^{\frac{1}{2}} \cong k\left(\frac{E_f}{E_m}\right)^{\frac{1}{2}} \qquad 7.4$$

Equation 7.4 shows that the shear lag theory predicts a square root dependence of the critical aspect ratio on the fibre/matrix modulus ratio [6]. If in a comparison between different matrix materials the assumptions are made that the fibre diameter D, the test sample thickness (≅ R) and the matrix Poisson's ratio ν_m remain constant, then the factor in front of the modulus ratio can be considered to be a constant, which is depicted as k in equation 7.4.

In contrast to the square root dependence of the L_c/D on the ratio of moduli E_f/E_m found by using the shear lag theory, Termonia [8] has found a linear dependence for E_f/E_m ratios below 20 by using finite difference modelling. At higher values for the E_f/E_m ratio a deviation from the linear relationship was found [9], approaching the square root relationship. Pegoretti et al. [10] suggested that the deviation from the square root relationship at low values of E_f/E_m in Termonia's results is caused by the additional stress transfer via the fibre ends, which is ignored in the analysis based on the shear lag theory with a cylindrical matrix. In the SFFT the ends of the broken fibres are not loaded, hence the square root relationship is assumed to be the most accurate to describe the influence of the moduli on the results. Asloun et al. [7] have analysed various experimental results from literature to determine the influence of the

fibre and matrix moduli on the L_c/D and the value of the factor k. From the large amount of literature results gathered by them it became clear that almost all experimental data fit the square root relationship. When the specific properties and dimensions of the fibres, matrix and composite test samples for all different matrix and fibre types analysed by Asloun [7] are combined in equation 7.4 to calculate the theoretical value for k, this leads to values between 2 and 3. However, a plot of the experimental values for L_c/D versus E_f/E_m showed that almost all experimental data fit best to equation 7.4 with a factor k that is higher than the theoretical value of 2-3. In fact, all thermoset and thermoplastic matrices showed higher k-values to fit the data, except for elastomeric matrices where a lower value of k gave the best fit. According to the authors the higher value of k (they found an average value of $k \cong 4.7$) is due to the assumption of perfect bonding between fibres and matrix, which is not valid in reality. In other words, a reduced adhesion would lead to a higher value of k, while the square root relationship remains valid.
For the analysis of the experimental data the data are plotted as the critical aspect ratio versus the modulus ratio E_f/E_m to see to what extend it follows the square root relationship.

7.2.3 Influence of the maximum strain of the matrix

Besides the influence of the matrix yield stress and the modulus, the maximum strain of the matrix is also very important. If the matrix breaks before fragmentation saturation is reached, the results of the test are irrelevant, because the critical fibre length is not yet reached. Tripathi and Jones [11] have found with finite element modelling that for matrices with low yield strain, the critical fibre fragment length is higher than for matrices with high yield strain, with the assumption of both matrices having equal yield stress in an ideal elastic-plastic matrix, even though the level of interfacial shear stress is constant. Therefore it is important to make sure that the strain is high enough to reach fragmentation saturation. Galiotis et al. [6] have shown that for single fibre composites at global strains above 1 % the increase in fibre strain is equal to the increase in composite strain, and Tripathi et al. [11] indicated that the matrix should be able to reach a strain of at least three times the fibre failure strain. For SFF tests on glass fibre composites this means that a strain of at least 8 % [12] is necessary for a reliable test, which can be difficult for crosslinked thermoset matrices, but is feasible for thermoplastic matrices such as PA6.

7.2.4 The influence of the melt flow behaviour

The melt flow behaviour of the matrix during the production of the composite could have an influence on the wetting of the fibres, and the wetting of the fibres has an influence on the adhesion and therefore on the results of the SFF test [12]. Because the addition of nanoparticles has a large influence on the melt flow behaviour [13] (see chapter 5), it is interesting to include the melt flow properties of the matrix materials to see if a connection with the fibre fragmentation results exists.

7.2.5 Determination of the critical aspect ratio from the test data

The critical aspect ratio is related to the average aspect ratio via $L_c/D = 4/3\ L_{average}/D$ [3] if a random distribution of fragments between ½ L_c and L_c is assumed. The critical aspect ratio can be derived from a measurement of the average fibre aspect ratio, which could be obtained from simply dividing the original fibre length by the number of fractures. However, unusually large fragments caused by local imperfect wetting or bad adhesion would have a large influence on the result. Therefore, a different approach is used to determine the critical fibre aspect ratio based on an analysis of all the fragments, which will be described below.

In the ideal case any fibre fragment longer than the critical length L_c will be broken in two, and any fibre fragment shorter than the L_c will not be broken. Consequently, in the ideal case the longest fibre that would exist after fragmentation saturation in the test has been reached is equal to L_c, while the smallest fragment is equal to ½ L_c. The shortest length is ½ L_c because a fibre fragment with a length of L_c experiences the maximum stress in the centre, therefore a fragment with a length L_c will be broken into two identical pieces with a length of ½ L_c. The fragment lengths are initially randomly generated, caused by failure at the weakest points and it is assumed that the fibre fragment lengths obtained from the SFFT measurement vary uniformly between ½ L_c and L_c. In the analysis of the data the length and diameter of each fragment are measured and the fragments are sorted to increasing L/D. In figure 7.1 a hypothetical example is shown, where on the x-axis the cumulative fraction of fibres is plotted, and it can be seen that the L/D values then show a straight line (see the dotted line in figure 7.1) with slope and intercept both equal to ½(L_c/D), as described by equation 7.5.

$$\left(\frac{L}{D}\right)_{SFFT} = \frac{1}{2}\frac{L_c}{D}\cdot P + \frac{1}{2}\frac{L_c}{D} \qquad 7.5$$

In equation 7.5 P represents the cumulative fraction of fibre fragments, which is a number between 0 and 1, obtained by dividing the number of each fragment by the total number of fragments.

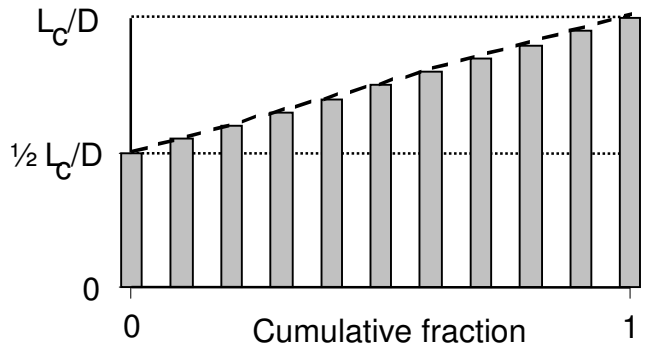


Figure 7.1: Example of fibre fragment length distribution with Lc/D analysis.

When sorted to increasing length, each fragment receives a number, 1 for the first (smallest), 2 for the second, and so on. Then each number is divided by the total number of fragments for that material, resulting in a value between 0 and 1 for each fragment. The aspect ratio of each fragment is plotted as a function of this number P between 0 and 1. This way of plotting the data means that L_c/D can be found by fitting a straight line based on equation 7.5 to the experimental data. In reality fragments below ½(L_c/D) can occur due to incidental defects in the fibres leading to premature failure. Fragments longer than L_c/D can be found in the case of local imperfect wetting, imperfect alignment or imperfect fragmentation saturation. Using the best fit based on the model as represented by equation 7.5 it is possible to eliminate these artefacts by inspection of all the experimental data, resulting in a more reliable value for the critical aspect ratio than would be obtained by just dividing the original length by the number of fracture points.

7.3 Experimental

7.3.1 Materials

Polyamide 6

- Akulon® K122D, injection-moulding grade PA6 from DSM, the Netherlands.
  M_n = 16000, M_w = 32000 g/mol, T_m = 220 °C
  (Similar in properties to K222D and K123 used in other chapters.)

Nanofillers

- Somasif® MEE from Unicoop, Japan: synthetic mica modified with coco bis(2-hydroxyethyl) methyl ammonium surfactant (28.5 wt%).
- Somasif® ME-100 from Unicoop, Japan: unmodified water-swellable synthetic mica.

Fibres

- E-glass fibres with a modulus of 76 GPa [12] coated with various PA6 compatible sizings (coupling agents) were obtained from different companies. The different fibres are designated A to E and the diameters and characteristics of the fibre sizings, as far as these are known, are listed in table 7.1.

E-glass fibre	Fibre diameter (μm)	Sizing	E [GPa]	L_c/D
A	6-9	Unknown silane based	76	26 ± 2
B	6-9	A-1100 amino-silane	76	27 ± 2
C	10	Unknown PA6 compatible	76	31 ± 2
D	6-9	Volan chrome complex	76	28 ± 2
E	7.5-11.5	A-1100 amino-silane	76	26 ± 2

Table 7.1: Properties E-glass fibres with different sizings and critical aspect ratios.

7.3.2 Preparation

The route for the preparation of PA6 nanocomposites consists of melt-compounding PA6 with Somasif® MEE and Somasif® ME-100 by means of a co-rotating twin-screw extruder (Werner & Pfleiderer ZDS-K28) at 240 °C. For the Somasif® MEE nanocomposite materials, first an 11 wt% MEE master batch was compounded. To obtain the various concentrations of the MEE nanocomposite the master batch was extruded for a second time without dilution for the 11 wt% nanocomposite, or diluted with PA6 to concentrations of 6.1 and 2.7 wt%. The 2.5 wt% Somasif® ME-100 nanocomposite material was produced by diluting a 10 % ME-100 master batch obtained from DSM with PA6 in the extruder. All mentioned percentages are weight percentages silicate as measured with a Perkin Elmer TGA-7 thermo-gravimetric analyser after heating for 40 minutes at 800 °C in air.

Two demands for the preparation of the single fibre fragmentation specimens have to be met: the fibre must be straight in the centre of the specimen, and the matrix

material of the specimen must be thin enough to be transparent, because the fibre fragments are measured using an optical microscope.

A Fontijne hot plate press heated to 240 °C was used to produce the films necessary for the SFFT specimen preparation. Single fibres were extracted from a fibre bundle and placed at a distance of approximately 2 cm parallel to each other between the PA6 or nanocomposite films. The hot plate press at 240 °C was used to melt the polymer films and a pressure of 0.8 N/mm^2 was applied for 30 seconds to provide the necessary bonding with the fibre. After cooling between cold metal plates, a tensile test specimen with dimensions as shown in figure 7.2 and a thickness of ± 0.2 mm is cut out with the fibre in the centre.

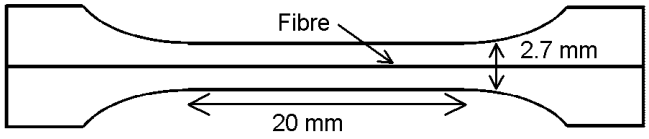


Figure 7.2: Single fibre composite specimen with an effective gauge length of 20 mm.

The tensile modulus and yield stress of the matrix materials were determined on larger injection moulded samples. The dumbbell shaped samples according to ISO 527 standards were produced on an Arburg Allrounder 150-45 injection-moulding machine.

All SFFT and injection moulded samples were dried at 80 °C in a vacuum oven for at least 48 hours. The mass was determined using a Mettler AE240 balance with an accuracy of 0.01 mg. The moisture conditioned samples were allowed to absorb moisture in a climate chamber at a temperature of 70 °C and relative humidity of 62 %, which leads to the same moisture content as conditioning at 23 °C and 50 % RH, but at an accelerated rate. The weight increase was monitored until it reached a constant level, indicating that the samples had reached the equilibrium moisture content.

7.3.3 Testing

Tensile tests

The SFFT specimens were subjected to a tensile strain using a Zwick 1445 test machine with a crosshead speed of 0.5 mm/min at room temperature (23 °C). The test was stopped after a maximum in the stress-strain curve was reached. This moment coincides with neck-formation, and the test was stopped because at that point the maximum uniform strain was reached.

The injection moulded samples for modulus and yield point determination were tested according to ASTM D638M at 5 mm/min in the same machine.

Rheology

A Rheometrics RMS-800 rheometer was used for melt flow measurements of the matrix materials at the processing temperature of 240 °C.

Fragmentation analysis

Single fibre fragmentation samples were observed using a polarising optical microscope and photographs were taken with an attached digital camera. The fragmentation lengths and fibre diameters were measured using an ocular with a calibrated measuring scale. The fragment lengths were obtained by measuring the size of each individual fragment. The fragment lengths were divided by the measured values for the diameter of the fibres to obtain the values for the aspect ratio L/D. To determine the critical aspect ratios the L/D of all fibre fragments were ordered from low to high and these values were plotted versus the cumulative fraction of fibre fragments as explained in section 7.2.5 and shown in figure 7.1. The resulting plot of aspect ratios in order of increasing L/D versus an x-axis ranging between 0 and 1 was used to find a best fit of a straight line with slope and intercept of ½(L_c/D) through the data points according to equation 7.5, as was shown by the dotted line in figure 7.1. This way outlying fragment lengths are easy to identify and will not influence the experimentally found critical aspect ratio, since this is based on a best fit through the majority of data points. The value for the L_c/D is determined from the best fit of a line starting at ½ L_c/D and ending at L_c/D.

7.4 Results and Discussion

To check if all specimens had reached fragmentation saturation the fragmented fibres were observed with the optical microscope. When saturation is reached, the fibre fragments are pulled through the matrix, leaving voids in between the fibre fragments, which can be seen in figure 7.3. The presence of these voids between all broken fragments at strains above 8 % was regarded as proof that the fibre fragmentation process had reached saturation for all matrix materials in all conditions.

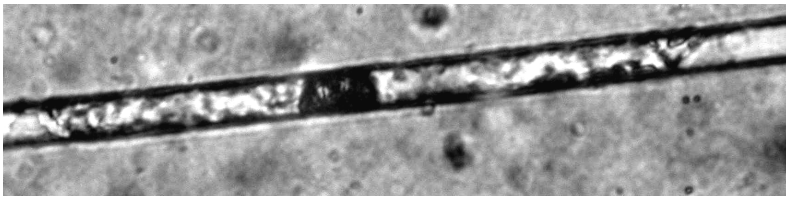


Figure 7.3: Pullout and de-bonding near fibre fragment ends (2.7% MEE dry)

7.4.1 SFFT PA6 and glass fibres with various sizings

In order to find the glass fibre sizing that provided the highest level of bonding with PA6, SFFT samples with different fibres and a dry unfilled PA6 matrix were tested.

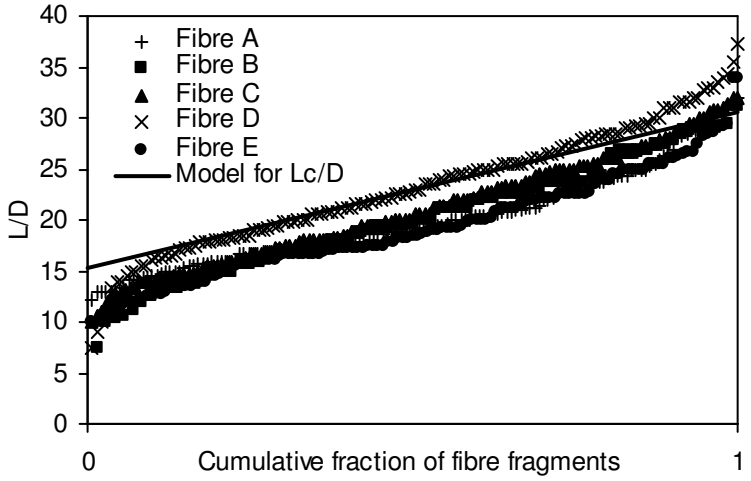


Figure 7.4: L/D values for the different fibres with dry PA6 matrix.

The specimens were tested until neck formation occurred, which was around 13.6 % strain. The data of the fibre aspect ratios are arranged according to increasing length and shown in figure 7.4. For fibre type D the line according to the model in equation 7.5 is plotted to show how the method works and how the fibre fragment aspect ratios fit to this model. For the other samples in figure 7.4 these lines are not plotted, because the data are so close together that the lines would make the results unclear. The resulting critical aspect ratios are shown in table 7.1 (last column) and it is clear that the differences are small; fibre type E was used for the tests with the different matrix materials.

7.4.2 SFFT glass fibres and dry PA-6 nanocomposites

Single fibre fragmentation tests on glass fibres and PA6 nanocomposites were performed to study whether different silicate nanocomposites yield different values for the critical aspect ratio L_c/D. PA6 / silicate nanocomposites with approximately 2.5 wt% silicate were used and compared with unfilled PA6. The dry nanocomposites were strained until failure, because the nanocomposites are more brittle than the unfilled PA6. Single fibre fragmentation tests on dry nanocomposites with a silicate concentration higher than 2.7 wt% were not possible, because the samples failed in a brittle mode at very low strains and fibre fragmentation saturation was not reached. The L/D results are shown in figure 7.5. The data for the unfilled matrix are the same as shown in figure 7.4 for fibre type E.

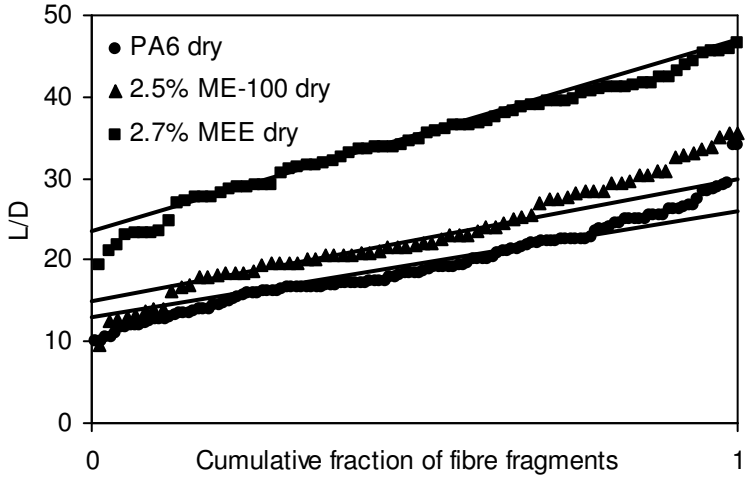


Figure 7.5: L/D values for dry unfilled PA6 and dry nanocomposites.

Through each data set a line is plotted according to equation 7.5, which is used to determine the L_c/D for each sample. It can be seen in figure 7.5 that the experimental fibre fragment distribution follows equation 7.5 reasonably well. The maximum strains and the critical aspect ratios are shown in table 7.2. As can be seen in figure 7.5 and table 7.2 the unfilled PA6 matrix gave the smallest fragments, the nanocomposites filled with 2.5 % Somasif® ME-100 gave results close to the values for unfilled PA6, and the nanocomposites filled with Somasif® 2.7 % MEE produced much longer fragments. The maximum strains for these samples are decreasing upon addition of ME-100 and MEE silicate, but in all cases fibre pullout between all fragments was visible (as shown in figure 7.3), which supports the idea that fragmentation saturation was reached.

Dry / Conditioned	Matrix material	$(L_c/D)_{Exp}$	ε_{max} [%]	E_m [GPa]	σ_{max} [MPa]	$(L_c/D)_{Kelly\text{-}Tyson}$ (Equation 7.2)
Dry	K122D	26 ± 2	13.6	3.0	84.0	21
Dry	2.5% ME-100	30 ± 2	9.1	3.2	86.5	20
Dry	2.7% MEE	47 ± 3	8.4	4.0	85.5	20
Conditioned	K122D	50 ± 3	18.6	1.5	57.0	30
Conditioned	2.5% ME-100	52 ± 3	13.6	1.9	57.0	30
Conditioned	2.7% MEE	57 ± 3	13.7	2.5	57.5	30
Conditioned	6.1% MEE	89 ± 6	10.7	3.5	56.0	31
Conditioned	11% MEE	126 ± 8	9.0	4.5	51.0	34

Table 7.2: Critical aspect ratios and mechanical properties of the matrix materials.

7.4.3 SFFT glass fibres and moisture conditioned PA-6 nanocomposites

Moisture absorption in PA6 leads to a decrease of the glass transition temperature, which causes a reduction of the modulus and yield stress at room temperature, and a higher ductility (see chapter 2). The use of these PA6 based composite materials will probably not be in a dry environment, but in an environment with a variable relative humidity. For this reason, the SFF test on moisture-conditioned samples is very useful to predict the bonding behaviour of the material in a normal environment. In addition to the change in ductility, modulus and yield behaviour, the fibre-matrix interaction might change as well due to the presence of water in the polymer.

Exposure to ambient moisture at 70 °C and 62 % relative humidity resulted in an equilibrium moisture concentration of approximately 2.8 % in both unfilled PA6 and nanocomposites, although the rate of moisture absorption is lower for nanocomposites. An advantage of moisture conditioning is that the ductility increases enough to be able to test nanocomposites with higher concentrations of silicate.

Samples with moisture saturated PA6 and nanocomposites with 2.5 wt% ME-100 silicate and 2.7, 6.1 and 11 % MEE silicate were tested and the L/D distributions are all shown together in figure 7.6 and the best fit of the line according to equation 7.5 is added for each nanocomposite. The resulting values for L_c/D and the maximum strain of the moisture-conditioned samples are shown in table 7.2. It is clear from table 7.2 that the L_c/D of the moisture-conditioned materials is higher than that of the dry materials, when identical compositions are compared. This could be caused by a reduction of fibre-matrix adhesion or by changes in mechanical properties of the matrix, such as modulus and yield stress. Nanocomposites show higher L_c/D values than unfilled PA6, which was also found for the dry samples, and at silicate contents above 2.7 % the L_c/D shows a dramatic increase. As can be seen from the maximum

strain data, this is probably not caused by a brittle fracture of the samples before fragmentation saturation: the strains are higher than in the dry state.

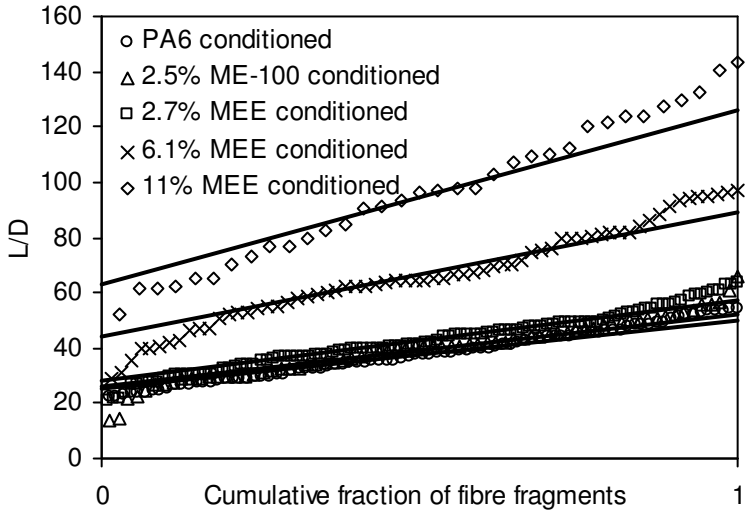


Figure 7.6: L/D values for moisture conditioned PA6 and nanocomposites.

7.4.4 Matrix properties: tensile modulus, yield stress, yield strain and melt flow behaviour

The maximum strain of the samples before neck-formation or fracture occurred are shown in table 7.2, and in all cases the maximum strain was high enough to reach fragmentation saturation as was made clear from the fact that fibre pull-out between all fragments could be seen (figure 7.3). Moisture conditioned samples show a higher maximum strain than dry samples when identical silicate concentrations are compared.

If the failure mechanism is by shear yielding of the matrix, the critical aspect ratio can be related to the matrix yield stress according to the Kelly-Tyson theory, as was shown in equation 7.1 and 7.2. However, shear yield failure of the matrix will only happen if the interfacial bond strength is higher than the inherent strength of the matrix material, which is limited by the matrix shear yield stress. Equation 7.2 can provide a rough estimation for the expected L_c/D when the matrix itself fails by shear yielding, and by comparing this with the experimental L_c/D the failure mechanism can be determined.

The values found for the yield stress σ_{max} (the maximum in the stress-strain curve at the point of neck-formation) for the various materials are displayed in table 7.2. The yield stress is hardly influenced by the addition of silicate fillers, but it shows a strong

reduction for moisture-conditioned samples. An E-glass fibre strength of 2.0 GPa [12] as the average strength of fragments with a length of a few hundred micrometers is used in the calculations. The strength of glass fibres is dependent on the length of the fibre: in general the apparent strength increases for shorter samples because shorter fibres show less flaws were a fibre would break [4]. The average fibre strength of 2.0 GPa for the length scale in these SFFT specimen was measured by tensile tests on fragments of this length scale [14]. The matrix shear yield stress is, according to the Von Mises criterion, equal to the matrix tensile yield stress divided by √3 [10]. In the last column of table 7.2 the calculated critical aspect ratios for a failure mode dominated by matrix shear yielding are shown and it is clear that the predicted values in all materials are significantly smaller than the measured values. In addition, the trend of increasing critical aspect ratio with addition of silicate fillers in the experiments is not seen in the calculations based on the matrix shear failure mechanism. Based on these results, it can be concluded that the failure mechanism is not by matrix failure but by interfacial de-bonding in all samples.

The matrix modulus can influence the stress transfer to the fibres [6,7] and, therefore, it can influence the results of the SFF test. In previous research a square root relationship between the critical aspect ratio and the ratio of fibre modulus / matrix modulus was found. The moduli of all matrix materials are shown in table 7.2 and a strong increase with addition of silicate fillers and a decrease with addition of moisture can be seen. To compare the data with the influence of the modulus that is predicted by the shear lag theory (summarized in equation 7.4) and observed in experiments and simulations, the critical aspect ratio L_c/D for each sample is plotted versus E_f/E_m in figure 7.7.

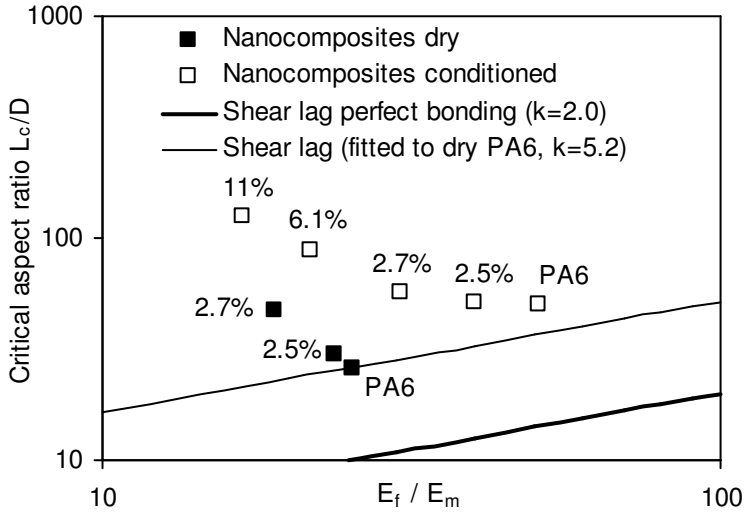


Figure 7.7: L_c/D versus ratio fibre/matrix modulus: experimental results and model (Eq. 7.4).

Next to each data point the composition of the specific matrix materials for that point is written, 2.5 % is 2.5 % ME-100, the other concentrations are MEE concentrations. Figure 7.7 contains data for E_m and L_c/D values as shown in table 7.2 and for E_f = 76 GPa [12] for all samples. The results in figure 7.7 will be discussed further in section 7.4.5.

The melt flow behaviour can have an influence on the wetting of the fibres and the resulting structure of the interface and, therefore, it can have an indirect influence on the results of the SFF test. The results for the viscosity measurement of the nanocomposites at the processing temperature of 240 °C are shown in figure 7.8.

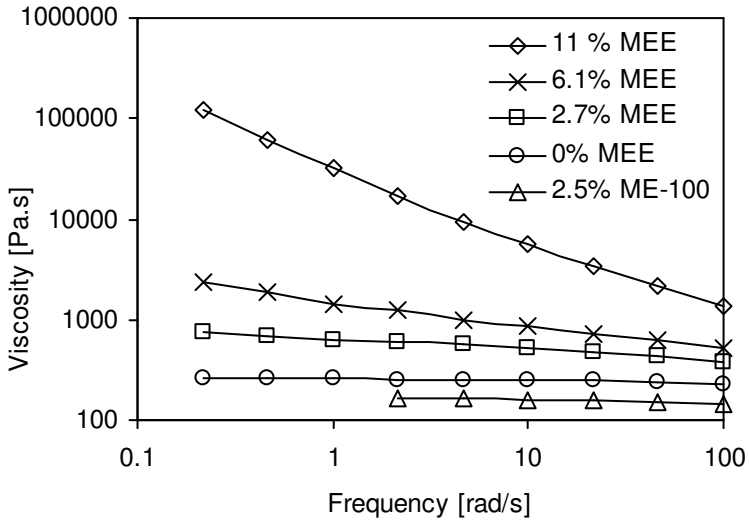


Figure 7.8: Viscosity of different silicate concentration nanocomposites in PA6 at 240 °C.

It can be seen that the 2.5 % ME-100 nanocomposite has a slightly lower viscosity than the unfilled matrix, which is a result of a small decrease of the molecular weight due to the extrusion process [15], this was also seen in the nanocomposites in chapter 5. The most striking behaviour, which can be seen at higher nanofiller concentrations, is a rise in viscosity for decreasing frequencies. The unfilled polymer does not show this rise in viscosity at decreasing frequencies, and this behaviour of the MEE nanocomposites is a result of a yield stress in the melt that is probably caused by the interaction of filler particles [13] (see also chapter 5).

7.4.5 General discussion of the results

One of the first questions that should be asked when analysing the data is if the fibre fragmentation process was completed for each sample, because if the fragmentation saturation is not reached, the critical fibre aspect ratios are not directly related to the adhesion. Figure 7.3 shows an example of fibre pullout between the fragments, and for all described samples this was observed between all fragments. In addition, the moisture conditioned matrix materials show higher maximum strains than the equivalent dry materials, but the critical fibre aspect ratios in the conditioned samples are higher than in the dry samples. This shows that the fragmentation state was reached in all samples and that the variation in maximum strain is not the reason for the observed differences in critical fibre aspect ratio.

In order to understand how the aspect ratios found with the SFF test can be influenced by the matrix properties, the theory of Kelly and Tyson [3] for the influence of the yield stress and the shear lag theory for the influence of the moduli on the stress transfer [5] are used.

The comparison between experimental L_c/D results and calculations based on equation 7.2 (see table 7.2) with the matrix shear yielding as failure mode shows that the interfacial bonding strength in reality is lower than the intrinsic shear strength of the matrix materials. Therefore, it appears that the failure mechanism in all samples is by interfacial de-bonding instead of matrix failure. In addition, it can also be seen in table 7.2 that the differences in yield stress with different silicate content are very small and only the amount of moisture has a large influence on the yield stress, and this is not reflected in the critical aspect ratios. To conclude, an influence of the yield stress of the matrix on the SFFT results is not expected, because the failure mode is not determined by the matrix shear yield stress and no relation is found between the SFFT data and the yield stress.

The modulus of the matrix shows large changes with both the addition of silicate nanofillers and the presence of moisture and almost all results in literature point to a square root relationship between the critical aspect ratio and the ratio of fibre modulus and matrix modulus, according to equation 7.4 [4,7,10,12]. The theoretical background for this behaviour is found in the shear-lag theory of Cox [5], which shows how (among other properties) the fibre and matrix modulus influence the stress transfer from matrix to fibre. To investigate how the experimental data fit the theory summarised by 7.4, the data are plotted as L_c/D versus E_f/E_m in a double logarithmic plot in figure 7.7. In the log/log plot the model based on equation 7.4 gives a straight line and the height depends on the value of the factor k (the factor

before the modulus ratio in equation 7.4). When the factor k is calculated for this system with $\nu_{m,\,PA6}$ = 0.35, D ≈ 10 μm and 2R = thickness sample ≈ 200 μm this leads to k ≅ 2. The Poisson ratio in the nanocomposites could be affected, depending on the orientation of the platelets, and there might be a variation in sample thickness and fibre diameter, but even with these variations taken into account this would only lead to a small (~10 %) variation of the value 2 for k. In figure 7.7 two lines based on equation 7.4 are added, one for k=2 which was calculated for the SFFT samples used in this chapter and one for k=5.2, which is based on the best fit with dry unfilled polyamide samples. The line for the shear lag theory with the assumption of "perfect adhesion", which corresponds to equation 7.4 with k=2 in these samples, predicts critical aspect ratios that are far below the experimental results. This was also noticed by Asloun *et al.* [7], who compared many experimental results from literature, and found that the experimental data obey the square root relationship, but with a factor k which is usually much higher. The average value for k based on experimental data from literature found by Asloun *et al.* was 4.7, and the authors attributed the higher value for k to a fibre-matrix adhesion that is less strong than the assumed "perfect" bonding. For the data shown in this chapter it can be seen in figure 7.7 that a value of k = 5.2 provides a fit with the data point for the dry PA6 matrix, but the critical aspect ratio for moisture conditioned samples of the same composition does not fit onto the same line. Therefore, it appears that moisture conditioning decreases the level of adhesion: the critical aspect ratio is not only higher because of the reduction of the modulus, but there is an additional mechanism that increases L_c/D. This mechanism could be the interference of the water molecules with the bonding between sizing and polymer. The water molecules can form hydrogen bonds between the polymer chains and the amino-silane sizing on the fibres and this way the mobility is increased and the level of bonding could be decreased [16].

The most important observation that can be made in figure 7.7 is that neither of the dry and moisture conditioned data series shows the trend that the shear lag theory [6] or simulations [8,9] predict and other experimental results confirmed [7,10]. For decreasing E_f/E_m a decrease in critical aspect ratio is expected based on all models and experimental results from literature, but the results with addition of silicate shows the opposite behaviour. Only when comparing dry and conditioned samples with the same composition, the trend of increasing aspect ratio with decreasing matrix modulus is followed in general. The nanocomposite matrix materials give much longer fragments than would be expected based on the modulus and the yield stress, and the effect is much more pronounced at higher filler levels. Therefore, it can be

concluded that the interfacial bonding decreases due to the addition of silicate nanofillers to the matrix material.

Two suggestions can be made to explain this behaviour: one is the occurrence of the yield stress in the melt, and the second is the low thermal stability of the organic surfactants. The fibre-matrix interfacial bonding will also depend on the perfection of the wetting of the fibres. Nanocomposites with higher concentrations of exfoliated silicate have no limiting zero-shear viscosity at low frequencies, which is shown in figure 7.8 and chapter 5. The continuously increasing viscosity indicates that the melt shows a yield stress, and the yield stress in the melt could mean that the melt flow around a fibre is not followed by perfect spontaneous wetting, but more research is required to prove this hypothesis.

The nanocomposite based on non-modified Somasif® ME-100 showed better adhesion with the fibres than the nanocomposite based on the organically modified silicate Somasif® MEE. It is known that the type of quaternary ammonium ion based surfactants, used in this type of modified silicate (MEE) as compatibilizer for improving the dispersion in the polymer, is not very stable at high temperatures. Above 200 °C thermal degradation starts [17] and at the processing temperature of 240 °C a part of the surfactant will decompose. It is possible that the degradation products (such as alkyl chains) can migrate through the nanocomposite to the surface and interfere with the interaction between the fibre and the matrix.

7.5 Conclusions

In this chapter the adhesion of nanocomposite matrix materials with glass fibres in both dry and moisture conditioned samples is tested using the single fibre fragmentation test. A simple method for determination of the critical fibre aspect ratio from the results obtained with the single fibre fragmentation test (SFFT) was introduced. The method is based on the assumption that the fragments are randomly distributed between ½ L_c/D and L_c/D and the experimental data fit this model reasonably well. The critical fibre aspect ratio was used as a relative measure for the adhesion.

Moisture conditioned samples show higher critical fibre aspect ratios than dry samples. Compared to the unfilled matrix material the samples with a nanocomposite matrix showed longer critical aspect ratios, with increasing aspect ratio for increasing silicate content. The maximum strains of all tested samples were regarded high enough to fulfil the requirement of fragmentation saturation. The yield stress of the

matrix decreased significantly with moisture conditioning, but only minor changes upon addition of silicate fillers are seen and no relationship with the critical aspect ratios is found. According to the shear lag theory and many experimental [7] and simulation results [8] the general trend is that a higher matrix modulus results in smaller critical aspect ratios due to improved stress transfer via the fibre-matrix interface. In the experimental results this trend can be observed when dry and moisture conditioned samples are compared, but when nanocomposites are used instead of unfilled PA6 the opposite trend is observed. Moisture conditioning gives larger aspect ratios than is expected based on the mechanical properties of the matrix. This points to a reduction of adhesion with moisture conditioning, which could be caused by water molecules interfering with the hydrogen bonding interactions between the fibre sizing and the PA6 matrix.

The large increase in critical aspect ratio with the use of nanocomposites, especially with higher silicate concentrations, is apparently also caused by a reduction of interfacial bond strength. The change in melt flow behaviour, which shows a yield stress in the melt at higher silicate concentrations, could deteriorate the spontaneous wetting behaviour of the matrix melt with the fibres, which might give a less perfect interface. Another possible reason could be the low thermal stability of the organic surfactants on the silicate, which could degrade and collect at the fibre-matrix interface reducing the bonding strength.

When these results are combined with the results of the melt yield stress from chapter 5 (figure 5.8), it seems that unmodified silicate such as ME-100 has a better potential for application as matrix material in continuous fibre composites than modified layered silicates.

7.6 References

1. Marissen R, Brouwer HR. The significance of fibre microbuckling for the flexural strength of a composite. Composites Science and Technology 1999;59(3):327-330.
2. Herrerafranco PJ, Drzal LT. Comparison of Methods for the Measurement of Fiber Matrix Adhesion in Composites. Composites 1992;23(1):2-27.
3. Kelly A, Tyson WR. Tensile Properties of Fibre-Reinforced Metals: Copper/Tungsten and Copper/Molybdenum. Journal of the Mechanics and Physics of Solids 1969;13:329-350.
4. Tripathi D, Jones FR. Single fibre fragmentation test for assessing adhesion in fibre reinforced composites. Journal of Materials Science 1998;33(1):1-16.
5. Cox HL. The Elasticity and Strength of Paper and other Fibrous Materials. British Journal of Applied Physics 1952;3:72-79.
6. Galiotis C, Young RJ, Yeung PHJ, Batchelder DN. The Study of Model Polydiacetylene Epoxy Composites .1. The Axial Strain in the Fiber. Journal of Materials Science 1984;19(11):3640-3648.

7. Asloun EM, Nardin M, Schultz J. Stress Transfer in Single-Fibre Composites - Effect of Adhesion, Elastic-Modulus of Fiber and Matrix, and Polymer-Chain Mobility. Journal of Materials Science 1989;24(5):1835-1844.
8. Termonia Y. Theoretical-Study of the Stress Transfer in Single Fiber Composites. Journal of Materials Science 1987;22(2):504-508.
9. Termonia Y. Dependence of Fiber Critical Length on Modulus in Single-Fiber Composites. Journal of Materials Science Letters 1993;12(10):732-733.
10. Pegoretti A, Fambri L, Migliaresi C. Interfacial stress transfer in nylon-6/E-glass microcomposites: Effect of temperature and strain rate. Polymer Composites 2000;21(3):466-475.
11. Tripathi D, Chen F, Jones FR. The effect of matrix yield strain on the data reduction technique of the single-filament fragmentation test. Composites Part a-Applied Science and Manufacturing 1996;27(9):709-715.
12. Hull D, Clyne TW. An Introduction to Composite Materials. Cambridge; 1996.
13. Krishnamoorti R, Yurekli K. Rheology of polymer layered silicate nanocomposites. Current Opinion in Colloid & Interface Science 2001;6(5-6):464-470.
14. Thomason JL, Kalinka G. A technique for the measurement of reinforcement fibre tensile strength at sub-millimetre gauge lengths. Composites Part a-Applied Science and Manufacturing 2001;32(1):85-90.
15. Korbee R; Process for the preparation of polyamide nanocomposite composition. NL patent WO 99/29767 DSM. 1999.
16. Plueddemann EP. Mechanisms of Adhesion through Silane Coupling Agents. Composite Materials 1974;6:174-216.
17. Xie W, Gao ZM, Pan WP, Hunter D, Singh A, Vaia R. Thermal degradation chemistry of alkyl quaternary ammonium montmorillonite. Chemistry of Materials 2001;13(9):2979-2990.

The results described in this chapter have been published as:

D.P.N. Vlasveld, P.P. Parlevliet, H.E.N. Bersee, S.J. Picken.

Fibre-matrix adhesion in glass-fibre reinforced polyamide-6 silicate nanocomposites.

Composites Part A: Applied Science and Manufacturing,

2005, Volume 36, Issue 1, page 1-11

Chapter 8

Continuous fibre reinforced thermoplastic composites with a PA6 nanocomposite matrix

8.1 Introduction

Continuous fibre reinforced thermoplastic composites have been developed as an alternative to thermoset fibre composites with a wide variety of matrix polymers, ranging from very cheap commodity plastics to very expensive high performance polymers. Polymer nanocomposites based on exfoliated layered silicate are a different type of composite material, containing extremely small particles with a thickness in the range of 1 nm. The length scales of the reinforcement in fibre composites and nanocomposites are so different that the two composites can be combined in a completely new type of three-phase composite. In this new three-phase composite the main reinforcing phase are continuous fibres, which are used at a high volume fraction (for example V_f = 0.5 in woven fibre composites). In the new composite the matrix is a composite too; in this case a nanocomposite. In figure 8.1 a schematic drawing illustrates this concept: the fibres are long and continue throughout the sample and the particles in the matrix material fit between the fibres, without reducing the fibre volume fraction. No fibres are replaced by nanoparticles, but the matrix-dominated properties of the fibre composite can benefit from the improved properties of the nanocomposite.

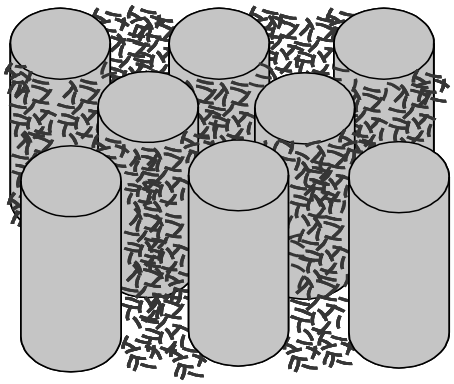


Figure 8.1: Nano-particle reinforcement of the matrix in a fibre composite.

PA6 is an interesting polymer for thermoplastic fibre composites because it combines good mechanical properties with low melt viscosity and a relatively low melting point. However, PA6 has a relatively low T_g and its tendency to absorb moisture from the environment lowers T_g further. The modulus decreases strongly above T_g and, therefore, the performance at high temperatures and in moist environments could be improved. As shown in the previous chapters, nanocomposites based on PA6 have a much higher modulus. They retain a relatively high modulus in the presence of absorbed moisture (chapter 2) and at temperatures above T_g (chapter 4), and have a strongly reduced creep compliance (chapter 6). Therefore, nanocomposites can reduce the disadvantages of PA6 as matrix material for fibre composites and increase the temperature range at which PA6 composites can be applied.

In continuous fibre composites with high fibre fractions the fibres dominate the modulus and the tensile strength. Therefore, the increased matrix modulus is not expected to provide a significant increase in the composite modulus or tensile strength. The nanoparticles in the matrix can improve the matrix-dominated properties of the fibre composite, such as the compressive and flexural strength. The compressive strength of continuous fibre composites is usually lower than the tensile strength, because the fibres tend to buckle under a compressive load. The compressive strength depends on the modulus of the matrix [1-5], because a higher modulus increases the lateral support of the fibres and, therefore, reduces the tendency for fibre micro buckling or kinking. The flexural strength of a continuous fibre composite is dominated by the compressive strength because failure usually starts at the compressive side by micro buckling, as can be seen in the PA6 glass fibre composite sample in figure 8.2.

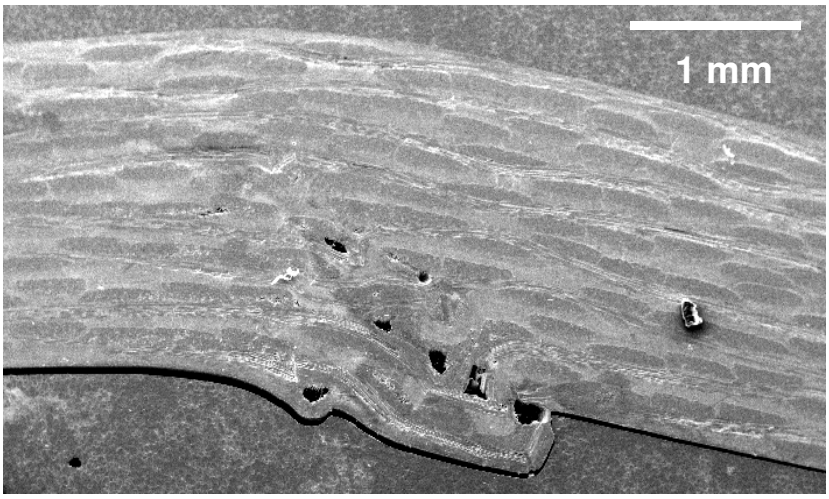


Figure 8.2: Compressive failure of a PA6 glass fibre composite sample in a flexural strength test.

For this reason, flexural measurements are a good and easy method to measure the effect of nanocomposite matrix materials on the matrix dominated properties of the fibre composites. Bending loads are often encountered in the applications of composite materials, so the flexural strength is also of great practical importance.
Previously published research on the concept of a nanocomposite matrix for continuous fibre composites based on epoxy resins did not lead to an improvement of the fibre composite properties [6-8], although one such composite based on a thermoset polyimide achieved improved properties [9] (see section 1.5.2 for more details). In this chapter the properties of a three-phase thermoplastic composite based on PA6 nanocomposites reinforced with woven glass and carbon fibres are described. The improvement of the flexural strength at various temperatures in both dry and moisture-conditioned samples shows the potential importance of this new class of composites.

8.2 Experimental

8.2.1 Materials

Fibre composite

- A commercially available glass fibre composite (TEPEX® Dynalite 102) and carbon fibre composite (TEPEX® Dynalite 202) based on PA6 as matrix from Bond Laminates, was used to investigate the strength versus temperature behaviour of this type of thermoplastic composite.

Matrix

PA6 reference material

- Akulon® K222D, injection-moulding grade PA6 from DSM, the Netherlands.
  $M_n \approx 16000$, $M_w \approx 32000$ g/mol, $T_m \approx 220$ °C
  (Similar in properties to K122D and K123 used in other chapters.)

Melt exfoliated PA6 nanocomposite

Based on:

- Akulon® K123, injection-moulding grade PA6 from DSM, the Netherlands
  $M_n \approx 16000$, $M_w \approx 32000$ g/mol, $T_m \approx 220$ °C

(K123 does not contain a nucleating agent, besides that it is similar in properties to K122D and K222D used in other chapters.)

Containing layered silicate nanoparticles:

- Somasif® ME-100 Synthetic Mica® (water-swellable synthetic fluorine mica) from Unicoop, Japan.

In-situ polymerized PA6 nanocomposite

- Unitika M1030D, from Unitika, Japan, containing 4.6% silicate.

Fibre reinforcement

- Glass fibres: Ten Cate Advanced Composites SS0303, 8 Harness satin weave E-glass fibres, 300 g/mm2, (Style 7781) (E=77 GPa).
- Carbon fibres: Ten Cate Advanced Composites CD0286, 5 Harness satin weave T300JB high strength carbon fibres, 300 g/mm2 (E=230 GPa).

8.2.2 Preparation

Somasif® ME-100 / Akulon® K123D nanocomposite

The nanocomposite with Somasif® ME-100 was made by feeding a mixture of cryogenically milled PA6 and ME-100 powder in a Werner and Pfleiderer ZSK 30/44 D co-rotating twin-screw extruder. To enhance the exfoliation of the water-swellable ME-100 silicate, water was injected into the extruder at a rate of 25 ml/min, and removed by venting at the end of the extruder [10]. The extruder was operated at a temperature of 240 °C at a rotation speed of 200 rpm and a feeding rate of approximately 10 kg/h.

Fibre composites

The fibre composites were made by film stacking and fibre impregnation in a hot plate press. The composite is build up by alternating layers of the matrix material and woven fibre reinforcement. In the glass fibres composites eight fibre layers were used and in the carbon fibre composites six fibre layers were used, both for a two mm thick composite plate. The matrix layer thickness was calculated to result in a fibre volume fraction of 50%. The matrix films were pressed from granules of the extruded PA6 or nanocomposite. The number of layers of matrix material was one more than the layers of fibres (nine for glass, seven for carbon), and the outside layers were half the thickness of the layers between the fibres because they only need to impregnate the fibres from one side. To reach a composite thickness of approximately two mm and a

volume fraction of 50% the total thickness of the combined films for each composite plate needed to be one mm. Using the density of the matrix material, the weight of each film was calculated and the exact amount of granules was measured to press each film. The films were pressed between five mm thick aluminium plates of 50x45 cm covered with a Teflon / glass fibre release film. The granules were spread evenly and heated at 240 °C for six minutes without pressure and subsequently pressed for six minutes at a pressure of 10 bar (PA6) or 25 bar (nanocomposites) at the same temperature. A higher pressure was used for the nanocomposites because of the higher melt viscosity. The films and fibre layers were stacked and heated for six minutes at 240 °C between the same plates. Subsequently, the composite plate was impregnated under a pressure of 20 bar for seven minutes and cooled under the same pressure. The press was cooled with water at a rate of approximately 20 °C per minute. The composite samples of 12.5 mm wide and 120 mm long were cut with a water-cooled diamond saw.

Injection moulding

Dumbbell shaped samples according to ISO 527 standards were injection moulded on an Arburg Allrounder 221-55-250 injection-moulding machine. The feeding zone was heated to 150 °C, the melting and mixing zones heated to 240 °C and the nozzle was heated to 270 °C to prevent solidification when the nozzle is in contact with the cold mould.

Determination of silicate content

Thermo-gravimetric analysis (TGA) measurements were done to determine the exact silicate content in the materials. A Perkin Elmer TGA-7 Thermal Gravimetric Analyzer was used to determine the weight fraction of silicate by heating a sample in air at 800 °C for 1 hour. The silicate levels mentioned are the weight percentages of the silicate filler as measured with TGA.

Conditioning

The dry samples were dried further after processing in a vacuum oven at 80 °C for at least 48 hours before testing. The moisture-conditioned samples were stored in a climate chamber at 62% RH and 70 °C (ISO 1110). These conditions lead to a moisture content of approximately 2.8 wt% in the PA6 phase. This moisture content is similar to the moisture content the material would reach at 23 °C and 50% RH, but the equilibrium concentration is reached much faster.

Measurement of the glass transition temperature

The glass transition temperatures (T_g) of the samples were determined with Dynamic Mechanical Analysis. Samples with a thickness of 0.2 mm were pressed at 240 °C and tested in a Perkin-Elmer DMA 7e at a temperature range from –100 °C to 200 °C. The temperature at the maximum of the loss modulus is used to represent $T_{g.}$

8.2.3 Testing

Density and fibre volume fraction

The density of the matrix materials and the composite samples was measured by weighing the samples in air and water. Two samples for each composite plate were measured and the fibre volume fraction V_f was calculated from the density of the components. For the small variation in V_f around 0.50 a fibre volume correction factor of ($0.5 / V_{f,\ measured}$) was calculated. This factor was used to correct the measured stresses for small deviations from the intended V_f.

Mechanical properties

All samples were tested on a Zwick 1445 universal test machine with a 10 kN force cell, equipped with a temperature chamber.

The modulus of the injection moulded matrix samples was measured in tension at a speed of 5 mm/min at 20 °C intervals according to the ISO 527 standard.

The fibre composites were tested in three point bending at 5 mm/min according to the ASTM D790M test standard. The samples were 12.5 mm wide (Bond Laminates composites 25 mm), and the span in the bending test was 80 mm, with the loading point in the centre. For each temperature and composition five samples were tested to determine the average values. The commercially available glass and carbon composites were tested at 20, 40, 60, 80, 100, 120, 140, 160 and 180 °C. The composites with a nanocomposite matrix and their reference materials were tested at 20, 80 and 120 °C, and some at 160 °C. The measured average failure stress was corrected for small deviations from the intended V_f of 0.50 by multiplying them with a fibre volume correction factor ($0.5 / V_{f,\ measured}$). This way the influence of the small deviations from the average V_f on the results was minimized. For all tests on the matrix and fibre composite samples, moisture conditioned at 80 °C, the specimen were transported shortly before the test from the climate chamber, which was at 70 °C, to the test machine. The samples were allowed to heat up to 80 °C for 5 minutes,

after which the test was started immediately to prevent as much as possible the loss of water in the relatively dry test chamber.

8.3 Results and Discussion

8.3.1 The influence of the temperature on the flexural strength of PA6 glass and carbon fibre composites

Commercially available PA6 based fibre composites containing 46 vol% woven glass and carbon fibres were tested at temperatures from 20 to 180 °C with 20 °C intervals. In figure 8.3 the results for the flexural strength of glass and carbon fibre composites are plotted as a function of the temperature.

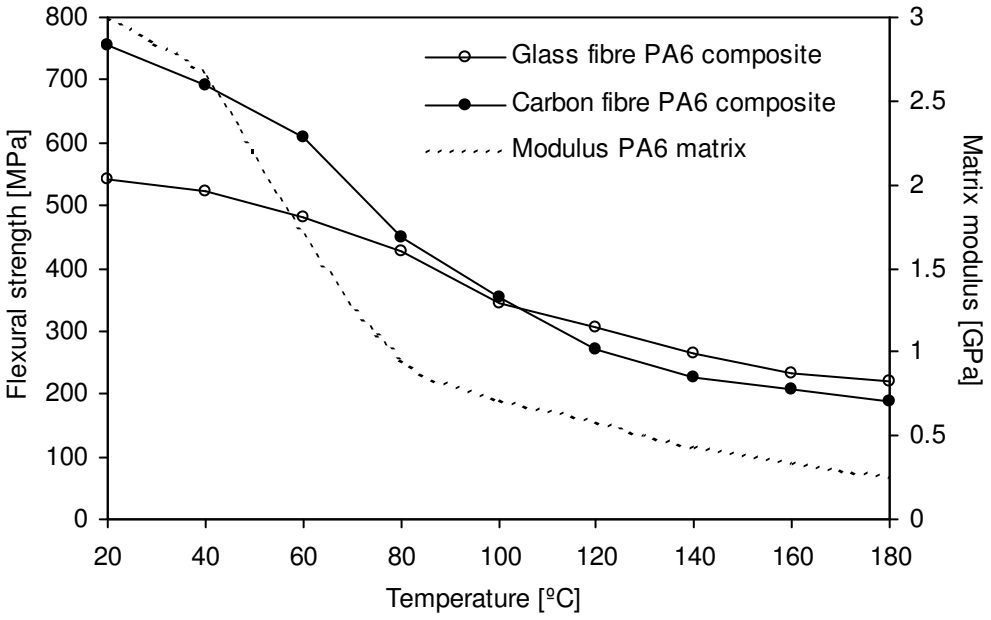


Figure 8.3: Flexural strength of dry commercially available glass and carbon fibre composites with PA6 matrix as a function of the temperature (46 vol% fibres).
The dotted line represents the matrix modulus as a function of the temperature.

In both composites the strength decreases at increasing temperature. The carbon fibre composites have a higher strength at room temperature than the glass fibre composites, as can be expected, but at higher temperature the difference is rapidly decreasing. At 80 °C the strength of both types of composite is almost identical, and above 100 °C the glass fibre composites have a slightly higher strength than the

carbon fibre composites. In bending of a composite a complex combination exists of tensile stresses on the fibres on the outside, compressive stresses on the fibres on the inside, and shear stress between the layers of the composite. With the ratio of the test length (l) to the composite thickness (t) used in this ASTM 790D test (l/t = 40) the shear stresses between the layers are low enough to prevent shear failure. The flexural strength is in this case limited by the compressive strength, as can be seen in the SEM picture of the cross section of a failed glass fibre specimen (figure 8.2). The compressive strength of the composite depends on the amount of buckling of the fibres, which depends on the lateral support provided by the matrix. The temperature dependence of the strength in figure 8.3 can be explained by the decrease in the matrix modulus, which occurs at increasing temperatures. To illustrate this, the modulus of the matrix (PA6) is plotted at the same temperature range in figure 8.3, with the modulus values on the right axis. The drop of the matrix modulus around T_g of PA6 shows a correlation with the composite strength. It is likely that the decrease in matrix modulus decreases the lateral support of the fibres, which leads to failure due to fibre buckling. Carbon fibre composites seem to be more sensitive to this effect, probably because of the lower failure strain of carbon fibres. Buckling of fibres with a lower failure strain will lead more quickly to fibre failure and subsequent composite failure. In figure 8.4 the composite strength of both fibre composites is plotted as a function of the matrix modulus.

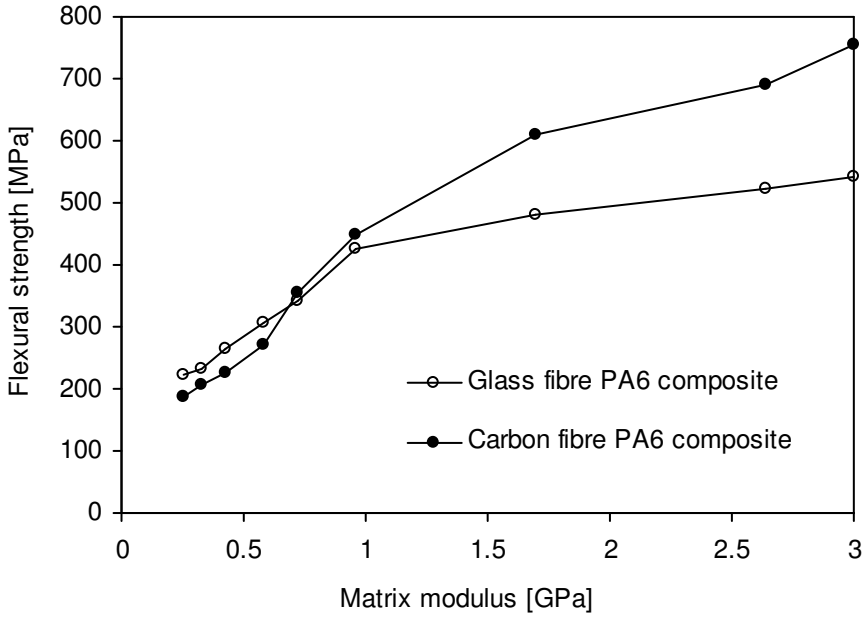


Figure 8.4: Flexural strength of dry commercially available PA6 glass and carbon fibre composites as a function of the matrix modulus (46 vol% fibres).

Figure 8.4 shows for both composites a decrease of the strength with decreasing matrix modulus, which is stronger for carbon fibre composites. The decrease of the strength is much stronger when the matrix modulus drops below approximately 1 GPa (note that this is close to the modulus at the heat distortion temperature (HDT)). In unfilled PA6 this modulus is reached at approximately 80°C in dry conditions (see figure 8.3).

8.3.2 Nanocomposite matrix materials

The new three-phase composite is made with two different nanocomposites as matrix material, and an unfilled PA6 matrix as reference. One is a commercially available PA6 nanocomposite (Unitika M1030D) and the other a nanocomposite (10% ME-100 in low MW PA6) that has been selected after various previous tests on mechanical properties (chapter 4), melt flow behaviour (chapter 5) and adhesion with the fibres (chapter 7) [11,12]. Initial attempts to produce melt-impregnated fibre composites with nanocomposites often resulted in fibre composites with more voids and (much) lower strength than the reference material. It proved to be difficult to achieve good fibre bundle impregnation and wetting with many PA6 nanocomposites, probably due to the melt flow behaviour, which is characterized by a higher viscosity and a yield stress. The adhesion of many nanocomposites with the fibres also proved to be often lower (chapter 7) [11]. The two types of nanocomposite described in this chapter do not show severe problems with respect to impregnation and adhesion, and they can therefore indeed show the expected advantages of nanocomposite matrix materials. In figure 8.5 the tensile modulus of the nanocomposites and the PA6 reference material is shown as a function of the temperature. The dotted lines show the results for moisture-conditioned samples at 20 and 80°C. Figure 8.6 shows the loss moduli obtained from DMA measurements on thin films; the peaks indicate the glass transition temperature. T_g is the same in unfilled PA6 and the nanocomposites, but it decreases from around 65 °C (dry) to around room temperature as a result of moisture conditioning. The decrease of ≈ 40 °C in T_g due to moisture conditioning translates to a decrease in the modulus that is similar to an increase of 40 °C in temperature. Both unfilled PA6 and nanocomposites show a strong decrease of the modulus above T_g (see figure 8.5), but even above T_g the nanocomposites have moduli that are more than 1 GPa higher than unfilled PA6 (at 80 °C). However, T_g and the temperature around which the modulus decreases does not change in nanocomposites compared to unfilled PA6 (figure 8.6).

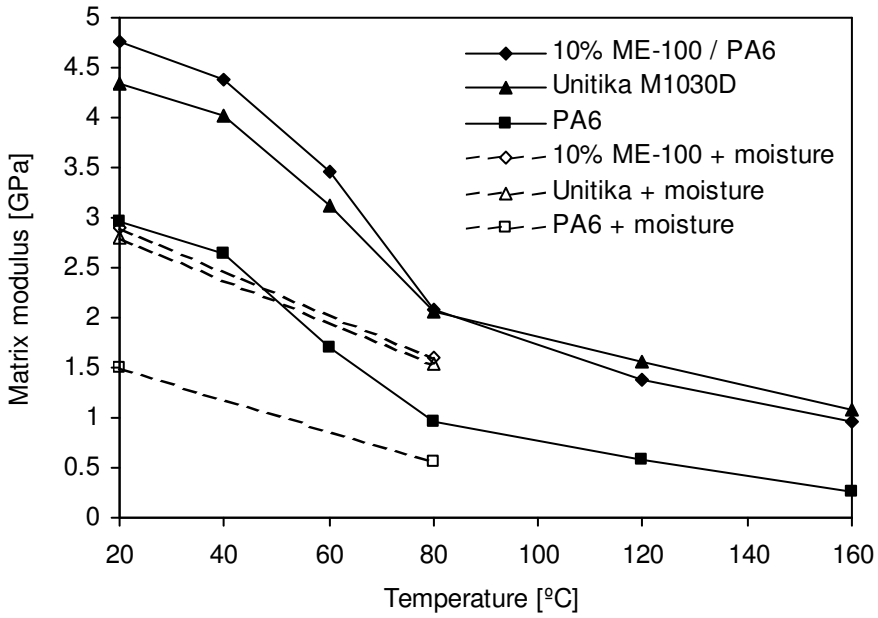


Figure 8.5: Modulus of unfilled PA6 and two nanocomposite matrix materials as a function of the temperature.

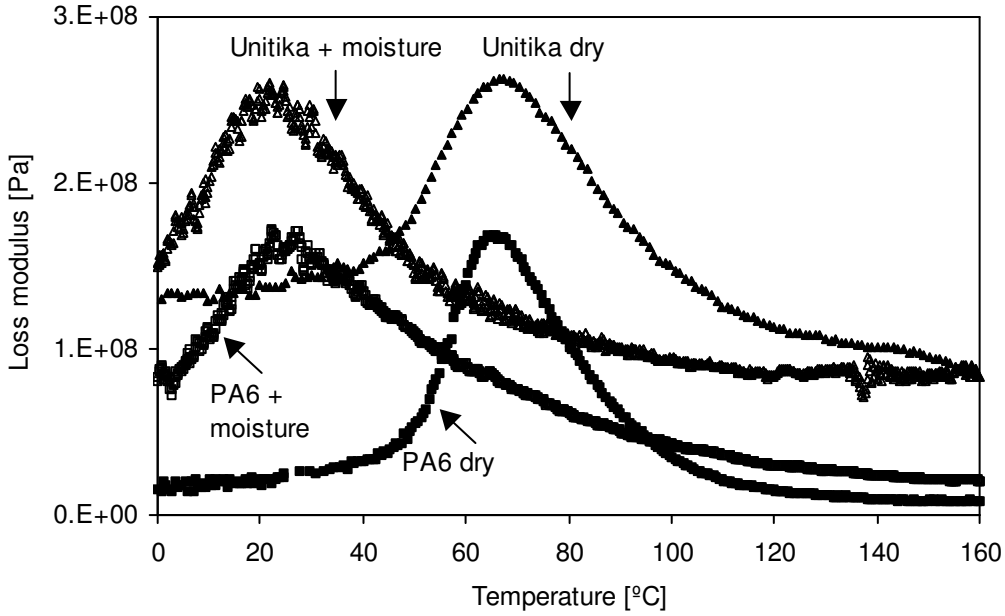


Figure 8.6: Loss moduli as a function of the temperature for dry and moisture-conditioned PA6 and a PA6 nanocomposite. The peak represents the glass transition temperature (T_g).

The potential benefits of nanocomposites for the use in fibre composites can be visualized when the results of figure 8.4 and figure 8.5 are combined: the nanocomposites have moduli above 1 GPa up to 160 °C, while the unfilled PA6 already has a lower modulus above 80 °C. In figure 8.4 it can be seen that at matrix

moduli below 1 GPa the flexural strength decreases rapidly. The 1 GPa "barrier" (although just an arbitrary value) is shifted up by 80 °C in these nanocomposites. Therefore, it can be expected that the strength of the fibre composites remains high up to much higher temperatures, significantly expanding the application window for PA6 as matrix material. A similar result can be expected for moisture-conditioned samples. It can be seen in figure 8.5 that the modulus of the moisture-conditioned nanocomposites is almost the same as the modulus of dry PA6. With the combination of moisture-conditioning and elevated temperature (80°C), the modulus of the nanocomposites is almost three times higher than in unfilled PA6, and still higher than moisture-conditioned PA6 at room temperature. Therefore, it can be expected that the negative effect of moisture absorption in PA6 on the fibre composite strength can be reduced to a large extend by using nanocomposites. The modulus of the two types of nanocomposite is similar, both in dry and moisture conditioned samples, despite the different amounts of nanoparticles. This can be explained by the fact that the exfoliation of the platelets is not perfect in the ME-100 nanocomposites, as a result of the lack of surfactant on the platelets. This leads to more stacks of un-exfoliated platelets and, therefore, to a lower average aspect ratio in the ME-100 nanocomposites (see chapters 4 and 5) [13]. In this material a higher volume fraction of nanoparticles is necessary to achieve the same modulus as with perfectly exfoliated particles, but the influence of reduced exfoliation on the melt flow properties is beneficial for fibre impregnation [12].

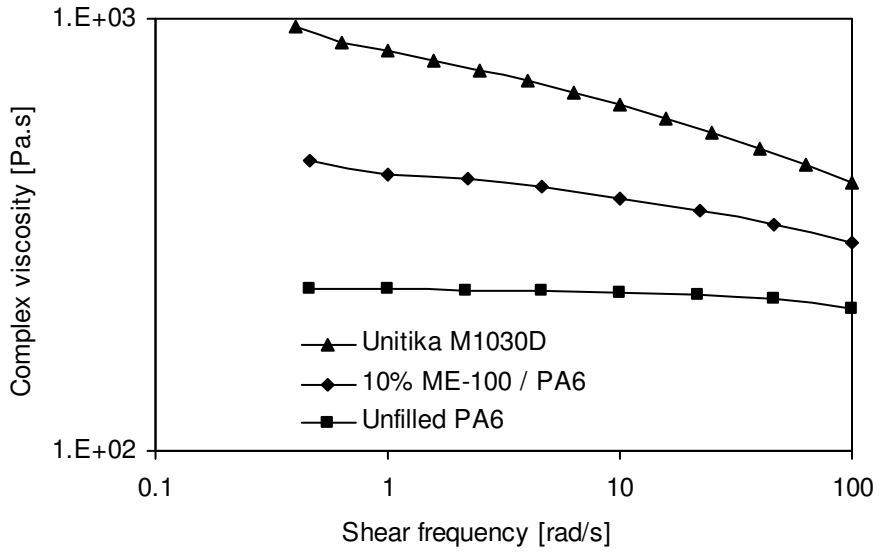


Figure 8.7: Viscosity as a function of the shear frequency for the three matrix materials.

In figure 8.7 the viscosity of the three matrix materials at the processing temperature of 240 °C is shown. The nanocomposite from Unitika has the highest melt viscosity and the unfilled PA6 the lowest. However, the viscosities are not very high in these matrix materials compared to many nanocomposites (see chapter 5, figure 5.11) [12] and no significant yield stress in the melt was found (see chapter 5, figure 5.8). It was possible to achieve good fibre bundle impregnation with these three matrix materials.

8.3.3 The flexural strength of fibre composites with a nanocomposite matrix

In figure 8.8 the flexural strength of the glass fibre composites with nanocomposite and PA6 matrix is shown as a function of the temperature. Note that the PA6 / glass fibre composites tested for the data in this figure are not the same as the commercial composites tested for the data in figure 8.3; therefore, the values can be different.

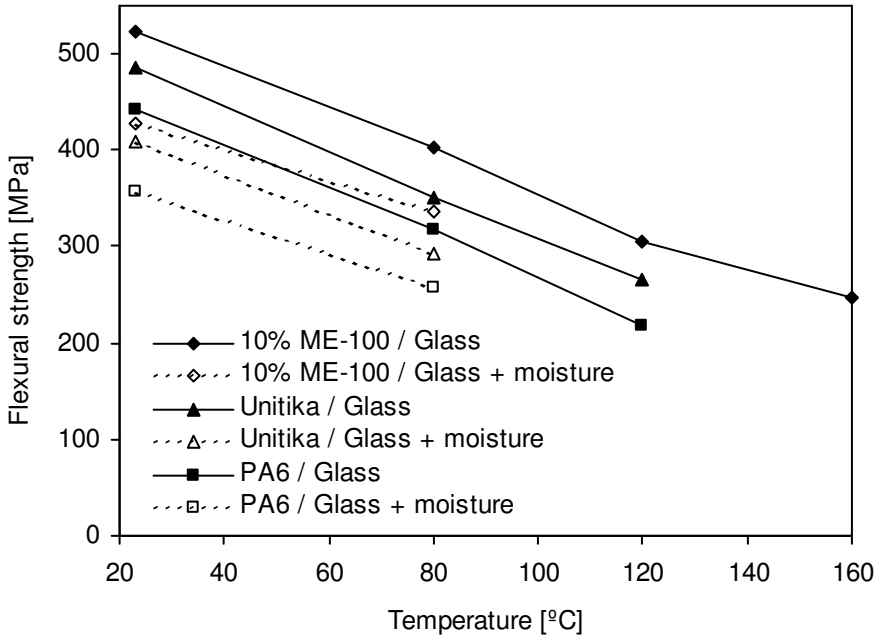


Figure 8.8: Flexural strength of glass fibre composites with PA6 and nanocomposite matrix as a function of the temperature (dry and moisture conditioned).

Both fibre composites based on a nanocomposite matrix have a higher strength at all temperatures compared to the PA6 fibre composite. At elevated temperatures the difference becomes relatively larger, with an increase in flexural strength of 42% at 120 °C for the 10% ME-100 nanocomposite. The strength with a nanocomposite matrix at 120 °C is similar to the strength with a PA6 matrix at 80 °C, and at 160 °C the strength is even higher than at 120 °C with the PA6 matrix. Therefore, with this

nanocomposite matrix it is possible to increase the temperature range at which the PA6 fibre composite can be used with 40 to 50 °C, without changing the processing temperature. A similar positive influence of the nanocomposite matrix was found for the moisture-conditioned samples. At 20 °C the moisture conditioned sample has a flexural strength close to the dry fibre composite with a PA6 matrix, so the nanocomposite matrix can compensate for the loss of strength due to moisture absorption in the PA6 matrix. At combined hot and moist conditions (80 °C, moisture-conditioned) the fibre composite with a 10% ME-100 matrix shows a 27 % higher flexural strength than the one with a normal PA6 matrix.

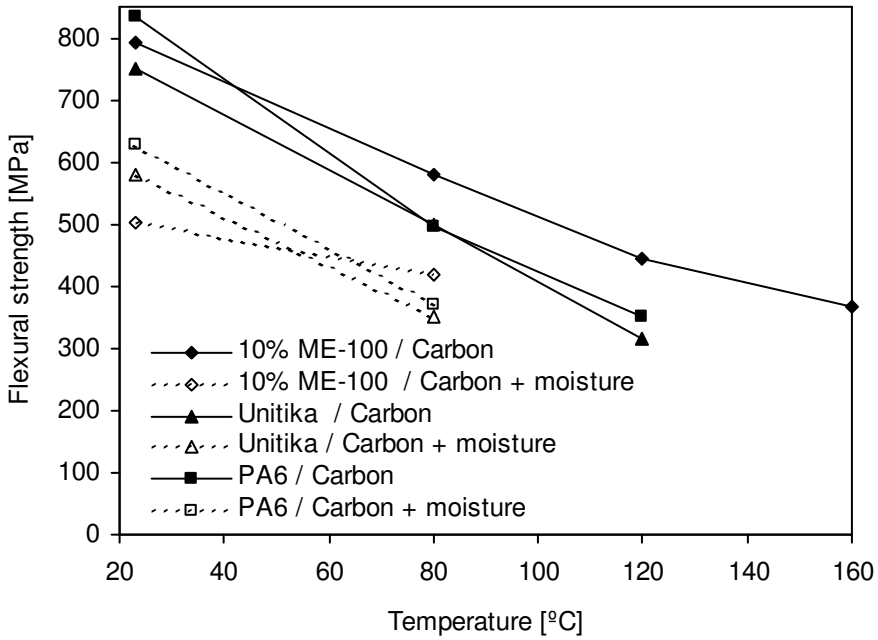


Figure 8.9: Flexural strength of carbon fibre composites with PA6 and nanocomposite matrix as a function of the temperature (dry and moisture conditioned).

In figure 8.9 the flexural strength of carbon fibre composites as a function of temperature is shown. Note that the PA6 / carbon fibre composites tested for the data in this figure are not the same as the commercial composites tested for the data in figure 8.3; therefore, the values can be different.

In this type of fibre composite the positive influence of the nanocomposite matrix is not evident at room temperature; at 20 °C the PA6 carbon fibre composite is stronger than the fibre composites with a nanocomposite matrix. However, at elevated temperatures the composite with 10% ME-100 nanocomposite as matrix material has a much higher strength than the one with the unfilled PA6 matrix. Remarkably, the fibre composite with the Unitika nanocomposite matrix does not show any

improvement in the strength. In moisture-conditioned samples none of the nanocomposites leads to an increased strength at room temperature, and only for the ME-100 composite a small increase is found at 80 °C. It is not clear why the nanocomposite matrix increases the flexural strength of glass fibre composites more than of carbon fibre composites. Based on figures 8.3 and 8.4, it could be expected that nanocomposites have an even better effect on the flexural strength of carbon fibre composites, because the influence of a decrease in matrix modulus (due to an increase in temperature) is stronger for carbon fibre composites. However, the sizing on the carbon fibre used in this research has not been specifically developed for use with PA6. Probably the adhesion can still be improved by optimizing the fibre surface treatment. The ME-100 matrix results in a larger increase in strength than Unitika M1030D in the glass fibre composites. In the carbon fibre composites it is the only nanocomposite that has a positive influence on the strength at elevated temperatures. The reason for the better performance ME-100 is probably not a difference in modulus; this is almost identical over the investigated temperature range, as can be seen in figure 8.5. However, what could be the reason behind the better performance of the ME-100 nanocomposite is the difference in the melt viscosity, as shown in figure 8.7. Maybe the higher viscosity of Unitika M1030D leads to a slightly worse fibre wetting at the processing conditions that were used, although no differences could be seen using SEM. Also the presence of the organic modification in the Unitika nanocomposite could influence the adhesion, as was already proposed in the conclusions of chapter 7. To investigate how the flexural strength depends on the matrix modulus in these samples, the strength (from figures 8.8 and 8.9) is plotted as a function of the matrix modulus (from figure 8.5).

In figure 8.10 the results for the dry and moisture conditioned glass fibre composites are shown and in figure 8.11 the same for the carbon fibre composites.

In these figures the points at lower matrix modulus correspond to higher temperatures. All lines through the data series are connected to the point where the modulus=0 and the strength=0, because obviously the bending strength approaches zero with a liquid (or no) matrix. In figure 8.10 it can be seen that the data for the glass fibre composites with PA6 matrix fit reasonably well on one curve, both the dry and the moisture-conditioned samples. The composites with a 10% ME-100 matrix are on the same curve as the PA6 samples for the higher matrix moduli, but at the lower moduli (higher temperatures) the strength is below this curve and, therefore, somewhat lower than could be expected.

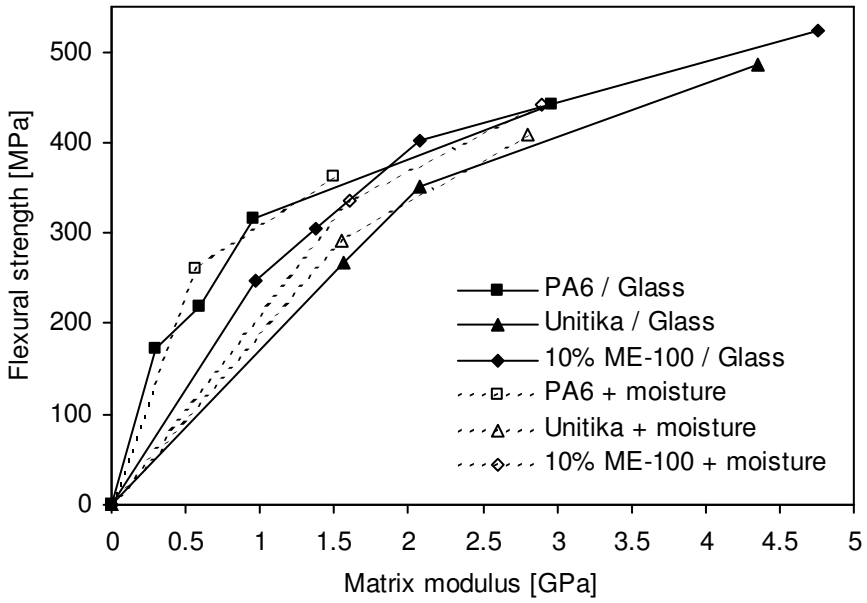


Figure 8.10: Flexural strength of glass fibre composites with PA6 and nanocomposite matrix as a function of the matrix modulus (dry and moisture conditioned).

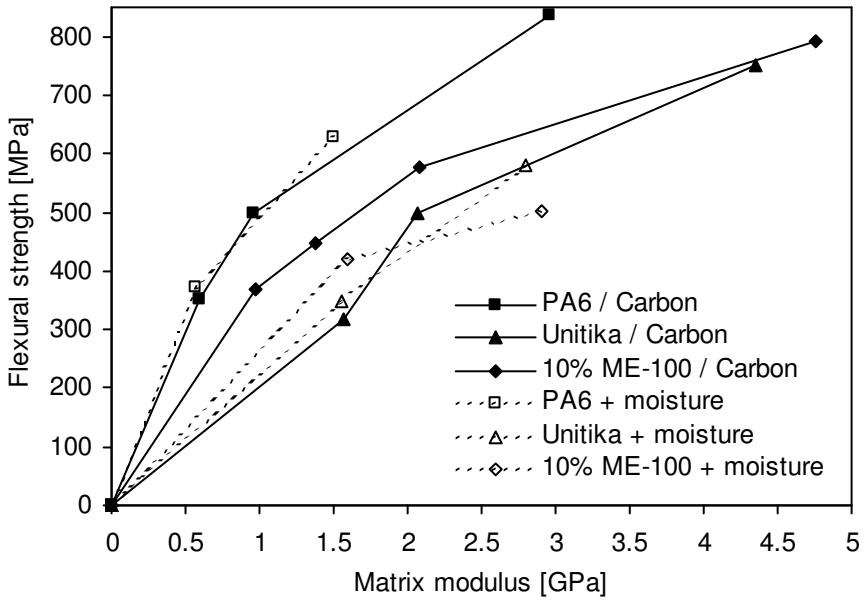


Figure 8.11: Flexural strength of carbon fibre composites with PA6 and nanocomposite matrix as a function of the matrix modulus (dry and moisture conditioned).

The glass fibre composites with a Unitika nanocomposite matrix are all on a different curve, and have a lower strength than could be expected based on the matrix modulus. This means that in this case another mechanism is responsible for a decrease in flexural strength, besides the increase caused by the increased matrix modulus. This mechanism is probably the adhesion of the fibres with the matrix.

Previous attempts to combine other nanocomposites with fibres often resulted in a strong decrease of the strength, clearly caused by a bad adhesion. In some cases the laminate would even delaminate instead of fail on the compressive side due to the bad adhesion. In the glass fibre composites with the Unitika matrix the adhesion is not so bad; the increased matrix modulus does indeed increase the strength, but probably the strength could be higher if the adhesion would be improved.
The results for the carbon fibre composites in figure 8.11 are different than for the glass fibre composites: the nanocomposites all are below the points of the unfilled PA6 matrix. In these composites the adhesion between the nanocomposites and the carbon fibres is probably worse than between the unfilled PA6 and the matrix, reducing the potentially positive influence of the increased matrix modulus. The strength versus matrix modulus of the composites with the unfilled PA6 matrix overlaps for dry and moisture conditioned samples, just as for glass fibre composites. For the composite with the Unitika nanocomposite matrix this is also true, although the curve is on a lower level. However, for the composite with the ME-100 matrix this is not the case: the moisture-conditioned samples have a much lower strength than expected, which cannot be explained by the modulus reduction alone. Maybe an additional reduction of the adhesion in the presence of moisture is responsible here, which is stronger in this type of nanocomposite. Clearly, more research is necessary on the adhesion between the nanocomposites and carbon fibres to reach the full potential of the improved matrix properties. However, for the glass fibre composites large increases in flexural strength have been achieved using an optimized matrix material.

8.4 Conclusions

The concept of combining nanocomposites as matrix material with continuous fibre composites in a new three phase composite has been shown to be very successful. The main goal of increasing the matrix dominated flexural strength by increasing the matrix modulus has been achieved, with different types of PA6 nanocomposite in combination with glass and carbon fibres. Based on flexural tests on thermoplastic PA6 glass and carbon fibre composites over a large temperature range up to near the melting point, it has become clear that for these fibre composites it is important to have a reasonably high matrix modulus. Both glass and carbon composites are very sensitive to a decrease of the matrix modulus below values around 1 GPa. Above this value, carbon fibre composites are more sensitive to the matrix modulus than

glass fibre composites. While the modulus of unfilled PA6 decreases below the 1 GPa level just above T_g, the nanocomposites used in this research have moduli that are much higher and stay above the 1 GPa level up to 160 °C, 80 °C higher than for unfilled PA6. The nanocomposites also show much higher moduli in moisture conditioned samples, and even in moisture conditioned samples tested at 80 °C the modulus is much higher than that of the dry unfilled samples, again well above 1 GPa. The increased modulus of the nanocomposites offers much more support to the fibres at increased temperatures and in moisture conditioned samples. The strength of the glass fibre composites has been increased by more than 40 % at elevated temperatures and the temperature at which the composite strength drops below a certain (arbitrary) value has been increased by 40-50 °C. The results for carbon fibre composites are less impressive, although they also show significant improvements at elevated temperatures. However, to reach the full potential of the higher matrix moduli more needs to be understood about the adhesion and probably also the impregnation and crystallization mechanism in this new type of composite, especially in combination with carbon fibres. With additional optimization of the fibre surface treatment and the composite production process the properties can probably be improved further, because the plots of strength versus matrix modulus suggest that higher flexural strengths than measured can be expected if all other factors are equal to the reference material.

The clear advantage of the use of nanocomposites over the use of different polymers to improve the high temperature behaviour of fibre composites is that the properties can be improved without any change in the melting temperature and processing conditions. The added cost of the nanocomposite matrix can be small due to the low amounts of filler necessary for a significant improvement. Also interesting is the fact that film extrusion (and probably also film blowing) is much easier with nanocomposites due to the altered melt flow behaviour: a low MW nanocomposite can replace a high MW unfilled polymer (results are not shown).

The results of the three-phase composite shown in this chapter are for PA6 as the matrix material, but the concept can be applied to many different matrix polymers. Nanocomposites have been developed with many different polymers over the last decade as has been shown in chapter 1. It has been shown that PA66 can be converted into a nanocomposite in the same way as PA6 with very good results (see chapter 4) [13], so this would be an interesting matrix for fibre composites as well. The same concept has been tried with epoxy resins in the past [6-8], unfortunately with little success, but the improvements in the epoxy matrix properties were also not very substantial. However, polymers such as polypropylene (PP), polyetherimide

(PEI), thermoplastic polyurethane (TPU) and polyesters (PET, PBT) could be upgraded by filling it with the appropriate nanoparticles. The improved properties of the nanocomposite matrix material can upgrade the properties of relatively low cost thermoplastic composites up to the level of the high performance composites and further increase the temperature resistance of existing high-performance composites. All of this can be achieved without an increase of the processing temperature or pressure and therefore with minimal additional cost.

8.5 References

1. Lager JR, June RR. Compressive Strength of Boron-Epoxy Composites. Journal of Composite Materials 1969;3:48-56.
2. Hahn HT, Williams JG. Compression Failure Mechanisms in Unidirectional Composites. In: Whitney JM, editor; 1986. American Society for Testing and Materials. p 115-139.
3. Lo KH, Chim SM. Compressive strength of Unidirectional Composites. J. Reinf. Plast. Compos. 1992;11:838-896.
4. Schultheisz CR, Waas AM. Compressive failure of composites .1. Testing and micromechanical theories. Prog. Aeosp. Sci. 1996;32(1):1-42.
5. Waas AM, Schultheisz CR. Compressive failure of composites .2. Experimental studies. Prog. Aeosp. Sci. 1996;32(1):43-78.
6. Rice BP, Chen CG, Cloos L, Curliss D. Carbon fiber composites: Organoclay-aerospace epoxy nanocomposites, Part I. Sampe J. 2001;37(5):7-9.
7. Chen CG, Curliss D. Resin matrix composites: Organoclay-aerospace epoxy nanocomposites, Part II. Sampe J. 2001;37(5):11-18.
8. Garcia R, Evans RE, Palmer RJ. Structural Property Improvements Through Hybridized Composites. In: Johnston NJ, editor. Toughened Composites. Volume ASTM STP 937. Philadelphia: American Society for Testing and Materials; 1987. p 397-412.
9. Campbell S, Scheiman D, Faile M, Papadopoulos D. PMR-15/ layered silicate nanocomposites for improved thermal stability and mechanical properties. 2002.
10. Korbee R; Process for the preparation of polyamide nanocomposite composition. NL patent WO 99/29767 DSM. 1999.
11. Vlasveld DPN, Parlevliet PP, Bersee HEN, Picken SJ. Fibre–matrix adhesion in glass-fibre reinforced polyamide-6 silicate nanocomposites. Composites Part A: Applied Science and Manufacturing 2005;36(1):1-11.
12. Vlasveld DPN, Jong Md, Bersee HEN, Gotsis AD, Picken SJ. The relation between rheological and mechanical properties of PA 6 nano- and micro-composites. Polymer 2005;46: In Press.
13. Vlasveld DPN, Vaidya SG, Bersee HEN, Picken SJ. A comparison of the temperature dependence of the modulus, yield stress and ductility of nanocomposites based on high and low MW PA6 and PA66. Polymer 2005;46(10):3452-3461.

The results described in this chapter have been published as:

D.P.N. Vlasveld, H.E.N. Bersee, S.J. Picken,

Nanocomposite matrix for increased fibre composite strength.

Polymer 2005, In Press.

Chapter 9

Conclusions

The main goal of the research described in this thesis was to improve the properties of a thermoplastic fibre composite by reinforcement of the matrix material with nanoparticles, which fit between the fibres. By using a nanocomposite as the matrix material the improved properties of the nanocomposite matrix can increase the strength of the fibre composite, especially at high temperatures. The advantage of the use of nanocomposites over the use of different polymers to improve the mechanical properties at high temperature is that the properties can be improved without any change in the melting and processing temperature. In this last chapter some issues will be discussed that appear in various chapters, and some links between the different chapters will be made.

9.1 Production processes

The nanocomposites described in this thesis are almost all based on PA6, and a few on PA66 (chapter 6). Most have been produced by mixing organically modified nanoparticles in the polymer melt using a co-rotating twin-screw extruder. A very good dispersion was achieved by making highly concentrated master batches that were diluted to the desired concentration in a second extrusion step. The exfoliation into high aspect ratio platelets resulted in a strong modulus increase over a large temperature range, both below and above T_g. Nanofillers modified with one long chain on each surfactant molecule exfoliate much better in PA6 than nanofillers with two chains, probably because the latter is too hydrophobic for an optimal interaction with PA6. The nanocomposites produced by mixing organically modified silicates with PA6 in the melt have similar moduli as the commercial in-situ polymerized nanocomposites for similar silicate content. Using the same extrusion process and a similar organically modified silicate a series of nanocomposites based on PA66 was successfully prepared at a higher extrusion temperature, apparently without problems with the heat-sensitive modified silicate. The modulus of the PA66 nanocomposites is

higher than of the PA6 nanocomposites due to the slightly higher matrix modulus, but the relative increase is similar. In addition, nanocomposites have been prepared with unmodified layered silicate using a water-assisted extrusion process to help the exfoliation of the silicate layers (chapter 4 and 5). These particles exfoliate to a lower degree, resulting in a lower modulus increase for the same silicate content. These nanocomposites proved to be very useful in combination with fibre reinforcement (chapter 7 and 8).

9.2 Brittleness

In all nanocomposites the modulus increase is accompanied by a small yield stress increase and a strongly reduced ductility, which became clear in chapter 2 and 4. Only the use of high MW polymer can compensate for the loss of ductility (chapter 4), but this can result in serious processing problems at higher filler content. The absorption of moisture improves the ductility, and physical ageing decreases it over time (chapter 2). In fibre composites the brittle fracture behaviour of nanocomposites is not such a problem. Because glass and carbon fibres have low failure strains, the matrix cannot reach large strains in a fibre composite without failure of the composite. Most nanocomposite matrices have a higher failure strain than the fibres, and, therefore, the reduced ductility is not problematic in fibre composites. However, for the adhesion test used in chapter 7 the low failure strain of some nanocomposites is a problem, due to the nature of the test.

9.3 Crystallization and orientation of crystals and particles

The presence of the nanoparticles causes an increased amount of gamma crystals compared to alpha crystals, but it does not have a large influence on the overall level of crystallinity, probably because most of the matrix polymers used already contains a nucleating agent (indicated by the “D” in the Akulon product code). A small decrease of the matrix modulus is expected because of the addition of the organic silicate modification (surfactant), which does not add stiffness to the matrix. For composite models this extra surfactant phase should be taken into account, because the volume fractions are similar to the volume fraction of filler and, therefore, not negligible (chapter 3). This surfactant phase is probably partially responsible for the

non-linear modulus increase with increasing nanofiller content, which is often observed in organically modified nanocomposites at high filler content.
WAXS measurements on injection-moulded samples have shown that the platelet shaped particles align in the flow direction during processing (chapter 3). The PA6 crystals show a certain degree of alignment at the local level, but the average crystal alignment in the entire injection moulded sample seems to be almost isotropic.

9.4 Water absorption and diffusion

Nanocomposites absorb water at a slower rate, but they are capable of absorbing similar quantities of water in the matrix phase as the unfilled polymer. The higher modulus of nanocomposites can compensate the modulus decrease of PA6 in wet conditions, at room temperature with 5-6 % exfoliated silicate (chapter 2). This compenzation for the absorbed moisture is also effective for creep (chapter 6) and in fibre composites: the strength of moisture conditioned fibre composites with a nanocomposite matrix can be higher than that of fibre composites with an unfilled PA6 matrix (chapter 8). The slower moisture diffusion means that nanocomposites will be in a non-equilibrium state for a longer time during moisture absorption, leading to changing mechanical properties for longer periods. Pre-conditioning at elevated temperatures can speed up the moisture absorption process and lead to more stable properties. However, the reduced moisture transport rate of nanocomposites means that the properties of nanocomposites will be less sensitive to fluctuations in environmental conditions.

9.5 Aspect ratios from the various models

Effective platelet aspect ratios have been estimated from three different properties, using different models: from moisture diffusion coefficients (chapter 2), from room temperature Young's moduli at different moisture levels (chapter 3) and from the intrinsic melt viscosity (chapter 5). The aspect ratios calculated from these three properties show a good agreement with each other and with TEM images. The models calculate lower aspect ratios for particles modified with double-chain surfactants (chapter 3) and unmodified particles (chapter 4 and 5), which are less compatible with PA6. This is due to the larger amount of multi-platelet stacks, which

were also observed in TEM images. One common feature of the estimations from moisture diffusion and Young's moduli is a decreasing aspect ratio with increasing silicate content, probably because of the appearance of small stacks of a few platelets at high concentrations. Calculations from the melt viscosity were only available for low filler content, because the intrinsic viscosity was used and the viscosity models are not reliable at high filler content. In general, the models using diffusion or modulus data lead to more accurate predictions of the aspect ratio at higher filler content, while the models using rheological data lead to more accurate predictions for very low filler content.

Changes on the molecular level due to the presence of the silicate layers apparently only have a small influence on the modulus, because the shape and modulus of the reinforcing particles is sufficient to account for the observed moduli at different matrix moduli using a standard composite model (chapter 3).

9.6 Creep and physical ageing

The creep compliance is reduced by the addition of layered silicate to the matrix polymer, which means that the time dependent deformation will be much smaller when the same load is applied. The physical ageing process is not changed much by the addition of the layered silicate, the shape of the curves does not change much and the curves for different ageing times can be overlapped onto one master curve by shifts on the time axis, just as in unfilled polymers below T_g. The shift rate is not changed much, although it seems to be slightly higher for nanocomposites indicating a slightly faster ageing rate in nanocomposites. The creep behaviour of moisture conditioned nanocomposites and at elevated temperatures shows that the effect of nanofillers is much stronger in these conditions. Creep compliances above T_g can be reduced by more than one decade using only a few percent of exfoliated silicate. It proved difficult to measure the effect of the reduced matrix creep in the fibre composites in bending, because of the low stresses on the matrix.

9.7 Melt flow behaviour and fibre impregnation

The modulus increase is higher for montmorillonite and synthetic mica platelets than for sepiolite fibres for the same volume fraction, because of the higher modulus and

because the platelets reinforce in two directions instead of one. In addition, the viscosity increases less for platelets than for fibres, which is supported by theories that predict a linear dependence on the aspect ratio for platelets and a quadratic one for fibres (chapter 5). Therefore, nano-fibre matrix reinforcement was not used in the fibre composites. The nanocomposites produced with unmodified nano-platelets have a much lower viscosity than those based on organically modified platelets. In modified silicate nanocomposites the melt yield stress increases rapidly above 5 wt% silicate, suggesting a strong structure of interacting particles. However, the nanocomposites with unmodified particles do not lead to a large yield stress, even up to 20 wt% filler. Therefore, despite the lower modulus compared to nanocomposites with modified silicate, this type of nanocomposite has very interesting properties for the use in fibre composites.

For low shear rate processes such as fibre impregnation and wetting, nanocomposites based on unmodified silicate have the advantage of a lower viscosity at the same modulus enhancement and a lack of yield stress, compared to those based on modified silicate. In addition, due to the lack of temperature sensitive modifications the high-temperature resistance can improve. The larger amount of particles necessary for a certain modulus increase can easily be compensated by the lower price of the unmodified particles and the fact that not half of the volume consists of the surfactant that does not increase the modulus (chapter 3).

For high shear rate processes, such as injection moulding, both types of nanocomposite show a similar increase in viscosity, probably because the platelets can align in fast flow fields. For these applications the modulus advantage of the modified platelets can be more important. For film blowing this higher viscosity of nanocomposites with modified particles can even be an advantage, since a low MW nanocomposite can replace a high MW unfilled polymer.

9.8 Adhesion

A reduction of the adhesion with moisture conditioning is observed, which could be caused by water molecules interfering with the hydrogen bonding interactions between the fibre sizing and the PA6 matrix. The modified silicate nanocomposite matrix shows a decrease in adhesion with increasing silicate content. The unmodified silicate shows much less decrease of the adhesion, and is for this reason the preferred type of nanocomposite. Possibly the high viscosity and the yield stress in the melt of modified silicate nanocomposites is responsible for this effect. It could deteriorate the wetting behaviour of the fibre surface, which might result in a less

perfect interface. Another possible reason could be the low thermal stability of the organic surfactants on the modified silicate, which could degrade and collect at the fibre-matrix interface, reducing the bonding strength.

9.9 Combination nanocomposites and continuous fibres

The concept of combining nanocomposites with continuous fibres in a new three phase composite has been very successful for certain types of nanocomposite. The only nanocomposites that have resulted in increasing the (matrix dominated) flexural strength of the glass fibre composite by increasing the matrix modulus are an unmodified silicate nanocomposite and an in-situ polymerized nanocomposite. In carbon fibre composites the expected increase in strength could only be achieved at elevated temperatures using the unmodified silicate nanocomposite. From tests on PA6-based fibre composites at elevated temperatures it became clear that it is very important for fibre composites to have a reasonably high matrix modulus: glass and carbon composites are very sensitive to a decrease of the matrix modulus below values around 1 GPa. Above 1 GPa carbon fibre composites are much more sensitive to the matrix modulus than glass fibre composites. Because the modulus of most nanocomposites stays above the 1 GPa level up to 160 °C or higher, while the modulus of unfilled PA6 decreases below 1 GPa just above T_g, nanocomposites can increase the temperature at which the modulus becomes too low for fibre composites by up to 80-100 °C. Moisture conditioned nanocomposites also show much higher moduli. Even in moisture conditioned samples tested at 80 °C the modulus is much higher than of dry unfilled PA6, well above 1 GPa. This large increase of the application window for PA6 as a fibre composite matrix material has been clearly shown in glass fibre composites. The flexural strength of the glass fibre composites with nanocomposite matrix shows a smaller decrease with increasing temperature, which means a much larger relative increase at elevated temperatures. The strength can be increased by more than 40 % at elevated temperatures. When the increase in temperature range is considered, the temperature at which the fibre composite strength drops below a certain (arbitrary) value increases by 40-50 °C. The carbon fibre composites also show significant improvements at elevated temperatures, but at room temperature no improvement was found. Especially for carbon fibre composites more knowledge on the impregnation and adhesion is necessary to reach the full potential of nanocomposite matrix materials.

These results show that the concept of nanocomposites as matrix material for fibre composites is very successful for PA6, but the concept could also be applied to many other matrix polymers. The improved properties of the nanocomposite matrix material can be used to upgrade the properties of relatively low cost thermoplastic fibre composites to a higher level, while usually more expensive polymers with higher processing temperatures would have to be used to provide the required properties. It can also further increase the temperature range for application of existing high-performance composites.

Besides the increased modulus, additional advantages of nanocomposites are the decreased creep (chapter 6) and a reduced flammability [1-4]. The reduced creep can be beneficial to improve the long-term performance of thermoplastic composites. The reduced flammability can open up new applications in demanding environments such as aircraft interiors, if necessary in combination with additional fire retardants. Using nanocomposites, all these improvements can be achieved without increasing the processing temperature or pressure, and, therefore, with minimal additional cost and easy implementation in existing processes. The added cost of the nano-filled matrix can be small due to the low amounts of filler necessary for a significant improvement.

9.10 Recommendations

- More needs to be understood about the adhesion and wetting of the fibres with nanocomposites, especially in combination with carbon fibres. The influences of the temperature on the adhesion, and the combination with moisture conditioning are also still unknown factors.
- It is not clear how the different crystal morphology in this new type of composite influences the final properties of the fibre composite. More detailed research on the crystallization behaviour of PA6 in the presence of fibres and nanoparticles could possibly reveal possibilities for improvement of the fibre-matrix adhesion and thereby the fibre composite strength.
- In addition to the previous point, further optimization of the fibre composite production process and the fibre surface treatment can probably lead to a larger improvement of the fibre composite properties. The plots of flexural strength versus matrix modulus in chapter 8 suggest that higher flexural strengths than measured could be expected if all other factors would be equal.

- Pultrusion can be used to produce fibre composites with perfectly aligned fibres. In a perfectly aligned unidirectional composite it is possible to measure the true compressive strength, which can subsequently be used for modelling.
- It would be interesting to investigate how the particles flow around the fibres, and how the resulting anisotropic matrix properties influence the fibre composite properties.
- PA66 and PA46 nanocomposites based on the same nanoparticles could be used for the fibre composites to improve the high temperature behaviour further.
- A different way to produce thermoplastic fibre composites with a PA6 matrix is to use anionically polymerized PA6. In this method a liquid monomer containing a catalyst system can be injected into a mould filled with the fibre reinforcement, and polymerized after complete impregnation of the fibres. The same advantages of nanofillers can be expected for this type of PA6 matrix, with the added advantage of the low viscosity of the polymer precursor. Some initial investigation has been done on this concept, both on anionic PA6 with fibres and anionic PA6 with nanofillers [5,6]. However, it proved to be difficult to incorporate nanoparticles in anionic PA6, because the catalyst system is very sensitive and looses its reactivity easily with many types of impurity, such as water, in the system. More research should be done on which layered silicates are compatible with the catalyst, exfoliate in caprolactam and remain stable in the monomer melt without flocculation.
- Other interesting thermoplastic composite matrix polymers such as polypropylene (PP), polyetherimide (PEI), polyphenylenesulfide (PPS), thermoplastic polyurethane (TPU) and polyesters (PET, PBT) could be improved by filling it with the appropriate nanoparticles. To make nanocomposites from these other polymers, not only extrusion processes could be used, but the particles could also be added in a solution of the polymer or during the polymerization step. Preliminary research has shown that PP nanocomposites can be successfully produced using maleic-anhydride modified PP, and that PEI nanocomposites can be successfully produced from solution.

9.11 References

1. Morgan AB, Gilman JW, Nyden M, Jackson CL. New approaches to the development of fire-safe materials. Gaithersburg, MD: NIST, National Institute of Standards and Technology; 2000. Report nr NISTIR 6465.
2. Morgan AB, Gilman JW, Kashiwagi T, Jackson CL. Flammability of polymer-clay nanocomposites. NIST, National Institute of Standards and Technology; 2000.
3. Kashiwagi T, Harris RH, Zhang X, Briber RM, Cipriano BH, Raghavan SR, Awad WH, Shields JR. Flame retardant mechanism of polyamide 6-clay nanocomposites. Polymer 2004;45(3):881-891.
4. Qin HL, Su QS, Zhang SM, Zhao B, Yang MS. Thermal stability and flammability of polyamide 66/montmorillonite nanocomposites. Polymer 2003;44(24):7533-7538.
5. Van Rijswijk K, Vlasveld DPN, Van Rhijn P, Bersee HEN, Beukers A, Picken SJ. Process considerations for liquid molding of composites based on anionic polyamide 6. 2003; San Diego, USA. p 1569.
6. Van Rijswijk K, Vlasveld DPN, Bersee HEN, Picken SJ. Vacuum Injection of Anionic Polyamide 6. 2003; Durban, South Africa. p 508-513.

Summary

Fibre reinforced polymer nanocomposites

In this thesis the results are described of the research on a combination of two types of composites: thermoplastic nanocomposites and continuous fibre composites. In this three-phase composite the main reinforcing phase consist of continuous glass or carbon fibres, and the matrix consists of a polyamide 6 / layered silicate nanocomposite. To be able to produce and understand this new type of thermoplastic composite, several aspects of the individual components needed to be understood first. The first part of this thesis concerns the study of the nanocomposite matrix material, followed by an investigation of the properties of the new three-phase composite.

In **chapter 1** a general introduction describes nanocomposites, nanoparticles, thermoplastic fibre composites and the current knowledge on the combined three-phase composite.

In **chapter 2** the influence of the amount of layered silicate filler and the amount of absorbed moisture on the mechanical properties of PA6 nanocomposites is discussed. Diffusion coefficients have been determined from moisture absorption experiments and it was found that similar amounts of water were absorbed by the nanocomposites with different silicate concentrations. The modulus of the nanocomposites increases with increasing amount of silicate and decreases with increasing amount of absorbed moisture. However, the ductility of the nanocomposites decreases with increasing amount of silicate and increases with increasing moisture content. A more hydrophobic modification of the particles results in a reduction of the degree of exfoliation in PA6, and consequently in a lower modulus, a higher ductility and an increased diffusion coefficient compared to nanocomposites with particles that are better exfoliated. PA6 nanocomposites can compensate for the decrease of the modulus of PA6 when water is absorbed from the environment.

In **chapter 3** the modulus data of nanocomposites with three different moisture levels that were described in chapter 2 have been analysed with a Halpin-Tsai composite model. In addition, the crystallinity and the orientation of the crystals and the silicate platelets in injection-moulded samples have been studied using DSC and WAXS. Based on this data, the model is used to calculate the matrix modulus in the

nanocomposites based on the crystallinity, the amount of surfactant and the moisture content. Subsequently, the measured modulus of the nanocomposites with different moisture content was used to calculate the effective aspect ratios of the reinforcing particles with the Halpin-Tsai model. The calculated aspect ratio for each nanocomposite is independent of the moisture concentration. This indicates the validity of this composite model to describe nanocomposites, despite the small particle size. The results suggest that changes on the molecular level due to the presence of the silicate layers only have a small influence on the modulus, because the modulus can be explained with a composite model. The reduced efficiency of reinforcement at increasing filler levels can be partially explained by the reduction of the matrix modulus due to surfactant and a very slightly reduced crystallinity, and partially by the occurrence of small stacks of platelets.

In **chapter 4** several different types of nanocomposites were studied, including a comparison between nanocomposites based on organically modified and unmodified silicate. A series of concentrations has been prepared using low and high molecular weight grades of PA6 and this was compared with a series based on a low MW grade of PA66 and several commercially available PA6 nanocomposites. Mechanical properties have been tested at temperatures ranging from 20 to 120 °C. The modulus increase in all nanocomposites with organically modified silicate is similar: at room temperature an increase of the modulus of approximately 10% for each wt% of silicate is found. PA66 nanocomposites display an identical (relative) modulus increase as PA6 nanocomposites, while unmodified silicate nanocomposites show a smaller increase of the modulus. The yield stress also increases with the addition of layered silicate, but low MW PA6 and PA66 nanocomposites show brittle fracture behaviour at room temperature, and only high MW PA6 nanocomposites are ductile. With increasing temperature all nanocomposites become ductile at a certain temperature. It became clear that unmodified layered silicate is not as effective as modified silicate, but it can lead to substantial improvements in properties as well. High MW PA6 leads to more ductile nanocomposites, but the high viscosity leads to processing problems with high filler fractions. PA66 can be used with equal success as PA6 as matrix polymer.

In **chapter 5** a series of nanocomposites based on modified and unmodified silicate with different levels of exfoliation, was used to study the dynamic properties in the solid state and the melt. The results were compared with micro-composites containing various shapes of glass filler. The higher modulus of nanocomposites at higher concentrations is accompanied by an increase in melt viscosity and the occurrence of a yield stress in the melt. Both the modulus in the solid state and the

melt viscosity are influenced by the aspect ratio and the concentration of the filler particles. These results were used to calculate the aspect ratios of the reinforcement using the Halpin-Tsai composite model and several modified Einstein viscosity models. The experiments showed that the Simha theory for oblate and prolate spheroids predicts platelet aspect ratios from melt viscosity data that are close to the results from the Halpin-Tsai composite model and from TEM observations. The results of the analysis show the advantages and disadvantages of the various shapes and sizes of fillers and the level of exfoliation, both from a processing and a mechanical properties point of view.

In **chapter 6** the creep and physical aging behaviour of various types of PA6 nanocomposites and unfilled PA6 are described. After annealing far above T_g the samples were quenched to room temperature and tested after various ageing times. The creep compliance shows a significant reduction with the addition of exfoliated layered silicate to the PA6. The shape of the creep curves of the nanocomposites is similar to unfilled PA6 and time - ageing time superposition is possible with all materials. The shift rate for superposition is in the same range, but slightly higher in nanocomposites. The creep behaviour of nanocomposites conditioned with an equilibrium amount of moisture and dry samples at elevated temperatures shows that the effect of nanofillers is much stronger under these conditions.

In **chapter 7** the interfacial bonding between glass fibres and PA6 and PA6 nanocomposites is studied. Two different types of nanocomposite were used with different degrees of exfoliation of the silicate layers: one with non-modified silicate and one with an organically modified silicate. The fibre-matrix interfacial bonding properties of these fibre-reinforced nanocomposites were studied with the single fibre fragmentation test (SFFT). This test provides the critical fibre aspect ratio, which is used to compare the interfacial bonding for different systems. The following parameters and their influence on interfacial bonding are studied: fibre surface treatment, type and concentration of the silicate filler, and moisture content. The mechanical properties of the matrix materials such as the modulus and the yield behaviour are studied to find out how they could influence the test results. The SFFT results for the various nanocomposite matrix materials are compared with various models that describe the critical aspect ratio as a function of the mechanical properties. The failure mechanism is by interfacial de-bonding and not by matrix failure. Both the addition of nanoparticles and moisture conditioning has a negative effect on the bonding between the matrix and the fibres. Unmodified silicate nanocomposites seem to lead to a better adhesion than modified silicate nanocomposites.

In **chapter 8** a new type of thermoplastic composite has been made, consisting of a main reinforcing phase of woven glass or carbon fibres and a PA6 nanocomposite matrix. Nanocomposites have the potential to improve the matrix dominated flexural and compressive strength by increasing the matrix modulus. Good quality fibre composites have been made with several types of PA6 nanocomposite and a PA6 reference material in combination with glass and carbon fibre reinforcement. Flexural tests on commercial PA6 fibre composites have shown the amount of decrease of the flexural strength upon increasing temperature and the link with the decrease of the matrix modulus. The nanocomposites used in this research have moduli that are much higher than unfilled PA6, also above T_g and in moisture conditioned samples. The strength of glass fibre composites can be increased by more than 40 % at elevated temperatures and the temperature range for applications can be increased by 40-50 °C. Carbon fibre composites also show significant improvements at elevated temperatures, but not at room temperature. An improved understanding and optimization of the production method and the fibre-matrix adhesion is needed to reach the full potential of the higher matrix moduli. With the use of nanocomposites the fibre composite properties can be improved without change in the processing conditions.

In **chapter 9** the various subjects covered in the previous chapters are combined and discussed, followed by some recommendations for further research on this subject.

Samenvatting

Vezelversterkte polymeer nanocomposieten

In dit proefschrift zijn de resultaten beschreven van het onderzoek naar een combinatie van twee typen composieten: thermoplastische nanocomposieten en continu vezelversterkte composieten. In dit driefasen composiet bestaat de belangrijkste versterkende fase uit continue glas of koolstof vezels en de matrix bestaat uit een polyamide 6 / gelaagd silicaat nanocomposiet. Om dit nieuwe type thermoplastische composiet te kunnen produceren en begrijpen, moeten er eerst verschillende aspecten van de individuele componenten begrepen worden. Het eerste deel van dit proefschrift behandelt het nanocomposiet matrix materiaal, gevolgd door een onderzoek naar de eigenschappen van het nieuwe driefasen composiet.

In **hoofdstuk 1** beschrijft een algemene inleiding nanocomposieten, nanodeeltjes, thermoplastische vezelcomposieten en de huidige kennis op het gebied van gecombineerde driefasen composieten.

In **hoofdstuk 2** wordt de invloed van de hoeveelheid gelaagd silicaat en de hoeveelheid geabsorbeerd vocht op de mechanische eigenschappen van PA6 nanocomposieten behandeld. Diffusie coëfficiënten zijn afgeleid van vochtopname experimenten, welke uitwezen dat de hoeveelheid opgenomen vocht in de matrix nauwelijks beïnvloed wordt door de concentratie silicaat. De modulus van de nanocomposieten stijgt met toenemende hoeveelheid silicaat en neemt af met toenemende hoeveelheid geabsorbeerd vocht. De taaiheid van de nanocomposieten neemt echter af met toenemende hoeveelheid silicaat en neemt toe met meer geabsorbeerd vocht. Een meer hydrofobe modificatie van de silicaatplaatjes (met dubbele alifatische staarten) leidt tot een reductie van de exfoliatie, en daardoor tot een lagere modulus, een hogere taaiheid en een hogere diffusiesnelheid in vergelijking met nanocomposieten met beter verdeelde plaatjes. PA6 nanocomposieten kunnen de modulusverlaging door water absorptie uit de omgeving compenseren.

In **hoofdstuk 3** zijn de moduli van de nanocomposieten met drie verschillende vochtgehaltes die beschreven zijn in hoofdstuk 2 geanalyseerd met behulp van een Halpin-Tsai composiet model. Tevens zijn de kristalliniteit en de oriëntatie van de kristallen en de silicaatplaatjes in gespuitgiete teststaafjes bestudeerd met DSC en

WAXS. Met deze gegevens is het model gebruikt om de modulus van de matrix te berekenen als functie van de kristalliniteit, de hoeveelheid surfactant en de hoeveelheid vocht. Vervolgens is de gemeten modulus van de nanocomposieten met verschillende vochtgehaltes gebruikt om de effectieve as-verhouding (aspect ratio) van de versterkende deeltjes te berekenen met het Halpin-Tsai model. De berekende as-verhouding is onafhankelijk van het vochtgehalte. Dit geeft aan dat dit composietmodel goed bruikbaar is om nanocomposieten te beschrijven, ondanks de kleine deeltjesgrootte. De resultaten suggereren dat de veranderingen op moleculair niveau door de aanwezigheid van de silicaatplaatjes slecht een kleine invloed op de modulus hebben, want de modulus kan verklaard worden door een composietmodel. De afnemende effectiviteit van de versterkende deeltjes bij toenemende hoeveelheid silicaat kan deels verklaard worden door de reductie van de matrix modulus door de toegevoegde surfactant en de zeer licht gedaalde kristalliniteit, en deels door een toename van kleine aggregaten met meerdere plaatjes.

In **hoofdstuk 4** zijn verschillende soorten nanocomposieten bestudeerd, waaronder een vergelijking tussen nanocomposieten gebaseerd op organische gemodificeerde en ongemodificeerde silicaten. Concentratiereeksen zijn gemaakt op basis van laag molgewicht en hoog molgewicht PA6, en die zijn vergeleken met een concentratiereeks op basis van een laag molgewicht PA66 en twee commercieel verkrijgbare nanocomposieten. De mechanische eigenschappen zijn getest bij temperaturen van 20 tot 120 °C. De modulusstijging bij alle nanocomposieten op basis van organische gemodificeerde silicaten is ongeveer gelijk: bij kamertemperatuur is een modulusstijging van ongeveer 10% voor elk gewichts% silicaat gevonden. PA66 nanocomposieten laten een identieke (relatieve) modulus stijging zien als de PA6 nanocomposieten, maar nanocomposieten met ongemodificeerde silicaatplaatjes laten een lagere stijging zien. De vloeispanning stijgt ook licht met het toevoegen van gelaagd silicaat, maar laag molgewicht PA6 en PA66 nanocomposieten vertonen een bros breukgedrag bij kamertemperatuur, en alleen hoog molgewicht nanocomposieten zijn taai en vertonen een vloeipunt. Bij toenemende temperatuur worden alle nanocomposieten taai bij een bepaalde temperatuur. De resultaten maakten duidelijk dat hoewel ongemodificeerde silicaat niet zo effectief is als gemodificeerde, het toch ook tot aanzienlijke verbeteringen van de eigenschappen kan leiden. Hoog molgewicht PA6 leidt wel tot taaiere nanocomposieten, maar de hoge viscositeit kan tot verwerkingsproblemen leiden bij hogere vulgraad. PA66 kan met evenveel succes worden gebruikt als nanocomposiet matrix als PA6.

In **hoofdstuk 5** zijn twee concentratiereeksen, gebaseerd op gemodificeerde en ongemodificeerde silicaten, met een verschillende exfoliatie gebruikt om de dynamische eigenschappen in de vaste toestand en in de smelt te bestuderen. De resultaten zijn vergeleken met microcomposieten met verschillende vormen glasdeeltjes. Naast de hogere modulus van nanocomposieten bij toenemende concentratie is er ook een hogere viscositeit en een vloeispanning in de smelt te zien. Zowel de modulus in de vaste toestand als de smelt viscositeit wordt beïnvloed door de concentratie en de as-verhouding van de deeltjes. De resultaten zijn gebruikt om de as-verhoudingen van de deeltjes te berekenen met het Halpin-Tsai composiet model en enkele gemodificeerde Einstein viscositeitmodellen. De resultaten van de experimenten en berekeningen lieten zien dat de theorie van Simha voor oblate en prolate ellipsoïden as-verhoudingen uit viscositeiten voorspelt die goed overeenkomen met de resultaten van het Halpin-Tsai model en TEM observaties. De resultaten van de analyse laten de voor- en nadelen van de verschillende vormen en groottes van de deeltjes zien, zowel wat betreft de verwerking als de mechanische eigenschappen.

In **hoofdstuk 6** is het kruipgedrag en de fysische veroudering van verschillende typen PA6 nanocomposieten beschreven. Na een thermische behandeling ver boven de T_g zijn de teststaafjes snel afgekoeld naar kamertemperatuur en getest na verschillende verouderingstijden. De kruipcompliantie vertoont een aanzienlijke reductie door de toevoeging van de silicaatplaatjes. De vorm van de kruipcurves van de nanocomposieten lijkt erg op die van ongevuld PA6 en tijd – verouderingstijd superpositie is mogelijk met alle materialen. De verschuiving over de tijd-as voor superpositie is in dezelfde ordegrootte, maar een klein beetje hoger voor nanocomposieten. Het kruipgedrag van vochtgeconditioneerde materialen en het kruipgedrag boven de T_g laat zien dat de reductie van de kruip met de nanodeeltjes onder deze omstandigheden veel groter is.

In hoofdstuk 7 is de hechting tussen glasvezels en PA6 en nanocomposieten bestudeerd. Twee verschillende soorten nanocomposiet zijn gebruikt met een verschillende exfoliatie, gemaakt met gemodificeerde en ongemodificeerde silicaatplaatjes. De vezel-matrix hechting van de vezelversterkte nanocomposieten is gemeten met een enkele-vezel fragmentatie test. Deze test levert een kritische vezel as-verhouding op die gebruikt is om de hechting tussen de verschillende systemen te vergelijken. Factoren zoals de oppervlaktebehandeling van de vezels, het type en de concentratie van de nanodeeltjes en de invloed van vocht zijn gemeten. Tevens zijn de mechanische eigenschappen van de matrix getest om de invloed hiervan op de testresultaten te bestuderen. De resultaten met de verschillende matrix materialen

zijn vergeleken met enkele modellen die de kritische as-verhouding van de vezelfragmenten voorspellen als functie van de matrix eigenschappen. Het faalmechanisme blijkt door het loslaten op het grensvlak te zijn, en niet door het falen van de matrix. Zowel het toevoegen van nanodeeltjes als het conditioneren met vocht blijkt een nadelig effect te hebben op de hechting tussen matrix en vezel. Nanocomposieten met ongemodificeerde silicaatplaatjes blijken een betere hechting te geven dan die met organisch gemodificeerde silicaatplaatjes.

In **hoofdstuk 8** is een nieuw type thermoplastisch composiet beschreven, bestaande uit een versterkende fase van geweven glas of koolstof vezel en een matrix van een PA6 nanocomposiet. De nanocomposieten kunnen de matrixgedomineerde compressie- en buigsterkte van de vezelcomposiet verhogen door de matrix modulus te verhogen. Vezelcomposieten van goede kwaliteit zijn gemaakt met verschillende soorten nanocomposiet en PA6 referentiemateriaal, zowel met glas- als koolstofvezels. Buigproven aan commercieel verkrijgbare PA6 vezelcomposieten hebben de daling van de sterkte bij toenemende temperatuur aangetoond, evenals de link met de dalende matrix modulus. De hier gebruikte nanocomposieten hebben een veel hogere modulus dan ongevuld PA6, ook boven T_g en in vochtige toestand. De sterkte van de glasvezel composieten is met meer dan 40% verhoogd bij hogere temperaturen en de temperatuur waarbij deze composieten toegepast kunnen worden kan daardoor met 40-50 °C verhoogd worden. Koolstofvezel composieten lieten ook een aanzienlijke verbetering zien van de sterkte bij hoge temperaturen, maar niet bij kamertemperatuur. Een beter begrip en een verbetering van de productiemethode en de vezel-matrix hechting is nodig om het volledige potentieel van de hogere matrix moduli te benutten. Met het gebruik van nanocomposieten als matrix kunnen de vezelcomposiet eigenschappen sterk verbeterd worden zonder veranderingen in de verwerkingscondities.

In **hoofdstuk 9** zijn de onderwerpen die in de voorgaande hoofdstukken behandeld zijn gecombineerd en bediscussieerd, gevolgd door enkele aanbevelingen voor verdergaand onderzoek op dit gebied.

Curriculum vitae

Daniël Vlasveld kwam op 25 maart 1975 ter wereld in Leiderdorp. Heel wat jaren later bracht hij de periode van 1987-1993 door aan het Adelbert College te Wassenaar, waar de voorkeur voor chemie en natuurkunde echt duidelijk werd. Nadat het VWO diploma was behaald vertrok hij richting Enschede voor een studie Chemische Technologie aan de Universiteit Twente. Daar ging de aandacht steeds meer uit richting de polymeren, wat daardoor vervolgens ook de afstudeerrichting werd. Na een afstudeerproject op het gebied van slagvastheid van polyketon-rubber blends, afgerond in 2000, was de onderzoeksinteresse echt goed aangewakkerd en werd er snel gekozen voor het doen van een promotieonderzoek. Weer terug aan de westelijke kant van het land werd er in oktober 2000 begonnen aan de TU Delft aan een promotieonderzoek over nanocomposieten en de toepassing als vezelcomposiet matrix materiaal. Het resultaat van dit onderzoek is beschreven in dit boekje. Na afronding was de interesse voor nanocomposieten nog niet verdwenen, en is hij in 2005 aan een postdoctoraal onderzoek begonnen op het gebied van aramide nanocomposieten in samenwerking met Teijin Twaron.

Publications

Nanocomposite matrix for increased fibre composite strength.
D.P.N. Vlasveld, H.E.N. Bersee, S.J. Picken
Polymer 2005 (46) In Press

The relation between rheological and mechanical properties in PA 6 nanocomposites and microcomposites.
D.P.N. Vlasveld, M. de Jong, A.D. Gotsis, H.E.N. Bersee, S.J. Picken
Polymer 2005 (46) In Press

Moisture absorption in polyamide-6 silicate nanocomposites and its influence on the mechanical properties
D.P.N. Vlasveld, J. Groenewold, H.E.N. Bersee, S.J. Picken
Polymer 2005 (Revised version under review)

Creep and physical aging behaviour of PA6 nanocomposites.
D.P.N. Vlasveld, H.E.N. Bersee, S.J. Picken
Polymer (Under review)

A comparison of the temperature dependence of the modulus, yield stress and ductility of nanocomposites based on high and low MW PA6 and PA66.
D.P.N. Vlasveld, S.G. Vaidya, H.E.N. Bersee and S.J. Picken
Polymer 2005 (46) 3452-3461.

Analysis of the modulus of polyamide-6 silicate nanocomposites using moisture controlled variation of the matrix properties
D.P.N. Vlasveld, J. Groenewold, H.E.N. Bersee, E. Mendes, S.J. Picken
Polymer 2005 (46) 6102-6113.

Fibre–matrix adhesion in glass-fibre reinforced polyamide-6 silicate nanocomposites
D.P.N. Vlasveld, P.P. Parlevliet, H.E.N. Bersee and S.J. Picken
Composites Part A, issue 1, January 2005, 1-11

Nanocomposite matrices for continuous fibre reinforced thermoplastic composites
D.P.N. Vlasveld, H.E.N. Bersee and S.J. Picken
Proceedings of the 25th International SAMPE Europe Conference 2004

Creep in thermoplastic nano- and fibercomposites
K. van Rijswijk, K.H. Boonstra, D.P.N. Vlasveld, H.E.N. Bersee and S.J. Picken
Proceedings of the 25th International SAMPE Europe Conference 2004

Influence of sample thickness on fracture behaviour of a polyketone and a polyketone-rubber blend
W.C.J. Zuiderduin, D.P.N. Vlasveld, J. Huétink and R.J. Gaymans
Polymer 2005 (46) In Press

Mechanical properties of polyketone terpolymer/rubber blends
W.C.J. Zuiderduin, D.P.N. Vlasveld, J. Huétink and R.J. Gaymans
Polymer 2004 (45) 3765-3779.